NASA Conference Publication 10014

Polar Ozone Workshop

Abstracts

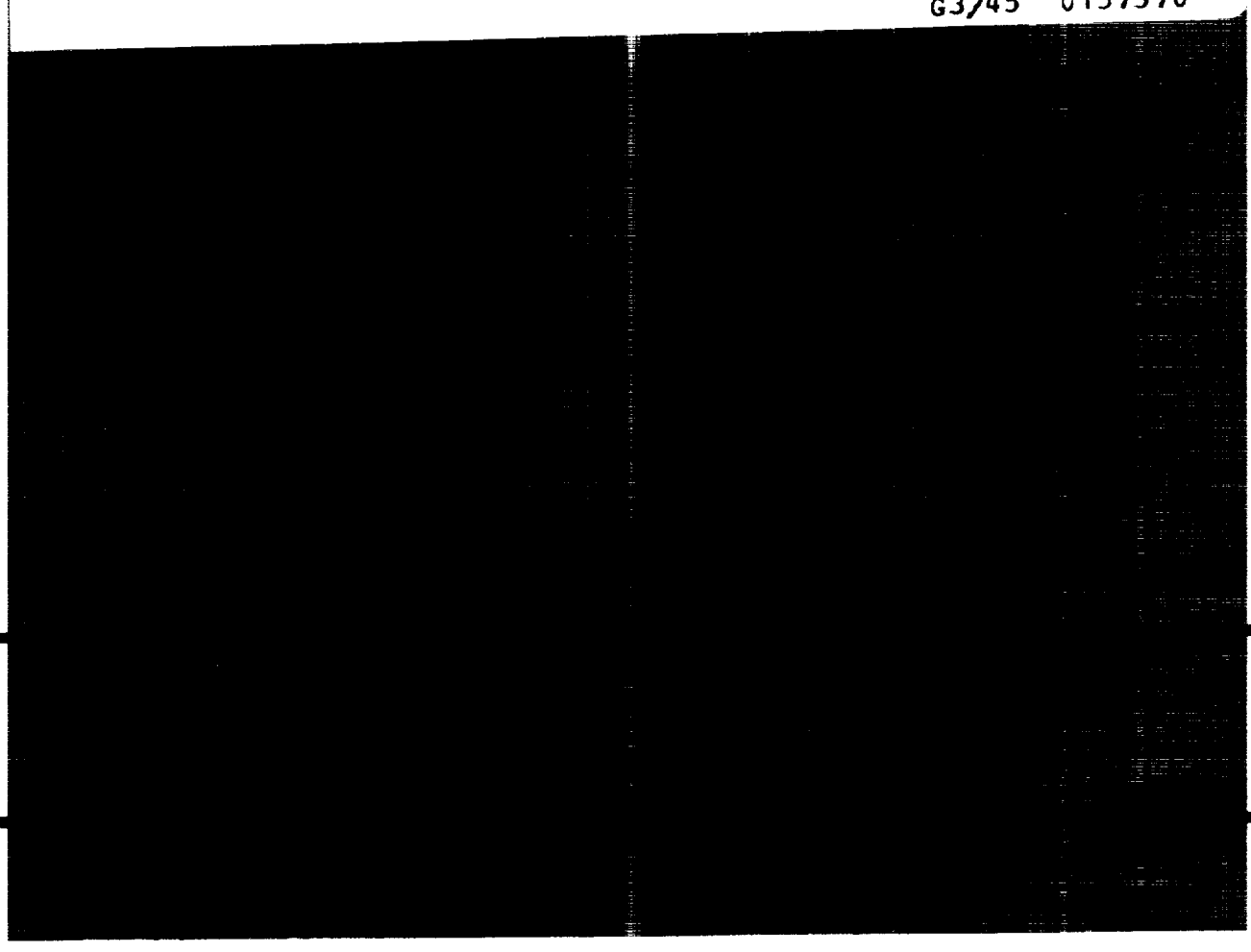

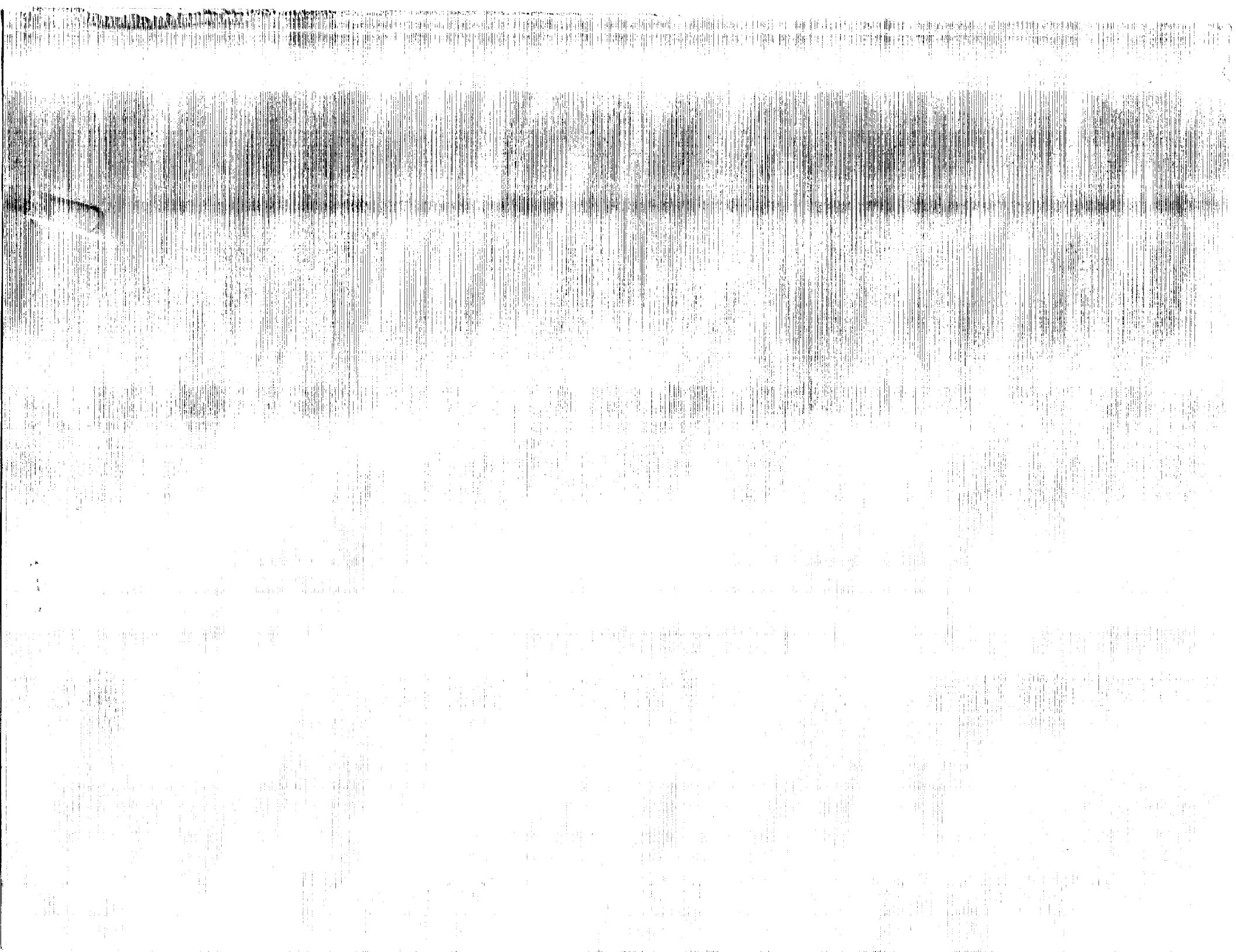

NASA Conference Publication 10014

Polar Ozone Workshop

Abstracts

Proceedings
of the Polar Ozone Workshop
held in Snowmass, Colorado, U.S.A.
and Sponsored by the National
Aeronautics and Space
Administration, National Oceanic
and Atmospheric Administration,
National Science Foundation,
Chemical Manufacturers
Association, World Meteorological
Organization, and the United Nations
Environment Program
May 9-13, 1988

National Aeronautics and
Space Administration

1988

POLAR OZONE WORKSHOP

Snowmass, Colorado

May 9-13, 1988

Executive Committee

Daniel L. Albritton, National Oceanic and Atmospheric Administration

Michael J. Kurylo, National Aeronautics and Space Adminstration

John Lynch, National Science Foundation

Mack McFarland, Fluorocarbon Program Panel of the Chemical Manufacturers Association

Robert T. Watson, National Aeronautics and Space Administration

Program Committee

Arthur C. Aikin - Executive Secretary, NASA Goddard, Greenbelt, MD

Shigeru Chubachi, Meteorological Research Institute, Tsukuba, Japan

Paul Crutzen, Max Planck, Mainz, FRG

Joe C. Farman, British Antarctic Survey, Natural Environment Research Council, UK

Dennis L. Hartmann, University of Washington, Seattle, WA

David J. Hofmann, University of Wyoming, Laramie, WY

Ivar S.A. Isaksen, University of Oslo, Norway

John Lynch, National Science Foundation, Washington, DC

Mack McFarland, Fluorocarbon Program Panel of the Chemical Manufacturers Association, Washington, DC

Michael McIntyre, Cambridge University, Cambridge, UK

John Pyle, University of Cambridge, Cambridge, UK

Susan Solomon, NOAA Aeronomy Laboratory, Boulder, CO

N. Sundararaman, World Meteorological Organization, Geneva, Switzerland

Adrian Tuck, NOAA Aeronomy Laboratory, Boulder, CO

Peter Usher, United Nations Environment Program, Nairobi, Kenya

Robert T. Watson - Chairman, NASA Headquarters, Washington, DC

Flo Ormond - Conference Coordinator, ORI, Inc./NASA Headquarters, Washington, DC

TABLE OF CONTENTS

Polar Ozone Workshop Agenda
May 9-13, 1988
Snowmass, Colorado

SESSION I - Observations of Ozone and Temperature
Presiding, J. Anderson, Harvard University
Monday Morning, May 9 - 9:00 AM

Author(s)	Affiliation	Title of Abstract	Time
D. Albritton	NOAA/Aeronomy Laboratory Boulder, CO	Overview	15
J. Farman	British Antarctic Survey Cambridge, UNITED KINGDOM	Ozone Observations	20
S. Chubachi	Meteorological Research Institute JAPAN	Total Ozone by Lunar Dobson Observation at Syowa, Antarctica	20
A. J. Krueger	NASA/Goddard Space Flight Center Greenbelt, MD	Total Ozone Changes in the 1987 Antarctic Ozone Hole	20
P. Newman M. Schoeberl	Applied Research Corporation Landover, MD NASA/Goddard Space Flight Center Greenbelt, MD	The Breakup of the Southern Hemisphere Spring Polar Ozone and Temperature Minimums From 1979 to 1987	20
W. J. Randel P. Newman	National Center for Atmospheric Research, Boulder, CO Applied Research Corporation Landover, MD	Observations of Stratospheric Temperature Changes Coincident with the Recent Antarctic Ozone Depletions	20
J. C. Larsen M.P.McCormick	ST Systems Corporation Hampton, VA NASA/Langley Research Center Hampton, VA	Antarctic Measurements of Ozone by SAGE II in the Spring of 1987	12
A. C. Aikin R. D. McPeters	NASA/Goddard Space Flight Center Greenbelt, MD	The Three-Dimensional Morphology of the Antarctic Ozone Hole	12

SESSION II - Polar Stratospheric Clouds - A
Presiding, J. Margitan, Jet Propulsion Laboratory
Monday Afternoon, May 9

M.P.McCormick C. R. Trepte	NASA/Langley Research Center Hampton, VA ST Systems Corporation Hampton, VA	Persistence of Antarctic Polar Stratospheric Clouds	20

SESSION II - Polar Stratospheric Clouds - A, Cont.
Presiding, J. Margitan, Jet Propulsion Laboratory
Monday Afternoon, May 9

Author(s)	Affiliation	Title of Abstract	Time
C. V. Ferry	NASA/Ames Research Center Moffett Field, CA	Comparison of *In Situ* Aerosol Measurements with SAGE II and SAM II Aerosol Measurements during the Airborne Antarctic Ozone Experiment	20
M.P.McCormick	NASA/Langley Research Center Hampton, VA		
R. F. Pueschel	NASA/Ames Research Center Moffett Field, CA		
J.M.Livingston	SRI International Menlo Park, CA		
D. J. Hofmann	University of Wyoming	Stratospheric Aerosol and Cloud Measurements at Mcmurdo Station Antarctica during the Spring of 1987	20
J. M. Rosen	Laramie, WY		
J. W. Harder	"		
J. M. Rosen	University of Wyoming	Balloon Borne Antarctic Frost Point Measurements and their Impact on Polar Stratospheric Cloud Theories	20
D. J. Hofmann	Laramie, WY		
J. R. Carpenter	"		
J. W. Harder	"		
S. J. Oltman	GMCC NOAA Boulder, CO		
E. V. Browell	NASA/Langley Research Center	Large-Scale Variations in Ozone and Polar Stratospheric Clouds Measured with Airborne Lidar during Formation of the 1987 Ozone Hole over Antarctica	20
Lamont R. Poole	Hampton, VA		
M. P. McCormick	"		
S. Ismail	"		
C. F. Butler	"		
S. A. Kooi	"		
M. Szedlmayer	"		
R. Jones	Meteorological Office GREAT BRITAIN		
A. J. Krueger	NASA/Goddard Space Flight Center Greenbelt, MD		
A. Tuck	NOAA/Aeronomy Laboratory Boulder, CO		
B. W. Gandrud	National Center for Atmospheric Res.	Filter Measurements of Chemical Composition during the Airborne Antarctic Ozone Experiment	20
P. D. Sperry	Research, Boulder, CO		
L. Sanford	"		

Author(s)	Affiliation	Title of Abstract	Time
R. F. Pueschel K. G. Snetsinger J. K. Goodman G. V. Ferry V. R. Oberbeck S. Verma W. Fong	NASA/Ames Research Center Moffett Field, CA San Jose State University San Jose, CA NASA/Ames Research Center Moffett Field, CA Thermo Analytical Systems Inc. Richmond, CA Information Management Inc. Palo Alto, CA	Antarctic Polar Stratospheric Aerosols: The Roles of Nitrates, Chlorides and Sulfates	20

Reception for Poster Presentations
In Hoagland Room
Immediately Following Session II

SESSION III - Polar Stratospheric Clouds - B
Presiding, S. Wofsy, Harvard University
Tuesday Morning, May 10, 1988

D. W. Fahey D. M. Murphy C. S. Eubank G. V. Ferry K. R. Chan J. M. Rodriquez	NOAA Boulder, CO " NASA/Ames Research Center Moffett Field, CA Atmospheric and Environmental Res. Cambridge, MA	*In Situ* Measurements of Total Reactive Nitrogen, Total Water Vapor, and Aerosols in Polar Stratospheric Clouds in the Antarctic Stratosphere	20
L. R. Poole M. P. McCormick E. V. Browell D. Fahey K. Kelly G. Ferry R. Pueschel R. Jones	NASA/Langley Research Center Hampton, VA " NOAA Boulder, CO NASA/Ames Research Center Moffett Field, CA U. K. Meteorological Office UNITED KINGDOM	Multi-Wavelength Backscatter and Extinction Measurements of Polar Stratospheric Clouds during the 1987 Airborne Antarctic Ozone Experiment: Implications for Microphysical Processes	20
D. Hanson K. Mauersberger	University of Minnesota Minneapolis, MN	Laboratory Studies of HNO3/H2O Mixtures at Low Temperatures	15
V. Ramaswamy	Princeton University Princeton, NJ	Evolution of Polar Stratospheric Clouds during the Antarctic Winter	20
R. P. Turco O. B. Toon	R & D Associates Marina del Rey, CA NASA/Ames Research Center Moffett Field, CA	Heterogeneous Physicochemistry and Microphysics of Polar Stratosphere Clouds	10
O. B. Toon	NASA/Ames Research Center Moffett Field, CA	Polar Ice clouds and the Seasonal Cycle of Water Vapor	10

Author(s)	Affiliation	Title of Abstract	Time
M. A. Tolbert	SRI International Menlo Park, CA	Heterogeneous Chemistry Related to Antarctic Ozone Depletion: Reaction of ClONO2 and N2O5 on Ice Surface	15
M. J. Rossi D. M. Golden	" "		
D. Worsnop	Aerodyne Research Inc.	Mass Accommodation Coefficient Measurements for HNO3, HCl and N2O5 on Water, Ice and Sulfuric Acid Droplet Surfaces	15
M. Zahniser	Billerica, MA		
C. Kolb	"		
L. Watson	Boston College		
J. V. Doren	Chestnut Hill, MA		
J. Jayne	"		
P. Davidovits	"		
M.-T. Leu	Jet Propulsion Laboratory Pasadena, CA	Laboratory Studies of Sticking Coefficients and Heterogeneous Reactions Important in the Antarctic Stratosphere	15

SESSION IV - Remote Sensing of Trace Gases
Presiding, R. Turco, R & D Associates
Tuesday Afternoon, May 10, 1988

J. G. Keys	Physics and Engineering Lab.	Stratospheric Column NO2 Measurements From Three Antarctic Sites	15
P. V. Johnston	Central Otago, NEW ZEALAND		
R. W. Sanders	CIRES, University of Colorado Boulder, CO	Ground-based Measurements of O3,NO2,OClO, and BrO20 during the 1987 Antarctic Ozone Depletion Event Including Observations of the Diurnal Variations of BrO and OClO	20
S. Solomon	NOAA/Aeronomy Laboratory		
M. A. Carroll	Boulder, CO		
A. L. Schmeltekopf	"		
A. Wahner	CIRES, University of Colorado	Near UV Atmospheric Absorption Measurements from the DC-8 Aircraft the 1987 Airborne Antarctic Ozone Experiment	20
R. O. Jakoubek	Boulder, CO		
A. R. Ravishankara	NOAA/ERL		
G. H. Mount	Boulder, CO		
A. L. Schmeltekopf	"		
M. T. Coffey	NCAR	Infrared Measurements of Column Amounts of Stratospheric Constituents in the Antarctic Winter, 1987	20
W. G. Mankin	Boulder, CO		
G. C. Toon	Jet Propulsion Laboratory	Infrared Aircraft Measurements of Stratospheric Composition over Antarctica during September 1987	20
C. B. Farmer	Pasadena, CA		
L. L. Lowes	"		
P. W. Schaper	"		
J. F. Blavier	"		
R. H. Norton	"		
F. J. Murcray	University of Denver	Infrared Measurements in the Spring 1987 Ozone Hole	20
D. G. Murcray	Denver, CO		
A. Goldman	"		
J. G. Keys	Lauder Dept. of Sciencific and		
W. A. Matthews	Industrial Res., NEW ZEALAND		

Author(s)	Affiliation	Title of Abstract	Time
R. deZafra	State University of New York	Quantitative Observations of Anomalous	10
P. Solomon	Stony Brook, NY	Low Altitude ClO in the Antarctic Spring	10
M. Jaramillo	"	Stratosphere, 1987: Diurnal Behavior and	
J. Barrett	"	Retrieval Accuracy	
L. Emmons	Milltech Corporation		
A. Parrish	South Deerfield, MA		

SESSION V - In-Situ Measurements of Chemical Species and Their Interpretation - A
Presiding, S. Solomon, NOAA/Aeronomy Laboratory
Wednesday Morning, May 11, 1988

J. G. Anderson	Harvard University	*In Situ* Observations of ClO and	30
W. H. Brune	Cambridge, MA	BrO in the Antarctic: Evidence for	
M. J. Profitt	NOAA/Aeronomy Laboratory	Chlorine-Catalyzed Destruction	
	Boulder, CO	of Ozone	
W. Starr	NASA/Ames Research Center		
K. R. Chan	Mountain View, CA		
D. W. Fahey	NOAA	Measurements of NO and Total	10
D. M. Murphy	Boulder, CO	Reactive Odd Nitrogen, NOy, in the	
C. S. Eubank	"	Antarctic Stratosphere	
G. V. Ferry	NASA/Ames Research Center		
K. R. Chan	Moffett Field, CA		
J. M. Rodriquez	Atmospheric and Environ. Res.		
	Cambridge, MA		
J. F. Vedder	NASA/Ames Research Center	Mixing Ratios of Trace Gases in the	20
	Moffett Field, CA	Austral Polar Atmosphere During	
L. E. Heidt	NCAR	August and September, 1987	
	Boulder, CO		
W. H. Pollock	NCAR		
B. E. Henry	Boulder, CO		
R. A. Leub	"		
J. R. Podolske	NASA/Ames Research Center	Southern Hemispheric Nitrous	20
M. Loewenstein	Moffett Field, CA	Oxide Measurements Obtained During	
L. E. Strahan	"	the 1987 Airborne Antarctic Ozone	
K. L. Chan	"	Experiment	
B. L. Gary	Jet Propulsion Laboratory	Observational Results of Microwave	20
	Pasadena, CA	Temperature Profile Measurements	
		From the Airborne Antarctic	
		Ozone Experiment	
R. L. Jones	Meteorological Office	Photochemical Trajectory Modeling	20
D. S. McKenna	UNITED KINGDOM		
J. Austin	"		

SESSION VI - In-Situ Measurements of Chemical Species and Their Interpretation - B
Presiding, M. McIntyre, University of Cambridge
Wednesday Afternoon, May 11, 1988

Author(s)	Affiliation	Title of Abstract	Time
A. F. Tuck K. K. Kelly D. W. Fahey M. H. Proffitt D. M. Murphy R. L. Jones D. S. McKenna L. E. Heidt G. V. Ferry M. Loewenstein J. R. Podolske K. R. Chan	NOAA/Aeronomy Laboratory Boulder, CO NOAA/Aeronomy Laboratory CIRES, Boulder, CO " Meteorological Office UNITED KINGDOM Nat'l Center for Atmos. Res. Boulder, CO NASA/Ames Research Center Moffett Field, CA " "	Synoptic and Chemical Evolution of the Antarctic Vortex in Winter and Spring, 1987	30
K. K. Kelly A. F. Tuck D. W. Fahey M. H. Proffitt R. L. Jones D. S. McKenna L. E. Heidt G. V. Ferry M. Loewenstein J. R. Podolske K. R. Chan	NOAA/Aeronomy Laboratory Boulder, CO NOAA/Aeronomy Laboratory CIRES, Boulder, CO Meteorological Office UNITED KINGDOM Nat'l Center for Atmos. Res. Boulder, CO NASA/Ames Research Center Moffett Field, CA " "	Dehydration in the Lower Antarctic Stratosphere in Late Winter and Spring	30
M. H. Proffitt J. A. Powell A. F. Tuck D. W. Fahey K. K. Kelly M. Loewenstein J. R. Podolske K. R. Chan	NOAA/Aeronomy Laboratory CIRES, Boulder, CO NOAA/Aeronomy Laboratory Boulder, CO " NASA/Ames Research Center Moffett Field, CA "	Temporal Trends and Transport within and around the Antarctic Polar Vortex during the Formation of the 1987 Antarctic Ozone Hole	15
D. M. Murphy A. F. Tuck K. K. Kelly M. Loewenstein J. R. Podolske S. E. Strahan K. R. Chan	NOAA/Aeronomy Laboratory CIRES, Boulder, CO NOAA/Aeronomy Laboratory Boulder, CO NASA/Ames Research Center Moffett Field, CA " "	Small Scale Structure and Mixing at the Edge of the Antarctic Vortex	15

SESSION VI - In-Situ Measurements of Chemical Species and Their Interpretation - B
Wednesday Afternoon, May 11, 1988

Author(s)	Affiliation	Title of Abstract	Time
D. Hartmann	University of Washington Seattle, WA	Transport into the South Polar Vortex during Early Spring	30
L. Heidt	Nat'l Center for Atmos. Res. Boulder, CO		
M. Lowenstein	NASA/Ames Research Center		
J. Podolske	Moffett Field, CA		
W. Starr	"		
J. Vedder	"		
R. Chan	"		
J. Podolske	"		
B. Gary	Jet Propulsion Laboratory Pasadena, CA		
M. Schoeberl	NASA/Goddard Space Flight Center Greenbelt, MD		
M. R. Schoeberl	NASA/Goddard Space Flight Center Greenbelt, MD	The Evolution of AAOE Observed Constituents with the Polar Vortex	20
P. A. Newman	Applied Research Corporation		
R. Martin	Landover, MD		
L. Lait	NASA/Goddard Space Flight Center Greenbelt, MD		
M. Loewenstein	NASA/Ames Research Center		
J. Podolske	Moffett Field, CA		
J. Anderson	Harvard University Cambridge, MA		
J. M. Rodriquez	Atmos. and Environ. Res. Inc.	Photochemical Modeling of the Antarctic Stratosphere: Observational Constraints from the Airborne Antarctic Ozone Experiment and Implications for Ozone Behavior	20
N. D. Sze	Cambridge, MA		
M. K. W. Ko	"		
J. G. Anderson	Harvard University Cambridge, MA		
E. Browell	NASA/Langley Research Center Hampton, VA		
R. Chan	NASA/Ames Research Center Moffett Field, CA		
M. Coffey	Nat'l Center for Atmos. Res.		
W. Mankin	Boulder, CO		
D. Fahey	NOAA Boulder, CO		
C. B. Farmer	Jet Propulsion Laboratory Pasadena, CA		
L. Heidt	Nat'l Center for Atmos. Res.		
J. Vedder	Boulder, CO		
P. McCormick	NASA/Langley Research Center Hampton, VA		
A. Wahner	NOAA		
R. Jakoubek	Boulder, CO		

SESSION VII - Arctic Measurements
Presiding, I. Isaksen, University of Oslo
Thursday Morning, May 12, 1988

Author(s)	Affiliation	Title of Abstract	Time
R. S. Stolarski A. J. Krueger	NASA/Goddard Space Flight Center Greenbelt, MD	Variations of Total Ozone in the North Polar Region as Seen by TOMS	20
N. Harris F. S. Rowland R. Bojkov P. Bloomfield	University of California Irvine, CA Atmospheric Environ. Services CANADA North Carolina State University	Winter time Losses of Ozone in High Northern Latitudes	20
U. Schmidt R. Bauer G. Kulessa E. Klein B. Schubert	Institut fur Atmospharische Chemie FEDERAL REPUBLIC OF GERMANY " " "	Observations of Stratospheric Source Gas Profiles During the Arctic Winter	15
F. Arnold O. Mohler K. Pfeilsticker H. Ziereis G. Knop	Max-Planck-Institut fur Kernphysik FEDERAL REPUBLIC OF GERMANY " " " "	Rocket- and Aircraft-Borne Trace Gas Measurements in the Winter Polar Stratosphere including Stratospheric Nitric Acid Vapor Measurement in the Cold North Polar Vortex - Implications for HNO3/H2O-Nucleation and Polar Ozone Detection	20
W. H. Brune D. W. Toohey J. G. Anderson E. F. Danielsen W. Starr	Harvard University Cambridge, MA " NASA/Ames Research Center Mountain View, CA	*In Situ* Observations of ClO in the Wintertime Northern Hemisphere: ER-2 Aircraft Results From 21N to 61N Latitude	15
G. H. Mount R. W. Sanders R. O. Jakoubek A. L. Schmeltekopf S. Solomon	NOAA Boulder, CO University of Colorado Boulder, CO " NOAA Boulder, CO "	Visible and Near-Ultraviolet Spectrosopy at Thule AFB (76.5N) From January 28 - February 15, 1988	15
J. P. Pommereau	CNRS, 91371 - Verrieres le Buisson FRANCE	Ozone and Nitrogen Dioxide Ground Based Monitoring by Zenith Sky Visible Spectrometry in Arctic and Antarctic	15
W. F. J. Evans J. B. Kerr H. Fast	Atmospheric Environment Service Ontario, CANADA "	Canoze Measurements of the Arctic Ozone Hole	15

SESSION VIII - Dynamical Simulations
Presiding, J. Pyle, University of Cambridge
Thursday Afternoon, May 12, 1988

Author(s)	Affiliation	Title of Abstract	Time
L. Lait P. A. Newman M. Schoeberl R. Stolarski	NASA/Goddard Space Flight Center Greenbelt, MD Applied Research Corporation Landover, MD NASA/Goddard Space Flight Center Greenbelt, MD	The QBO and Interannual Variations in Total Ozone	20
M. K. W. Ko D. Weisenstein J. M. Rodriquez N. D. Sze	Atmos. and Environ. Res. Inc. Cambridge, MA " "	Antarctic Ozone Decrease: Possible Impact on the Seasonal and Latitudinal Distribution of Total Ozone as Simulated by a 2-D Model	15
M. J. Prather M. M. Garcia	GISS New York, NY Columbia University New York, NY	Global Impact of the Antarctic Ozone Hole: Simulations with a 3-D Chemical Transport Model	15
D. S. McKenna R. L. Jones J. Austin	Meteorological Office UNITED KINGDOM "	Diagnostic Studies of the 1987 Antarctic Spring Vortex: Studies Relating to the Air-borne Antarctic Ozone Experiment (1987) Employing the UK Meteorological Office Global Analysis	20
M. McIntyre	Dept. of Applied Math. and Theor. Phys., UNITED KINGDOM	Polar Vortex Dynamics	20
B. A. Boville J. T. Kiehl B. P. Briegleb	National Center for Atmos. Res. Boulder, CO "	Evolution of the Antarctic Polar Vortex in Spring: Response of a GCM to a Prescribed Antarctic Ozone Hole	20
H. Yang K. K. Tung E. Olaguar	Clarkson University Potsdam, NY "	Theoretical Study of Polar and Global Ozone Changes Using a Coupled Radiative-Dynamical 2-D Model	20
M. A. Geller M.-F. Wu E. R. Nash	NASA/Goddard Space Flight Center Greenbelt, MD Applied Research Corporation Landover, MD	Comparison of the Poleward Transport of Ozone in the Northern and Southern Hemispheres	20

SESSION IX - Chemistry and Chemical Modeling
Presiding, M. Kurylo, National Bureau of Standards
Friday Morning, May 13, 1988

Author(s)	Affiliation	Title of Abstract	Time
M. J. Molina T.-L. Tso F. C. Y. Wang	Jet Propulsion Laboratory Pasadena, CA "	Chemistry of Chlorinated Species in the Antarctic Stratosphere	10

Author(s)	Affiliation	Title of Abstract	Time
R. R. Friedl S. P. Sander	Jet Propulsion Laboratory Pasadena, CA	Studies of ClO and BrO Reactions Important in the Polar Stratosphere: Kinetics and Mechanisms of the ClO + BrO and ClO + ClO Reactions	10
R. A. Cox G. D. Hayman	Engineering Sciences Division UNITED KINGDOM	Stability and Photochemistry of ClO Dimers Formed at Low Temperature in the Gas Phase	10
J. B. Burkholder J. J. Orlando P. D. Hammer C. J. Howard A. Goldman	NOAA/Aeronomy Laboratory Boulder, CO " " University of Denver Denver, CO	Measurements of the ClO Radical Vibrational Band Intensity and the ClO + ClO + M Reaction Product	10
W. B. DeMore E. T. Roux	Jet Propulsion Laboratory Pasadena, CA University of Calgary CANADA	Chemistry of the ClO Dimer at Low Temperatures	10
M. Chipperfield J. A. Pyle	University of Cambridge UNITED KINGDOM	Modelling the Antarctic Lower Stratosphere	20
R. J. Salawitch S. C. Wofsy M. B. McElroy	Harvard University Cambridge, MA "	The Chemistry of Antarctic Ozone 1960-1987	20
P. J. Crutzen C. Bruhl	Max-Planck Inst. for Atmos. Chemie FEDERAL REPUBLIC OF GERMANY "	Modelling the "Antarctic Ozone Hole"	20
F. S. Rowland D. R. Blake	University of California Irvine, CA	Stratospheric Feedback from Continued Increase in Tropospheric Methane	10

Polar Ozone Workshop Agenda

POSTER PRESENTATIONS

SESSION I - Observations of Ozone and Temperature

 # 8

P.K. Bhartia, A. J. Krueger, S. Taylor, C. Wellemeyer
Science Applications Research (NASA/Goddard Space Flight Center), Greenbelt, MD
"Estimation of Errors in the TOMS Total Ozone Measurement during the Antarctica Ozone Compaign of August/September 1987"

 # 3

M. E. Gelman, P. A. Newman
Climate Analysis Center, NMC, NOAA, Washington, DC
"NMC Stratospheric Analyses during the 1987 Antarctic Expedition"

 # 15

J. W. Harder
Cooperative Institute for Research in Environmental Sciences, University of Colorado/NOAA, Boulder, CO
"The UW Ozonesonde: Characteristics and Flow Rate Calibration"

 # 7

D. F. Heath
NASA/Goddard Space Flight Center, Greenbelt, MD
"Seasonal and Temporal Changes in the Vertical Profile of Polar Stratospheric Ozone: 1978-1986"

 # 14

D. J. Hofmann, J. M .Rosen, J. Hereford, J. Carpenter, J. Harder
Department of Physics and Astronomy, University of Wyoming, Laramie, WY
"Ozone Profile Measurements at McMurdo Station Antarctica during the Spring of 1987"

 # 6

G. M. Keating, W. E. Bressette, C. Chen, M. C. Pitts, J. Craven
Atmospheric Sciences Division, NASA/Langley Research Center, Hampton, VA
"Dynamics Explorer I Spin-Scan Ozone Images of the "Antarctic Ozone Hole"

 # 5

G. M. Keating
"Short-term Changes in Antarctic Ozone Hole Measured by Nimbus-7 TOMS"

 # 2

P. Newman
Applied Research Corporation, Landover, MD (NASA Goddard Space Flight Center), Greenbelt, MD
L. R. Lait and M. R. Schoeberl
NASA Goddard Space Flight Center, Greenbelt, MD
"The Morphology and Meteorology of Southern Hemisphere Spring Total Ozone Mini Holes"

 # 4
C. R. Stearns
Department of Meteorology, University of Wisconsin, Madison, WI
"GHOST Balloons Around Antarctica" and "Antarctic Automatic Weather Stations: 1988"

 # 12
A. L. Torres, G. Brothers
NASA GSFC/Wallops Flight Facility, Wallops Island, VA
"Ozone Profiles above Palmer Station, Antarctica"

#11
W. D. Komhyr, R. D. Grass, P. J. Reitelbach, P. R. Franchois, M. C. Fanning, S. E. Kuester
"Total Ozone, Ozone Vertical Distributions, and Stratospheric Temperatures at South Pole, Antarctica in 1986 and 1987"

 # 13
S. E. Strahan, M. Loewenstein, J. R. Podolske, W. L. Starr, M. H. Proffitt, K. K. Kelly, K. R. Chan
"Correlation of N2O and Ozone in the Southern Polar Vortex During the 1987 AAOE"

SESSION II - Polar Stratospheric Clouds - A

#38
S. A. Kinne, O. B. Toon, G. G. Toon, C. B. Farmer, E. V. Browell
NASA/Ames Research Center, Moffett Field, CA
"PSC Measurements with the MARK IV Interferometer"

#83
G. Visconti, G. Pitari
Dipartimento di Fisica, Universita degli Studi-L'Aquila, L'Aquila, ITALY
"Formation of Polar Stratospheric Clouds Simulated in a Two Dimensional Model of the Atmosphere (Progress Report)"

#40
M. Pat McCormick, L. Poole, V. Trepte
"PSC's in the Arctic"

 # 37
M. Tolbert, M .Rossi, D. M. Golden
"Heterogeneous Interactions of $ClONO_2$, HCl, & HNO_3 on Sulfuric Acid Surfaces at Stratospheric Temperatures"

 # 88
J. Goodman, O.B. Toon, R.F. Pueschel, K.G. Snetsinger, S. Verma
"Antarctic Stratospheric Ice Crystals:09

SESSION III - Polar Stratospheric Clouds - B

#43
B. M. Morley
SRI International, Menlo Park, CA
"Lidar Observations of Polar Stratospheric Clouds at McMurdo, Antarctica, during NOZE-2"

#42
J. C. Wilson, M. Loewenstein, S. D. Smith, S. Scott, J. M. Piasecki, G. V. Ferry
University of Denver, Department of Engineering, Denver, CO
"CN Observations in AAOE: Implications for Air Motions, Cloud Processes and Particle Formation"

#41

J. Van Doren, L. Watson, J. Gardner, J. Jayne, P. Davidovits, D. Worsnop, M. Zahniser, C. Kolb
"Mass Accomodation Coefficients on Droplets Aqueous H2SO4, H2O, Ice"

#44

P Solomon, J. Barrett, P. Jaramille, R. de Zafra, A. Parrish, L. Emmons
"Daytime Altitude Profiles of ClO over McMurdo in September 1987 and the Mechanism for Ozone Depletion"

SESSION IV - Remote Sensing of Trace Gases

#61

A. Wahner, R. O. Jakoubek, A. R. Ravishankara, G. H. Mount
"Remote Sensing Observations of NO2 Column and Night Time OClO Column During the Antarctic Ozone Experiment, 1987"

#39

C. B. Farmer, P. W. Schaper, G. C. Toon, J. F. Blavier, G. Mohler, D. C. Peterson
Jet Propulsion Laboratory, Pasadena, CA
"An FTIR Spectrometer for Remote Measurements of Atmospheric Composition"

#60

M. T. Coffey, W. F. Mankin
National Center for Atmospheric Research, Boulder, CO
"Temporal and Spatial Distributions of Stratospheric Trace Gases Over Antarctica in August and September, 1987"

#55

W. L. Starr, J. F. Vedder
NASA/Ames Research Center, Moffett Field, CA
"Measurements of Ozone in the Antarctic Region during August and September of 1987"

#62

R. W. Sanders, S. Solomon
"Ground-based Measurements of O3, NO2, OClO and BrO During the 1987 Antarctic Ozone Depletion Event"

SESSION V - In-Situ Measurements of Chemical Species and Their Interpretation - A

#19

K. R. Chan, S. G. Scott, T. P. Bui, S. W. Bowen, J. Day
NASA/Ames Research Center, Moffett Field, CA
"Temperature and Horizontal Wind Measurements on the ER-2 Aircraft during the 1987 Airborne Antarctic Ozone Experiment"

54

L. E. Heidt, J. F. Vedder, W. H. Pollock, B. E. Nenny, R. A. Lueb
NCAR, Boulder, CO
"Trace Gas Measurements From Whole Air Samples Collected Over the Antarctic Continent"

31

S. G. Scott, T. P. Bui, K. R. Chan, S. W. Bowen
NASA/Ames Research Center, Moffett Field, CA
"The Meteorological Measurement System on the NASA ER-2 Aircraft"

 # 78
A. F. Tuck, R. T. Watson, E. P. Condon, J. J. Margitan
NOAA/Aeronomy Laboratory, Boulder, CO
"The Planning and Execution of ER-2 and DC-8 Aircraft Flights Over Antarctica, August and September, 1987

#51
J. Anderson, W. H. Brune, W. Starr, M. Loewenstein, J.R. Podolske, K.R. Chan, M.H. Proffitt
"In-situ observations of ClO and BrO in the Antarctic Polar Vortex"

SESSION VI - In-Situ Measurements of Chemical Species and Their Interpretation - B

 # 81
Y. Iwasaka
"Effect of Aerosol Particle Motion on Ozone Hole Chemistry"

 # 79
D. M. Murphy,A. F. Tuck, Klaus Kunzi, M. Low, J. R. Podolske, S. Strahan, K. R. Chan
"Small Scale Structure and Mixing at the Edge of the Antarctic Vortex"

SESSION VII - Arctic Measurements

 # 65
J. B. Kerr
W. F. J. Evans, Atomspheric Environment Service, Downsview, Ontario, CANADA
"Brewer Spectrophotometer Measurements in the Canadian Arctic"

 # 86
S. H. H. Larsen
Department of Physics, University of Oslo, Oslo, NORWAY
"Ozone Measurements During Wintertime, in the Arctic, Made in the Years 1950-1958, are re-evaluated. Comparison with Recent Measurements at the Same Places are Made"

 # 63
S. J. Oltmans, P. J. Sheridan, R. Schnell, J. W. Winchester, L. Barrie, J. D. Kahl
Geophysical Monitoring for Climatic Change, Air Resources Laboratory, NOAA/ERL, Boulder, CO
"Springtime Surface Ozone Fluctuations at High Arctic Latitudes and Their Possible Relationship to Atmospheric Bromine"

 # 64
R. C. Schnell, P. J. Sheridan, R. E. Peterson, S. J. Oltmans
CIRES, University of Colorado, Boulder, CO
"Airborne Measurements of Tropospheric Ozone Destruction and Particulate Bromide Formation in the Arctic"

 # 66
W. J. Brune, D. W. Toohey, J. Anderson, E. Danielsen, W. Stan
"In situ Observations of ClO in the Wintertime Northern Hemisphere: ER-2 Aircraft Results from 21N to 61N Latitude"

 # 68
R. S. Stolarski, A. J. Krueger
"Variations of Total Ozone in the North Polar Region as Seen by TOMS"

 # 69
J. Pommereau, F. Goutail
"Ozone and Nitrogen Dioxide Ground Based Monitoring by Zenith Sky Visible Absorption in Arctic and Antarctic"

 # 52
U. Schmidt, R. Bauer, G. Kulessa, E. Klein, B. Schubert
"Observations of Stratospheric Source Gas Profiles During the Arctic Winter"

SESSION VIII - Dynamical Simulations

#30
M. Prather
"Global Imapct of the Antarctic Ozone Hole: Simulations with a 3-D Chemical Transport Model"

 # 67
H. Akiyoshi
Department of Physics, Faculty of Science, Kyushu University, Fukuoka 812, JAPAN
"Radiative Aspects of Antarctic Ozone Hole in 1985"

 # 17
D. G. Dritschel
University of Cambridge, DAMTP, Cambridge, UNITED KINGDOM
"On the Origin of Steep Edges and Filaments in Vorticity and Potential Vorticity Fields"

 # 18
P. H. Haynes
University of Cambridge, DAMTP, Cambridge, UNITED KINGDOM
"High Resolution Dynamical Modelling of the Polar Vortex"

 # 21
Y. Yung, R. L. Shia, M. Allen, R. W. Zurek, D. Crisp, J. S. Wen
California Institute of Technology, Pasadena, CA
"Simulation of the Transport of Halogen Species from the Equatorial and Mid-Latitude Stratosphere to the Polar Stratosphere in a Two-Dimensional Model"

 # 20
L. J. Gray, J. A. Pyle
"A 2D Model of the Ozone QBO"

 # 76
S. Salstein, R. Rosen, A. J. Miller
"Use of Operational Analyses to Study the Dynamics of Troposphere-Stratosphere Interactions in Polar Regions.

SESSION IX - Chemistry and Chemical Modeling

 # 87
V. Lang, S. Sander, R. Friedl
Jet Propulsion Laboratory, Pasadena, CA
"High Resolution FTIR Spectroscopy of the ClO Radical" AND " Infrared Band Strength of the ClO Radical"

 # 90
B. Gary
"Mountain Wave Observations Over Antarctica"

 # 92
M. Pat McCormick, J. Larsen
"Springtime Observations of O3, H2O, and Aerosol Extinction by SAGE II"

 # 88
J. Goodman, O. B. Toon, R. F. Pueschel, K. G. Snetsinger, S. Verma
"Antarctic Stratospheric Ice Crystals"

SESSION I - Observations of Ozone and Temperature
Presiding, J. Anderson, Harvard University
Monday Morning, May 9 - 9:00 AM

TOTAL OZONE BY LUNAR DOBSON OBSERVATION AT SYOWA, ANTARCTICA

Shigeru Chubachi,

Meteorological Research Institute
1-1 Nagamine Tsukuba Ibaraki 305 Japan

Ryoichi Kajiwara and Kouji Kondoh

Aerological Observatory
1-2 Nagamine Tsukuba Ibaraki 305 Japan

Introduction The lunar Dobson observation is almost the only one way to get the total ozone in or around the polar night season at high latitudes where the total ozone observation by solar Dobson is not available. The total ozone observations by lunar Dobson were carried out at Syowa Station (69°S, 40°E), Antarctica in 1969, and 1982 - 1986, in the months from March to October. In this paper, we describe the method, the accuracy and the results of the lunar Dobson observation carried out at Syowa Station from 1982 to 1986.

1. Instrument. The Dobson instrument used for lunar Dobson observation at Syowa Station was Beck 122, but has been Beck 119 after February 1986. These Dobson instruments are the same with that used in the ordinary solar Dobson observation. The intensity of the moonlight is not so strong that a sun director for lunar Dobson is equipped with a quartz lens (f=45cm) to condense the moonlight. The position of the lens is set to get the maximum output in the "A" pair wavelengths. No microscope is used, however we are able to see the focused image of the moon on the input slit of the Dobson instrument.

2. Method. The total ozone measurement by lunar Dobson observation is carried out with the moon light in clear sky at night. It is possible even if thin cloud covers the moon. We need the clear image of the moon on the input slit. The observation should be carried out near the culmination of the moon. "A" and "D" wavelengths are used. The value of the extraterrestrial constant for lunar Dobson observation is the same value as that for the sun. To observe total ozone by lunar Dobson observation, five measurements with "A" and "D" pair wavelengths are carried out. The calculation of the total ozone from the data of the Dobson is made according to the WMO manual. The horizontal parallax is taken into consideration.

3. Night representative. Since the accuracy of the lunar Dobson when the height angle of the moon is not established. We call the total ozone amounts when the height angle of the moon is highest "Night representative" value. This value should be the representative in the night 12 hour before and after the culmination of the moon.

4. Accuracy. The results of the comparison of the night representative of lunar Dobson observation with the daily representative of solar Dobson is shown in Figure 1. This shows that the total ozone at night by lunar Dobson observation is about 18 matm-cm greater than that in the daytime by solar Dobson. It is necessary to check that this bias is common or not among other instruments and other station.

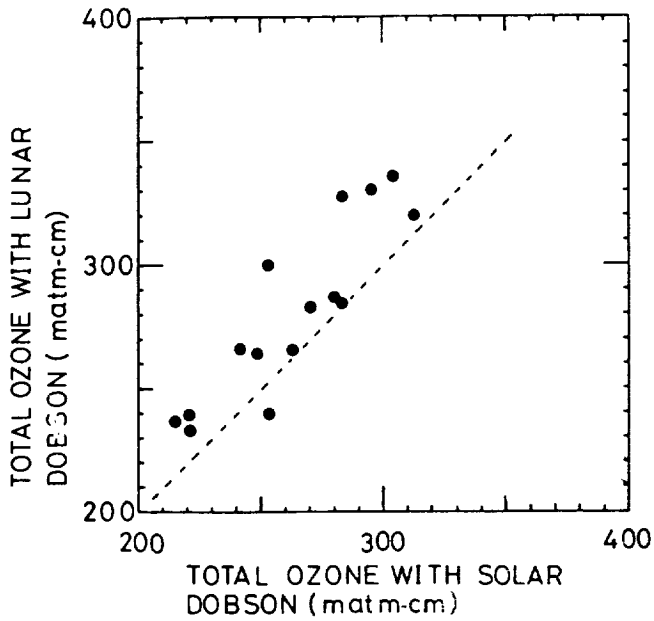

Fig.1 Comparison of the total ozone of night representative with that of the daily representative. If both daily representatives are available, The abscissa shows the mean value of the daily representative before and after the night when the lunar Dobson is carried out, else it shows the either of them. It is shown the 18 matm-cm bias in night representative by lunar Dobson.

5. Total ozone in polar night at Syowa Station. By the use of the lunar Dobson observation, we are able to get the seasonal change of the total ozone at Syowa Station including Polar night season. Figure 2 shows the 4 year mean of the daily representative total ozone at Syowa Station between February 1982 to January 1986, superimposed with the 20 year mean of the daily representative between 1961 to January 1982. It is shown that the spring time decrease starts in early or middle August. It becomes minimum in early or middle October. Then it turns to increase. it becomes maximum in early December and then decreases.

6. vertical profile of ozone decrease. Figure 3 shows the difference of the monthly means of the vertical profiles between above two periods., i.e. 1966 to January, 1982 and February 1982 to January 1986. This figure shows that the maximum decrease occurs between 150mb and 70mb in October and in November. It should be noticed that an increasing area exist at the height upper than 50 mb .

References

Ishida, K., Suzuki, T., and Sakai, S.,(1971): Syowa Kiti ni okeru 1969-nen no ozon zenryo kansoku Total ozone observation at Syowa Station, Antarctica in 1969). Nankyoku Shiryo (Antarct Rec.) 39,32-38.

Chubachi, S., Preliminary result of ozone observation at Syowa Station from February 1982 to January 1983, Mem. Natl INST. Polar Res., Spec. Issue, 34, 13-19

Komher, W. D.(1980): WMO Global Ozone Research and Monitoring Project Report No. 6 (Operation handbook ozone observations with a Dobson Spectrophotometer)

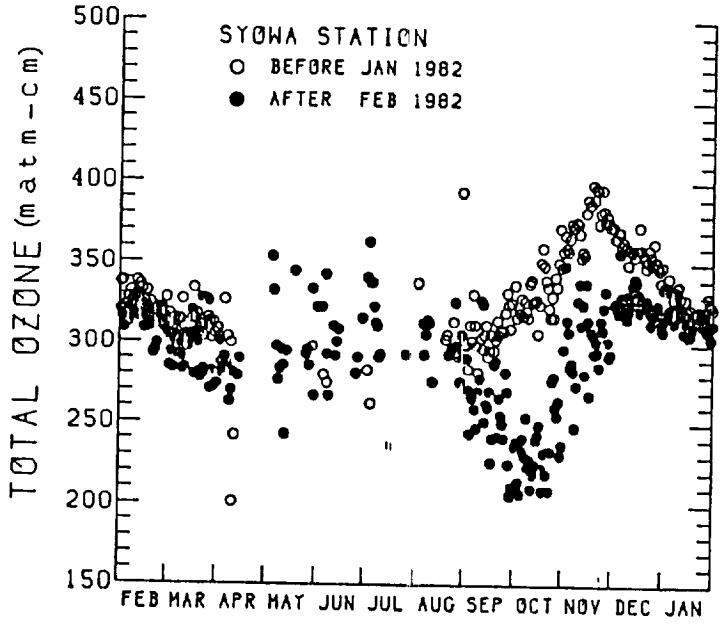

Fig.2 Closed circles shows the 4 years mean of the daily representative total ozone at Syowa Station from February 1982 to January 1986. Open circles shows the 20 years mean of the ones from 1961 to January 1982.

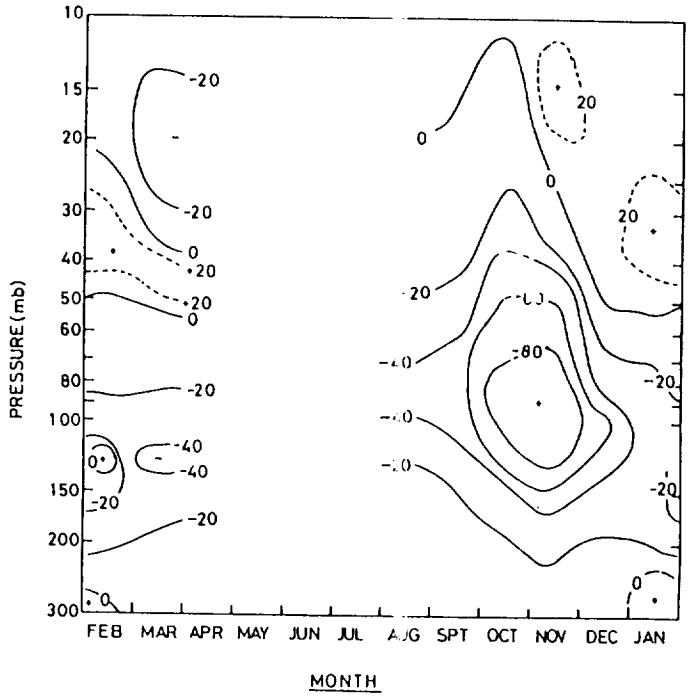

Fig.3 The difference of the monthly means of the vertical profiles of ozone partial pressure between the 1966 to January 1982 and February 1982 to January 1986.

N89-14505

Total Ozone Changes in the 1987 Antarctic Ozone Hole

Arlin J. Krueger, Mark S. Schoeberl, Scott D. Doiron,
Frank Sechrist, and Reginald Galimore

The development of the Antarctic ozone minimum was observed in 1987 with the Nimbus 7 TOMS instrument. In the first half of August the near-polar (60 and 70 deg S) ozone levels were similar to those of recent years. By September, however, the ozone at 70 and 80 deg S was clearly lower than any previous year including 1985, the prior record low year. The levels continued to decrease throughout September until October 5 when a new record low of 109 DU was established at a point near the South Pole. This value is 29 DU less than the lowest observed in 1985 and 48 DU less than the 1986 low. The zonal mean total ozone at 60 deg S remained constant throughout the time of ozone hole formation.

The ozone decline was punctuated by local minima which formed away from the polar night boundary at about 75 deg S. The first of these, on August 15-17, formed just east of the Palmer Peninsula and appears to be a mountain wave. The second major minimum formed on September 5-7 again downwind of the Palmer Peninsula. This event was larger is scale than the August minimum and initiated the decline of ozone across the polar region. Possible underestimation of ozone due to high clouds associated with the mountain wave is treated in a separate paper at this symposium.

The 1987 ozone hole was nearly circular and pole centered for its entire life. In previous years the hole was perturbed by intrusions of the circumpolar maximum into the polar regions, thus causing the hole to be elliptical. The 1987 hole also remained in place until the end of November, a few days longer than in 1985, and this persistence resulted in the latest time for recovery to normal values yet observed.

The Breakup of the Southern Hemisphere Spring Polar Ozone and Temperature Minimums from 1979 to 1987

Paul A. Newman[1] and Mark R. Schoeberl[2]

[1]Applied Research Corporation, 8201 Corporate Dr., Landover, MD 20785
[2]NASA/Goddard Space Flight Center, Greenbelt, MD 20771

I. Introduction

During the late southern hemisphere (SH) spring, the total ozone field has a broad scale polar minimum surrounded by a circumpolar maximum located at 40-60°S. During the spring polar vortex breakup or final warming, the ozone minimum increases, and is usually displaced off of the pole into the western hemisphere as the circumpolar ozone maximum intrudes onto the pole. The polar ozone minimum rapidly fills prior to the breakup.

Recently, it has been suggested that the October Antarctic ozone depletion may be influencing the timing of the polar vortex breakup (Kiehl et al., 1988). The breakup timing change would result from the reduced heating of the polar lower stratosphere because of the depleted lower stratospheric ozone mixing ratios. Since the vortex would be colder, zonal mean winds would be stronger, and these stronger zonal winds would inhibit the vertical propagation of waves into the stratosphere. The net effect is that the colder vortex is stabilized against erosion by Rossby waves, resulting in a delayed polar vortex breakup.

The purpose of this study is to quantify the observations of the polar vortex breakup. The data used in this study consist of Total Ozone Mapping Spectrometer (TOMS) data, and National Meteorological Center (NMC) analyses. The final warming is diagnosed using the difference between zonal means at 80° and 50°S for temperature, ozone, and layer mean temperature. The polar vortex breakup can also be diagnosed by the onset of weak zonal mean zonal winds (i.e. u, overbar denotes a zonal average) at 60°S.

II. Analysis

The polar vortex begins to erode in September at the high stratospheric altitudes; this is subsequently followed by irreversible erosion at lower levels later in the season as the jet descends. The final 100 mb breakup usually occurs in late-November (Farrara and Mechoso, 1986). The final warming during 1987 is illustrated in Fig. 1a using NMC $\bar{u}$ at 60°S and 100 mb (short dash), $\bar{T}(80°S)-\bar{T}(50°S)$ (hereafter referred to as the temperature difference) at 100 mb (solid), and the 80°-50°S 100-150 mb layer mean temperature difference (long dash). Weak zonal winds (i.e. winds less than 20m/s) appear on December 12, 1987, the 100 mb temperature difference reverses on December 9, 1987, and the 150-100 mb layer mean temperature difference reverses on December 6, 1987. The higher levels have breakup dates which are earlier (e.g. the 10 mb 80°-50°S temperature difference reverses on October 3, 1987). Figure 1b displays the ozone hole breakup using the zonal mean 80°-50°S total ozone difference (solid) and the the polar map minimum total ozone values (dashed). The rapid breakup in late-November is accompanied by an increase of total ozone values in the polar minimum. Other years show similar evolution with time.

The breakup dates of the polar ozone minimum for all years 1979-1987 are shown in Fig. 2 using the 80°-50°S zonal mean total ozone differences (solid),

100 mb temperature difference (long dash), and 100 mb zonal mean wind (short dash). The figure shows a general trend toward later final warmings. However, the earliest 100 mb warming took place in 1986. Note also the excellent correlation between the 100 mb temperature and the total ozone differences. Comparisons at other stratospheric levels are inconclusive because of the large interannual variance of the breakdown date and the fact that total ozone reflects lower stratospheric processes.

Finally, Fig. 3 shows a plot of the breakdown date (from the 100 mb temperature difference) versus the total ozone October map minimum value. Generally, the figure reveals reduced ozone in October is associated with a later breakdown date. Although this trend is significant at the 95% confidence interval, at higher altitudes, the trend is not significant at the 95% C.I.

Individual plots of TOMS total ozone data for late November (not shown here) indicate that the ozone minimum is remaining intact for a longer period in the later years of the TOMS data set (i.e. 1985, 1986, 1987) than the earlier years (i.e. 1979, 1980, 1981, and 1982).

III. Summary and Conclusions

Computations of the polar vortex breakdown date using NMC meteorological data and TOMS total ozone data indicate that the breakdown is occurring later in the spring in the lowest portion of the stratosphere. At altitudes above 100 mb, the large interannual variance of the breakdown date renders any trend determination of the breakdown date difficult. Individual plots of TOMS total ozone indicate that the total ozone minimum remains intact for a longer period of time than is observed in earlier years.

References

Farrara, John D., and Carlos R. Mechoso, An Observational Study of the Final Warming and Polar Vortex Disappearance During the Southern Hemisphere Spring, Geophys. Res. Lett., 13, 1232-1235, 1986

Kiehl, J.T., Byron A. Boville, and Bruce P. Briegleb, Response of a General Circulation Model to a Prescribed Antarctic Ozone Hole, submitted to Nature, 1988.

Figure Captions

Figure 1. Spring 1987 line plots of: a) NMC 80°-50°S 100 mb temperature difference (solid), NMC 80°-50°S zonal mean 100-150 mb layer mean temperature difference (long dash), and zonal mean zonal wind at 60°S (short dash); and b) TOMS total ozone 80°-50°S difference (solid), and TOMS total ozone map minimums (short dash).

Figure 2. Polar vortex breakup dates (Julian day) versus year as diagnosed from: a) 100 mb 80°-50° temperature differences (long dash), b) total ozone 80°-50°S zonal mean difference (solid), and 100 mb zonal winds (short dash).

Figure 3. Breakdown date from the 80°-50°S 100mb temperature gradient plotted against the TOMS October average map minimum.

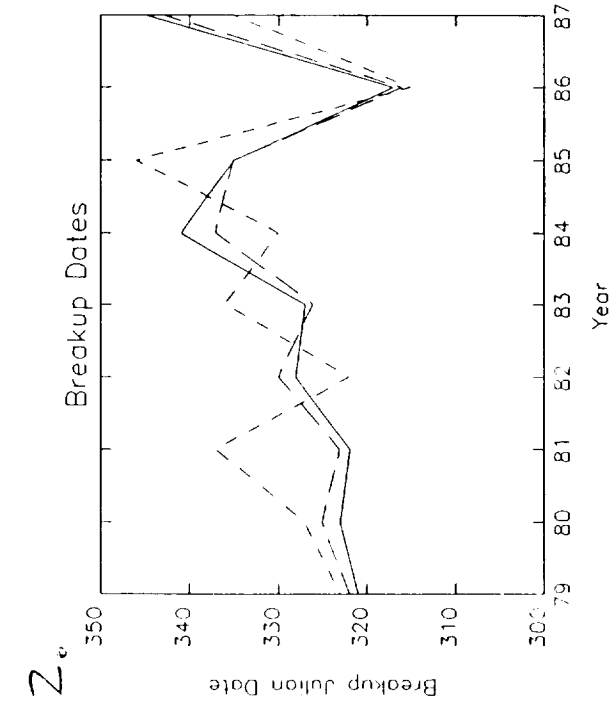

2e.

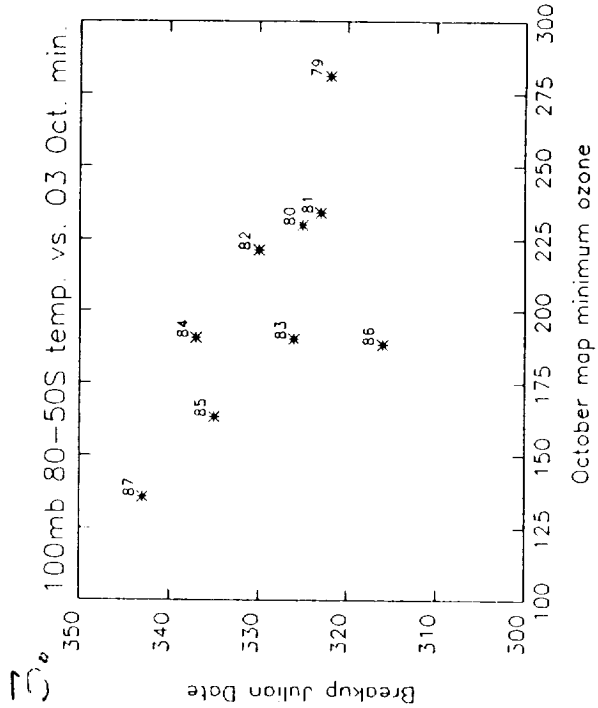

5e.

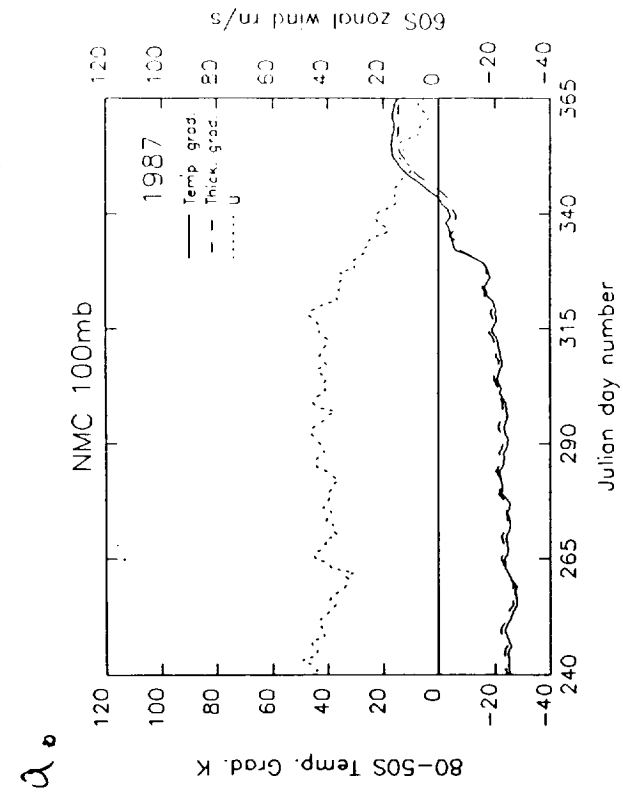

1a.

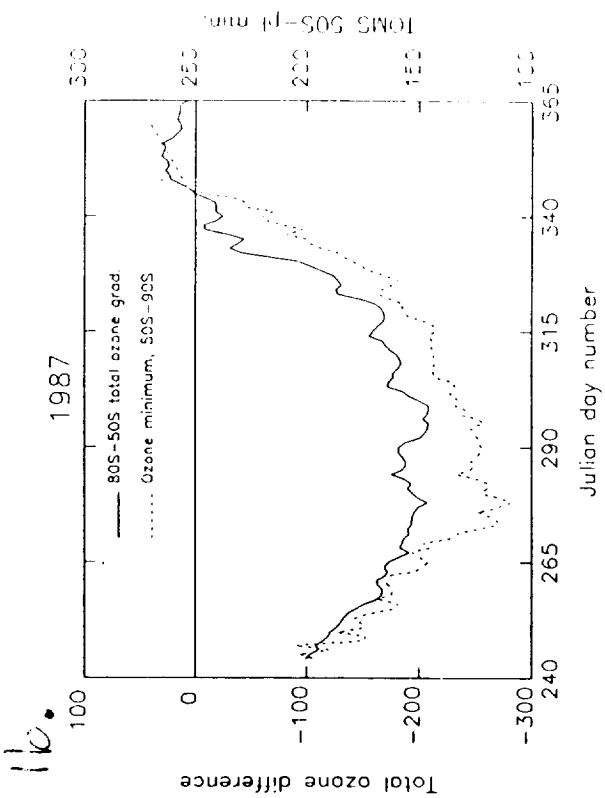

1k.

N89-14507

OBSERVATIONS OF STRATOSPHERIC TEMPERATURE CHANGES COINCIDENT WITH THE RECENT ANTARCTIC OZONE DEPLETIONS

William J. Randel

National Center for Atmospheric Research
Boulder, CO 80307

Paul Newman

Applied Research Corporation
Landover, MD 20785

1. INTRODUCTION

A high degree of correlation between the recent decline in Antarctic total ozone and cooling of the stratosphere during Austral spring has been noted in several recent studies (e.g., Sekiguchi, 1986; Angel, 1986). This study analyzes the observed temperature trends in detail, focusing on the spatial and temporal aspects of the observed cooling. Ozone losses and stratospheric cooling can be correlated for several reasons: 1) ozone losses (from an unspecified cause) will directly reduce temperatures due to decreased solar ultraviolet absorbtion (Shine, 1986), and/or 2) changes in both ozone and temperature structure due to modification of stratospheric circulation patterns (Mahlman and Fels, 1986). In order to scrutinize various ozone depletion scenarios, detailed information on the observed temperature changes is necessary; our goal is to provide such data.

The data used here are National Meteorological Center (NMC) Climate Analysis Center (CAC) derived temperatures, covering 1000–1 mb (0–48 km), for the period 1979–1987. Discussions on data origin and quality (assessed by extensive comparisions with radiosonde observations), along with other details of these observations, can be found in Newman and Randel (1988).

2. OBSERVED TEMPERATURE TRENDS

Figure 1 shows October average values of total ozone and 70 mb (~19 km) temperature at the South Pole for 1979–1987 (the total ozone data is from Total Ozone Mapping Spectrometer (TOMS) observations, as discussed in Schoeberl et al. (1986)). Strongly correlated interannual variability is observed in both variables in Fig. 1, along with a general decline over 1979–1987. The dashed lines show linear slopes calculated over 1979–1986, and we use similar linear trend analysis as an objective method to locate regions and times of large temperature changes over this period. (We note here that linear trends over eight years of data should not be interpreted as monotonic climate variations—this is discussed below in light of longer records of observations.)

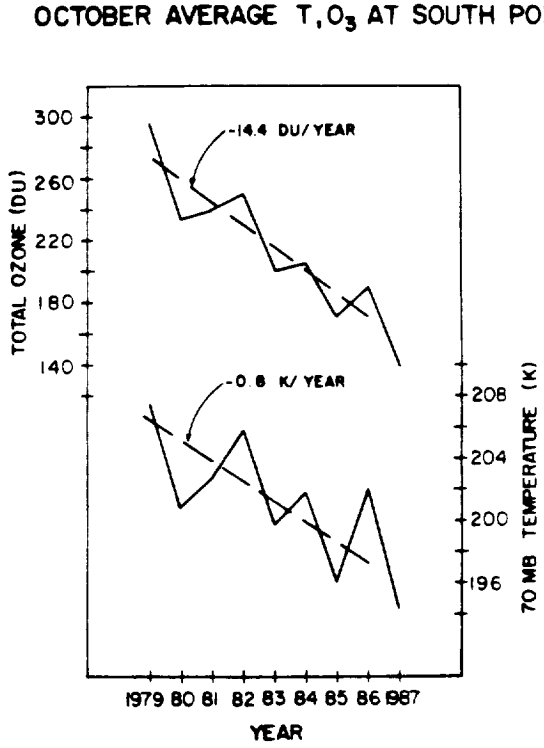

Fig. 1. October average values of total ozone (top) and 70 mb temperature (bottom) at the South Pole over 1979–1987. The linear trends of each series over 1979–1986 are indicated by dashed lines.

Figure 2 shows polar orthographic plots of 1979–1986 trends in October average total ozone (left), and 70 mb (~19 km) temperature (right); here the trends have been calculated separately at each horizontal grid point. The similarity in patterns and details between the ozone and temperature trends is intriguing; note not only the strong negative trends in both quantities centered near the east coast of Antarctica, but correlated positive trends west of South America near 50°S. These highly spatially correlated trends illustrate the coherent nature of interannual ozone-temperature variations.

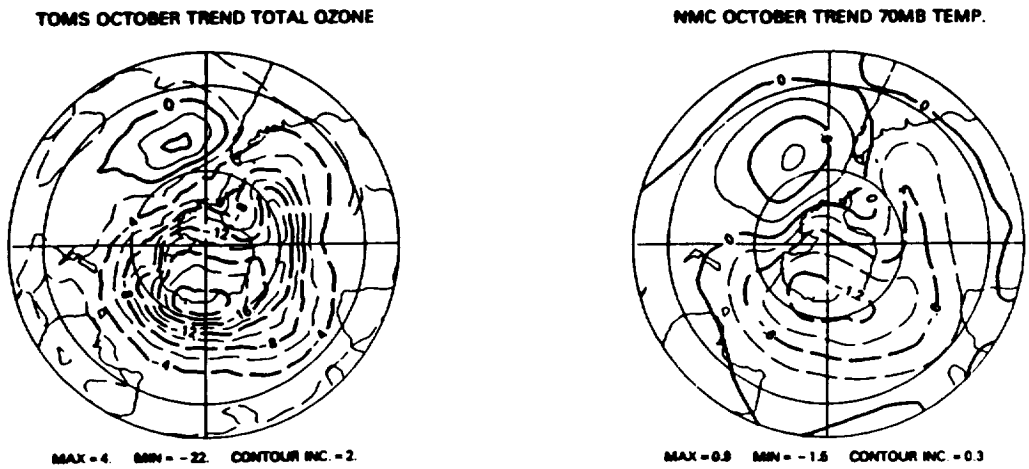

Fig. 2. Polar orthographic plots of 1979–1986 linear trends in October average total ozone (left) and 70 mb temperature (right). The outer latitude is 20° S. These diagrams are constructed by calculating the linear trend independently at each horizontal grid point. Units of DU/year and K/year, respectively.

Further spatial and temporal characteristics of the NMC derived temperature trends are illustrated in Fig. 3, which show meridional cross sections of trends in zonal mean temperature (because of interannual variability in data acquisition procedures, trends in Fig. 3 above 10 mb are not reliable, and should be viewed skeptically). Trends calculated in Fig. 3 include the 1987 data. The strongest zonal mean cooling is observed in October poleward of 40°S over 200–10 mb, and in November poleward of 60°S over 200–30 mb.

A latitude-time section of the zonal mean temperature trends at 50 mb (~21 km) is shown in Fig. 4b to highlight the temporal evolution (a low pass filter has been applied to the data in Fig. 4 to remove fluctuations with periodicities below 50 days). Also shown in Fig. 4a is the 1979–1987 mean temperature evolution at 50 mb. The trends (Fig. 4b) highlight strongest polar cooling in October and November, with a mid-latitude cooling band extending into December (note the lack of high latitude cooling beyond November), along with high latitude warming during August-September. Comparison of the trends (Fig. 4b) with the mean evolution (Fig. 4a) show that although the spring warming progresses somewhat slower during October-November (*i.e.*, the negative trends), temperatures in high latitudes following the final warming (*i.e.*, beyond November) have changed little over this period.

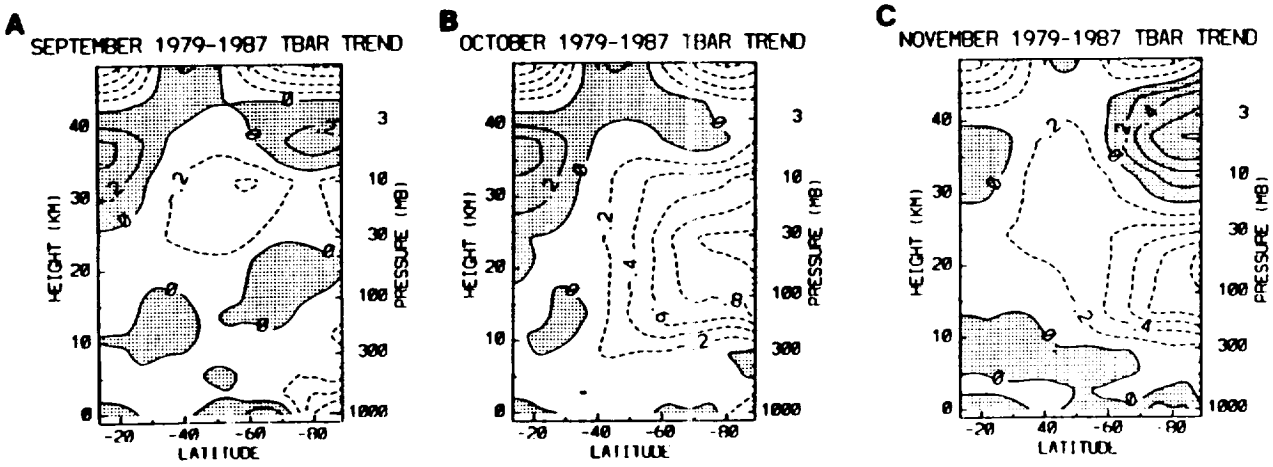

Fig. 3. Linear trends over 1979–1987 of zonal mean temperature during (a) September, (b) October, and (c) November. Units of K/year.

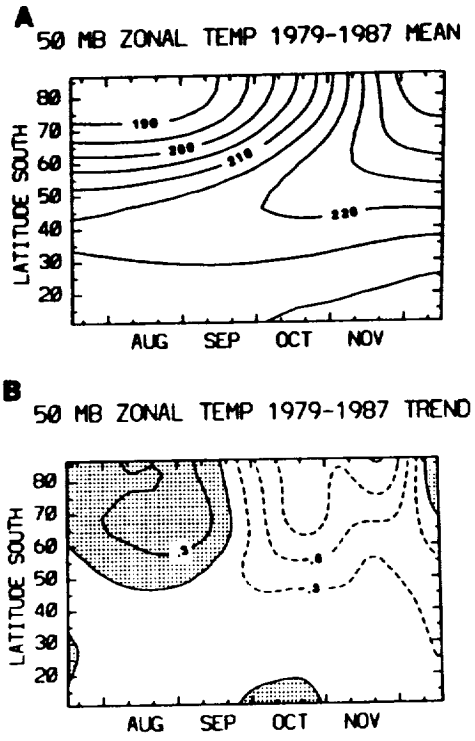

Fig. 4. Latitude-time sections at 50 mb of the (a) zonal mean temperature (K) averaged over 1979–1987, and (b) 1979–1987 linear trend in zonal mean temperature (K/year). These diagrams have been constructed using a low pass filter applied to daily data.

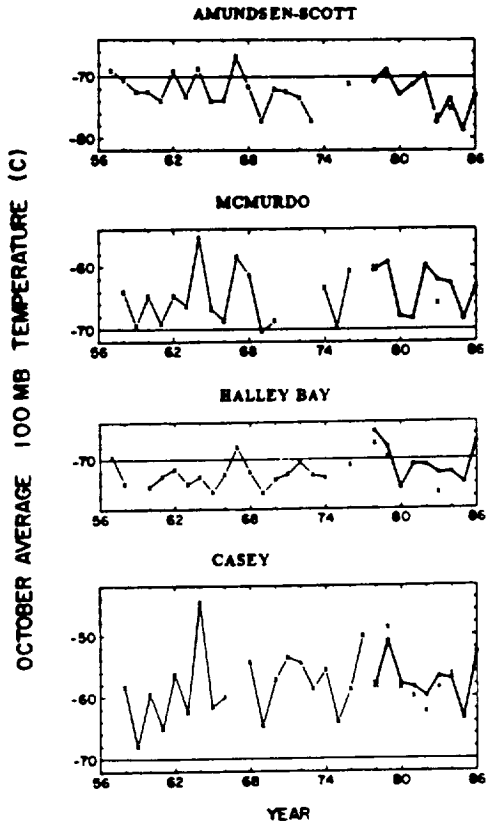

Fig. 5. Time series of October average 100 mb temperature (°C) at four selected stations around Antarctica. The ×'s and light lines denote monthly mean radiosonde observations, while the heavy lines over 1978–1986 are from the NMC analyses.

To evaluate longer term temperature fluctuations, and check on the NMC data quality, we have studied available monthly mean stratospheric radiosonde observations (RAOBS). Figure 5 shows time series of 100 mb October average temperatures at four selected Antarctic stations (these four have relatively complete RAOB records over 1957–1984—more extensive comparisons are shown in Newman and Randel, 1988). Although direct NMC RAOB comparions are restricted to 1978–1984, overall good agreement is seen between the two data sets (in particular, similar sized interannual differences). Furthermore, inspection of these longer term records shows no evidence for monotonic climatic trends, in spite of the decrease in temperatures seen over 1979–1986. These data lead to the conclusion that linear trends derived from limited time samples (such as the eight years studied here) should not be treated as representative of long term variations.

3. SUMMARY

Large decreases in October average total ozone in the Southern Hemisphere over 1979–1987 are highly spatially correlated with contemporaneous cooling of the lower and middle stratosphere. This study analyzes the spatial and temporal nature of the observed temperature changes, with the following main results:

1) Stratospheric polar cooling is strongest in October-November, extending over 200–10 mb (11–32 km) (Figs. 3 and 4b), and the patterns are highly zonally asymmetric (Fig. 2). Local temperature differences between October 1979 and October 1986 of 12K and 16°K are observed at 70 and 30 mb, respectively, coincident with a local column ozone decrease of 160 DU. Seasonal and zonal mean estimates of temperature changes result in substantial underestimates.
2) Inspection of the 1979–1987 trends in light of the longer historical record from RAOB data shows no evidence of monotonic climatic variations; the 1979–1987 temperature declines are not distinguishable from other decadal time scale fluctuations.

References

Angel, J. K., 1986: *Geophys. Res. Lett.*, **13**, 1240–1243.

Mahlman, J. D., and S. B. Fels, 1986: *Geophys. Res. Lett.*, **13**, 1316–1319.

Newman, P. A., and W. J. Randel, 1988: Submitted to *J. Geophys. Res.*

Schoeberl, M. R., A. J. Krueger, and P. A. Newman, 1986: *Geophys. Res. Lett.*, **13**, 1217–1220.

Setiguchi, Y., 1986: *Geophys. Res. Lett.*, **13**, 1202–1205.

Shine, K. P., 1986: *Geophys. Res. Lett.*, **13**, 1331–1334.

ANTARCTIC MEASUREMENTS OF OZONE, WATER VAPOR, AND AEROSOL EXTINCTION BY SAGE II IN THE SPRING OF 1987

J. C. Larsen, ST Systems Corp., Hampton, VA 23666

M. P. McCormick, NASA Langley Research Center, Hampton, VA 23665-5225

Realization that springtime ozone abundances have declined rapidly in the past decade (Farman et al., 1985; Stolarski et al., 1986) led to several intensive measurement campaigns (NOZE, 1986; NOZE II, 1987; and AAOE, 1987) with the goals of characterizing chemical and dynamical conditions in the Antarctic region to better understand the depletion phenomenon. Concurrent with these campaigns, and also in 1985, the Stratospheric Aerosol and Gas Experiment II (SAGE II) obtained simultaneous measurements of ozone, water vapor, and multiple wavelength aerosol extinction at high southern latitudes in September and October.

SAGE II uses the solar occultation technique to measure the extinction of aerosols and trace gases during spacecraft sunrise/sunset. Fifteen sunset and sunrise measurements evenly distributed over longitude along a latitude circle are obtained daily. The highest latitudes reached in September and October are approximately 66°S and 72°-73°S, respectively. Although the vortex typically remains centered on the pole during this time period, it is not entirely zonal, thus providing measurement opportunities over a wide range of meteorological conditions each day. The extent to which SAGE II penetrates the vortex each day can be estimated by comparing the 50-mb temperatures at the SAGE II measurement locations to 50-mb map temperature minimums. By October 4 in all three years, SAGE II encountered 50-mb temperatures within 1 to 2 degrees of the daily map minimum. Figure 1 displays the daily minimum total ozone profiles (which generally correspond to the daily minimum 50-mb temperature) observed by SAGE II for 10 days in October 1985, 1986, and 1987. The top frame presents the ozone profiles as concentration versus altitude, the primary SAGE II data product. In the middle frame are the same profiles expressed as ozone partial pressure versus pressure with the help of the NMC temperature data shown in the bottom frame. The loss region extends from about 13 to 22 km for 1985/1987, while for 1986 the upper boundary of the loss region is about 1 km lower. Thus, the 1986 profiles display peak ozone values some 5 to 20 nbars higher than the 1985/1987 peaks of 70 to 80 nbars at 35 mbars altitude. Minimum ozone values within the depletion region are 10 nbars on October 8, 1985/1986, and fall below 5 nbar on October 7 and 9, 1987. Despite a gradual shift northward of the extreme measurement latitudes, the 1987 ozone depletion is considerably greater than either 1985 or 1986. The October 9, 1987, profile is notable in that minimum values on 5 nbar extend over a 4-km layer. The minimum concentration for this profile, which is also the monthly minimum, dropped to less than 1.0E + 11 (molecules/cm^3) at 16 km which is considerably lower than the 1985/1986 monthly minimum attained on October 8 of 4.0E + 11 (molecules/cm^3). The daily total ozone (100-mb base) minimums in 1987 dropped 17 percent relative to 1985, the previous worst year.

In this talk we will present recent measurements of ozone, water vapor, and aerosol extinction from the spring of 1987, compare them to 1985 and 1986, and relate the observed changes to variations in meteorological conditions in the vortex for these three years. March ozone data at similar latitudes for these three years will be used to investigate coupling between the severity of the springtime depletion and early fall values. We will also investigate correlations between the measured species of water vapor, ozone, and aerosols throughout the vortex region.

REFERENCES

Farman, J. C., B. G. Gardiner, and J. D. Shanklin, 1985: Large losses of total ozone in Antarctica reveal seasonal $C\ell O_x/NO_x$ interaction, Nature, 315, 207-210.

Stolarski, R. S., A. J. Krueger, M. R. Schoeberl, R. D. McPeters, P. A. Newman, and J. C. Alpert, 1986: Nimbus 7 SBUV/TOMS measurements of the springtime Antarctic ozone hole, Nature, 322, 808-811.

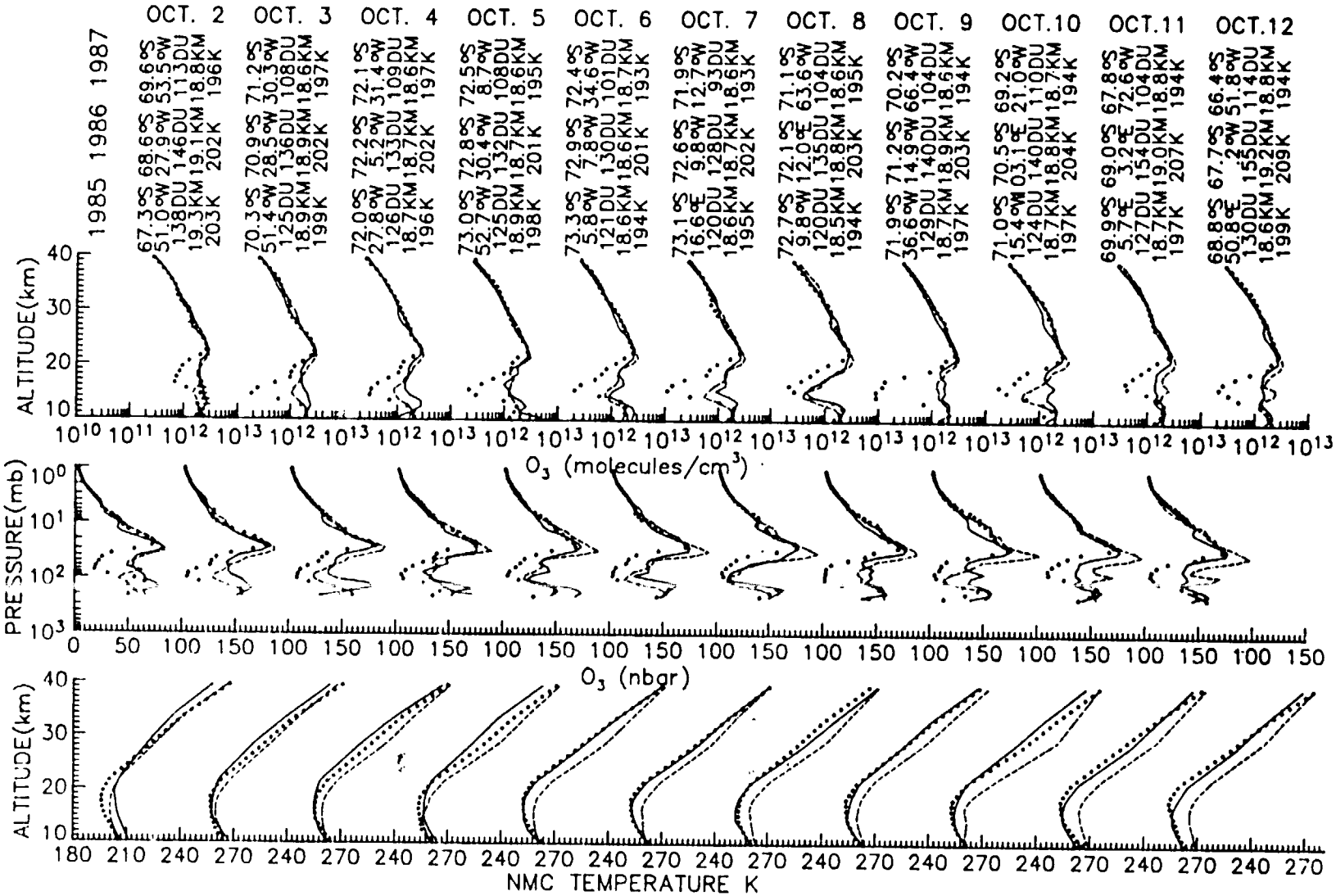

Figure 1. Daily minimum total ozone profiles measured by SAGE II for October 2 to 12, 1987 (dots), 1986 (dashed), and 1985 (solid). Top frame presents the ozone profiles as concentration versus altitude, the primary SAGE II data product. In the middle frame, the ozone profiles have been converted to partial pressure versus pressure using the NMC supplied temperature profiles shown in the bottom frame. Above each day's profiles are shown the measurement latitude and longitude, total ozone calculated with a 100-mb column base and the 50-mb geopotential height and temperature.

The Three-Dimensional Morphology of the Antarctic Ozone Hole

A. C. Aikin and R. D. McPeters

Laboratory for Atmospheres, NASA/Goddard Space Flight Center

Abstract

The three-dimensional morphology of the spring antarctic ozone distribution as determined by the Nimbus 7 SBUV instrument is presented for the period 1 to 11 October in 1986. The data show that a clearly defined minimum in ozone relative to the local ozone field extends throughout the stratosphere from the tropopause to above 50 km, though decreasing in intensity with altitude. Near 18 km ozone in the ozone hole is 50% less than the average surrounding ozone. But even at 50 km the ozone is 20% less than the surrounding ozone field. The ozone minimum in the upper stratosphere is displaced about 6 degrees toward the equator so that observations at a fixed station may provide the illusion that the ozone minimum is restricted only to low altitudes. While the ozone minimum is spatially coherent throughout the stratosphere, there are differences in the behavior of ozone at different altitudes that suggest the existence of at least three distinct altitude domains. Below 30 km ozone is characterized by classic "ozone hole" behavior. Between 33 and 43 km ozone is more stable, actually increasing during September and October. Above 43 km ozone has always decreased during September to a minimum in October, but it has suffered a long term decrease of 7-12% since 1979 similar to that seen at low altitudes.

ESTIMATION OF ERRORS IN THE TOMS TOTAL OZONE MEASUREMENT DURING THE ANTARCTICA OZONE CAMPAIGN OF AUGUST/SEPTEMBER 1987

P.K.Bhartia
Science Applications Research/
National Space Science Data Center
Goddard Space Flight Center, Code 633
Greenbelt, Md. 20771

A.J.Krueger
NASA/Goddard Space Flight Center, Code 616
Greenbelt, Md. 20771

S.Taylor and C.Wellemeyer
S T Systems Corporation
9701J Philadelphia Court
Lanham, Md. 20706

The TOMS instrument on the Nimbus-7 satellite provides the primary source of total ozone data for the study of total ozone in the polar regions of the earth. There are no comparable instruments either on the ground or on the satellites that provide the coverage, the accuracy and the spatial resolution of TOMS necessary for understanding the dynamical and chemical processes that may have triggered the formation of the ozone hole in the Antarctica region.

However, by the time of the Antarctica Ozone campaign of Aug/Sept 1987, TOMS had completed almost nine years of continuous operation in space during which there has been degradation in the instrument's performance resulting in significant calibration drifts and increased noise. In addition, the unusual atmospheric conditions prevailing in the Antarctica ozone hole, such as very low stratospheric temperatures, stratospheric clouds, and extremely low ozone amounts were not anticipated in the design of the TOMS retrieval algorithm. The purpose of this paper is to quantify the errors in the TOMS total ozone measurements resulting from both the instrument degradation and the retrieval algorithm.

There are two types of instrument related errors: a slowly developing drift in the instrument calibration since the launch of the instrument in October 1978 and an increase in the measurement noise beginning April, 1984. We estimate that by October 1987, the accumulated error in the TOMS total ozone measurement due to instrument drift is about 6 m-atm-cm. The sign of the error is such that the TOMS is slightly overpredicting the long-term decrease of the Antarctica ozone. The increase in the measurement noise is more difficult to quantify affecting some measurements by as much as 10 D.U. and others not at all. A

detailed analysis of this error and its potential impact on the studies of total ozone from TOMS will be provided.

There are three categories of algorithmic errors: 1) error due the unusual shape of the ozone profile in the ozone hole 2) error caused by very low atmospheric temperatures in the ozone hole affecting the ozone absorption cross-sections at the TOMS wavelengths, and 3) errors resulting from occasionally thick stratospheric clouds that sometimes reach to 20km in the ozone hole .

Simulation results indicate that the TOMS ozone retrieval technique is quite robust; even for the highly unusual ozone and temperature profiles found in the ozone hole the algorithm returns total ozone values close to the correct answer. Very close to the terminator the current TOMS algorithm may underestimate the total ozone by as much as 10 m-atm-cm but the error decreases rapidly with decreasing solar zenith angle. We will propose some simple algorithmic modifications, such as giving more weight to the longer (more penetrating) wavelength pairs, that can reduce this error even further.

Errors in the presence of clouds are harder to quantify since little information is available about the total optical thickness and vertical distribution of these clouds. Though the satellite measurements such as SAGE II and SAM II and the measurements from the aircraft detect significant amounts of stratospheric aerosols/ice clouds before and during the ozone hole episode, these clouds are generally too thin to produce significant error in the TOMS total ozone determination. Normal tropospheric clouds found in the south polar regions also produce little or no errors in the TOMS measurements. There are, however, aircraft reports of very high altitude (10-15 km) cirrus type clouds that may have large enough optical thickness to produce significant error in the determination of the TOMS total ozone.

Lacking the necessary information about the optical properties of the stratospheric clouds, we will provide results of sensitivity calculations for clouds of various optical thicknesses at different heights in the atmosphere. Further studies- a careful analysis of visible and infrared pictures from the AVHRR instrument on the NOAA satellites coupled with the aircraft measurements and the ultraviolet reflectivity data from TOMS - will be necessary before one can provide reasonable upper and lower bounds on the errors due to stratospheric clouds.

NMC STRATOSPHERIC ANALYSES DURING THE 1987 ANTARCTIC EXPEDITION

By Melvyn E. Gelman, Climate Analysis Center, NMC, NOAA
Washington D C. 20233
and Paul A. Newman, Applied Research Corporation
Landover MD 20785

INTRODUCTION

Stratospheric constant pressure analyses of geopotential height and temperature, produced as part of regular operations at the National Meteorological Center (NMC), were used by several participants of the Antarctic Ozone Expedition. This paper gives a brief description of the NMC stratospheric analyses and the data that are used to derive them. In addition, comparisons of the analysis values at the locations of radiosonde and aircraft data are presented to provide indications for assessing the representativeness of the NMC stratospheric analyses during the 1987 Antarctic winter-spring period.

THE NMC STRATOSPHERIC ANALYSES

Since 24 September 1978 daily global fields of temperature and geopotential height at eight stratospheric levels (70, 50, 30, 10. 5, 2, 1, and 0.4 mb, approximately 18 to 55 km) have been produced at NMC, Climate Analysis Center (Gelman et al 1986). This series of stratospheric analyses is separate from the NMC Global Data Assimilation System (GDAS) (Dey and Morone, 1985) analyses from 1000 to 50 mb. There are two levels (70 and 50 mb) that are analyzed both in the GDAS and stratospheric series. The GDAS analyses are available at both 00 GMT and 1200 GMT for use in the NMC numerical forecast system, while the stratospheric analyses, not part of the forecast system, are done only for 1200 GMT. Since the GDAS 70 and 50 mb analyses are within the top layer of the NMC numerical model, the limitations implicit in the top boundary are most evident there. While every analysis system has its own limitations, the analyses from the stratospheric series at 70 and 50 mb and higher are the fields that are most used for research purposes.

A principal data source for the stratospheric analyses comes from the Tiros Operational Vertical Soundings (TOVS) derived from the NOAA satellites. The TOVS system (Smith et al, 1979) is made up of the Stratospheric Sounding Unit (SSU), the High Resolution Sounder (HIRS-2), and the Microwave Sounding Unit (MSU). The TOVS soundings derived by the National Environmental Satellite Data and Information Service (NESDIS) provide layer mean temperature between the standard pressure levels. Updating relationships used to derive temperature profiles from the satellite radiance measurements is different for differents layers. For the layers from 1000 to 10 mb, the relationships (regression coefficients or eigenvectors) are based on a coincident sample of radiosonde and satellite measurements collected for the past week (or up to 3 weeks in areas of sparse data). For layers from 10 to 0.4 mb, the regression coefficients are not updated from their pre-launch values, because of lack of sufficient in-situ data to perform this function. Temperatures at the NMC stratospheric analysis levels are found by linear interpolation in log pressure of the layer mean temperatures. The geopotential heights are derived by interpolating from the GDAS field the 100 mb height to the location of each TOVS temperature profile. The hypsometric equation is then used to calculate

heights above 100 mb at each NMC analysis level.

The NMC stratospheric analyses use only TOVS data for all levels in the southern hemisphere and for 5 to 0.4 mb in the northern hemisphere. The northern hemisphere 70 to 10 mb analyses also use radiosonde data which are analyzed to modify the first guess field produced from the TOVS data.

DATA COMPARISONS

Figure 1 shows results of comparisons of radiosonde data with TOVS data colocated within 150 km and 3 hours of each other. The summaries for August, September, and October 1987 for the region 60 to 90 South shows how the average differences, especially at the upper levels, vary over this region. While some of the bias may be attributed to radiosonde error, much of the difference is due to limitations on the vertical resolution of the TOVS data and lags in the TOVS coefficients, based on recent past radiosonde data, due to rapid seasonal changes. Over most areas and pressure levels, however, the TOVS data provide very good information for use in meteorological analyses.

Figure 2 shows a comparison of temperature values from the ER-2 special flights over Antartica during July and August 1987 with NMC analysis values interpolated to the aircraft pressure and location. Again there is very good agreement over most of the range. The large differences at higher temperatures occur at lower tropospheric levels, while the differences at the lowest temperatures are probably due to an NMC underestimate of the extremely low temperatures.

Figure 3 shows time series from mid July to mid October 1987 of 70, 50, and 30 mb temperature values interpolated from the NMC analyses to the locations of three radiosonde stations. There is reasonably good overall agreement in the temporal changes shown from the NMC values as compared with radiosonde temperatures. Most difference is seen at the upper level, consistent with the biases shown in figure 1. Correlation coefficients range from .98 at 30 mb South pole to .56 at 50 mb McMurdo.

REFERENCES

Dey, C. H., and L. L. Morone, 1985: Evolution of the National Meteorological Center Global Data Assimilation System: January 1982-December 1983, Mon. Wea. Rev., Vol. 113, pp. 304-318.

Gelman, M. E., A. J. Miller, K. W. Johnson, and R. M. Nagatani, 1986: Detection of Long-Term Trends in Global Stratospheric Temperature from NMC Analyses Derived from NOAA Satellite Data, Adv. Space Res., Vol. 6, No. 10, pp. 17-26.

Smith, W. L., H. M. Woolf, C. Hayden, D. Q. Wark, and L. M. McMillin, 1979: TIROS-N Operational Vertical Sounder, Bull. Amer. Meteor. Soc. Vol. 60, pp. 1177-1197.

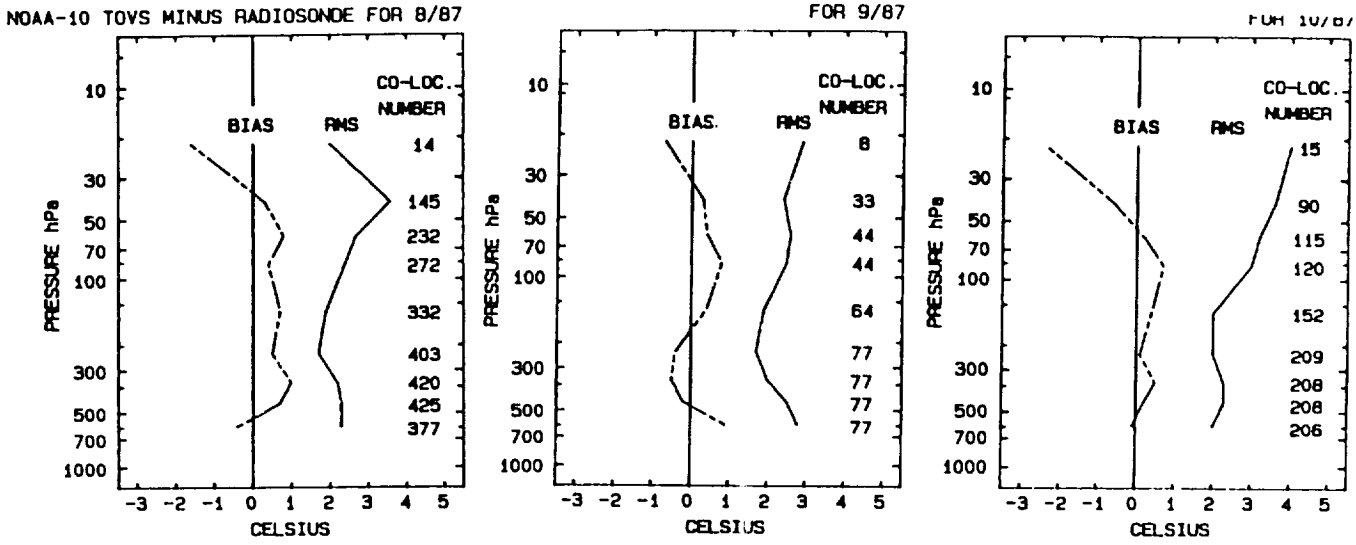

Figure 1. Temperature differences (Celsius degrees) between NOAA-10 TOVS layer mean temperatures and colocated radiosonde data from 60 to 90 S for August, September and October 1987. The number of colocations for each level appears on the right side of each diagram.

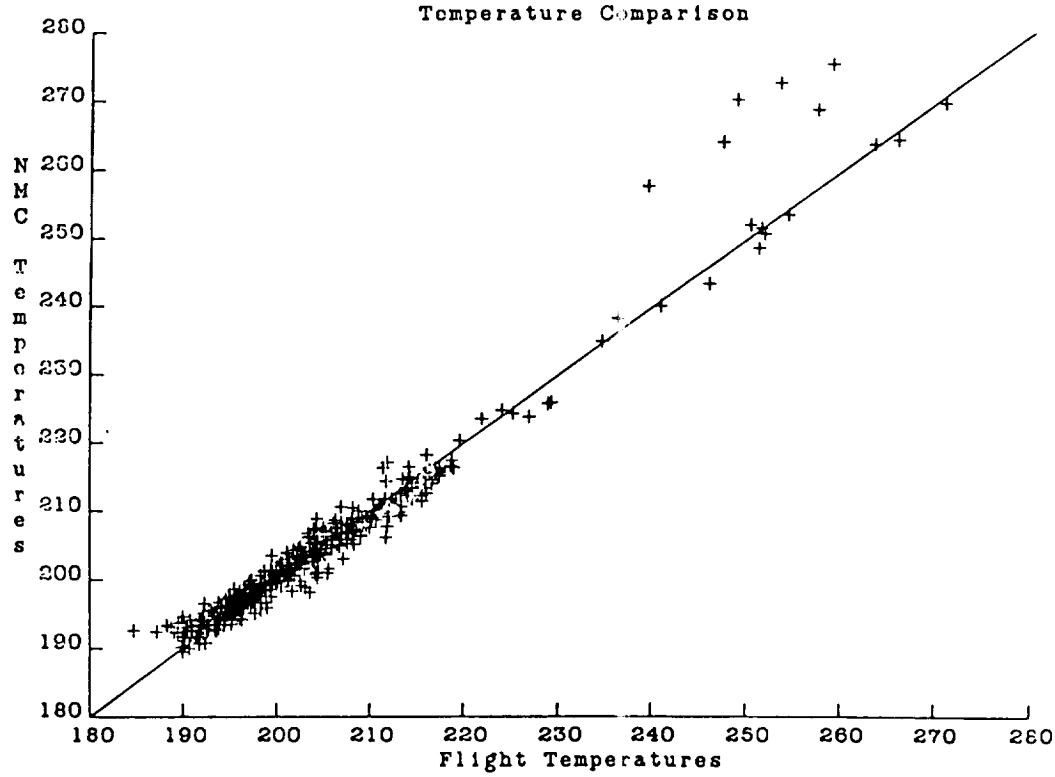

Figure 2. Comparison of temperatures from the ER-2 aircraft with interpolated NMC analysis values.

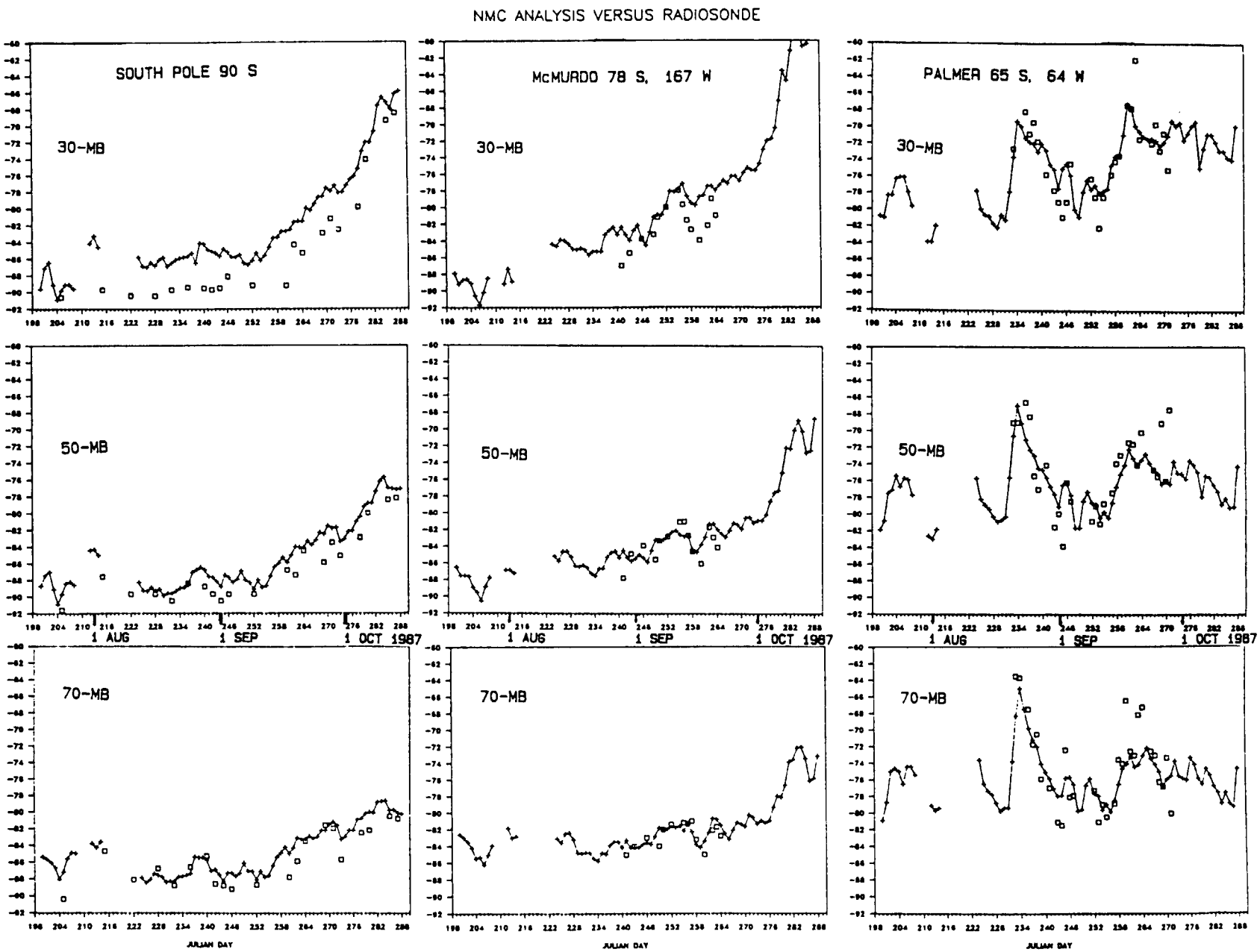

Figure 3. Comparison of 70, 50, and 30 mb radiosonde temperatures at South Pole, McMurdo, and Palmer with NMC temperatures interpolated to the station locations.

THE UW DIGITAL OZONESONDE: CHARACTERISTICS AND FLOW RATE CALIBRATION.

J.W. Harder
Cooperative Institute for Research in Environmental Sciences
University of Colorado/NOAA, Boulder, Colorado 80309-0449

D.J. Hofmann, J.M. Rosen, and N.T. Kjome
Department of Physics and Astronomy
University of Wyoming, Laramie, WY 82071

During the austral springs of 1986 and 1987, a series of balloon soundings were conducted to characterize the temporal and vertical development of Antarctic ozone depletion using the electrochemical concentration cell method (ECC). An important part of this study was to perform correlative studies between ozone and aerosol particles. In order to facilitate these simultaneous measurements, a digital ozonesonde system was developed to interface with aerosol counters. The ozone measurements will be described herein. The ozonesonde modification was accomplished by converting the current output of the sonde to a frequency and adding this digital signal to the serial data stream of a Vaisala Corporation RS-80 radiosonde under microprocessor control. This system has a number of advantages over the standard ozonesonde system currently in use, namely:

1) The high quality compensated operational amplifier used in the current-to-frequency conversion of the electrochemical current produces a linear cell response transfer function.

2) A measurement of pressure, temperature, humidity, ozone partial pressure, and (if present) aerosol concentration is transmitted every 5.24 seconds using a standard 403 MHz transmitter and FSK telemetry. Once the incoming signal has been received and decoded, IBM compatible computer hardware can store the data on floppy disk ready for detailed analysis.

3) A measurement of ozone partial pressure every 5.24 seconds permits complete resolution of electrochemical response time of the ECC (about 20 seconds).

4) Any sensor that has a TTL compatible frequency output can be interfaced to this system. But, the system can still be used as a stand-alone ozonesonde and is inexpensive enough to be used as a "throw away" instrument.

The multiple instrument capability of this system was utilized to study the response variability of two independent ozonesondes in the balloon flight environment prior to Antarctic deployment. These dual unit flights demonstrated that for pressures greater than about 50 mb (in the ozone hole region) agreement between units is quite good, on the order of 5%. However, for pressures less than 50 mb significant variations were observed, suggesting the need for individual pump efficiency calibration of each ozonesonde before balloon flight. The apparatus used to find the pump efficiency as a function of pressure is shown in Figure 1.

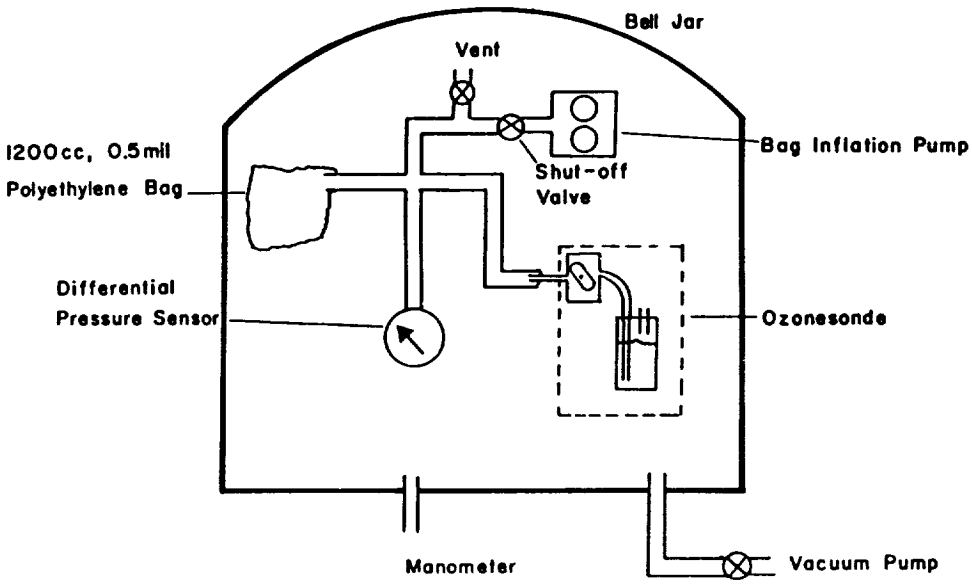

Figure 1. Apparatus used to perform ozonesonde pump calibrations.

This system essentially measures the length of time required to pump out a fixed volume of air. The differential pressure sensor measures the endpoints of when the bag is empty and full. The result of 45 individual ozonesonde pump calibrations is given in Figure 2.

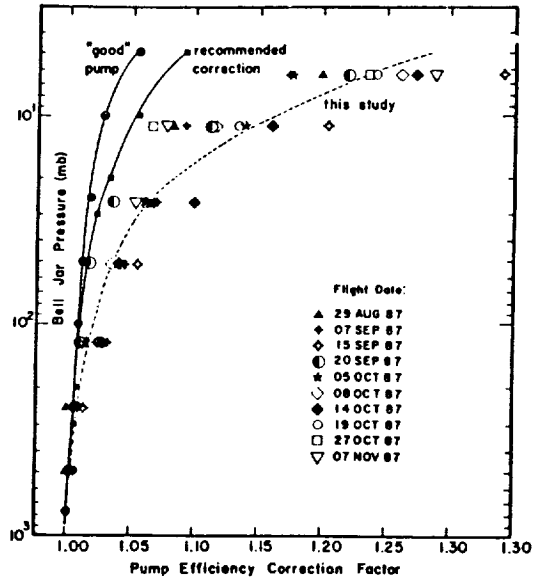

Figure 2. Measured flow rate correction as a function of pressure for the average of 45 ozonesondes (dashed curve), individual data for 10 sondes in this data set, the recommended pump calibration, and the calibration of a good pump. See text for details.

This figure shows the average of 45 pump efficiency factors (dashed curve), and the pump calibrations for ten ozonesondes in this data set (labeled according to the date that they were flown). Also shown in this figure is the efficiency of a "good" pump. This pump consists of a gear pump that has the bearings and gear teeth coated with vacuum grease to prevent any air leakage. This test demonstrates the response of a leak free pump and that the bag deflation technique gives reasonable results for a pump that behaves differently from the ozonesonde pump. Finally, the figure shows the pump efficiency correction factor quoted in the Ozonesonde Operations Handbook (NOAA Technical Memorandum ERL ARL-149). This pump correction factor is markedly different from the one found in this study. The differences are most significant at higher altitudes and can be as large as 15%. Figure 3 shows the differences between these two pump calibrations for two flights in Antarctica in 1987.

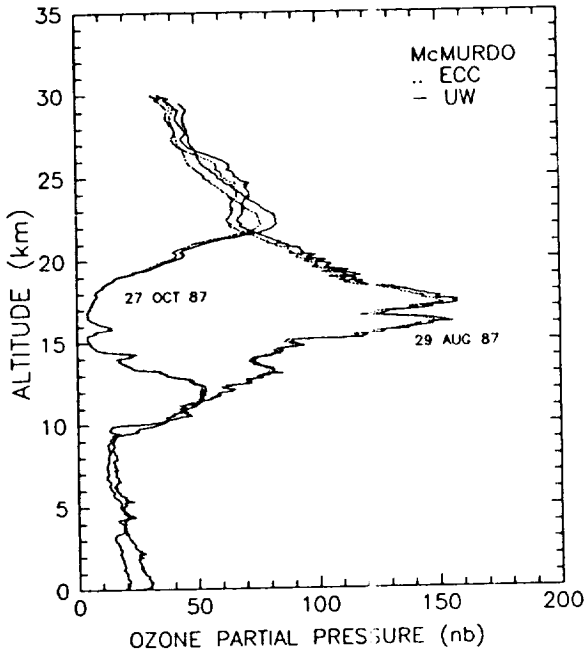

Figure 3. Comparison of pump correction factors for two flights in 1987. The dashed curve used the recommended flow rate correction factor, the solid curve used the pump calibrations found in this study.

In this figure, the profiles marked ECC are profiles derived from the recommended pump calibration, the profiles labeled UW are the profiles found using the individual pump corrections. Using the UW corrections, the integrated ozone was found to be 274 DU on August 29, and 148 DU on October 27. Using the standard correction, the derived integrated ozone columns would be 260 and 137 respectively. Figure 4 shows a comparison of the total ozone found from the Total Ozone Mapping Spectrometer and from integrated ozonesonde data in 1987. Agreement is generally quite good except for early in the season when the ozonesonde tends to give higher total ozone values.

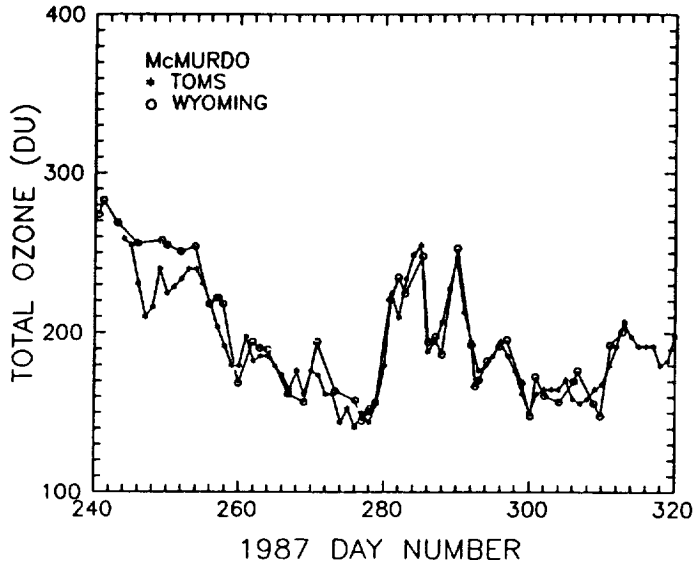

Figure 4. Comparison of total ozone as found by the Total Ozone Mapping Spectrometer, and that found by integrating the ozonesonde height profiles in 1987.

Acknowledgements. This research was supported by the National Science Foundation, Division of Polar Programs and Atmospheric Sciences and the National Aeronautics and Space Administration.

Seasonal and Temporal Changes in the Vertical Profiles of Polar Stratospheric Ozone: 1978-1986

Donald F. Heath
NASA Goddard Space Flight Center
Laboratory for Atmospheres
Greenbelt, MD 20771

NOAA/ERL/ARL
325 Broadway
Boulder, CO 80303

The long-term changes in stratospheric ozone in both Antarctic and Arctic regions during the period November 1978 - October 1986 exhibit significant interhemispheric differences in terms of time of onset, altitude, latitude, longitude, and phase. The 8-year data set of stratospheric ozone derived from observations with the Nimbus 7 SBUV instrument were deseasonalized by subtracting monthly deviations from 6-year monthly means for 10° bands centered at latitudes 80°S-80°N and the 64x64 standard NMC grid at standard pressure levels in the atmosphere. Linear trends are derived from the linear regression of monthly deviations from long term monthly means in terms of annual and monthly trends for the latitude region 55°-81° in both hemispheres. An assessment has been made of the SBUV instrument drift from analyses of annual deviations from long term annual means of stratospheric ozone in north temperate regions from 25°N-55°N with corresponding Umkehr observations from 5 stations at latitudes from 36°N-52°N which have been corrected for stratospheric aerosols derived from 5 lidar stations (DeLuisi and Mateer, 1988).

Antarctic Region (55°S-81°S)

The vertical distribution of ozone depletion in the Antarctic region can be separated into two altitude regions, above 10 mb and below 15 mb. At altitudes above 10 mb up to 0.3 mb, the maximum ozone depletion which is about 3% y^{-1} at 1.0 mb is observed during the months of May, June and July, (winter) which is the period of coldest temperatures at high latitudes in the Southern Hemisphere. In the lower stratosphere a maximum ozone depletion of about 5.5% y^{-1} is observed at 40-50 mb during October which is about two months after the coldest high latitude temperatures at the 40-50 mb level.

The geographical location of the zonally symmetric strongest poleward gradients of ozone depletion is the same in both the upper (altitudes 2 mb and below) and lower stratosphere, offset from the pole along the 30°E longitude meridian. In the upper stratosphere and lower stratosphere ozone ° depletion accelerates after early 1981.

Arctic Region (55°N-81°N)

The seasonal variation of the profile of ozone depletion in the region 55°N-81°N suggests the existence of two altitude regions of high values of ozone depletion in the upper stratosphere above 3 mb and the middle-lower stratosphere, 5 mb-40 mb with the maximum seasonal differences observed near the 1.0 mb and 10-15 mb levels.

Maximum rates of ozone depletion are observed during February and March in the upper stratospheric region and during February in middle stratospheric region. These maximum rates of ozone depletion are observed approximately two months after the coldest zonal mean high latitude stratospheric temperatures in the Northern Hemisphere. At altitudes of 2-5 mb and in the vicinity of the 30 mb level strong poleward gradients are observed in the geographical distribution which are centered slightly offset from the pole along the longitude meridian of about 30°E. An acceleration in the rates of ozone depletion in the Arctic region is observed beginning in early 1982. This onset of an acceleration of ozone depletion begins approximately one year later in the Northern Hemisphere than in the Southern Hemisphere.

The characteristics of high latitude rates of ozone depletion suggest that dynamical processes are important as well as photochemical and radiative processes in the formation of regions of enhanced ozone depletion in the Antarctic and Arctic regions.

OZONE PROFILE MEASUREMENTS AT MCMURDO STATION ANTARCTICA DURING THE SPRING OF 1987

D. J. Hofmann, J. W. Harder, J. M. Rosen, J. Hereford, and J. Carpenter
Department of Physics and Astronomy
University of Wyoming
Laramie, WY 82071

During the Antarctic spring of 1986, 33 ozone soundings were conducted from McMurdo Station. These data indicated that the springtime decrease in ozone occurred rapidly between the altitudes of 12 and 20 km. During 1987, these measurements were repeated with 50 soundings between 29 August and 9 November. Digital conversions of standard electrochemical cell ozonesondes were again employed. The ozonesonde pumps were individually calibrated for flow rate as the high altitude performance of these pumps have been in question. While these uncertainties are not large in the region of the ozone hole, they are significant at high altitude and apparently resulted in an underestimate of total ozone of about 7% (average) as compared to the Total Ozone Mapping Spectrometer (TOMS) in 1986, when the flow rate recommended by the manufacturer was used. At the upper altitudes (≈30 km) the flow rate may be overestimated by as much as 15% using recommended values (see Harder et al., "The UW Digital Ozonesonde: Characteristics and Flow Rate Calibration", poster paper, this workshop). These upper level values are used in the extrapolation, at constant mixing ratio, required to complete the sounding for total ozone.

The first sounding was on 29 August, prior to major ozone depletion, when 274 DU total ozone (25 DU extrapolated) was observed. By early October total ozone had decreased to the 150 DU range; it then increased during mid-October owing to motion of the vortex and returned to a value of 148 DU (29 DU extrapolated) on 27 October. The recommended ozonesonde flow rate would have given 137 DU (25 DU extrapolated) on 27 October. TOMS recorded 150 DU on this day over McMurdo (A. Krueger personal communication, 1988). In general, agreement with TOMS was very good except for the period 3-9 September when the soundings indicated more ozone than derived from TOMS data (see Figure 1).

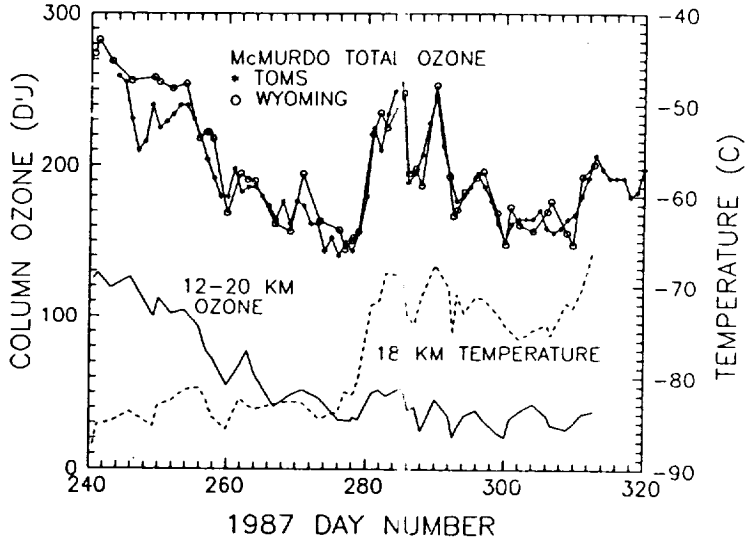

Figure 1. Total ozone at McMurdo in 1987 as determined by ozonesondes (circles) and TOMS satellite data (stars). Also shown is the 12-20 km ozone column and the 18±1 km average temperatures from the ozonesonde data.

The differences in early September are larger than can be accounted for by ozonesonde uncertainties. This apparent discrepancy may be related to the effect of high clouds on remotely sensed data at this time. Warmer temperatures at 18 km and high ozone above this altitude from about 7-24 October marked a period when McMurdo was near the edge of the ozone hole region. However, this did not affect the 12-20 km ozone column substantially (see Figure 1) where ozone fell sharply in September and remained low throughout October and early November. A major portion of the decrease (about 50 DU) occurred between 13 and 17 September (see Figure 1). The average rate of ozone mixing ratio decrease at 18 km in September was greater than in 1986 with a halflife, for an exponential decay, of 12.4 days as compared to 25 days.

The 16 km ozone partial pressure decreased from about 150 nbar in late August to about 3-5 nbar in early October representing a reduction in excess of 95% (see Figure 2). This may be compared to a minimum of about 10 nbar at McMurdo in 1986. Since the minimum ozone partial pressures in 1987 are near the background level of the electrochemical sensor under the prevailing conditions, and since some ozone may have diffused into the minimum region, the depletion may in fact have been total at some earlier time in this air mass. It may thus be difficult to determine the strength of the depletion mechanism from such measurements.

The 1987 ozone hole was also greater in vertical extent, reaching to 23 km as compared to about 20 km in 1986. The lower boundary was similar (about 12 km) with ozone depletion delayed at 12 km until about mid-September. In order to reach total ozone values as low as 105-110 DU, as reportedly observed in limited regions by TOMS, and restrict the depletion region to 12-23 km as observed in the McMurdo ozonesonde data, one would have to totally deplete ozone over that entire region. It is thus possible that the depletion extended to somewhat higher altitudes in limited regions. Again the possible effect of spatially limited dense clouds on remotely sensed ozone data needs to be investigated.

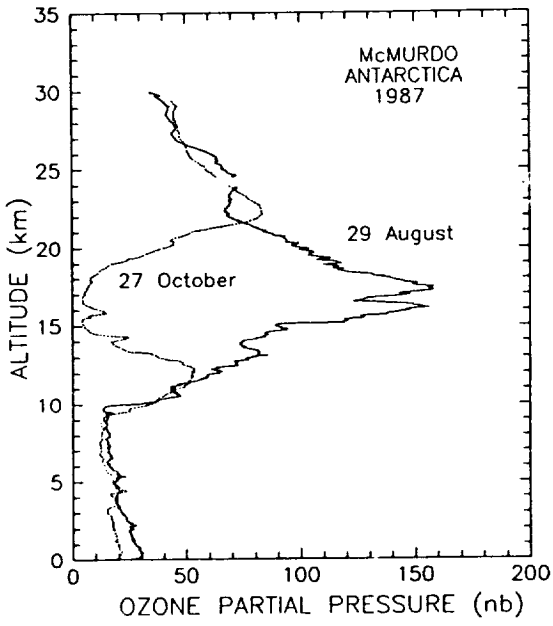

Figure 2. Comparison of ozonesonde profiles before (29 August) and after (27 October) development of the 1987 ozone hole at McMurdo.

The large variability observed in ozone profiles in the hole region in October 1986 was again observed in 1987 mainly in the 7-24 October period when McMurdo was farthest from the center of the hole. This suggests that most of these ozone layers are probably associated with the walls of the ozone cavity or polar vortex region. On September 20, reductions in ozone in ≈1 km layers in the 12-18 km region were correlated with reductions in temperature. The latter were near the frost point for water (see Rosen et al., "Balloonborne Antarctic Water Vapor Measurements and their Impact on PSC Theories," this workshop) and cloud formation may have played a role. However, on this occasion the associated ozone variations appear to be the result of adiabatic mixing in 1-2 km thick layers and are probably related to mountain generated waves and the formation of nacreous clouds which were observed at this time. Major nacreous cloud events were observed at McMurdo on 17 September in 1986 and on 20 September and 5 October in 1987.

Other than on the somewhat rare occasions associated with mountain lee waves, temperature and ozone mixing ratio profiles showed no evidence for general vertical motions with constant mixing ratio during the formation of the ozone hole (see Figure 3). The dominant depletion mechanism appears to begin in the 20 km altitude region and creates ozone mixing ratios which decrease with altitude in the hole region suggesting a local sink rather than transport of ozone out of the region. Small regions of vertical motion, as associated with the unusual temperature profile of 20 September may be important in ozone variations in the lower stratosphere especially after mid-September.

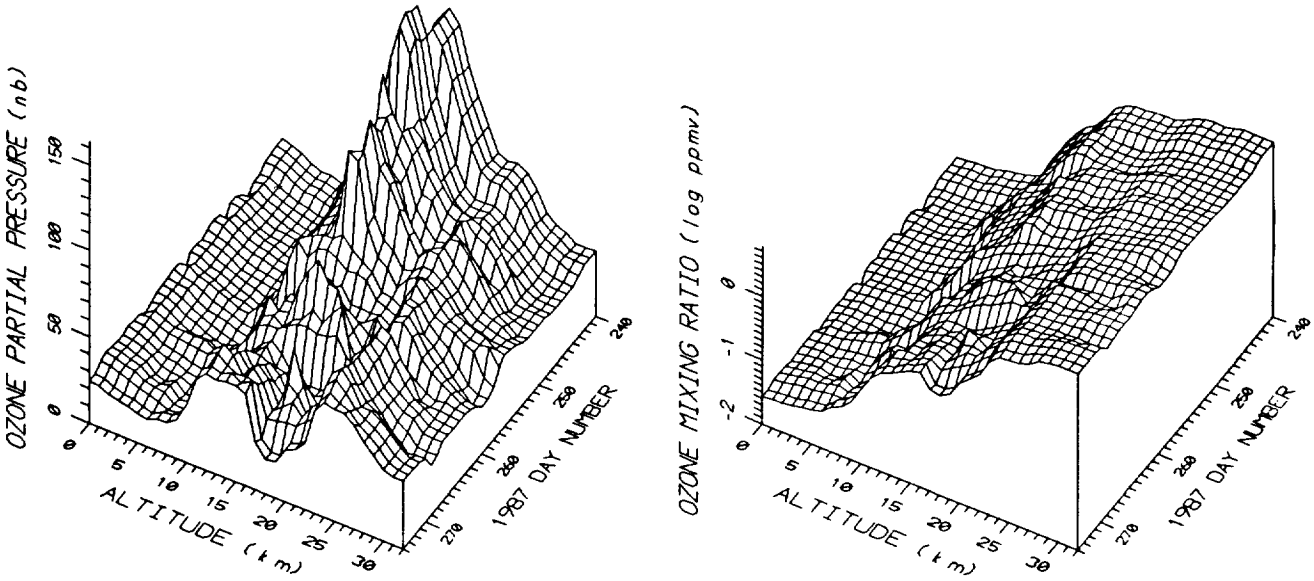

Figure 3. Three-dimensional ozone partial pressure and mixing ratio surfaces versus time and altitude constructed from 18 soundings during the 29 August to 30 September 1987 period at McMurdo.

Acknowledgements. This research was supported by the National Science Foundation, Division of Polar Programs and Atmospheric Sciences and the National Aeronautics and Space Administration.

DYNAMICS EXPLORER I SOI IMAGES OF THE "ANTARCTIC OZONE HOLE"

G. M. Keating[1], W. E. Bressette[1], C. Chen[2], M. C. Pitts[2], and J. Craven

[1]Atmospheric Sciences Division, NASA Langley Research Center, Hampton, VA 23665-5225
[2]ST Systems Corporation, Hampton, VA 23666
[3]University of Iowa, Iowa City, IA

The Dynamics Explorer satellite (DE) carries an Auroral Imaging Package which contains filters designed for performing backscatter ultraviolet measurements to measure total column ozone in the Earth's middle and lower atmosphere. Measurements are obtained at 317.5 mm (to measure ozone absorption) and 360 nm (to measure scene reflectivity). This subset of the Auroral Imager is called the Spin Scan Ozone Imager (SOI). Using the spin of the spacecraft (in conjunction with a scanning mirror), a spin-scan image of the Earth may be obtained every 12 minutes. The apogee of the spacecraft is extraordinarily high (23,000 km) compared, for example, with the Nimbus 7 apogee (955 km), and this allows global scale ozone images to be obtained of the illuminated Earth in just 12 minutes. With the high apogee, both temporal variations at a location can be studied for hours at a time, and synoptic images of larger portions of the ozone field can be obtained than from previous BUV-type measurements.

In October 1985 and 1986, measurements were obtained near apogee of the Antarctic "ozone hole." The only other high spatial resolution measurements were obtained from the Nimbus 7 TOMS experiment. In October 1987, the Dynamics Explorer apogee had precessed into the Northern Hemisphere preventing measurements of the ozone hole. However, measurements should be obtained from DE of the ozone hole in both 1988 and 1989. Considering that the Nimbus 7 TOMS instrument has long exceeded its expected lifetime, the DEI SOI experiment could easily play a crucial role in studies of the ozone hole over the next few years.

Shown in Fig. 1 is a contour chart of the ozone hole obtained from the DE SOI experiment for October 12, 1985. Notice the three-sided configuration of the ozone hole and that the hole is not centered on this day on the Pole. Shown in Fig. 2 is a comparison of the DE SOI measurements with ground-based total column ozone measurements from various Dobson stations. The provisional measurements from Halley Bay are somewhat lower than the extraordinarily low ozone values measured by the DE-SOI experiment. However, the general agreement with the Dobson stations is quite good.

Shown in Fig. 3 are contours of the NMC temperatures at 70 mb for October 12, 1985. At mid-latitudes, it may be seen that generally

maximum temperatures appear near the location of maximum column ozone, and minimum temperatures occur near minimum total ozone. The correspondence of high ozone and high temperature may be partially attributed to subsidence resulting in adiabatic heating and also in convergence of the ozone field.

The Antarctic ozone hole, where lowest temperatures and ozone concentrations occur, is shielded and shaped by the polar vortex, which results in the temperature and ozone contours in the hole having similar shapes. A study of satellite data reveals rapid hourly changes of the evolution of contours of minimum ozone within the ozone hole, suggesting that daily maps do not necessarily represent mean daily conditions of ozone within the hole.

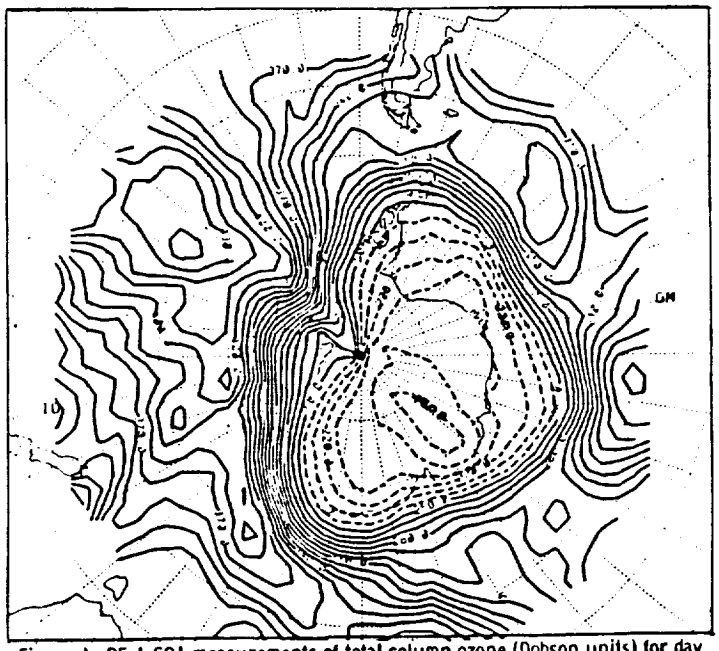

Figure 1. DE-1 SOI measurements of total column ozone (Dobson units) for day 285 of 1985 over the South Pole. The latitude and longitude intervals are 10 degrees and the heavy dashed lines are for contour intervals of less than 250 Dobson units.

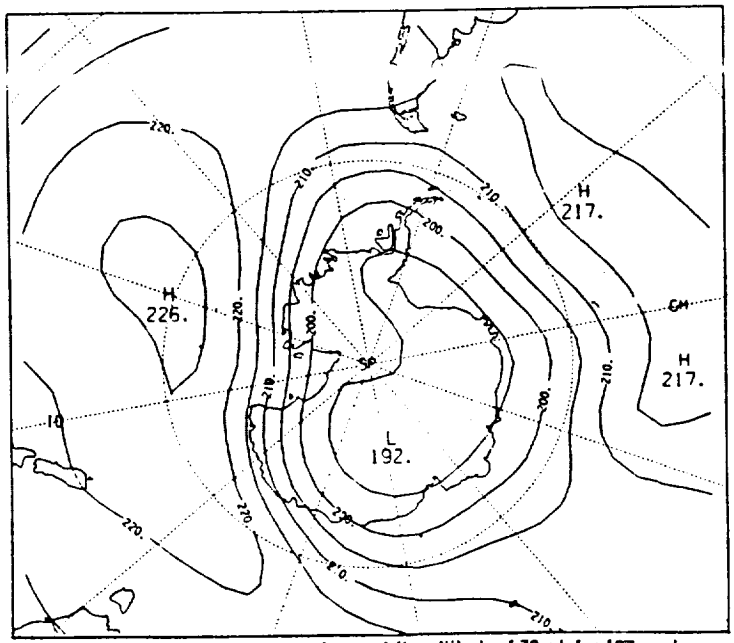

Figure 3. NMC temperature contours at the altitude of 70 mb for 12Z on day 285 of 1985 over the South Pole. Latitude and longitude intervals are 30°.

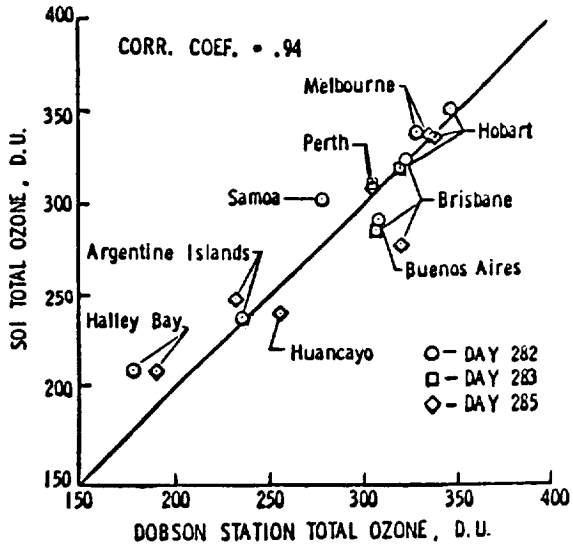

Figure 2. SOI total ozone versus southern hemisphere Dobson ground station total ozone data.

The Morphology and Meteorology of Southern Hemisphere Spring Total Ozone Mini-Holes

Paul A. Newman[1], Leslie R. Lait[2], and Mark R. Schoeberl[3]

[1]Applied Research Corporation, 8201 Corporate Dr., Landover, MD 20785
[2]National Research Council, NASA/Goddard, Code 616, Greenbelt, MD 20771
[3]NASA Goddard Space Flight Center, Code 616, Greenbelt, MD 20771

I. Introduction

On August 13 and September 2, 1986, rapid declines of total ozone in the south polar region were observed in Total Ozone Mapping Spectrometer (TOMS) data (Mark Schoeberl, personal communication). The two events were labeled mini-holes because of their rapid decline rates, and their small horizontal scales (1000-3000 km), as opposed to the long-term decline rate and planetary scale of the ozone hole. Two more mini-holes were observed on August 17 and September 5, 1987 during the Antarctic Airborne Ozone Experiment (AAOE).

The purpose of this paper is to describe the properties of mini-hole events. Both TOMS data and National Meteorological Center (NMC) meteorological analyses will be used to determine the horizontal, vertical and temporal characteristics of the mini-holes.

II. Analysis

As originally observed, the mini-holes showed horizontal spatial scales of 1000-3000 km, were usually located near the Palmer penninsula region (70°S 65°W), and produced rapid 20-30 DU reductions of the polar total ozone minimum value. Fig. 1 displays the 1987 map minimum total ozone values. These values were determined from the lowest gridded TOMS data value between 50°S and 90°S. The crosses on the figure denote days when the minimum value decreased by at least 20 DU over a single day. These sudden decreases are typical of each spring, usually occurring in August and September. The years 1979 and 1984 each had 6 mini-holes which resulted in at least a 20 DU decrease, while 1981 had only 1 mini-hole. Horizontal maps of mini-hole locations during August-September 1979 through 1987 indicate two preferential regions of intensification: 1) the Palmer penninsula (65-75°S, 60-80°W); and 2) the East Antarctica ice sheet (70-80°S, 40-100°E). The majority of mini-holes appeared over the first region.

In order to illustrate the temporal behavior of the mini-holes, the TOMS data have been band-pass filtered (half-amplitude points of 10 and 3 days). Fig. 2 shows these band-pass filtered data as a Hovmoller plot (only negative contours are plotted for ease of interpretation). The mini-holes are observed as the strong negative disturbances near 75°W on August 17 (day 16) and September 5, 1987 (day 35). It is now apparent that the mini-holes are eastward propagating disturbances which intensified in the 75°W region. In addition, the plot shows the detailed behavior of the mini-hole event of mid-August as two separate features. The first disturbance appeared on day 14 (August 15) near 120°W, moved rapidly eastward and intensified near 60°W by August 17. A second weak disturbance near 135°W appeared on August 16, intensified, and moved eastward to 60°W by August 19. The second mini-hole of September 5 can be traced from the weak disturbance mentioned previously which developed on August 16 near 135°W. This disturbance propagated completely around Antarctica at a phase speed of 10 m/s over a 17 day period and re-

intensified in the 65°W region.

Figs. 3 show polar stereographic projections of band-pass filtered total ozone (Fig. 3a), and band-pass filtered 100mb temperatures (Fig. 3b) on September 5, 1987. Excellent spatial correlation between these data sets is obvious. The mini-hole of September 5 is clearly identifiable in Fig. 3a as the low total ozone region which extends from the base of the Palmer penninsula (70°S, 60°W) into the region slightly west of South America. An identical feature is observed in the band-pass filtered 100mb temperatures in Fig. 3b. Thus, the total ozone field is highlyt correlated with lower stratospheric temperatures at small horizontal and short time scales. Note that the both filtered data sets show a distinct northwest-southeast tilt.

Band-pass filtered geopotential heights (not shown here) show an anti-cyclone which is closely associated with the mini-hole, but is phase shifted slightly to the west of the mini-hole on both Aug. 17 and Sep. 5. The unfilterd geopotential heights show stong northward flow in the mini-hole region. The vertical structure of the mini-hole features show a slight westward tilt with altitude for both the filtered temperatures and geopotential heights. Finally, the absolute value of Ertel's potential vorticity (Epv) shows a strong positive correlation, but with a slight phase shift of the Epv to the east of the mini-hole.

III. Summary

Mini-holes are rapidly developing (1-5 days), small horizontal scale (1000-3000 km) features which appear in the polar total ozone field during September and October of each year. Typically, a total of 1-6 mini-holes appear each year in either the Palmer penninsula region or over the East Antarctica ice sheet. The mini-holes do not develop over these two regions, but they intensify most dramatically there (possibly associated with the local orography). The mini-holes are associated with cold pools of air in the lower stratosphere, anti-cyclonic (geopotential height highs) disturbances to their west, high potential vorticity slightly to the east, and strong northward flow. These meteorological feature are baroclinic, having a distinct westward tilt with increasing altitude.

Figure Captions

Figure 1. TOMS total ozone minimum values for the southern spring 1987. The mapped minimum is the lowest total ozone value observed in the TOMS data between latitudes 50°S to 90°. The crosses denote map minimum decreases which exceeded 20 DU in a single day (Aug. 15, Aug. 17, and Sep. 5, 1987).

Figure 2. Hovmoller plot of band-pass filtered TOMS data. Only the -5 DU, -10 DU, -20 DU, and -30 DU contours are shown for ease of interpretation. The filter has half-amplitude points of 3 and 10 days.

Figure 3. Horizontal plots of band-pass filtered TOMS total ozone (3a, 10 DU contour increment), and NMC 100 mb temperatures (3b, 1°K contour increment). The band-pass filter has half-amplitude points of 3 and 10 days. TOMS data in 3a are omitted from 20°S to 32°S.

1.

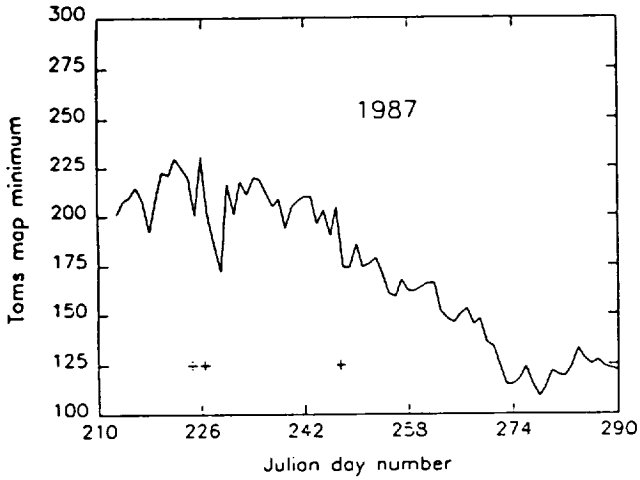

3a. TOMS TOTAL OZONE DU 9/ 5/87

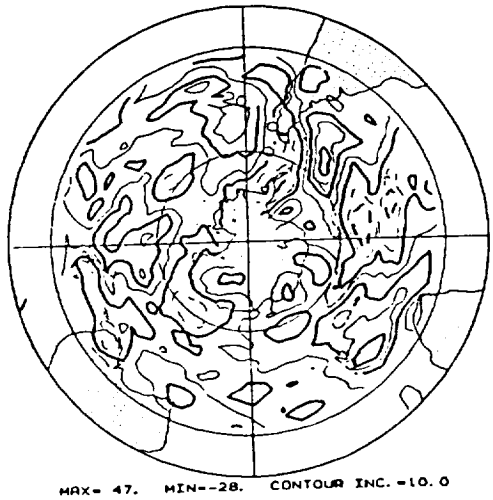

2.

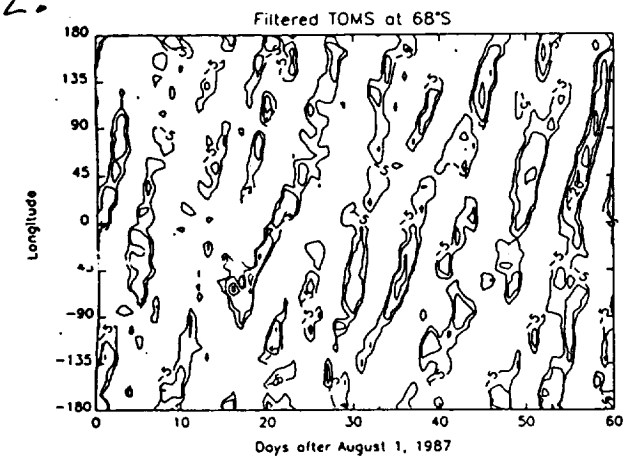

3b. NMC 100MB TEMP. 9/ 5/87

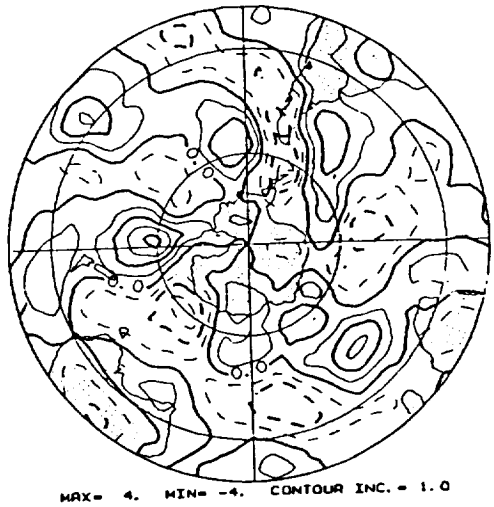

GHOST Balloons Around Antarctica

by

Charles R. Stearns
Department of Meteorology
University of Wisconsin
1225 W. Dayton St.
Madison, Wisconsin 53575

Abstract

Between 1966 and 1970 constant density GHOST balloons floating at a pressure of 100 and 200 mb were launched from Christchurch N.Z. The balloon positions were obtained from the sun's elevation angle and the radio direction to the balloon. The system is described and the balloon position data are given by Solot (1972).

The GHOST balloon position as a function of time data shows that the atmospheric circulation around the Antarctic Continent at the 100 mb and 200 mb levels is complex The GHOST balloons supposedly follow the horizontal trajectory of the air at the balloon level. Trajectories that are moving towards the South Pole could indicate air converging on the pole. The convergence would indicate a change in the vertical velocity at that level over Antarctica. The vertical motion could influence the processes associated with ozone growth and decay. The air moving towards the South Pole could also have an ozone content different from that of the displaced air.

Figure 1. shows the position of GHOST balloon 98Q for a three month period in 1968. The balloon moved to within 2 deg of the South Pole on 1 October 1968 and then by 9 December 1968 was 35 deg from the South Pole and close to its position on 1 September 1968. The balloon generally moved from west to east but on two occasions moved in the opposite direction for a few days.

Figure 2 gives the latitude of GHOST balloons 98Q and 149Z which was at 200 mb. Both balloons tended to get closer to the South Pole in September and October. Other GHOST balloons at the same pressure and time period may not indicate similar behavior.

GHOST balloon flights in adequete numbers should be made below, within, and above the ozone depletion region in Antarctica to possibly determine the role of the atmospheric circulation in the ozone depletion between June and December.

Reference:

Solot, S.B. (1972): "Complete 100- and 200- mb GHOST Balloon Data: 1966-1970", NCAR Technical Notes, National Center for Atmospheric Research, Boulder, Colorada.

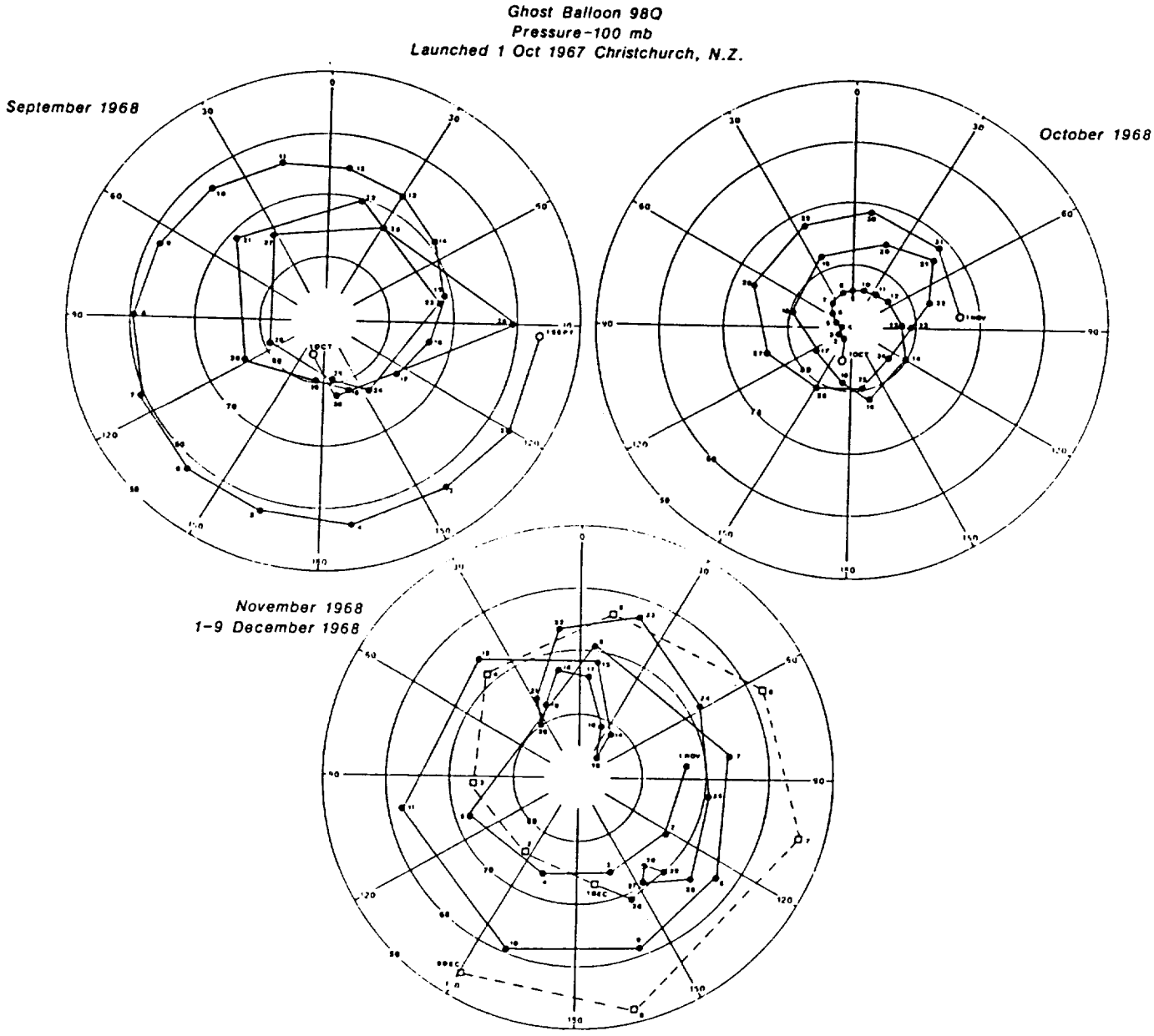

Figure 1. Position at 0000 GMT of GHOST balloon 98Q for September, October, November, and part of December 1968. The positions are connected by a straight line.

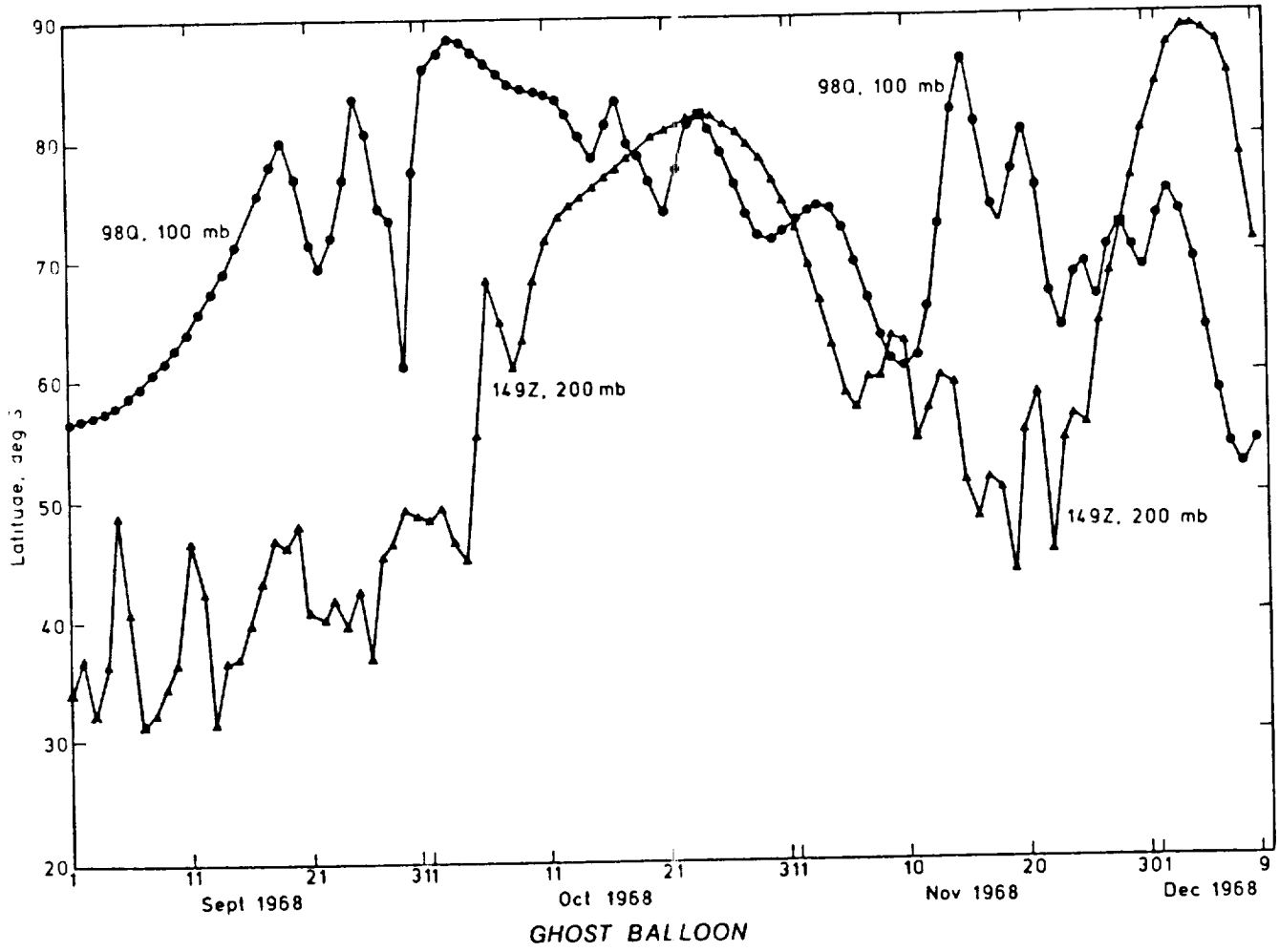

Figure 2. Latitude of GHOST balloons 98Q and 149Z for the period 1 September to 9 December 1968. Balloon 149Z was at a pressure of 200 mb.

OZONE PROFILES ABOVE PALMER STATION, ANTARCTICA

Arnold L. Torres
NASA GSFC/Wallops Flight Facility
Wallops Island, VA 23337

George Brothers
CHEMAL, Inc.
Wallops Island, VA 23337

Both NASA and the NSF sponsored major expeditions in 1987 aimed at studying the Antarctic ozone depletion phenomenon. In a cooperative effort between these two ventures, NASA's GSFC/Wallops Flight Facility conducted a series of 52 balloon-borne measurements of vertical ozone profiles over the NSF research facility at Palmer Station, Antarctica ($64^{o}46'S$, $64^{o}3'W$) between August 9 and October 24, 1987. High resolution measurements were made from ground level to an average of 10 mb.

Ozone measurements were made with Electrochemical Concentration Cell (ECC) ozonesondes (Science Pump Corporation, Camden, NJ) coupled to meteorological radiosondes for data transmission to a ground receiving station. Prior to its use in a sounding, each sonde was calibrated relative to a UV-absorption ozone monitor (Dasibi Environmental Corp.) that was, in turn, calibrated against a 3-meter UV absorption photometer at Wallops. The sonde's precision in the stratosphere below 10mb is estimated to be 5% (one sigma).

The temporal behavior of the vertical structure of ozone over Palmer Station was rather complex. Meteorological distortions and movements of the polar vortex about the Antarctic continent resulted in Palmer being in the region of maximum ozone depletion on some days, and outside of this region on other days. Figure 1 illustrates this, using two ozone profiles obtained three days apart. The profile of 10/6/87 is "normal," while that of 10/9/87 shows ozone partial pressures to be less than 10nb in the 50-80mb altitude region. Clearly, these profiles were measured in two entirely different air masses. The 9/24/87 profile shown in Figure 2 demonstrates the complex structure sometimes observed in the ozone distribution over Palmer. These features probably result from horizontal mixing between the two types of air masses when the polar vortex boundary is near the Palmer site.

While much variation was seen in the profile amounts of ozone, it is clear that a progressive depletion of ozone occurred during the measurement period, with maximum depletion taking place in the 17-19km altitude region. Ozone partial pressures dropped by about 95% in this region. In Figure 3 are plotted time dependences of ozone amounts observed at 17km and at arbitrarily selected altitudes below (13km) and above (24km) the region of maximum depletion. Ozone partial pressure at 17km is about 150nb in early August, and has decreased to less than 10nb in the minimums in October. The loss rate is of the order of 1.5%/day.

During this same period, there is only a slight decline in ozone amounts at the higher and lower altitudes and, at 24km, there is a slight increase near the end of the period. (The mid-August gap in the 24km data is due to unusually cold stratospheric temperatures that caused premature balloon bursts.) The much smaller ozone differences across the vortex boundary at the lower and higher altitudes are indicated here by smaller day to day variations than are seen at 17km.

The total ozone overburden can be estimated from ozonesonde data by integrating the profiles up to the balloon burst point, and assuming a constant mixing ratio above this altitude. Figure 4 shows how the total ozone, in Dobson units, changed during the measurement period. Again there is a clear trend downward, until near the end of the measurement period. Initially, total ozone amounts sometimes exceeded 300 DU. By early October, minimums are as low as 150 DU. As might be expected given the behavior seen in Figure 3, fluctuations in total ozone closely follow changes in ozone partial pressure at 17km (linear correlation coefficient = 0.86).

In summary, a progressive depletion in stratospheric ozone over Palmer Station was observed from August to October, 1987. Maximum depletion occurred in the 17-19km range, and amounted to 95%. Total ozone overburden decreased by up to 50% during the same period.

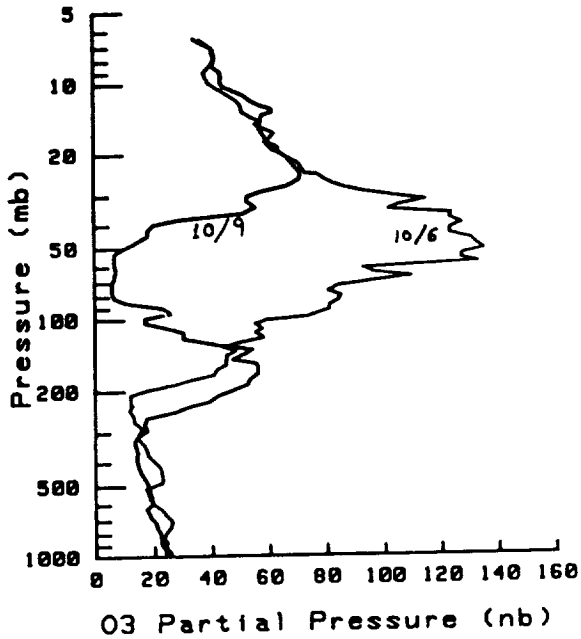

Figure 1. Ozone profiles outside (10/6/87) and inside (10/9/87) region of ozone depletion.

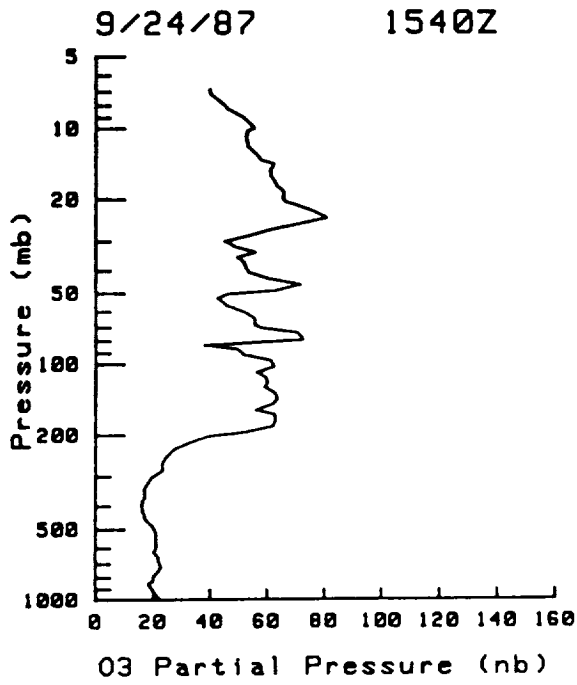

Figure 2. Ozone profile through mixed air masses.

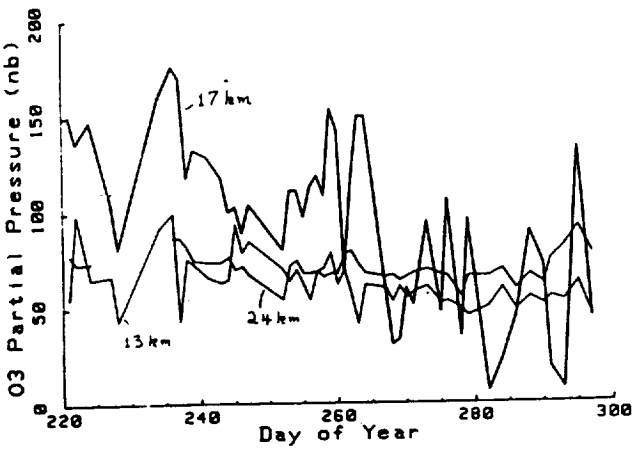

Figure 3. Ozone partial pressures below (13km), in (17km), and above (24km) region of maximum ozone depletion.

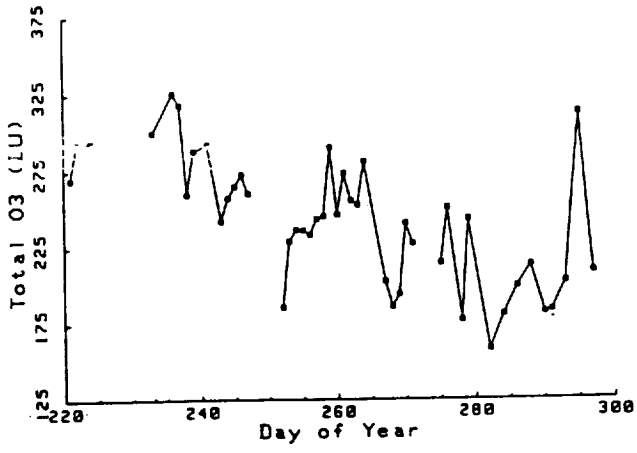

Figure 4. Trends in total ozone over Palmer Station.

Total Ozone, Ozone Vertical Distributions, and Stratospheric Temperatures at South Pole, Antarctica, in 1986 and 1987

W. D. Komhyr, R. D. Grass, and P. J. Reitelbach
NOAA Air Resources Laboratory, Boulder, Colorado

P. R. Franchois
Cooperative Institute for Research in Enviromental Sciences,
University of Colorado, Boulder, Colorado

S. E. Kuester
NOAA Corps, Rockville, Maryland

Seventy-six ECC ozonesondes were flown at South Pole, Antarctica, during 1987 in a continuing program to document year-round changes in Antarctica ozone that are dynamically and photochemically induced. Dobson spectrophotometer total ozone observations were also made. For the twilight months of March and September when Dobson instrument observations cannot be made at South Pole, total ozone amounts were deduced from the ECC ozonesonde soundings. ECC sonde total ozone data obtained during the polar night (April-August), furthermore, supplemented the sparse total ozone data obtained from Dobson instrument moon observations. Similar ozone profile and total ozone observations were made at South Pole in 1986.

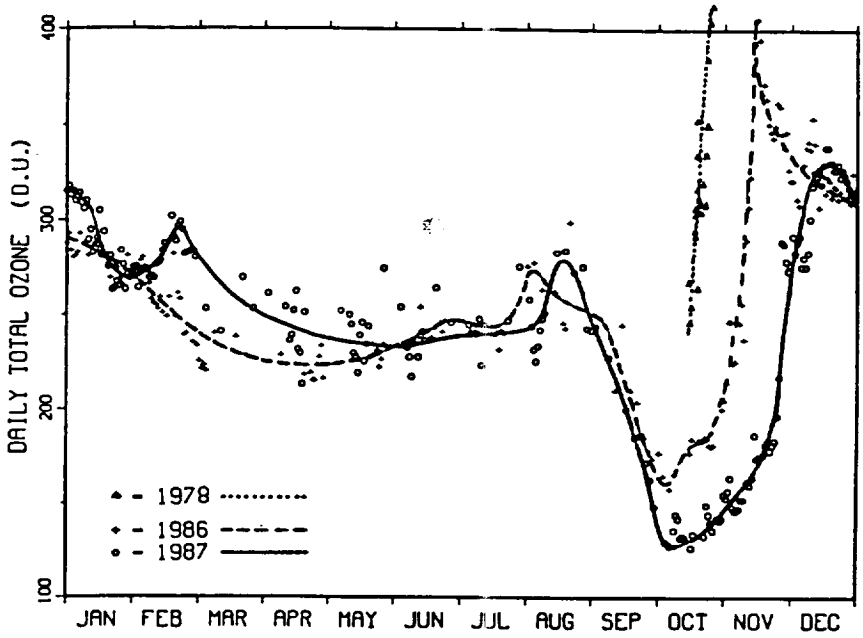

Figure 1. Daily total ozone amounts at South Pole in 1986 and 1987, including a portion of the 1978 total ozone record showing the springtime ozone increase that occurs each year in Antarctica.

As shown in Figure 1, the 1987 annual course of total ozone at South Pole differed significantly from that of 1986. For the time interval January-May, the average total ozone amount in 1987 was larger than in 1986 by about 8%. During the polar night of both years, total ozone increased from about 245 D.U. (D.U. = Dobson unit = milli-atm-cm ozone) in early June to 280-290 D.U. in August. Ozone decreased rapidly during September of both years to a low of 158 D.U. in early October 1986, but to an unprecedented low of 127 D.U. in early October 1987. Thereafter the ozone began to recover, with the recovery proceeding considerably more slowly (with a 3-4 week delay) in 1987 than in 1986. Compared to the time of the springtime ozone increase at South Pole in 1978 (Figure 1), the delay in the 1987 springtime ozone increase was 6-8 weeks. At year end for both 1986 and 1987, the total ozone amount at South Pole was 315 D.U.

The 1987 October (October 15-31) mean total ozone amount at South Pole was 138 D.U. The previous October mean low, of 161 D.U., occurred in 1985. The average total ozone amount for October months at South Pole during 1964-1979 was 292 D.U.

The 1987 November South Pole total ozone mean, of 184 D.U., was also unusually low. The previous November mean low of 238 D.U. occurred in 1985. The 1964-1979 average total ozone amount for November months at South Pole was 351 D.U.

ECC ozonesonde observations showed the springtime reduction of ozone between 11 and 22 km (180 and 25 mb) in the stratosphere to be more pronounced in 1987 than in 1986 (Figure 2). Ozone volume mixing ratios (not shown) in

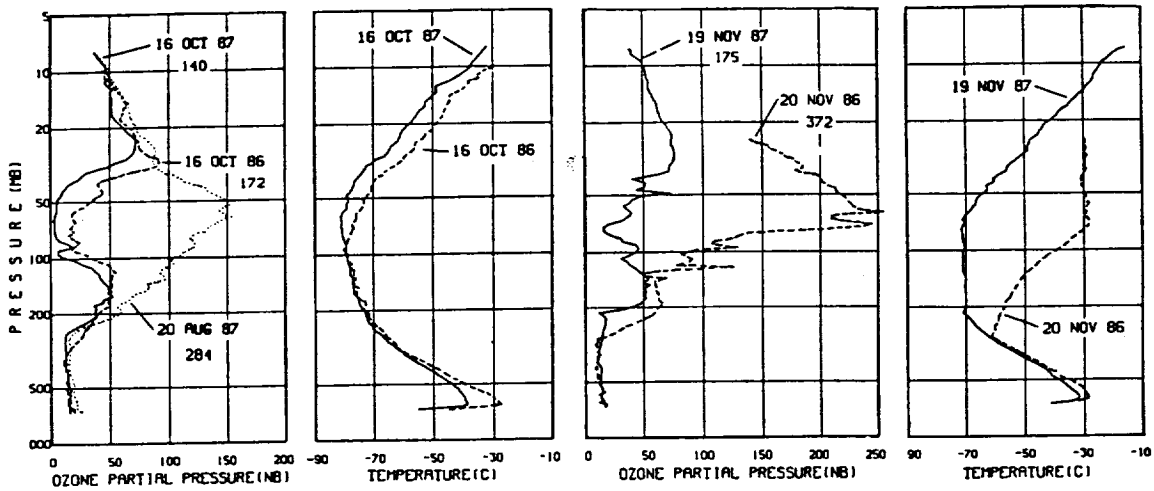

Figure 2. Comparison of South Pole October 16 and November 19-20 ozone and temperature profiles for 1986 and 1987. The August 20, 1987 profile depicts the character of the ozone vertical distribution at South Pole prior to the time of onset of the springtime ozone decrease phenomenon. Numbers under the date labels are total ozone amounts in D.U.

the heart of the ozone depletion region (at ~16 km altitude) ranged from 0.2 to 0.4 parts per million by volume (ppmv) in 1986, but approached 0.04 ppmv in 1987. (Such low ozone volume mixing ratios normally occur in the troposphere and in the low stratosphere). The observed mixing ratios of 0.04 ppmv may have been an artifact of ECC ozone sensor output current "tailing" that occurs at low output currents. Thus, depletion of ozone between 50 and 100 mb at South Pole during early October 1987 may have been virtually complete.

In 1986, at 16 km altitude, ozone decreased during August 20 to September 20 from about 2.0 to 1.0 ppmv, with an exponential decrease half-life of 34 days. During September 21 to October 15, the ozone was additionally reduced from 1.0 to 0.3 ppmv, with an exponential decrease half-life of 11 days.

The ozone reduction in the 16 km stratospheric region was more rapid in 1987. During August 20 to September 31, the ozone mixing ratio decreased from 2.3 to 0.6 ppmv, the exponential decrease half-life being 22 days. Additional ozone reduction during October 1 to 12, from 0.6 to 0.04 ppmv, proceeded with an exponential decay half-life of about 3 days.

Stratospheric temperatures near 50 mb over South Pole during August 20 to September 3 were 2°C colder in 1987 than in 1986 (-90°C vs -88°C). The temperature difference increased with time, becoming 6°C by November 1 (-70°C and -76°C in 1986 and 1987, respectively). With the break-up of the circumpolar vortex about November 15, 1986, the temperature at 50 mb over South Pole soared to -28°C. Cold stratospheric temperatures at 50 mb persisted, however, throughout much of the latter one-half of November 1987, with the temperatures being nearly 40°C colder than in 1986. With breakdown of the circumpolar vortex in late November-early December, 1987, the 50 mb stratospheric temperatures for 1986 and 1987 became comparable at about -33°C.

Bibliography

Komhyr, W. D., P. R. Franchois, B. C. Halter, and C. C. Wilson, ECC ozonesonde observations at South Pole, Antarctica, during 1986, NOAA Data Report ERL ARL-11, 213 pp., 1987.

Komhyr, W. D., S. J. Oltmans, and R. D. Grass, Atmospheric ozone at South Pole, Antarctica, in 1986, J. Geophys. Res., in press, 1988.

Komhyr, W. D., P. R. Franchois, S. E. Kuester, P. J. Reitelbach, and M. L. Fanning, ECC ozonesonde observations at South Pole, Antarctica, during 1987, NOAA Data Report ERL ARL-15, 319 pp., in press, 1988.

Correlation of N2O and Ozone in the Southern Polar Vortex during the Airborne Antarctic Ozone Experiment

S. E. Strahan (1,2), M. Loewenstein (2), J. R. Podolske (2), W. L. Starr (2) , M. H. Proffitt (3), K. K. Kelly (3), K. R. Chan(2)

(1) National Research Council Research Associate
(2) NASA Ames Research Center, Moffett Field, CA 94035
(3) NOAA/ERL/Aeronomy Laboratory, 325 Broadway, Boulder, CO 80303

In situ N2O mixing ratios, measured by an airborne laser spectrometer (ATLAS), have been used along with in situ ozone measurements to determine the correlation of N2O and ozone in the Antarctic stratosphere during the late austral winter.

At all latitudes, N2O has a constant mixing ratio of ~300 ppbv in the troposphere, but decreases with increasing altitude above the tropopause. Ozone has a very mixing ratio in the troposphere, which increases rapidly above the tropopause and peaks near 35 km; its mixing ratio decreases above 35-40 km. In the lower stratosphere, where they are neither produced or destroyed, N2O and ozone are conservative tracers. Their strong anticorrelation provides a signature of lower stratospheric air. Regions where this correlation is altered may serve as a diagnostic for sites of ozone loss.

During the 1987 Airborne Antarctic Ozone Experiment (AAOE), N2O data were collected by a laser absorption spectrometer on board the ER-2 on five ferry flights between Ames Research Center (37°N) and Punta Arenas, Chile (53°S), and on twelve flights over Antarctica (53°S to 72°S). Vertical profiling between 14 and 20 km on the flight of September 29 (flying from 53°S to 41°S) produced an average stratospheric correlation coefficient for N2O and ozone of -0.87(23). Averaging over all AAOE flights south of Punta Arenas between 53°S and 56°S,

the correlation coefficient of N2O and ozone was -0.81(25).

The first flight out of Punta Arenas, on August 17, revealed N2O/O3 correlations between 53°S and 67°S that were similar to those observed on the ferry flights. However, from August 23 to September 22, all flights reveal a different yet consistent pattern of information. Between 53°S and 72°S, we observed that the N2O/O3 correlation coefficient is always positive at the edge of the polar vortex as defined by the wind speed maximum. Inside the vortex, in the lower wind region where wind speed drops by a factor of 2 or more from the maximum, N2O and ozone have a negative correlation. The low ozone mixing ratios observed inside the vortex, however, differentiate this air from negatively correlated lower stratospheric air outside the vortex. The lowest ozone mixing ratios observed each flight were usually found inside the vortex in the lower wind region, near the boundary with the high wind region.

Of all the trace gas species measured by instruments on board the ER-2, only one showed a relationship to the N2O/O3 correlations in the vortex. With few exceptions, positive N2O/O3 correlations coincided with total water mixing ratios of greater than 2.9 ppmv, and total water mixing ratios of less than 2.9 ppmv corresponded to negative correlations. The lower water mixing ratios, or "dehydrated regions," are colocated with the negative correlations within the vortex, while the wetter regions always occur near the vortex edge.

N2O mixing ratios in the vortex range from 85 to 200 ppbv between 17 and 21 km. According to global averages [WMO, 1982], these mixing ratios correspond to seasonally averaged midlatitude observations at altitudes of 22 to 31 km. Because the anti-correlation of N2O and ozone extends to roughly 40 km, regions of positively correlated air are not evidence of subsidence. Changes in N2O mixing ratio may be used to indicate regions of ozone loss, even when ozone mixing ratios remain constant, due

to the strong anticorrelation that N2O and ozone exhibit in unperturbed lower stratospheric air. We conclude that regions of positive correlation between N2O and ozone may be interpreted as either evidence of a chemical depletion process, which may have occurred elsewhere, or as evidence of horizontal mixing of normal lower stratospheric air with ozone-depleted vortex air. Because air outside the vortex is relatively high in both N2O and ozone, and air within the vortex is low in both N2O and ozone, horizontal mixing between these two regions would produce a "transition zone" where N2O and ozone both decrease, resulting in positive correlation. The return to negative correlation within the vortex, while ozone mixing ratios remain low, implies a region of less severe ozone depletion because the ozone is increasing.

The relationship between N2O/O3 correlation and water mixing ratio is a striking phenomenon. The positively correlated regions with low ozone and high water near the vortex edge may be in a region of horizontal mixing, perhaps in the process of "mixing out" of the vortex, having already been chemically processed. The low ozone, dehydrated regions with negative correlation within the vortex may point to regions of ongoing ozone loss.

SESSION II - Polar Stratospheric Clouds - A
Presiding, J. Margitan, Jet Propulsion Laboratory
Monday Afternoon, May 9

PERSISTENCE OF ANTARCTIC POLAR STRATOSPHERIC CLOUDS

M. P. McCormick, NASA Langley Research Center, Hampton, VA 23665-5225

C. R. Trepte, ST Systems Corp., Hampton, VA 23666

It has recently been recognized that Polar Stratospheric Clouds (PSCs) may have multiple stages of growth (Poole and McCormick, 1988a): the preliminary stage consisting of binary HNO_3-H_2O particles (Type I) at temperatures slightly above the frost point (Toon et al., 1986, and Crutzen and Arnold, 1986) and another stage composed predominantly of ice (Type II) below the frost point. Crutzen and Arnold (1986), McElroy et al. (1986), and Toon et al. (1986) have suggested that the formation of PSC particles may effectively immobilize the gaseous NO_x reservoir and allow for the catalytic removal of ozone in the early Antarctic spring. In light of these developments, the persistence of PSCs observed by the Stratospheric Aerosol Measurement (SAM) II satellite sensor over a 9-year period is compared and contrasted. Details of the SAM II experiment are contained in McCormick et al. (1979) and McCormick et al. (1982). Histograms of the SAM II 1.0-μm extinction ratio data (aerosol extinction normalized by the molecular extinction) at an altitude of 18 km in the Antarctic have been generated for three 10-day periods in the month of September and are presented in Figures 1-3. Statistics for eight different years (1979-1982 and 1984-1987) are shown in separate panels for each figure.

Examination of Figure 1 (September 1-10) shows a wide range of extinction ratio values in each panel. For the most part, minimum values approach 0.25 whereas maximum values for each case vary considerably over the range from 10-100. It is not apparent from the shapes of the histograms that a preferred mode exists, but the plots do show a tendency for more larger values to be present in the later 4 winters than in the earlier set. Based on the inverse temperature-extinction relationship reported by McCormick et al. (1982), the higher extinction ratio values sighted should be accompanied by colder temperatures. Associated temperature data, obtained from the NMC temperature analysis and not shown here, do not exhibit distinctly colder conditions in the later 4 years. This inconsistency may be partially explained by uncertainties in the NMC analysis or by real changes in the environmental concentration of water vapor or nitric acid vapor as the result of particle sedimentation. The second 10-day period, September 11-20, is presented in Figure 2. It shows that the mode of the distribution has shifted toward smaller extinction ratios, which continues into the last 10-day period displayed in Figure 3 (September 21-30). These very low values are likely due to particle evaporation and the vertical redistribution of the aerosol layer by subsidence and sedimentation that takes place over the course of winter. Usually by the end of September, the lower stratosphere above about 17 km is "cleansed" of smaller particles present prior to PSC formation. Unlike any of the other years, PSCs (values >10) are clearly evident in the 1987 data set throughout September and into the first week of October. Although data are not presented in this abstract on PSCs at other altitudes, clouds tend to persist slightly longer at lower heights (16 km) and also disappear earlier at higher altitudes (20 km). In fact, extinction ratio values >10 were observed for the first time at 16 km throughout September in 1985 and again in 1987. Further, PSCs persisted through mid-September 1987 for the first time at 20 km.

Since the SAM II system is a solar occultation experiment, observations are limited to the edge of the polar night and no measurements are made deep within the vortex where temperatures could be colder. For this reason, we make use of the NMC global gridded fields and the known temperature-extinction relationship to infer additional information on the occurrence and areal coverage of PSCs. Calculations of the daily areal coverage of the 195 K isotherm will be presented for this same period of data. This contour level lies in the range of the predicted temperature for onset of the Type I particle enhancement mode at 50 mb (Poole and McCormick, 1988b) and should indicate approximately when formation of the binary HNO_3-H_2O particles begins.

REFERENCES

Crutzen, P. J., and F. Arnold, 1986: Nitric acid cloud formation in the cold Antarctic stratosphere: A major cause for the springtime "ozone hole," Nature, 324, 651-655.

McCormick, M. P., P. Hamill, T. J. Pepin, W. P. Chu, T. J. Swissler, and L. R, McMaster, 1979: Satellite studies of the stratospheric aerosol. Bull. Amer. Meteor. Soc., 60, 1038-1046.

McCormick, M. P., H. M. Steele, P. Hamill, W. P. Chu, and T. J. Swissler, 1982: Polar stratospheric cloud sightings by SAM II. J. Atmos. Sci., 39, 1387-1397.

McElroy, M. B., R. J. Salawitch, S. C. Wofsy, and J. A. Logan, 1986: Antarctic ozone: Reductions due to synergistic interactions of chlorine and bromine, Nature, 321, 759-762.

Poole, L. R. and M. P. McCormick, 1988a: Airborne lidar observation of Arctic polar stratospheric clouds: Indications of two distinct growth modes. Geophys. Res. Lett., 15, 21-23.

Poole, L. R. and M. P. McCormick, 1988b: Polar stratospheric clouds and the Antarctic ozone hole. Accepted for publication in J. Geophys. Res.

Toon, O. B., P. Hamill, R. P. Turco, and J. Pinto, 1986: Condensation of HNO_3 and HCℓ in the winter polar stratosphere. Geophys. Res. Lett., 13, 1284-1287.

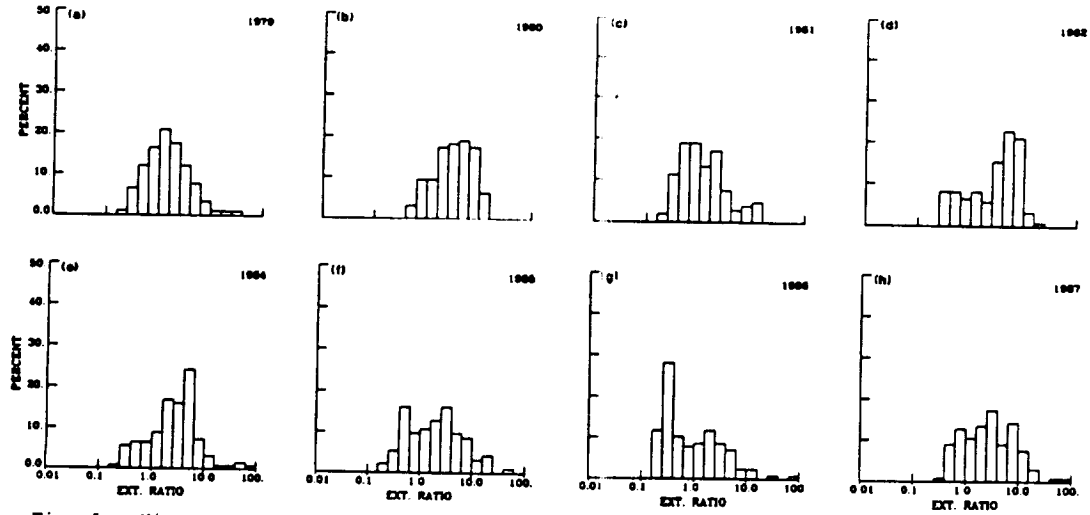

Fig. 1. Histograms displaying the probability distribution of the SAM II 1.0 μm aerosol extinction ratio data in the Antarctic region for a 10-day period, September 1-10. Each panel represents a separate year: (a) 1979, (b) 1980, (c) 1981, (d) 1982, (e) 1984, (f) 1985, (g) 1986, (h) 1987.

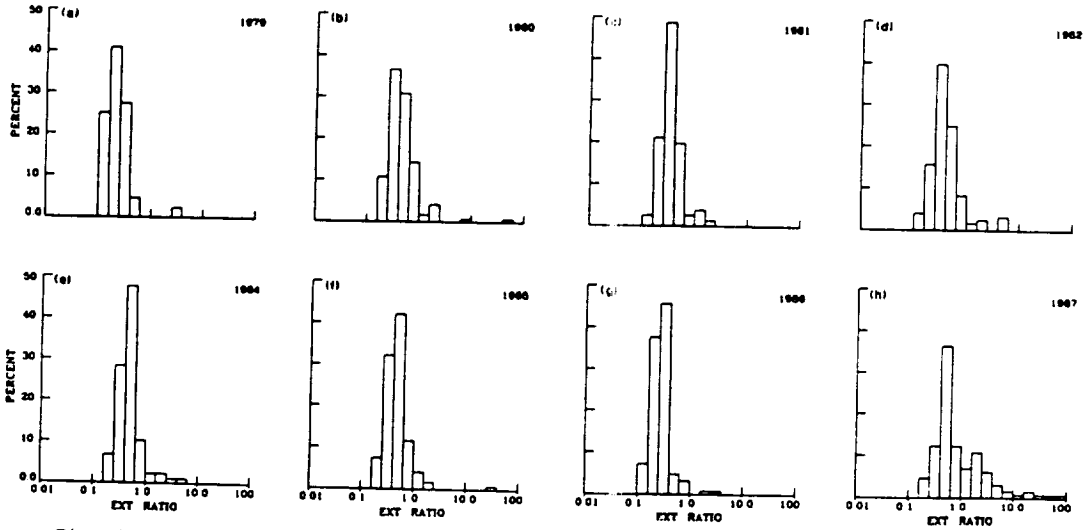

Fig. 2. Same as Fig. 1 except that the 10-day period covers September 11-20.

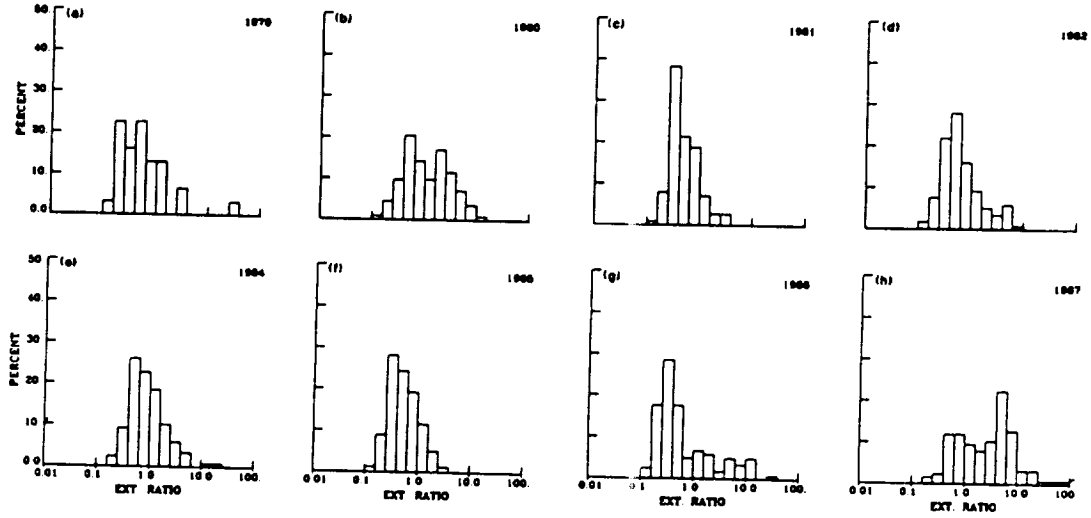

Fig. 3. Same as Fig. 1 except that the 10-day period covers September 21-30.

Comparison of In Situ Aerosol Measurements with SAGE II and SAM II Aerosol Measurements during the Airborne Antarctic Ozone Experiment

G. V. Ferry(1), M. P. McCormick(2), R. F. Pueschel(1), and J. M. Livingston(3)

(1) NASA Ames Research Center, Moffett Field, CA 94035.
(2) NASA Langley Research Center, Hampten, VA.
(3) STI International, Menlo Park, CA.

Models indicate that stratospheric aerosols play a major role in the destruction of ozone during the Austral winter. Although many in situ measurements of stratospheric aerosols were made during the Airborne Antarctic Ozone Experiment, changes of aerosol concentration and size distributions across the polar vortex are important to understanding changes of chemical species taking place during this time. Therefore comparison the in situ measurements with measurements made by satellites scanning wider areas are will give a clearer picture of the possible role played by aerosols during this period.

The SAM II instrument consists of a single-channel sun photometer designed to measure atmospheric extinction at a wavelength of 1 micrometer (McCormick et al.,1979) during local satellite sunrise and sunset. At this wavelength the attenuation of sunlight by gaseous absorption is negligible, and the extinction due to molecular scattering can be removed so that the measured irradiance data can be reduced and inverted to give an aerosol extinction profile with a 1-km vertical resolution (Chu and McCormick, 1979).

The SAGE II instrument is a seven-channel sun photometer similiar to SAM II (Mauldin, et al., 1985). SAGE II provides verticle profiles of ozone, NO2, water vaper and aerosol extinctions at 1.02, 0.525, 0.453, and 0.385 micrometer wavelengths. In general, the lower altitude limit for the aerosol extintion at 1.02 micrometers is the cloud top (as is SAM II), the lower altitude limit for the aerosol extinction at 0.525, 0.453, and 0.385 micrometers are 6.5 km, 10.5 km, and 14.5 km altitudes, respectively, if they are above the cloud top.

SAM II measurements are all made at polar latitudes of 64 to 80 S and 64 to 80 N. SAGE II coverage is from 80 S to 80 N latitudes varying with season.

In situ measurements were made by Particle Measuring Systems ASAS-X and FSSP particle spectrometers, and by NASA-Ames Research Center's Wire Impactor. The ASAS-X aerosol spectrometer sizes aerosol particles from 0.1 to 3.0 micrometers diameter. The FSSP aerosol spectrometer sizes particles from 1.0 to 8.0 micrometers. The wire impactor collects particles on 500 micrometer diameter wires and then sizes them using scanning electron microscope images.

The wire impactor size distributions are compared to those from the aerosol spectrometers and a best fit size distribution determined. Aerosol extinctions are calculated from the in situ measurements and compared to the extinctions measured by the satellites. Five comparisons are made with SAGE II and four with SAM II. Extinctions agree as close as a factor of two.

STRATOSPHERIC AEROSOL AND CLOUD MEASUREMENTS AT MCMURDO STATION ANTARCTICA DURING THE SPRING OF 1987.

D. J. Hofmann, J. M. Rosen, and J. W. Harder
Department of Physics and Astronomy
University of Wyoming
Laramie, WY 82071

Measurements of stratospheric aerosols with balloonborne optical particle counters on 6 occasions at McMurdo Station (78°S) in the spring of 1986 indicated subsidence of the stratospheric sulfate layer during the time that the ozone hole was forming (Hofmann et al., 1988). Since dynamic models of ozone depletion involving upwelling in the spring polar vortex would suggest the opposite, we repeated the measurements with an increased frequency (about one sounding per week) in 1987. During 3 of the aerosol soundings in 1986, temperatures in the 15-20 km range were low enough (<-80°C) for HNO_3 to co-condense with water according to several theories of polar stratospheric cloud formation. However, particles were not observed with the characteristic size suggested by theory (≈0.5 μm). For this reason, it was proposed that polar stratospheric clouds may predominantly consist of large (≈5-50 μm) ice crystals at very low (≈10^{-4}-10^{-3} cm^{-3}) concentrations (Rosen et al., 1988). The particle counter employed would be relatively insensitive to these low concentrations. With the increased frequency of soundings in 1987, and adding additional size discrimination in the 1-2 μm region, this hypothesis could be verified if suitably low temperatures were encountered.

Between August 29 and November 6, ten 8-channel (r ≥ 0.15 to 2 μm) aerosol detectors were flown. Of these, 8 returned size distribution information to altitudes in excess of 20 km, well above the sulfate layer at 10-15 km. As in 1986, no evidence for vertical motions could be found in the aerosol profiles during the time that the ozone hole was forming (see Figure 1).

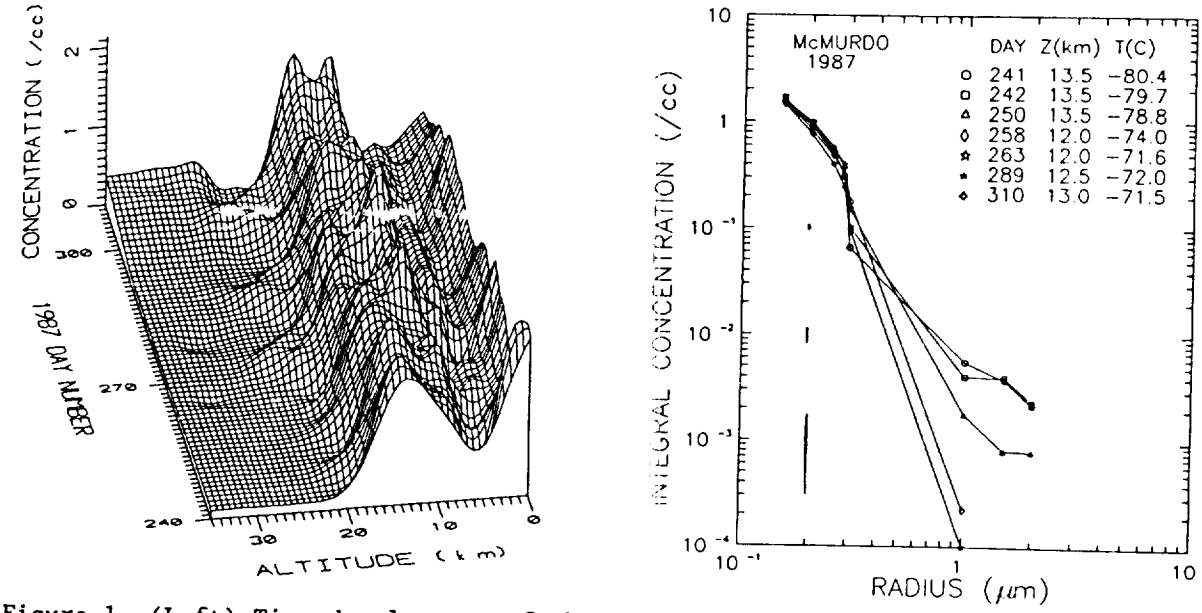

Figure 1. (Left) Time development of the aerosol concentration profile for radii greater than 0.15 μm and (Right) the size distribution (½km averages) at the stratospheric concentration maximum at McMurdo Station between August 29 and November 6, 1987. Vertical bars indicate the statistical uncertainty in the number of particles counted in ½km at the corresponding concentrations.

Size distributions in the stratospheric sulfate layer indicated the presence of large ($r \approx 1$-2 μm) particles at concentrations of 10^{-3} - 10^{-2} cm^{-3} in late August and early September (see Figure 1). By the middle of September the large particles were absent. Although sizes greater than 2 μm could not be resolved, the size distributions are not inconsistent with concentrations in the 10^{-4} - 10^{-3} cm^{-3} range for particles of 5-10 μm size. The large particles in the sulfate layer disappeared when temperatures were in excess of about -79°C (after about September 15) except on October 5 when 1-2 μm particles were observed at concentrations as high as 0.1 cm^{-3} and temperatures as high as -74°C in the 11-13 km region (see Figure 2). This event was observed in lidar data at McMurdo (B. Morley, personal communication) with scattering ratios <3 and nacreous clouds were observed that evening.

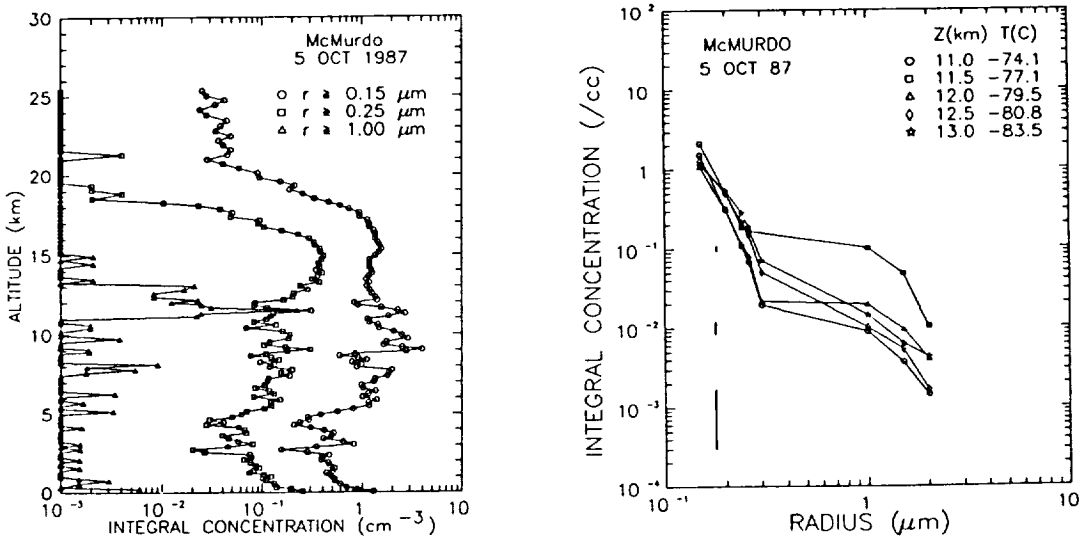

Figure 2. (Left) Aerosol concentration profiles and (Right) the associated size distribution (½km averages) at McMurdo on October 5, 1987. Vertical bars indicate the statistical uncertainty in the number of particles counted in the ½km at the corresponding concentrations.

An unusual event was observed in the 17-20 km region on August 29 when temperatures from -85° to -87°C were encountered. Both the small particle (0.15-0.3 μm) and large particle (1-2 μm) modes were enhanced with concentrations ranging from 10-80 cm^{-3} for $r \geq 0.15$ μm and 0.1-2.0 cm^{-3} for $r \geq 1$ μm. Malfunction of the instrument above 20 km prevented observation of the top of this apparent cloud. A pronounced twilight reddening of the sky indicated clouds at altitudes in the 20 km region that evening. A successful sounding 22 hours later under similar temperature conditions did not reveal unusual particle concentrations in this altitude range. Twilight observations could not be made owing to cloud cover that evening. The McMurdo lidar was not operating during this period. A measurement of the total aerosol concentration (condensation nuclei, $r \geq 0.01$ μm) 47 hours later with about 2°C higher temperatures indicated concentrations of about 10-15 cm^{-3} in this altitude range. Although the measurement on August 29 could not be confirmed, inverse correlations in the two size modes and the shape of the size distributions are physically reasonable. The small particle mode indicated a mass of about 50 ppb ($\rho = 1.2$) while that in the large particle mode suggested a lower limit (having no size resolution above 2 μm) of about 0.35 ppm ($\rho = 1$). These numbers translate into about 12 ppbv HNO_3 for a 50% HNO_3 aerosol in the small particle mode and about 0.55 ppmv for water in the large particle mode.

Measurements of condensation nuclei (CN) were conducted on 7 occasions in 1987. In 1986 a pronounced layer of CN ($\approx$50 cm^{-3}) was observed on all 3 soundings just above the ozone hole ($\approx$22-24 km). No CN measurements were made prior to ozone hole formation in 1986 so it was not known if this unusual CN layer formed during the polar winter or at the time of ozone hole formation. In 1987 a successful CN sounding was conducted on August 31, before major ozone depletion had begun. While CN concentrations were relatively high ($\approx$ 10-20 cm^{-3}) in the 20-25 km region, no distinct layer of $\approx$50 cm^{-3} was observed. However, by mid-October the layer had developed with concentrations as high as 100 cm^{-3} from 20-23 km (see Figure 3). It thus appears that this phenomenon is related to photochemistry. Temperatures in the region of the CN layer of -60° to -70°C again indicates that the composition of these small particles must be a sulfuric acid - water mixture similar to the sulfate layer. While their connection to the ozone hole phenomenon remains a mystery, they suggest unusual photochemistry, possibly related to OCS conversion to H_2SO_4, taking place in the springtime polar vortex.

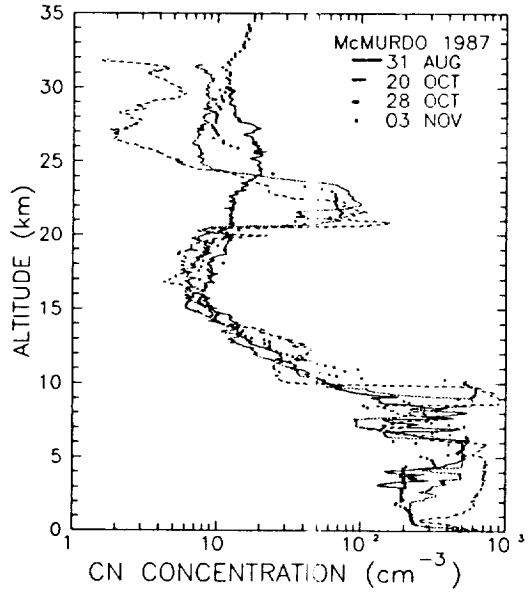

Figure 3. Condensation nuclei profiles before (August 31) and after (October 20, 28, November 3) formation of the ozone hole at McMurdo in 1987.

REFERENCES

Hofmann, D. J., J. M. Rosen, and J. W. Harder, Aerosol measurements in the winter/spring Antarctic stratosphere 1. Correlative measurements with ozone, J. Geophys. Res., 93, 665-676, 1988.

Rosen, J. M., D. J. Hofmann, and J. W. Harder, Aerosol measurements in the winter/spring Antarctic stratosphere 2. Impact on polar stratospheric cloud theories, J. Geophys. Res., 93, 677-686, 1988.

Acknowledgements. This research was supported by the National Science Foundation, Division of Polar Programs and Atmospheric Sciences and the National Aeronautics and Space Administration.

BALLOON BORNE ANTARCTIC FROST POINT MEASUREMENTS AND THEIR IMPACT ON POLAR STRATOSPHERIC CLOUD THEORIES

James M. Rosen, D.J. Hofmann
J. R. Carpenter and J. W. Harder
Dept. of Physics and Astronomy
University of Wyoming
Laramie, WY 82071
and
S. J. Oltmans
GMCC NOAA
Boulder CO 80303

ABSTRACT

The first balloon borne frost point measurements over Antarctica were made during September and October, 1987 as part of the NOZE II effort at McMurdo. The results indicate water vapor mixing ratios on the order of 2 ppmv in the 15 to 20 km region which is somewhat smaller than observed at mid-latitude and significantly smaller than the typical values currently being used in polar stratospheric cloud (PSC) theories. The observed water vapor mixing ratio would correspond to saturated conditions for what is thought to be the lowest stratospheric temperatures encountered over the Antarctic. Through the use of available lidar observations there appears to be significant evidence that some PSCs form at temperatures higher than the local frost point (with respect to water) in the 15 to 20 km region thus supporting the nitric acid theory of PSC composition. Clouds near 15 km and below appear to form in regions saturated with respect to water and thus are probably mostly ice water clouds although they could contain relatively small amounts of other constituents. Photographic evidence suggests that the clouds forming above the frost point probably have an appearance quite different from the lower altitude iridescent, colored nacreous clouds.

LARGE-SCALE VARIATIONS IN OZONE AND POLAR STRATOSPHERIC CLOUDS MEASURED WITH AIRBORNE LIDAR DURING FORMATION OF THE 1987 OZONE HOLE OVER ANTARCTICA

Edward V. Browell, Lamont R. Poole, M. Patrick McCormick, Syed Ismail, Carolyn F. Butler[a], Susan A. Kooi[a], Margaret M. Szedlmayer[a], Rod Jones[b], Arlin Krueger[c], and Adrian Tuck[d]

Atmospheric Sciences Division
NASA Langley Research Center
Hampton, VA 23665-5225 U.S.A.

A joint field experiment between NASA and NOAA was conducted during August-September 1987 to obtain in situ and remote measurements of key gases and aerosols from aircraft platforms during the formation of the ozone (O_3) hole over Antarctica. The ER-2 (advanced U-2) and DC-8 aircraft from the NASA Ames Research Center were used in this field experiment. The NASA Langley Research Center's airborne differential absorption lidar (DIAL) system was operated from the DC-8 to obtain profiles of O_3 and polar stratospheric clouds in the lower stratosphere during long-range flights over Antarctica from August 28 to September 29, 1987. The airborne DIAL system was configured to transmit simultaneously four laser wavelengths (301, 311, 622, and 1064 nm) above the DC-8 for DIAL measurements of O_3 profiles between 11-20 km ASL (geometric altitude above sea level) and multiple wavelength aerosol backscatter measurements between 11-24 km ASL. A total of 13 DC-8 flights were made over Antarctica with 2 flights reaching the South Pole.

Polar stratospheric clouds (PSCs) were detected in multiple thin layers in the 11-21 km ASL altitude range with each layer having a typical thickness of <1 km. Two types of PSCs were found during this experiment. Prior to September 15, 1987, many PSCs had aerosol backscattering ratios (aerosol backscattering/molecular backscattering) of >50 at 1064 nm and >10 at 622 nm, which are typical for predominantly water ice clouds (Type II PSC). This was also the period when the temperatures over Antarctica were the coldest with many regions below 190 K. After that date, the predominant type of PSC had aerosol scattering ratios an order of magnitude lower than those of the ice clouds. The scattering characteristics of these PSCs (Type I), which are expected to be present when temperatures are between 190-195 K, are consistent with the modeling of binary solid nitric acid/water clouds discussed in a companion paper (Poole et al.). Type I PSCs were also found in the warmer regions adjacent to Type II PSCs, and Type II PSCs were found as late as September 29 at latitudes >75°S on the last DC-8 mission. Many PSCs were found to be very large in vertical and horizontal extent. The larger PSCs were observed to extend from below 13 km ASL to above 18 km ASL with considerable vertical structure. These PSCs were found to extend more than 5° in latitude at the lower altitudes and more than 10° in latitude at the upper altitudes. The source of some of the thin layers seen at the upper altitudes in other locations was the result of wind shear and advection of air from the tops of these larger systems. Figure 1 shows an example of the atmospheric backscattering ratio (aerosol backscattering ratio + 1) profiles across a major PSC event with temperatures below 190 K across the 13-17 km ASL altitude

[a]ST Systems Corporation, Hampton, Virginia
[b]Meteorological Office, Bracknell Berkshire, Great Britain
[c]NASA Goddard Space Flight Center, Greenbelt, Maryland
[d]NOAA Aeronomy Laboratory, Boulder, Colorado

region. At these low temperatures, the aerosols are expected to be composed of ice crystals, and the magnitude of the backscattering ratio and the wavelength dependence of the aerosol backscattering ratio are also consistent with this assumption. The multilayer structure seen in both the 622 and 1064 nm scattering ratio profiles was common to most of the PSCs observed during this experiment. An example of the backscattering ratios observed from PSCs following the large-scale warming over Antarctica between September 14 and 16 is shown in Figure 2. The aerosol scattering ratios found for these Type I PSCs were more than an order of magnitude smaller than those found in the colder temperature regions prior to the warming, and temperatures across the 13-22 km ASL altitude region were in the 190-195 K range. These characteristics are both consistent with the modeling of the binary solid nitric acid/water PSCs.

Two distinct altitude regions were observed for aerosols across the polar vortex "wall." Below 13-14 km ASL, there was not a significant change in the aerosol properties upon going from outside to inside the vortex. This is consistent with other evidence that there is not a strong barrier to meridional transport across the vortex "wall" below 14 km ASL. At the upper altitudes (>14 km ASL), PSCs were found in conjunction with cold temperatures (<190 K) at latitudes typically >64°S. Over the period of this experiment, the tops of the highest aerosol layers at latitudes >75°S were observed to descend from 19.5 to 18.5 km ASL at a rate of about 1.5 km mo^{-1}. This is consistent with the subsidence rate determined from SAM-II (Stratospheric Aerosol Measurement-II) satellite aerosol extinction data. Over this same period, the tops of the primary PSCs were found to have a nearly constant average height of 17.1 km ASL. Details of the distribution and scattering characteristics of the PSCs observed during the O_3 hole formation are discussed in this paper.

Large-scale cross sections of O_3 distributions were obtained between 11-20 km ASL inside and outside the vortex with vertical and horizontal resolutions of 300 m and 12 km, respectively. Trends seen in the airborne DIAL O_3 data compared well with the trends in the O_3 column abundance data obtained from the TOMS (Total Ozone Mapping System) satellite instrument. Figure 3 shows an example of the trend in the DIAL O_3 data integrated between 13-18 km ASL as a function of latitude. The same relative trend was seen in the TOMS data with the major change in the O_3 column content along the outbound flight track at about 64°S. The location of the maximum horizontal gradient in the DIAL measured O_3 was found to consistently occur near the 250 DU (Dobson Unit) O_3 isopleth obtained from TOMS. The O_3 depletion trend seen by TOMS inside the vortex was strongly reflected in the DIAL measurements above 100 mb. Figure 4 shows the variation in the average O_3 concentration at high latitudes (>76°S) in two altitude regions from late August until late September. The average concentration of O_3 did not change substantially below 15 km ASL over that period; however, between 15-20 km ASL, O_3 decreased by more than 50%. Measurements on September 26 provided evidence that even strong O_3 depletion was taking place near 21 km ASL. At 72°S, where TOMS had indicated an O_3 level of 170 DU, the DIAL measured an O_3 mixing ratio of 0.5 ppmv, which was the lowest level observed at 21 km in real time during this field experiment.

Evidence was found for tropopause fold events occurring inside the vortex. During DIAL measurements on September 5, a tongue of high O_3 air in a layer having a thickness of about 2 km was observed near 68°S to be inclined from above 17 km ASL to below 14 km ASL. This layer also had low aerosol scattering, which is also an indicator of a descending clean, dry air mass. An enhancement in the O_3 mixing ratio was also noted by in situ O_3 instruments

on the DC-8 at an altitude of 9.4 km ASL. These data provide additional information about a potentially important transport mechanism that may influence the O_3 budget inside the vortex. There is also some evidence that strong low pressure systems in the troposphere are associated with regions of lower stratospheric O_3. The implications of these transport processes in affecting the O_3 depletion inside the vortex are addressed in other papers at this conference. This paper discusses the spatial and temporal variations of O_3 inside and outside the polar vortex region during the development of the O_3 hole and relates these data to other measurements obtained during this field experiment.

The authors would like to thank Neale Mayo, William McCabe, and Jerry Williams for assisting in acquiring the airborne DIAL data during this experiment; Patricia Robinette for producing the color display graphics for the reduced DIAL data; and Arlen Carter, James Siviter, Jr., Neale Mayo, William McCabe, Jerry Williams, Robert Allen, Noah Higdon, Byron Meadows, and Loyd Overbay for modifying the DIAL system for this mission and for installing it for the first time in the DC-8.

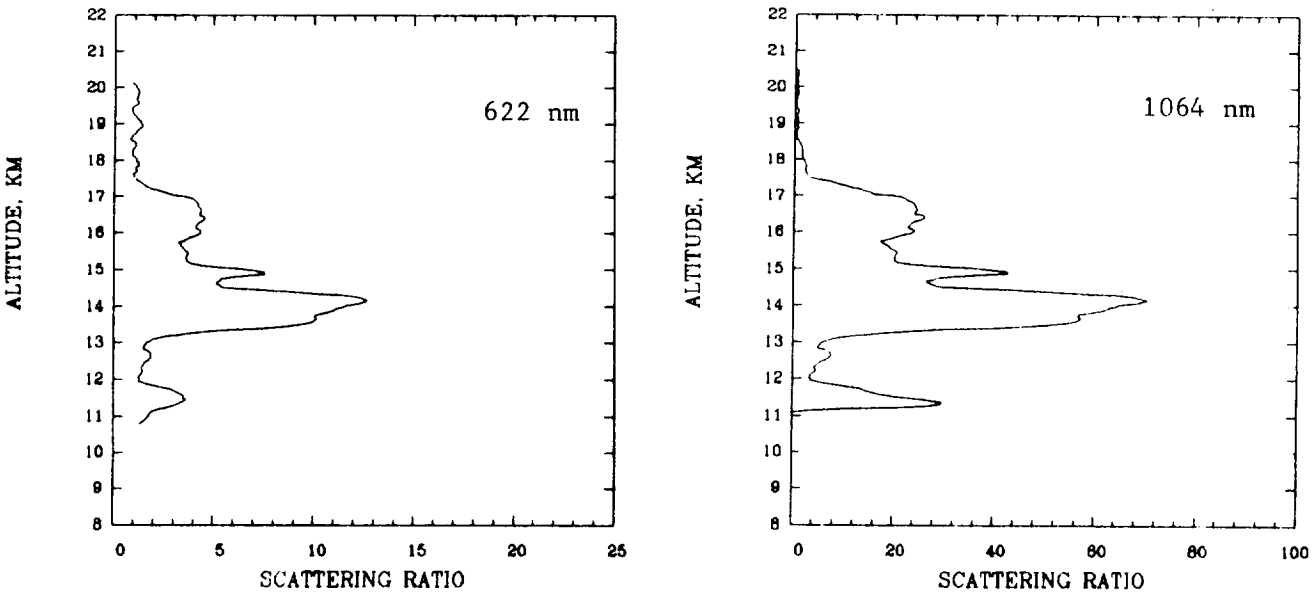

Figure 1. Atmospheric backscattering ratios on September 14, 1987, at 1125 UT and 77°S/48°W.

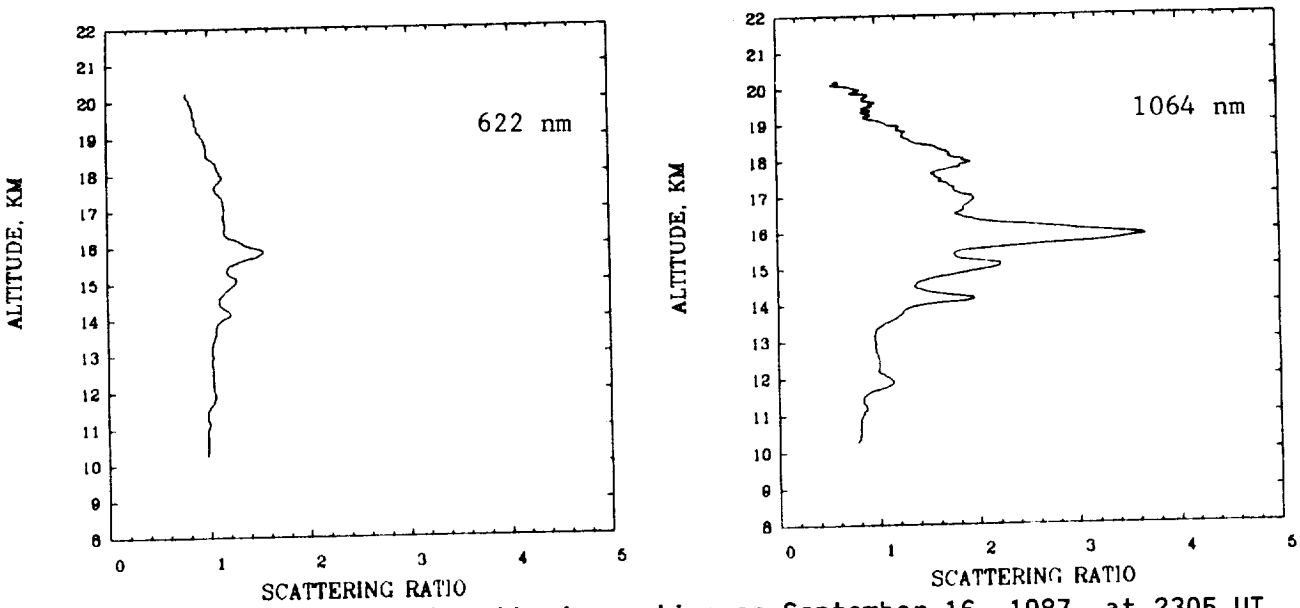

Figure 2. Atmospheric backscattering ratios on September 16, 1987, at 2305 UT and 75°S/56°W.

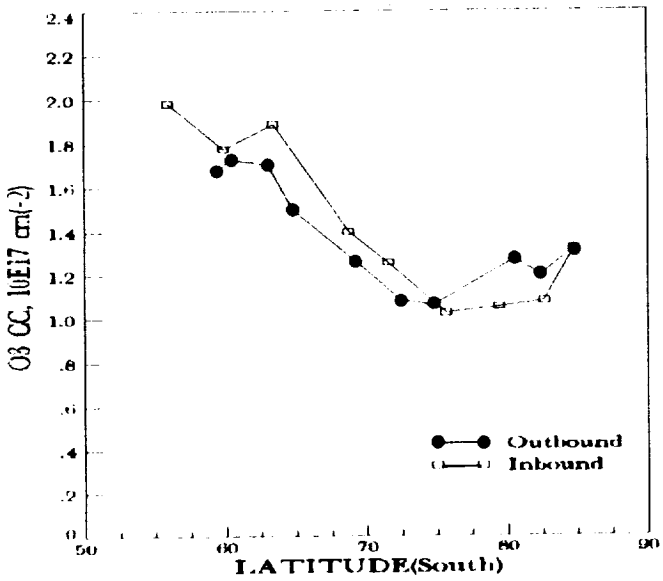

Figure 3. Ozone column content between 13-18 km ASL on September 16, 1987.

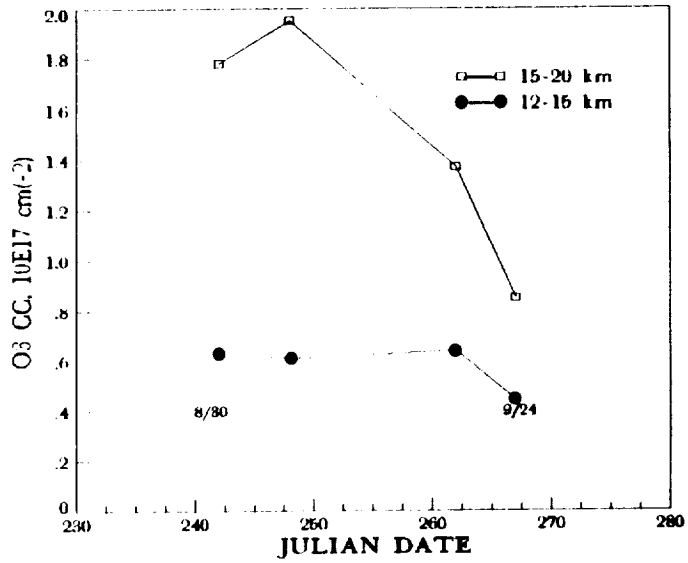

Figure 4. Ozone column content in two altitude regions at latitudes >76°S.

Filter Measurements of Chemical Composition During the Airborne Antarctic Ozone Experiment

B.W. Grandrud, P.D. Sperry and L. Sanford
National Center for Atmospheric Research
P.O. Box 3000
Boulder, Colorado 80307

During the Airborne Antarctic Ozone Experiment campaign, a filter sampler was flown to measure the bulk chemical composition of the aerosol and gas phase. On three of the flights, a separation of the aerosol and the acidic vapor composition was affected with a pre-filter to collect the aerosols followed by an impregnated filter to collect the acidic vapors. The Multi Filter Sampler (MFS) that was flown was the same sampler used in the past with the addition of NH_3 to the filter storage compartment. The filter storage compartment was also modified so that it could be maintained at near dry ice temperature to further retard volatilization of the collected aerosol.

The background sulfate aerosol was measured in regions inside and outside of the chemically perturbed region (CPR) of the polar vortex. The mass ratio of sulfate outside to inside was 2.8. This is indicative of a cleansing mechanism effecting the CPR or of a different air mass inside versus outside. The absolute value of the sulfate mixing ratio shows that the background aerosol has not been influenced by recent volcanic eruptions. The sulfate measured on the ferry flight returning to NASA Ames shows a decrease towards the equator with increasing concentrations in the northern hemisphere.

Nitrate in the aerosol phase was observed on 2 flights. The largest amount of nitrate measured in the aerosol phase was 44% of the total amount of nitrate observed. Other samples on the same flights show no nitrate in the aerosol phase. The presence of nitrate in the aerosol is correlated with the coldest temperatures observed on a given flight.

Total nitrate (aerosol plus acidic vapor nitrate) concentrations were observed to increase at flight altitude with increasing latitude north and south of the equator. Total nitrate was lower inside the CPR than outside.

Chloride and fluoride were not detected in the aerosol phase. From the concentrations of acidic chloride vapor, the ratio of acidic vapor Cl to acidic vapor F and a summing of the individual chloride containing species to yield a total chloride concentration, there is a suggestion that some of the air sampled was dechlorinated. Acidic vapor phase fluoride was observed to increase at flight altitude with increasing latitude both north and south of the equator. The acidic vapor phase fluoride was the only compound measured with the filter technique that exhibited larger concentrations inside the CPR than outside.

Antarctic Polar Stratospheric Aerosols: The Roles of Nitrates, Chlorides and Sulfates.

R.F. Pueschel (1), K.G. Snetsinger (1), J.K. Goodman (2), G.V. Ferry (1), V.R. Oberbeck (1), S. Verma (3), W. Fong (4).

(1) NASA Ames Research Center, Moffett Field, CA 94035.
(2) San Jose State University, San Jose, CA 95192.
(3) Thermo Analytical Systems Inc., Richmond, CA 94804.
(4) Information Management Inc., Palo Alto, CA 94303.

Nitric and hydrochloric acids have been postulated to condense in the winter polar stratosphere to become an important component of polar stratospheric clouds. One implication is that the removal of NOy from the gas phase by this mechanism allows high Clx concentrations to react with O_3, because the formation of $ClNO_3$ is inhibited.

Contributions of NO_3 and Cl to the stratospheric aerosol were determined during the 1987 Airborne Antarctic Ozone Experiment by testing for the presence of nitrates and chlorides in the condensed phase. Aerosol particles were collected on four 500 um diameter gold wires, each pretreated differently to give results that were specific to certain physical and chemical aerosol properties. One wire was carbon-coated for concentration and size analyses by scanning electron microscopy; X-ray energy dispersive analyses permitted the detection of S and Cl in individual particles. Three more wires were coated with Nitron, barium chloride and silver nitrate, respectively, to detect nitrate, sulfate and chloride in aerosol particles.

All three ions, viz., sulfates, nitrates and chlorides were detected in the Antarctic stratospheric aerosol. In terms of number concentrations, the aerosol was dominated by sulfates, followed by chlorides and nitrates. An inverse linear regression can be established between nitrate concentrations and ozone mixing ratio, and between temperature and nitrates.

N89-14528

On the Size and Composition of Particles in Polar Stratospheric Clouds

Stefan Kinne, NASA Ames Research Center, Moffett Field, CA,94035
Owen B. Toon, NASA Ames Research Center, Moffett Field, CA 94035
Goeff Toon, NASA JPL, 4800 Oak Grove Drive, Pasadena, CA 91109
Crofton B. Farmer, NASA JPL, 4800 Oak Grove, Pasadena, CA 91109
Edward V. Browell NASA Langley, Mail 401A, Hampton, VA 23665

Attenuation measurements of the solar radiation between 1.5 and 15 μm wavelenghts were performed with the airborne (DC-8) JPL MARK IV interferometer during the 1987 Antarctic Expedition. The opacities not only provide information about the abundance of stratospheric gases but also about the optical depths of polar stratospheric clouds (PSCs) at wavelengths of negligible gas absorption (windows).

The optical depth τ of PSCs can be determined for each window once the background attenuation, due to air-molecules and aerosol has been filtered out with the simple extinction law (the 'λ' subscript is used to indicate the wavelength dependency) :

$$\frac{I_{PSC,\lambda}}{I_{B,\lambda}} = \frac{I_{0,\lambda}\, F_\lambda \exp -[(\tau_{PSC,\lambda} + \tau_{B,\lambda})/\mu]}{I_{0,\lambda}\, F_\lambda \exp -[\tau_{B,\lambda}/\mu]} = \exp -[\tau_{PSC,\lambda}/\mu]$$

where I_{PSC}, I_B and I_0 represent measured attenuations of solar radiation for clouds, background aerosols and clear conditions, respectively. F is an instrument function and μ is the cosine of the almost horizontal solar zenith angle (83 to 89 degrees).

The ratio of optical thicknesses at different wavelengths reveals information about particle size and particle composition. Figure 1 shows the calculated extinction ratios for six different log-normal particle size distributions. Small particles rapidly loose their ability to attenuate at large wavelengths, while the attenuation of large particles has almost no spectral dependency. Figure 2 displays calculated extinction ratios for ice and water particles for one log-normal particle size distribution. Their difference is depicted by the shaded area. Sampling in PSCs has shown that sub-micron particles carry nitric acid. Thus, values for four nitric acid solution of different concentrations are graphed in Figure 2 as well. The behavior of the extinction ratios is so different, that the concentration of nitric acid in sub micron size cloud particles may be detected.

Among the almost 700 measured spectra only a few PSC cases exist. PSC events are identified by sudden reductions in the spectrally integrated intensity value and are also verified with backscttering data from an upward directed lidar instrument, that was mounted on the DC-8. For the selected case on September 21st at 14.40 GMT, lidar data indicate an optically thin cloud at 18km and later an additional optically thick cloud at 15km altitude.

Equivalent vertical optical depths were calculated based on the cosine dependence of the solar zenith angle and are presented in Figures 3 and 4 for both cloud types. The cosine assumption, however, overestimates optical paths for solar zenith angles in excess of 85^{0}. Since the selected cases are associated with an angle of 88^{0}, actual vertical optical depths are about twice of that indicated in Figures 3 and 4.

A comparison with Figures 1 and 2 reveals for the high cloud a typical particle radius of about 0.5μm and a high nitric acid concentration, based in particular on the extinction behavior at 3μm wavelength. The low cloud in contrast displays particle sizes in excess of 5μm radius. Their relative large ice water content makes high nitric acid concentration unlikely.

Many more PSC measurements were analyzed. Their spectral extinction dependencies reveal particles heavily varying in size and composition. The similarity of most cases to either that of Figure 3 or 4, however, suggests a particle classification.

All results still suffer from (1) often arbitrary definitions of a 'clear' case, that often already may have contained PSC particles and (2) noise problems that restrict the calculations of optical depths to values larger than 0.001. Once these problems are handled, this instrument may become a valuable tool towards a better understanding of the role PSCs play in the antarctic stratosphere.

Figure Captions

Fig. 1 Illustrated are extinction ratios of log-normal particle size distributions for mean particle radii of .125, .25, .5, 1, 2 and 4μm. (s - shape factor, RI - Refractive Index [constant]).

Fig. 2 Illustrated are extinction ratios of 0.5μm log-normal particle size distributions for ICE, WATER and several NITRIC ACID solutions.

Fig. 3 Illustrated are cosinus corrected vertical optical depths for a high PSC-cloud at 18Km altitude.

Fig. 4 Illustrated are cosinus corrected vertical optical depths for a PSC-cloud at 15km altitude.

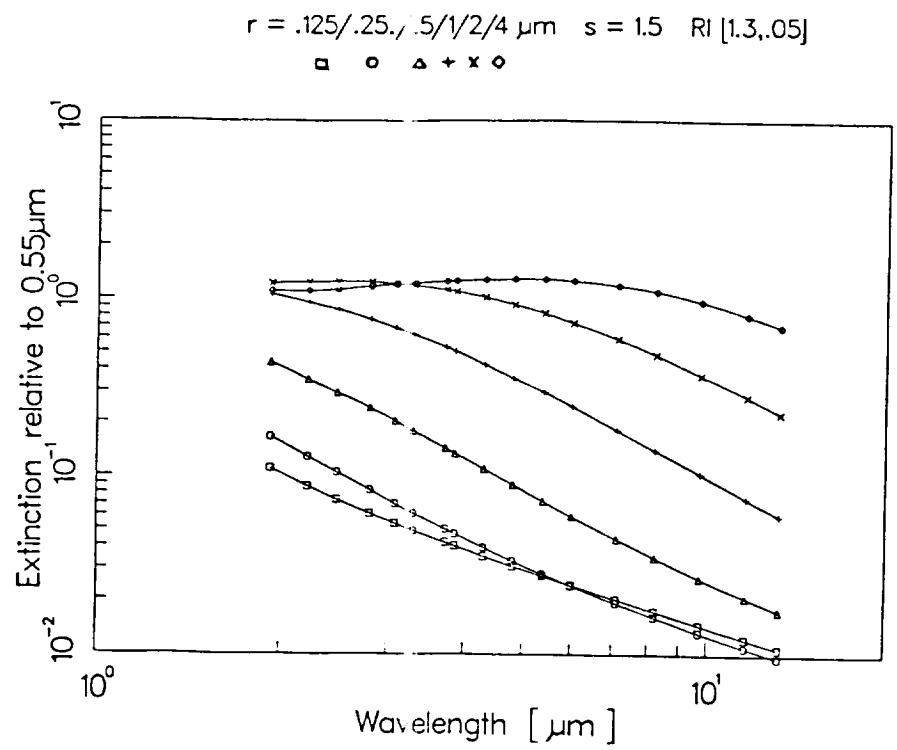

Figure 1

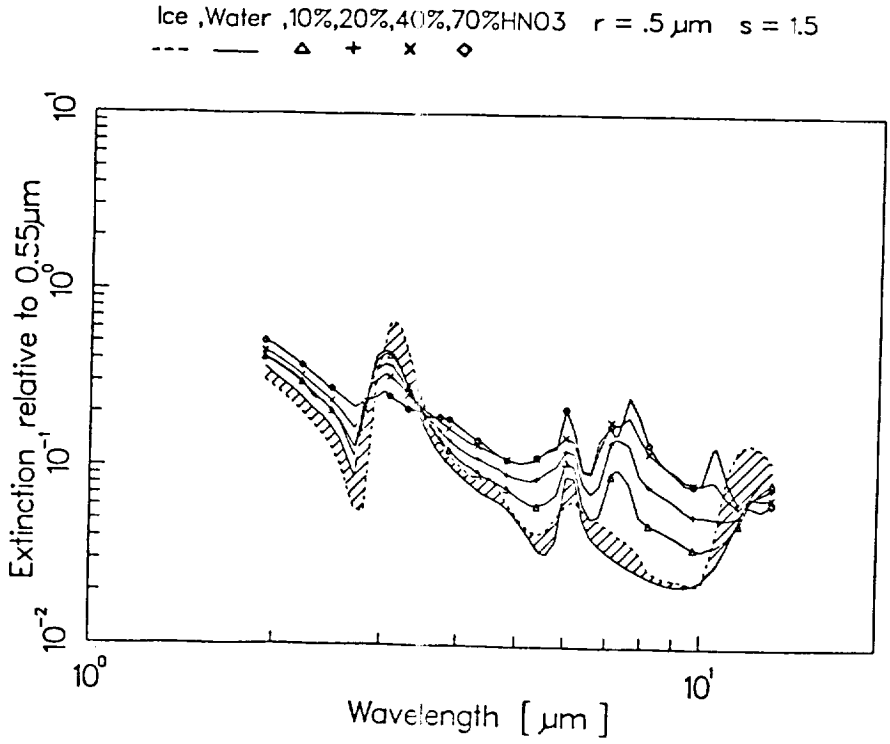

Figure 2

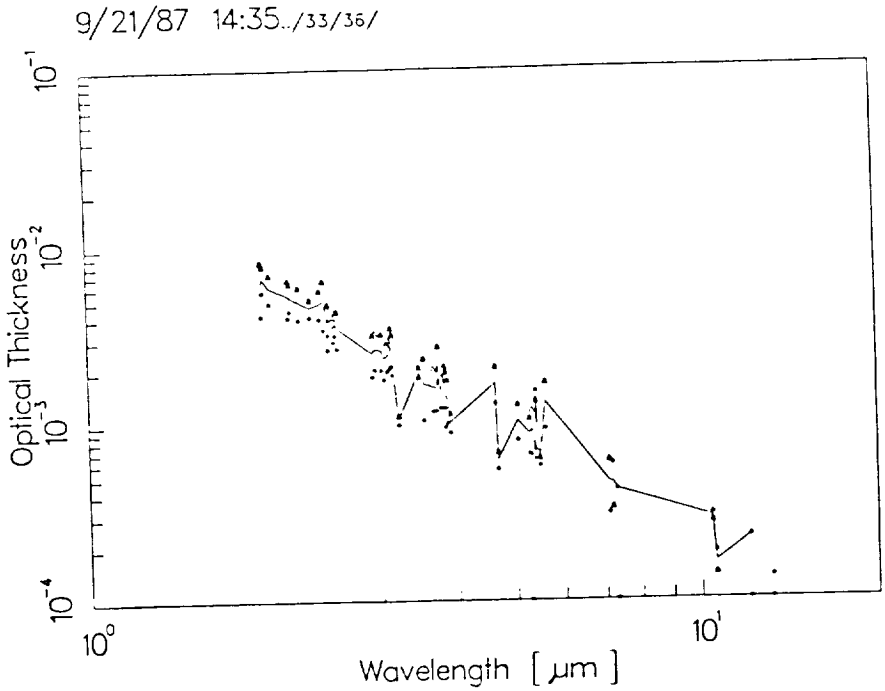

Figure 3

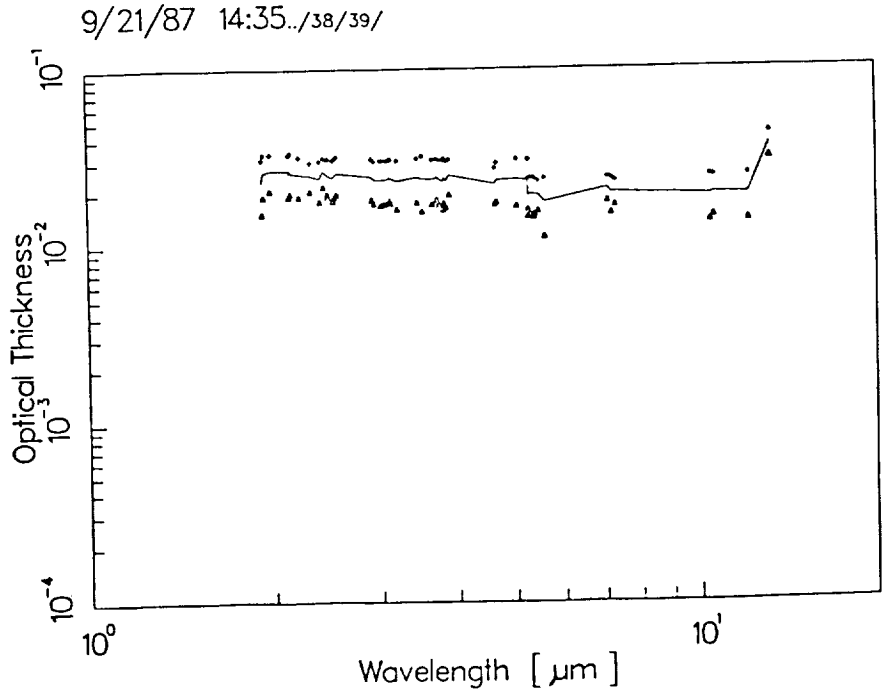

Figure 4

Formation of polar stratospheric clouds simulated in a two dimensional model of the atmosphere

Guido Visconti and Giovanni Pitari
Dipartimento di Fisica,Università degli Studi-L'Aquila
67100 L'Aquila,Italy

A microphysics code has been implemented in a two dimensional model of the atmosphere to study formation of polar stratospheric clouds containing HCl or HNO_3 .The model range from pole to pole in latitude and from the ground to about 20Km in altitude. Resolution in latitude is 10° and about 0.8Km in altitude. This is an eulerian model with prescribed eddy diffusion coefficients and the circulation obtained from observations. The chemistry of the model follows the family approach for NO_x ,Cl_x anf HO_x while the ozone is fixed and changed seasonally. The aerosol code is based on a assigned population of condensation nucleii and includes the processes of condensation,coagulation and sedimentation. Aerosol growth is simulated in nine different size bins ranging between 0.01u and 2.56u.

The model has been built to study aerosol layers formation in the upper troposphere and lower stratospherea and has been validated for sulfate aerosol resulting from a rather complex sulfur chemistry.

In order to simulate the effect of low temperature on the formation of polar clouds the basic temperature has been lowered in the winter polar region by a maximum of 10,20 and 30K. The optical thickness and cloudiness coverage can be estimated as well as the reduction in concentration of NOx. The resulting population of aerosol is analyzed in terms of the possible perturbation to the heating rates and the heterogeneous chemistry. Heating rates are calculated with an accurate radiative code which takes into account the effect of the particulate both in the solar and infrared wavelength range. Heterogeneous reaction rates are calculated by considering the size distribution of the aerosol and together with the changed chemical composition of the polar region can be used to estimate the depletion effects on ozone.

ICE IN THE ANTARCTIC POLAR STRATOSPHERE

J. Goodman (1), B. Toon (2), R. Pueschel (2), K. Snetsinger (2), and S. Verma (2)

(1) San Jose State University, San Jose, CA 95192.
(2) NASA Ames Research Center, Moffett Field, CA 94035.

ABSTRACT

On six occasions during the 1987 Airborne Antarctic Ozone Experiment, the PSC ice crystals were replicated over the Palmer Peninsula at approximately 70° South. The sampling altitude was approximately 60 to 65 thousand feet, the temperature range was -83.5°C to -72°C and the atmosphere was subsaturated in all cases. The collected crystals were predominantly complete and hollow prismatic columns with maximum dimensions up to 217 microns. Evidence of scavenging of submicron particles was detected on several crystals. While the replicated crystal sizes were larger than anticipated, their relatively low concentration results in a total surface area less than one tenth that of the sampled aerosol particles. The presence of large crystals (length > 100 microns) suggest that PSC ice crystals can play a very important role in stratospheric dehydration processes.

SESSION III - Polar Stratospheric Clouds - B
Presiding, S. Wofsy, Harvard University
Tuesday Morning, May 10, 1988

In-situ measurements of total reactive nitrogen, total water vapor, and aerosols in Polar Stratospheric Clouds in the Antarctic Stratosphere

by

D. W. Fahey [1], K. K. Kelly [1], G. V. Ferry [2], L.R. Poole [3], J.C. Wilson [4], D. M. Murphy [1,5], K. R. Chan [2]

[1] Aeronomy Laboratory
National Oceanic and Atmospheric Administration
325 Broadway R/E/AL6
Boulder, CO 80303

[2] Ames Research Center
National Aeronautics and Space Administration
Moffett Field, CA 94035

[3] Langley Research Center
National Aeronautics and Space Administration
Hampton, VA 23665

[4] University of Denver
Department of Mechanical Engineering
Denver, CO 80208

[5] Cooperative Institute for Research in Environmental Sciences
University of Colorado
Boulder, CO 80309

Measurements of total reactive nitrogen, NOy, total water vapor, and aerosols were made as part of the Airborne Antarctic Ozone Experiment conducted in Punta Arenas, Chile during August and September 1987. The measurements were made using instruments located onboard the NASA ER-2 aircraft which conducted twelve flights over the Antarctic continent reaching altitudes of 18 km at 72 S latitude. Each instrument utilized an ambient air sample and provided a measurement up to 1 Hz or every 200 m of flight path.

The data presented focus on the flights of August 17th and 18th during which Polar Stratospheric Clouds(PSC's) were encountered containing concentrations of 0.5 - 1.0 micron diameter aerosols greater than 1 cm^{-3}. The temperature during these events ranged as low as 184 K near 75 mb pressure, with H_2O values near 3.5 parts per million by volume(ppmv). With the exception of two short periods, the PSC activity was observed at temperatures above the frost point of water over ice.

For analysis, the PSC aerosol is assumed to form from the co-deposition of HNO_3 and H_2O on pre-existing sub-micron aerosols as $HNO_3.3H_2O$, with saturation vapor pressures extrapolated from the freezing point of the equivalent liquid mixtures. The degree of saturation for HNO_3 and H_2O mixing ratios over $HNO_3.3H_2O$ was calculated for each point along the flight track using the ambient pressure and temperature measurements. If the calculated vapor pressures are reduced by a factor of 0.5 below 200 K, then saturation conditions coincide with a PSC as defined by elevated aerosol concentrations.

If the aerosol volume is assumed to be $HNO_3.3H_2O$ containing ~54% HNO_3 by mass, then the peak volume observed on the 17th was equivalent to ~4 ppbv of HNO_3. This represents nearly 50% of the NOy reservoir observed outside of the PSC region. The NOy level and the HNO_3 fraction both agree favorably with results from 2-D photochemical models.

The anisokinetic feature of the NOy sampling probe results in the enhancement of the concentration of aerosols in the inlet by a factor of ~6. NOy species incorporated in these aerosols evaporate in the heated inlet lines and add to the NOy gas phase level. The effective enhancement can be calculated along the flight track from the measured aerosol concentration and size distribution. This effective enhancement, the aerosol volume and assumed HNO3 mass fraction, and an estimate of the non-condensing fraction of the NOy reservoir can then be combined to predict the NOy signal. The resulting agreement between the measured and calculated NOy provides strong independent evidence that NOy species are incorporated in the PSC aerosol.

EXTINCTION AND BACKSCATTER MEASUREMENTS OF ANTARCTIC PSC'S, 1987: IMPLICATIONS FOR PARTICLE AND VAPOR REMOVAL

L. R. Poole, M. P. McCormick, and E. V. Browell
NASA Langley Research Center, Hampton, VA 23665-5225

C. R. Trepte, ST Systems Corporation, Hampton, VA 23666

D. W. Fahey and K. K. Kelly, NOAA Aeronomy Laboratory, Boulder, CO 80302

G. V. Ferry and R. Pueschel, NASA Ames Research Center, Moffett Field, CA 94035

R. L. Jones, U. K. Meteorological Office, Bracknell, United Kingdom

Observations since 1979 of aerosol extinction at 1.0 μm by the SAM II (Stratospheric Aerosol Measurement II) sensor have shown recurring synoptic-scale, optically thin clouds in both winter polar stratospheres (McCormick et al., 1982) which are highly correlated with cold temperatures (<195K). Steele et al. (1983) initially proposed that PSC's consist of pure ice particles forming at temperatures below the frost point, but subsequent papers (Toon et al., 1986; Crutzen and Arnold, 1986) proposed a preliminary stage of binary HNO_3-H_2O particles forming at temperatures above the frost point. These authors suggested that a large fraction of the gaseous NO_x reservoir in the Antarctic stratosphere could be depleted during such a process, thereby "preconditioning" the stratosphere for halogen-catalyzed ozone destruction.

Airborne lidar observations of Arctic PSC's by Poole and McCormick (1988a) support the idea of a two-stage (Types I and II) formation process. At temperatures above the frost point (the Type I regime) the authors found a signature indicative of particles significantly larger than the ambient aerosol, but probably of limited size (radii on the order of the lidar wavelength, ≈0.7 μm) and perhaps quasi-spherical in shape. In contrast, the authors found a signature typical of larger crystalline (Type II) particles in PSC's at temperatures near the frost point. In a separate paper, Poole and McCormick (1988b) gave theoretical results from a two-stage PSC microphysical model assuming Type I particles to be solid, fixed (stoichiometric) composition nitric acid trihydrate ($HNO_3 \cdot 3H_2O$) and Type II particles to be a homogeneous mixture of pure water ice and the trihydrate. The results compared favorably with the authors' Arctic experimental data and supported the earlier estimates by Toon et al. and Crutzen and Arnold that a large fraction of the ambient HNO_3 vapor supply could be consumed in the PSC formation process. Computed particle size distributions for Antarctic PSC's suggested that Type II particles may be large enough to fall rather quickly, thereby removing the condensed HNO_3 (i.e., gaseous NO_x) from the region in which the clouds were formed. Calculated optical properties also showed a distinctive temperature dependence, with threshold temperatures for Type I and Type II PSC particle formation being sensitive indicators of the HNO_3 and H_2O vapor supplies, and enhancements in extinction and backscatter (relative to those computed for the ambient aerosol) being closely related to the number and modal size of the PSC particles.

In this paper, we examine the temperature dependence of optical properties measured in the Antarctic during 1987 at the 70-mb level (near 18 km), a level chosen to correlate our results with in situ measurements made from the NASA Ames Research Center ER-2 aircraft during the 1987 Airborne Antarctic Ozone Experiment (AAOE). Our data set consists of extinction measurements by SAM II inside the

Antarctic polar vortex from May to October 1987; and backscatter measurements by the UV-DIAL (Ultraviolet Differential Absorption Lidar) system (Browell et al., 1983) aboard the Ames DC-8 aircraft during selected AAOE flights. We will compare observed trends with results from a revised version of Poole and McCormick's model (assuming variable-composition Type I PSC's; McElroy et al., 1986; Hanson and Mauersberger, 1988), to classify the PSC observations by Type (I or II) and infer the temporal behavior of the ambient aerosol and ambient vapor mixing ratios.

The sample figures show monthly ensembles of the 70-mb SAM II extinction ratio (the ratio of aerosol or PSC extinction to molecular extinction) as a function of NMC temperature at the beginning (June) and end (October) of the 1987 Antarctic winter. Both ensembles show two rather distinct clusters of points: one oriented in the near-vertical direction which depicts the change with temperature of the ambient aerosol extinction ratio; and a second cluster oriented in the near-horizontal direction whose position on the vertical scale marks a change in particle phase (i.e., PSC formation) and whose length (the extinction enhancement relative to that of the ambient aerosol) is an indicator of PSC type. Several points are of note: (1) The typical ambient aerosol extinction ratio is smaller by a factor 2-3 in October than in June, indicating a change in the ambient aerosol population due to subsidence or sedimentation (or both) over the course of the winter. We found that June values are approximated well by theoretical computations using an ambient aerosol size distribution derived from August ER-2 observations. (2) Most extinction enhancements observed in both months were of the order of 10 or smaller, signaling (by model calculations) Type I PSC's. (3) Type I PSC's occurred at 70-mb temperatures between 195-200K in June, suggesting HNO_3 and H_2O mixing ratios of 5-7 ppbv and 4-5 ppmv, respectively. These are similar to local pre-winter values measured by LIMS (Limb Infrared Monitor of the Stratosphere) in 1979 (Russell, 1986) and, for H_2O only, by SAGE II (Stratospheric Aerosol and Gas Experiment II) in 1987 (J Larsen, personal communication). (4) In contrast, Type I PSC's occurred at lower (by ≈5K) 70-mb temperatures in October, implying a marked reduction in ambient vapor mixing ratios over the winter. Our calculations suggest October mixing ratios of 1-2 ppbv for HNO_3 and ≈2 ppmv for H_2O, similar to those measured inside the vortex from the ER-2 during AAOE and (H_2O only) by SAGE II in October. We believe that the inferred changes in ambient vapor levels cannot possibly be attributed to subsidence, but must be due instead to losses via sedimentation of PSC particles.

Although our quantitative estimates are subject to uncertainties in the NMC temperatures and the saturation HNO_3 and H_2O vapor pressures used in our supporting calculations, we feel that the general trends shown here would be borne out by similar analyses using other data bases. The results strongly suggest that Antarctic PSC's act as a sink for HNO_3 and H_2O vapor, a process which, by examination of other monthly ensembles of SAM II data, appears to take place primarily during the August time frame.

References

Browell, E. V., A. F. Carter, S. T. Shipley, R. J. Allen, C. F. Butler, M. N. Mayo, J. H. Siviter, Jr., and W. M. Hall, 1983: NASA multipurpose airborne DIAL system and measurements of ozone and aerosol profiles. Appl. Opt., 22, 522-534.

Crutzen, P. J., and F. Arnold, 1987: Odd nitrogen incorporation in polar stratospheric clouds: A possible major cause for the springtime ozone decay in Antarctica. Nature, 324, 651-655.

Hanson, D., and K. Mauersberger, 1988: Laboratory studies of the nitric acid trihydrate: Implications for the south polar stratosphere. Submitted for publication to Geophys. Res. Lett.

McCormick, M. P., P. Hamill, T. J. Pepin, W. P. Chu, T. J. Swissler, and L. R. McMaster, 1979: Satellite studies of the stratospheric aerosol. Bull. Amer. Meteor. Soc., 60, 1038-1046.

McCormick, M. P., H. M. Steele, P. Hamill, W. P. Chu, and T. J. Swissler, 1982: Polar stratospheric cloud sightings by SAM II. J. Atmos. Sci., 39, 1387-1397.

McElroy, M. B., R. J. Salawitch, and S. C. Wofsy, 1986: Antarctic O_3: Chemical mechanisms for the spring decrease. Geophys. Res. Lett., 13, 1296-1299.

Poole, L. R., and M. P. McCormick, 1988a: Airborne lidar observation of Arctic polar stratospheric clouds: Indications of two distinct growth modes. Geophys. Res. Lett., 15, 21-23.

Poole, L. R., and M. P. McCormick, 1988b: Polar stratospheric clouds and the Antarctic ozone hole. J. Geophys. Res., in press.

Russell, J. M. III, ed., 1986: Middle Atmosphere Program, Handbook for MAP, Vol. 22, International Council of Scientific Unions Scientific Committee on Solar-Terrestrial Physics (SCOSTEP), 302 pp.

Steele, H. M., P. Hamill, M. P. McCormick, and T. J. Swissler, 1983: The formation of polar stratospheric clouds. J. Atmos. Sci., 40, 2055-2067.

Toon, O. B., P. Hamill, R. P. Turco, and J. Pinto, 1986: Condensation of HNO_3 and HCl in the winter polar stratospheres. Geophys. Res. Lett., 13, 1284-1287.

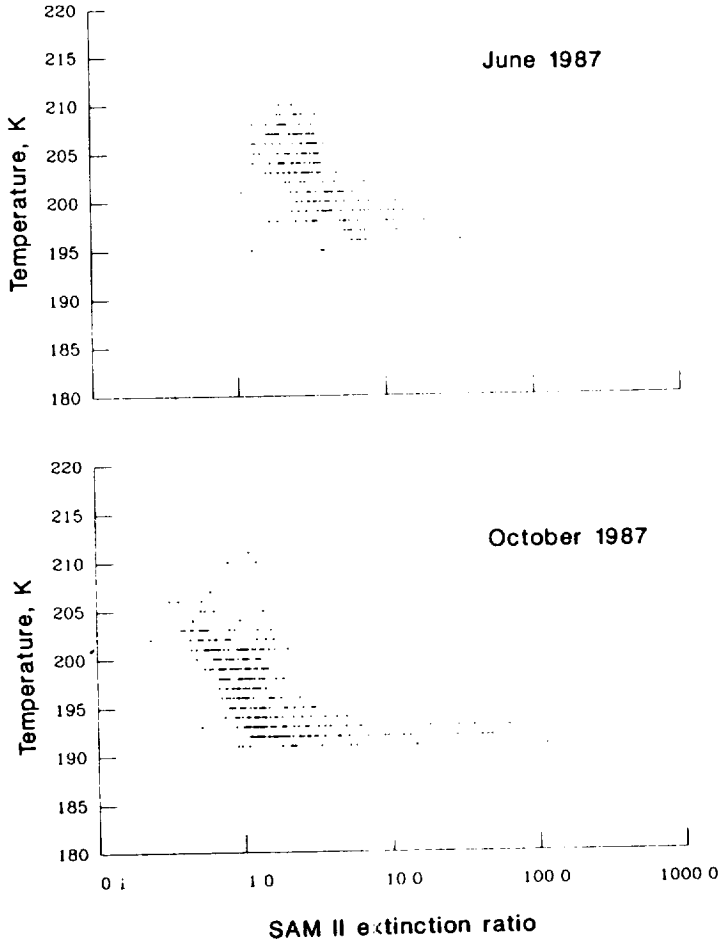

Ensembles of SAM II extinction ratio at 70 mb inside the Antarctic polar vortex, June and October 1987.

Laboratory Studies of HNO_3/H_2O Mixtures at Low Temperatures

David Hanson and Konrad Mauersberger

University of Minnesota, Minneapolis, Minn. 55455

The possibility of stratospheric HNO_3 condensing out of the gas-phase at low temperatures has become important in the chemical explanations of the rapid loss of antarctic ozone in spring. Consequently, knowledge about the behavior of the vapor pressures of H_2O and HNO_3 over HNO_3/H_2O mixtures at stratospheric temperatures is needed to determine if HNO_3 could condense, and by how much the HNO_3 vapor pressure could be depressed.

This paper describes laboratory investigations of vapor pressures above HNO_3/H_2O mixtures. Vapor pressures were initially measured over liquid and frozen bulk mixtures contained in a glass still which was attached to a stainless steel vacuum chamber. The total pressure in the chamber was monitored with a precision pressure sensor, and the vapor pressures of HNO_3, H_2O and impurities were analyzed with a mass spectrometer-beam system (1).

In a second set of experiments vapor deposits were made to produce ice and the mono- and trihydrate of HNO_3.

Temperatures of liquid and frozen HNO_3/H_2O bulk mixtures were varied from 200 to 260 K. The measured vapor pressures of HNO_3 and H_2O are in fairly good agreement with Clavelin and Mirabel's vapor pressure data (2) when extrapolated toward lower temperatures. For partially frozen bulk mixtures, the three phase equilibria solid/liquid/vapor and for frozen mixture trihydrate/monohydrate/vapor and trihydrate/ice/vapor were also investigated. These all resulted in one vapor pressure curve for both H_2O

and HNO_3 as expected from binary mixtures. The measured pressures for the freezing envelope (solid/liquid/vapor) were in close agreement with data obtained from freezing temperatures (3) and Clavelin and Mirabel's data (2).

Vapor deposits to form the trihydrate are initially made by establishing a 3-to-1 H_2O/HNO_3 gas mixtures in the vacuum chamber and rapidly cooling the glass still. Initially a thin, amorphous film over the whole glass surface is formed, which then changes to small crystalline structures. HNO_3 and H_2O vapor pressures have been determined for temperatures between 190 and 205 K. In addition, studies of the relevant solid/solid/vapor three-phase equilibria were again performed using vapor deposition to form the condensed phases. The ice/trihydrate/vapor equilibrium pressures were measured up to the eutectic temperatures of 230 K and a better determination of the HNO_3 pressure has been made. The H_2O pressure was essentially that of ice which was also found during bulk measurements. The trihydrate/monohydrate/vapor equilibrium was studied from 190 to 200 K and the vapor pressures were in general agreement with those measured over frozen bulk mixtures. As expected, the vapor pressures over the trihydrate lay in the region between these two three-phase equilibria and the H_2O and HNO_3 pressures over the trihydrate were seen to be well correlated.

From these data it can be concluded that the lower stratosphere becomes saturated with respect to the trihydrate about 5 K above the ice-saturation point. A strong temperature-dependence of the HNO_3 pressure over the trihydrate can also be demonstrated. As the temperature is lowered by 3 degrees and the H_2O pressure is kept constant, the equilibrium HNO_3 pressure over the trihydrate is lowered by a factor between 5 and 9. For comparison,

the HNO_3 pressure over the ice/trihydrate/vapor equilibrium is lowered by a factor of approximately 2 after a 3 degree cooling. This temperature dependence could lead to a wide variation in the local HNO_3 pressure and consequently to localized ozone destruction.

References

(1) K. Mauersberger, Rev. Sci. Instrum. 48, 1169 (1977).

(2) J.L. Clavelin and P. Mirabel, J. de Chim. Physique 76, 533 (1979).

(3) F.W. Kuster and R. Kremann, Z. amorg. Chem. 41, 1 (1904).

Evolution of Polar Stratospheric Clouds during the Antarctic Winter

V. Ramaswamy

Atmospheric and Oceanic Sciences Program

Princeton University

Princeton, NJ 08542.

The occurence of Polar Stratospheric Clouds (PSCs), initially inferred from satellite measurements of solar extinction, have now also been noted by the recent scientific expeditions in the Antarctic. The presence of such clouds in the Antarctic has been postulated to play a significant role in the depletion of ozone during the transition from winter to spring. The mechanisms suggested involve both dynamical and chemical processes which, explicitly or implicitly, are associated with the ice particles constituting the PSCs. It is, thus, both timely and necessary to investigate the evolution of these clouds and ascertain the nature and magnitude of their influences on the state of the Antarctic stratosphere.

To achieve these objectives, a detailed microphysical model of the processes governing the growth and sublimation of ice particles in the polar stratosphere has been developed, based on the investigations of Ramaswamy and Detwiler (Journal of the Atmospheric Sciences, 1986). The present studies focus on the physical processes that occur at temperatures below those required for the onset of ice deposition from the vapor phase. Once these low temperatures are attained, the deposition of water vapor onto nucleation particles becomes extremely significant.

First, the factors governing the magnitude of growth and the growth rate of ice particles at various altitudes are examined. These include the sizes and concentrations of the nucleation agents, and the temperature and water vapor profiles (which determine the saturation conditions). It is possible, for example, to predict whether ice growth or sublimation will occur at a given location and instant during the Antarctic winter, based on the temperature profile.

Second, the ice phase mechanisms are examined in the context of a column model with altitudes ranging from 100 to 5 mb. pressure levels. The model considers explicitly the growth and sublimation processes as well as the fallspeeds of the particles at different altitudes. Particles of different sizes and concentrations are considered, as given by a lognormal distribution. Particles of specific sizes are followed as they grow, decay or fall; no attempt is made to categorise them into bins of definite size range. This, in effect, implies that all particles, initially at specified levels in the column model, are continuously monitored. The forcing for the temporal evolution of the model is the time rate of decrease of temperature. Values considered include those appropriate during July, August and September in the Antarctic stratosphere. Various temporal resolutions have been considered to perform these

simulations, ranging from 1/2 minute to a hour. The principal features are the dependence of the cloud evolution on the rate of temperature decrease, water vapor mixing ratios and the particle characteristics. It is also seen that rapid changes in temperature cause rapid changes in the sizes of the ice particles.

In the third stage of the study, the column microphysical model has been used to perform simulations of the cloud evolution, using the observed daily temperatures. The simulations commence from June 1 and last till end of September; different years and geographical locations are considered in this part of the sensitivity study. The results indicate that particles grow large as a result of the ice deposition and, under favorable conditions, can fall down considerable distances. This, in effect, implies a depletion of water vapor and a reduction in the number concentration of nucleating particles at the higher altitudes of occurence of PSCs. These simulations are compared with the temporal evolution of the extinction measurements, as observed by the SAGE satellite.

The effects due to the growth of the particles on the radiation fields are also investigated using a one-dimensional radiative transfer model. Specifically, the perturbations in the longwave cooling and that in the shortwave heating for the late winter/early spring time period are analyzed.

HETEROGENEOUS PHYSICOCHEMISTRY OF THE WINTER POLAR STRATOSPHERE

R. P. Turco (R&D Associates, Marina del Rey, CA 90295)
O. B. Toon (NASA Ames Research Center, Moffett Field, CA 94035)

Present chemical theories of the antarctic ozone hole assume that heterogeneous reactions involving polar stratospheric clouds (PSC's) are the precursor of springtime ozone depletions. However, none of the theories quantify the rates of proposed heterogeneous processes, and none utilize the extensive data base on PSC's. Thus, all of the theories must be considered incomplete until the heterogeneous mechanisms are properly defined. This paper develops a unified treatment of the cloud related processes, both physical and chemical, and calibrates the importance of these processes using observational data. We also compare the rates of competitive heterogeneous processes to place reasonable limits on critical mechanisms such as the denitrification and dechlorination of the polar winter stratosphere. Among the subjects addressed here are the physical/chemical properties of PSC's, including their relevant microphysical, optical and compositional characteristics, mass transfer rates of gaseous constituents to cloud particles, adsorption, accommodation and sticking coefficients on cloud particles, time constants for condensation, absorption and other microphysical processes, effects of solubility and vapor pressure on cloud composition, the statistics of cloud processing of chemically-active condensible species, rate-limiting steps in heterogeneous chemical reactions, and the nonlinear dependence of ozone loss on physical and chemical parameters.

For purposes of analysis, we distinguish two distinct types of PSC's, which we refer to as Type-I and Type-II PSC's. These cloud types have distinct properties that lead

to different rates for specific mechanical and chemical processes (see Table 1). Such distinctions have been neglected in previous theoretical models of the ozone hole. The Type-I PSC's are apparently composed of nitric acid ices. The thermodynamics and physical chemistry of such ices suggests that the nitric acid trihydrate may be the predominant form, although laboratory spectroscopic evidence also points to the formation of impure and amorphous ice structures under conditions similar to those found in the polar winter stratosphere. Type-II clouds are most likely composed primarily of water ice. The Type-II clouds have a substantially larger particle mass than Type-I PSC's, and are probably responsible for the observed dehydration and denitrification of the polar winter stratosphere in the region of the ozone hole. Type-I clouds, on the other hand, may be dominant in catalyzing heterogeneous reactions that lead to the observed repartition of HCl, $ClONO_2$, and ClO. The frequency of occurrence of Type-I PSC's is roughly an order of magnitude greater than that of Type-II PSC's. Type-I clouds also fill a greater volume of the polar vortex over the course of winter.

The time constant for HCl absorption into ice particles is several hours or more in PSC's of either type. Although Type-I clouds may have only about 1% of the mass of Type-II clouds, they still have 10% or more of the surface area. The mass transfer rates of HCl to Type-I and II clouds occurs in different dynamical regimes: in Type-I clouds the HCl molecules reach ice surfaces by gas-kinetic transport; in Type-II clouds the HCl molecules diffuse toward particle surfaces in the transition flow regime lying between purely gas-kinetic and purely continuum flow. Gas-kinetic transport provides the more efficient mass transfer mechanism.

The removal of stratospheric trace gases condensed on PSC particles (e.g., HNO_3, H_2O and HCl) depends on the vapor

pressures of the condensates, the masses of condensates, the fallspeed of the particles, and the frequency and duration of cloud formation. The Type-I PSC ice particles have a gravitational fall velocity that is too low to account for the removal of substantial quantities of trace materials on short time scales (i.e., days to weeks). Nevertheless, the continuous sedimentation of these clouds over the course of winter can transfer materials downward by several kilometers on average. The measured particle sizes in Type-II clouds, by contrast, are large enough to carry condensed materials downward by several kilometers on time scales of hours to days.

The concentrations of trace constituents absorbed in ice particles also differs between the cloud types. In Type-I clouds, the HCl concentration could be ~1% by mass and the HNO_3 concentration ~50% by mass, while in Type-II clouds both the HCl and HNO_3 concentrations would be expected to lie below ~0.1% by mass. Such differences in concentrations are important in determining the rates of the heterogeneous chemical processes that involve chlorine species. For example, the short residence times and relatively low HCl concentrations of Type-II cloud particles implies that the reaction of $ClONO_2$ with condensed HCl might not proceed to completion in Type-II clouds. The competition between the processes of HCl condensation, HCl removal by cloud particle sedimentation, and HCl reaction with <u>in situ</u> $ClONO_2$ is thus sensitively dependent on the evolution of the Type-II PSC's and the dependence of the $ClONO_2$/HCl reaction rate on the trace composition of the ice. The estimated time constants for a number of heterogeneous chemical processes are compared in Table 1.

A number of other topics will be discussed, including the relationship between the time constants for heterogeneous processes and the long-term evolution of the ozone hole.

TABLE 1. POLAR STRATOSPHERIC CLOUD PROPERTIES AND TIME CONSTANTS

Property	Type-I	Type-II	Type-III[1]
Composition	$HNO_3/3H_2O$	H_2O+Trace[2]	H_2O+Trace[2]
Mass	~1 ppbm	$\lesssim$1 ppmm	~1 ppmm
Surface[3] Area	$\sim 10^{-8}$ cm^2/cm^3	$\sim 10^{-7}$ cm^2/cm^3	$\sim 10^{-5}$ cm^2/cm^3
Temperature Threshold[4]	~195 K	~187 K	~187 K
Relative Frequency[5]	~90%	~10%	~1%
Particle Diameter	~1 μm	~10-100 μm	~5 μm
Genesis Time[6]	$\sim 10^5$ sec	$\sim 10^3$-10^4 sec	$\sim 10^3$ sec
Cloud Particle Lifetime[7]	$\sim 10^5$-10^6 sec	$<10^5$ sec	$\sim 10^3$ sec
Time to Fall 1 km	$\sim 1\times10^7$ sec	$\sim 3\times10^3$-3×10^5 sec	$\sim 1\times10^6$ sec
HCl Absorption[8] Time	$\sim 1\times10^5$ sec	$\sim 1\times10^5$ sec	$\sim 10^2$-10^3 sec
HCl Concentration[9]	~0.01 g/g	~0.001 g/g	~0.001 g/g
$ClONO_2$ + HCl[10]	$\sim 1\times10^5$ sec	$\sim 2\times10^5$ sec	$\sim 10^3$ sec
$ClONO_2$ + H_2O[11]	$\sim 1\times10^6$ sec	$\sim 2\times10^5$ sec	$\sim 10^3$ sec
N_2O_5 + H_2O[12]	$\sim 2\times10^6$ sec	$\sim 4\times10^5$ sec	$\sim 10^3$ sec
N_2O_5 + HCl[13]	$\sim 2\times10^6$ sec	$\sim 4\times10^5$ sec	$\sim 10^3$ sec

Footnotes

1. These are lee wave clouds, similar in character to Type-II PSC's, which are formed near orographic features. The Type-III clouds may be considered as a subset of the Type-II clouds with shorter lifetimes and stronger geographical localization.
2. The ice will contain traces of a number of soluble gases such as HCl, HNO_3, HF and H_2SO_4, and the ice surfaces will hold many adsorbed vapors such as H_2O, $ClONO_2$, N_2O_5 and HOCl.
3. Total particle surface area per unit volume of air.
4. The temperature threshold corresponds to the local frost point of water for Type-II and III clouds, which varies with the ambient pressure for a fixed water vapor mixing ratio.
5. Based on a preliminary statistical analysis of SAM II satellite measurements of PSC extinction during hundreds of sunrise and sunset events. A fraction of the Type-I clouds may be denser, but localized, Type-II and III clouds.
6. The formation time of Type-II clouds depends sensitively on the local water vapor supersaturation and its variation with time. The values shown roughly correspond to an average supersaturation of ~1%.
7. For Type-I clouds, the lifetime is limited by dynamical (cooling) processes, for Type-II clouds, by particle fallout, and for Type-III clouds, by dynamical (lee wave) processing.
8. Assuming the HCl is absorbed into pre-existing ice particles with a "sticking coeficient", or accommodation coefficient, of 0.4 (Leu, 1988). If the HCL co-condenses with the clouds, then the absorption time is similar to the "Genesis Time" given above.
9. The HCl concentration in Type-I cloud particles is estimated using vapor pressures over solid solutions of HCl in pure water ice as determined in recent laboratory studies (Molina et al., 1987). The vapor pressures of HCl over concentrated nitric acid ices are unknown, but are expected to be similar to those for pure water ice. The concentration of HCl in Type-II and III clouds is estimated assuming nearly complete absorption of ambient HCl vapor to form solid solutions in the ice, which is consistent with the measured solubility of HCl in ice (Molina et al., 1987).
10. Reaction time of $ClONO_2$ for the HCl concentrations given in this table and a $ClONO_2$ "sticking coefficient" (or reaction efficiency per collision, in this case) of 0.25 for Type-I clouds (Leu, 1988) and 0.02 for Type-II clouds; the latter value is an extrapolation to low HCl concentrations based on data from Leu (1988), Molina et al., 1987) and Tolbert et al., 1987). The estimated reaction times do not take into account competitive chemical and physical processes, and assumes ideal and uniform surface properties.
11. Assuming a $ClONO_2$ "sticking coefficient" of 0.02 for for pure ice (Type-II and III clouds) as well as nitric acid trihydrate ice (Type-I clouds) in the presence of excess environmental (condensed) water vapor. Measured values of the sticking coefficient on pure ice range from ~0.009 @ 185 K (Tolbert et al., 1987), to ~0.02 @ 200 K (Molina et al., 1987), to ~0.06 @ 200 K (Leu, 1988).
12. Assuming an N_2O_5 "sticking coefficient" of 0.01 for ice surfaces in the presence of excess environmental water vapor; this value may represent a lower limit for the reaction on pure ice at temperatures of ~190-200 K (M.-T. Leu, prvt. comm., 1988).
13. Adopting an estimated N_2O_5 "sticking coefficient" of 0.01 for all types of PSC cloud surfaces and HCl concentrations (see Footnotes 11 and 12).

Physical Processes in Polar Stratospheric Ice Clouds

Owen B. Toon, NASA Ames Research Center, Moffett Field, CA 94035
Richard Turco, R&D Associates, Marina del Rey CA 90295
Joseph Jordan, Sterling Inc., Palo Alto CA 94304

A one dimensional model of cloud microphysics has been used to simulate the formation and evolution of polar stratospheric ice clouds. Some of the processes which are included in the model are outlined in Fig. 1 to 3. It is found that the clouds must undergo preferential nucleation upon the existing aerosols just as do tropospheric cirrus clouds. Therefore, there is an energy barrier between stratospheric nitric acid particles and ice particles implying that nitric acid does not form a continuous set of solutions between the trihydrate and ice. The Kelvin barrier is not significant in controlling the rate of formation of ice particles. We find that the cloud properties are sensitive to the rate at which the air parcels cool. In wave clouds, with cooling rates of hundreds of degrees per day, most of the existing aerosols nucleate and become ice particles. Such clouds have particles with sizes on the order of a few microns, optical depths on the order of unity and are probably not efficient at removing materials from the stratosphere. In clouds which form with cooling rates of a few degrees per day or less, only a small fraction of the aerosols become cloud particles. In such clouds the particle radius is larger than 10μm, the optical depths are low and water vapor is efficiently removed. Seasonal simulations (Fig 4, 5) show that the lowest water vapor mixing ratio is determined by the lowest temperature reached, and that the time when clouds dissappear is controlled by the time when temperatures begin to rise above the minimum values. Hence clouds occur in the early winter at temperatures which are higher than those at which clouds occur in the late winter. The altitude of the clouds declines during the winter because the temperatures in the Antarctic increase earlier at the higher altitudes. The rate of decline of cloud altitude is not an indication of particle fall speed or of vertical air motion as had been previously suggested. The ice clouds are not able to remove a significant amount of nitric acid through physical process such as coagulation or nucleation. Such removal must occur through other processes not included in our simulations such as vapor phase transfer. A considerable amount of further work could be done to improve upon our simulations. Improvements would include a

treatment of the three dimensional structure of wave clouds, a more complete treatment of the interactions between clouds and atmospheric motions on the seasonal time scale, and a treatment of the nitric acid vapor phase interactions with ice particles. Laboratory studies of the vapor pressures of water and nitric acid above ice crystals are needed. In addition laboratory investigations of the ice nucleating properties of nitric acid crystals would be useful. Direct observations of the sizes and concentrations of the particles in clouds formed over a few day time period are not available and are important to obtain since these dominate the sedimentation removal process.

Figure Captions

Fig. 1 Illustrated are the basic components of the cloud physics model. The preexisiting nitric acid aerosols nucleate to form impure ice crystals. These ice crystals grow by condensation of water. Once formed the ice particles begin to sediment, removing materials from the stratosphere. The model is one dimensional.

Fig. 2 Illustrated is the time required for hexagonal columns which are three times as long as they are wide to fall a distance of 1 km starting at altitudes of 20 km or 12 km. The fall time is not a strong function of the altitude, but it does vary greatly with the radius of the particles. Since ice clouds will generally have lifetimes on the order of a few days due to the varying temperatures experienced by air parcels as they move around the vortex, particle sizes on the order of 10μm are needed for substantial removal to occur during the lifetime of a cloud.

Fig. 3 Illustrated is the time required for a hexagonal column to double or half its size at a supersaturation of 100% assuming that 5ppmv of water vapor is present. When growth occurs the supersaturation will be reduced. In rapidly cooling clouds with many particles the supersaturation will become less than 1% and sizes will be limited. In slowly cooling clouds with a small number of particles the supersaturation may remain at the 10% level and large particles can form.

Fig. 4 Simulations of the seasonal evolution of ice cloud backscatter are compared with observations from the Syowa station in 1983 (Iwasaka et al., Geophys. Res. Lett. 13,1407,1986). With no energy barrier (m=1) all of the particles nucleate, clouds with optical depths

greater than 1 form and the clouds have more backscatter than observed. With a modest energy barrier (m=.95) only a few particles form , optical depths are order 10^{-2} and the backscatter is of the magnitude observed.

Fig. 5 The clouds are able to remove water vapor very effectively. Therefore the timing of water vapor removal and the amount of water removal are controlled by the temperatures. A further 2 degree cooling would have reduced the water to 2ppmv.

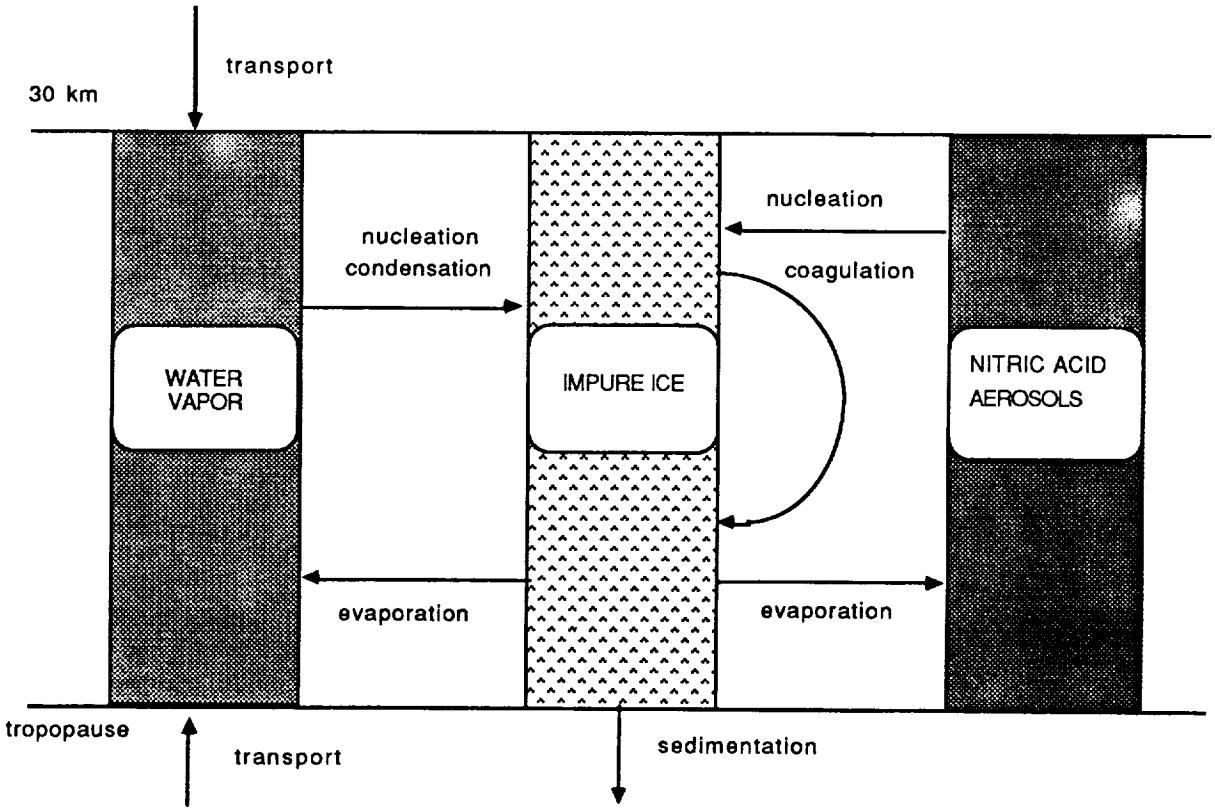

Fig. 1

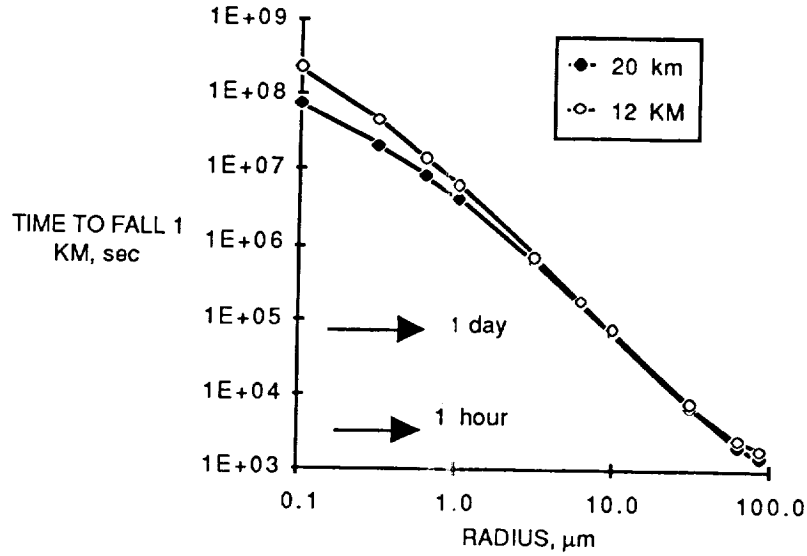
1E+09
1E+08
1E+07
1E+06
1E+05
1E+04
1E+03
TIME TO FALL 1 KM, sec
20 km
12 KM
1 day
1 hour
0.1
1.0
10.0
100.0
RADIUS, μm

Fig. 2

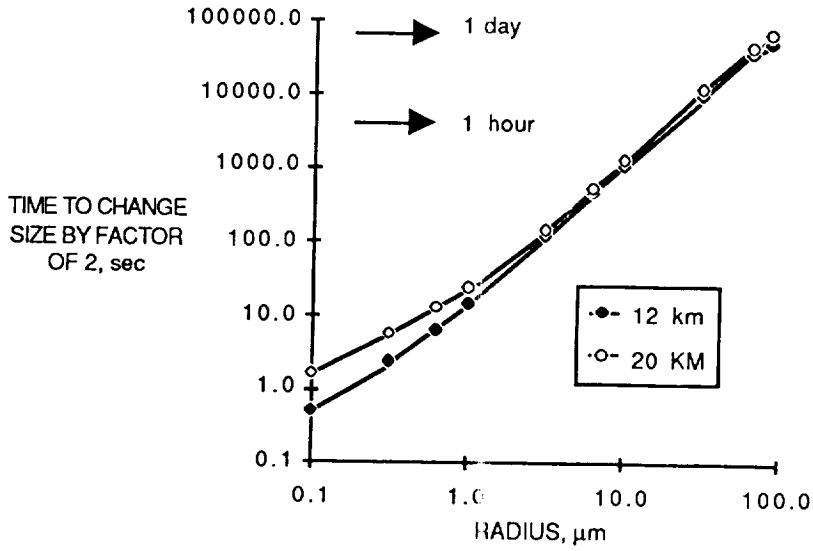
100000.0
10000.0
1000.0
100.0
10.0
1.0
0.1
TIME TO CHANGE SIZE BY FACTOR OF 2, sec
1 day
1 hour
12 km
20 KM
0.1
1.0
10.0
100.0
RADIUS, μm

Fig. 3

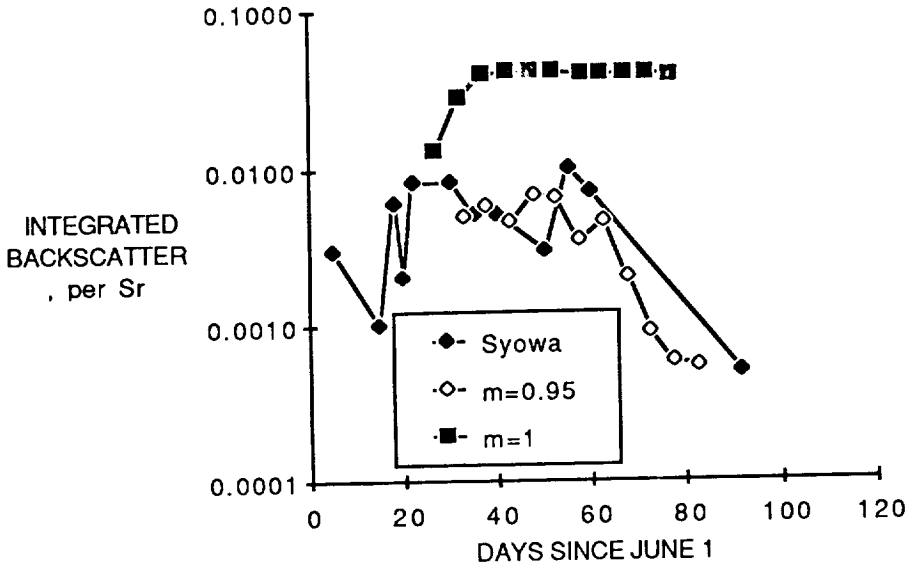
0.1000
0.0100
0.0010
0.0001
INTEGRATED BACKSCATTER , per Sr
Syowa
m=0.95
m=1
0
20
40
60
80
100
120
DAYS SINCE JUNE 1

Fig. 4

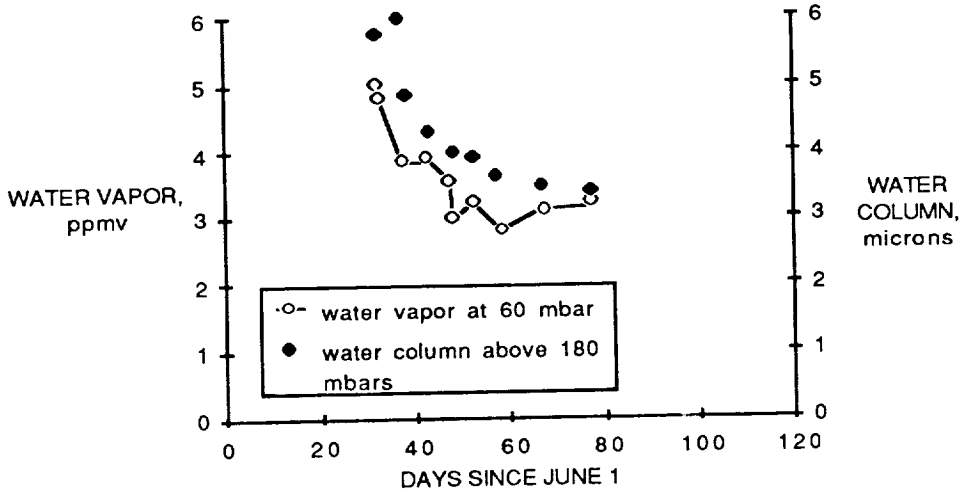
WATER VAPOR, ppmv
WATER COLUMN, microns
water vapor at 60 mbar
water column above 180 mbars
0
1
2
3
4
5
6
0
20
40
60
80
100
120
DAYS SINCE JUNE 1

Fig. 5

HETEROGENEOUS CHEMISTRY RELATED TO ANTARCTIC OZONE DEPLETION: REACTION OF $ClONO_2$ AND N_2O_5 ON ICE SURFACES

Margaret A. Tolbert, Michel J. Rossi, and David M. Golden
Department of Chemical Kinetics, Chemical Physics Laboratory
SRI International, Menlo Park CA 94025

Laboratory studies of heterogeneous reactions of possible importance for Antarctic ozone depletion have been performed. In particular, the reactions of chlorine nitrate ($ClONO_2$) and dinitrogen pentoxide (N_2O_5) have been investigated on ice and HCl/ice surfaces. Reactions 1 and 2, proposed to

$$ClONO_2 + H_2O \rightarrow HNO_3 + HOCl \quad (1)$$

$$ClONO_2 + HCl \rightarrow HNO_3 + Cl_2 \quad (2)$$

occur on the surfaces of polar stratospheric clouds (PSCs) over Antarctica,[1] transform the stable chlorine reservoir species ($ClONO_2$ and HCl) into photochemically active chlorine in the form of HOCl and Cl_2. Condensation of HNO_3 in the above reactions removes odd nitrogen from the stratosphere, a requirement in nearly all models of Antarctic ozone depletion.[1-4]

Reactions 3 and 4 may also be important for Antarctic ozone depletion.

$$N_2O_5 + H_2O \rightarrow 2\ HNO_3 \quad (3)$$

$$N_2O_5 + HCl \rightarrow HNO_3 + ClNO_2 \quad (4)$$

Like the reactions of chlorine nitrate, these reactions deplete odd nitrogen through HNO_3 condensation. In addition, reaction 4 converts a stable chlorine reservoir species (HCl) into photochemically active chlorine ($ClNO_2$). Reactions 1 - 4 were studied with a modified version of a Knudsen cell flow reactor.[5]

Heterogeneous Reactions of Chlorine Nitrate on Ice

Chlorine nitrate reacted readily with H_2O and HCl on ice surfaces at 185 K. Upon exposure of an ice surface to $ClONO_2$, gas phase HOCl was detected (reaction 1). Formation of gaseous Cl_2O was also observed. As discussed in [6], Cl_2O is thought to be formed in a secondary reaction. The other product of reaction 1, HNO_3, is not observed in the gas phase. However, when the surface is slowly warmed, HNO_3 is detected in thermal desorption spectrometry (TDS). Thus reaction 1 on ice produces gas phase HOCl and condensed phase HNO_3. The sticking coefficient for $ClONO_2$ on ice measured using m/e 46 is determined as 0.009 ± 0.002 (1 standard deviation).

The reaction of $ClONO_2$ with HCl on ice, reaction 2, may be especially important in the Antarctic stratosphere because it converts two chlorine reservoir species into photochemically active Cl_2. We and others[7,8] have observed this reaction to proceed readily. This reaction was studied on a surface prepared by co-condensing a 7:1 ratio of H_2O:HCl onto a wax-coated copper block at 185 K. When $ClONO_2$ was introduced into the Knudsen cell containing this

surface, gas phase Cl_2 was formed. Cl_2 does not stick to, or react with, ice at 185 K. The reaction of $ClONO_2$ on HCl/ice proceeded until at least 95% of the total deposited HCl was depleted, indicating rapid diffusion of HCl in ice.[7] As was the case for reaction 1, HNO_3 formed via reaction 2 was observed in TDS after the reaction by slowly warming the sample.

Heterogeneous Reactions of Dinitrogen Pentoxide on Ice

Dinitrogen pentoxide reacted readily with ice and HCl/ice at 185 K. When N_2O_5 was exposed to ice at this temperature, loss of N_2O_5 was indicated by a large decrease in the m/e 46 mass spectrometer signal. No new mass signals were observed in this reaction. Assuming that only N_2O_5 contributes to m/e 46, the sticking coefficient for N_2O_5 on ice is determined as 0.001 (± 50% in 10 determinations). To the extent that other species contribute to m/e 46, this should be considered a lower limit to the true value.

The product of reaction 3, HNO_3, was observed after the reaction in TDS. Figure 1a displays the nitric acid TDS signal after reaction of N_2O_5 on ice for 15 minutes at 185 K. Two desorption peaks are observed. Studies indicate that the lower temperature peak is due to overlayers of HNO_3, and the higher temperature peak is due to hydrates of HNO_3.[9] Figure 1b displays the HNO_3 signal after exposure of N_2O_5 at the same pressure to halocarbon wax-coated copper for 15 minutes at 185 K. The small signal in this figure is thought to be due to impurity HNO_3 in the N_2O_5. It can be seen that the HNO_3 produced from reaction 3 is much more abundant than that due to impurity.

The reaction of N_2O_5 with HCl was studied on a cold wax-coated copper surface and on ice. The Knudsen cell effluent for the reaction of N_2O_5 with HCl on waxed copper at 185 K is shown in Figure 2a. For comparison, the mass spectrum of $ClNO_2$ is shown in Figure 2b. The similarity in these two spectra suggests that $ClNO_2$ is a gas phase product of reaction 4. Similar spectra were obtained for the reaction of N_2O_5 on HCl/ice surfaces at 185 K. $ClNO_2$ did not stick to, or react with, ice at 185 K. As was the case for the reaction of $ClONO_2$ with HCl, reaction 4 proceeded until essentially all of the HCl in the ice was depleted. HNO_3 was observed in the ice after reaction using TDS.

Heterogeneous Reactions on Acidic Surfaces

As discussed above, reactions 1 - 4 proceed readily on ice surfaces at 185 K. Reaction 1 has also been studied on several acidic surfaces that may be more representative of the PSCs over Antarctica. It was found that reaction 1 occurs on only certain nitric acid/ice surfaces at 185 K. Of surfaces prepared by co-condensation of 1:2, 2:1, and 4.5:1 mixtures of H_2O:HNO_3, only the latter one promoted reaction 1.[6] These results suggest a critical amount of water is needed for the reaction to proceed.

Reaction 1 was also studied on sulfuric acid surfaces. It was found that this reaction proceeded readily on 95% H_2SO_4 at room temperature.[10] This reaction did not, however, occur on 95% H_2SO_4 at 185 K.[6] We are currently investigating reactions 1 and 2 on low temperature sulfuric acid surfaces of varying composition (65 - 85% H_2SO_4). The effects of temperature and acid concentration on the reaction efficiencies will be discussed.

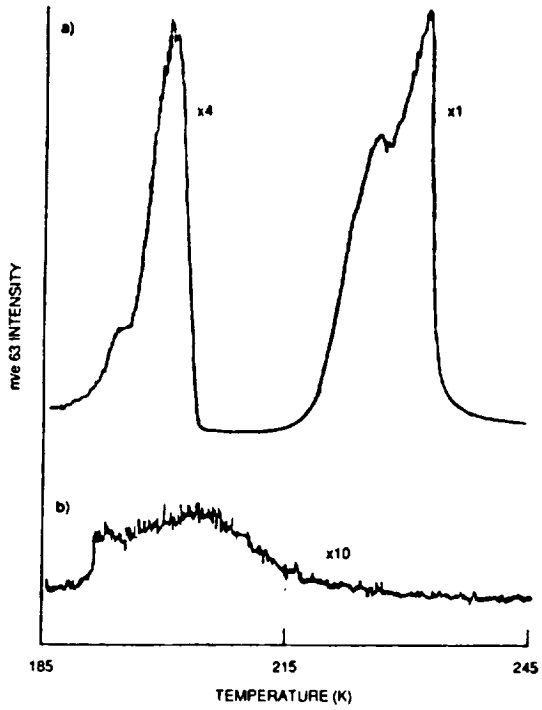

Figure 1 TDS scans of HNO_3 after a) exposure of ice to N_2O_5 (P = 1 mTorr) for 15 minutes and b) exposure of cold wax-coated copper to N_2O_5 at the same pressure for the same time.

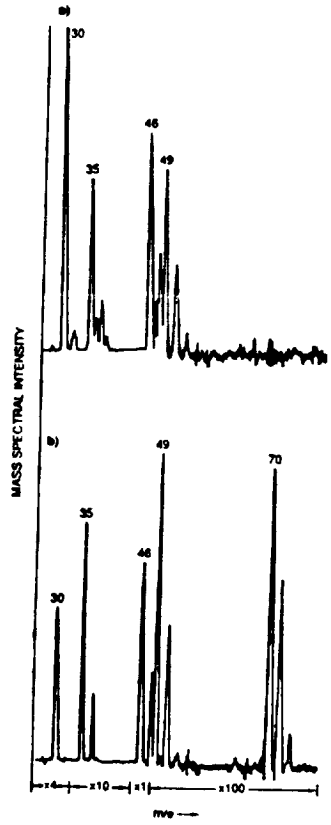

Figure 2 Mass scans for the Knudsen cell effluent for a) the reaction of N_2O_5 with HCl on wax-coated copper at 185 K and b) gas phase $ClNO_2$ with a 5% Cl_2 impurity.

References

1. S. Solomon, R. R. Garcia, F. S. Rowland, D. J. Wuebbles, Nature (London), 321, 755 (1986).
2. P. J. Crutzen and F. Arnold, Nature (London), 324, 51 (1986).
3. M. B. McElroy, R. J. Salawitch, S. C. Wofsy, Geophys. Res. Lett., 13, 1296 (1986).
4. O. B. Toon, P. Hamill, R. P. Turco, and J. Pinto, Geophys. Res. Lett., 13, 1284 (1986).
5. D. M. Golden, G. N. Spokes, S. W. Benson, Angew. Chem. Int. Ed. Engl., 12, 534 (1973).
6. M. A. Tolbert, M. J. Rossi, R. Malhotra and D. M. Golden, Science, 238, 1258 (1987).
7. M. J. Molina, T. L. Tso, L. T. Molina, F. C. Y. Wang, Science, 238, 1253, (1987).
8. M. T. Leu, Geophys. Res. Lett., 15, 17 (1988).
9. M. A. Tolbert, M. J. Rossi and D. M. Golden, Science, in press.
10. M. J. Rossi, R. Malhotra, D. M. Golden, Geophys. Res. Lett., 14, 127 (1987).

Mass Accomodation Coefficient Measurements for HNO_3, HCl and N_2O_5 on Water, Ice and Aqueous Sulfuric Acid Droplet Surfaces

Doulgas Worsnop, Mark Zahniser and Charles Kolb
Aerodyne Research, Inc., 45 Manning Road, Billerica, MA 01821

Lyn Watson, Jane Van Doren, John Jayne and Paul Davidovits
Department of Chemistry, Boston College, Chesnut Hill, MA 02167

We report preliminary results of the direct measurement of accommodation coefficients for HNO_3, N_2O_5 and HCl on water drops, aqueous sulfuric acid drops and ice particles. The heterogeneous chemistry of these species together with $ClONO_2$ has been implicated in the ozone depletion observed in the antarctic stratosphere during the spring in the last eight years. The most plausible chemical mechanism involves the removal of nitrogen oxide species via condensation on ice particles in polar stratospheric clouds resulting in an increase in the active chlorine species responsible for the ozone depletion. The observation of low NO_2 and high ClO densities in the antarctic stratosphere last summer appear to be consistent with such a mechanism.

This heterogeneous mechanism is also supported by ground breaking laboratory experiments at JPL (Molina et. al., 1987) and SRI (Tolbert et. al., 1987) which showed that key reactions have sufficiently large probability (> 10^{-3}) on ice surfaces at 200 K to be important in the antarctic stratosphere:

$$N_2O_5 + H_2O(s) \rightarrow 2HNO_3(s)$$

$$ClONO_2 + H_2O(s) \rightarrow HOCl(g) + HNO_3(s)$$

$$ClONO_2 + HCl(s) \rightarrow Cl_2(g) + HNO_3(s)$$

These reactions have the net effect of freeing active chlorine and removing odd nitrogen in the form of condensed nitric acid. However, because gas phase diffusion limits the rate of mass transport to the macroscopically large surfaces used in these experiments, many of the details of the surface reaction kinetics were unresolved in these first experiments. Furthermore, the combination of laboratory gas densities that are much larger than those in the atmosphere and the long gas/surface contact times (> 0.1 sec) may lead to surface saturation effects that are not representative of atmospheric conditions. There is also a need to extend heterogeneous reaction studies to sulfuric acid surfaces which are characteristic of global stratospheric aerosols.

Our experimental technique can directly measure heterogeneous uptake rates of gases corresponding to accommodation coefficients from 10^{-4} to 0.3 and larger. A measured flow of trace gas is exposed to a fast moving (20 meter/s) stream of droplets. The droplet stream provides a continuously renewed surface of well defined area. Depletion of trace gas is measured as a function of surface area to which the gas is exposed. Although laboratory gas densities are still larger than in the stratosphere, the potential for surface saturation effects is reduced by limiting the time of contact between the surface and trace gas to a millisecond or less. Operation at low pressure (down to 2 torr) and the use of small droplets (100 μm) maximizes gas phase

diffusion rates. Furthermore, gas phase mass transport rates can be deconvoluted from surface kinetics by varying the carrier gas pressure and composition.

Figure 1 shows a schematic of the apparatus. A stream of regular droplets is generated by pressurizing the liquid above a 60 μm orifice vibrated with a piezoelectric crystal. The size, spacing and velocity of the droplets are monitored with a cylindrically focussed He/Ne laser beam. The droplet stream is passed through two vacuum chambers before transversely crossing a 2.5 cm diameter flow tube. The stream is collected in a temperature controlled flask in a separate chamber. The composition of the atmosphere in each vacuum chamber is carefully controlled in order to maintain equilibrium between droplet temperature and water vapor pressure in the flow tube. The concentration of trace gas in the flow tube is monitored via diode laser absorption in a multiple pass cell downstream of the droplet stream.

Accommodation coefficients are calculated by comparing observed gas uptake ($\Delta n/n$) with the number of collisions of trace gas molecules with droplet surface as

$$\gamma = \frac{4F_g}{\bar{c}\, N\, A_d} \left(\frac{\Delta n}{n}\right)$$

where $\bar{c}$ is the trace gas average thermal velocity, F_g is the carrier gas volume rate of flow, and N and A_d are the number and surface area of droplets to which the trace gas is exposed.

Figure 2 plots the uptake rate, expressed as an observed accommodation coefficient, for HNO_3 as a function of the water vapor pressure in the flow tube. The variation in the water vapor pressure corresponds to a variation in the water droplet temperature, since the droplets actively cool by evaporation as they come into equilibrium with the ambient water vapor. This effect is shown in Figure 3, which plots accommodation coefficient versus inverse temperature.

The observed accommodation coefficients plotted in Figure 2 is a convolution of the "true" accommodation coefficient and the rate of gas phase diffusion of the trace gas to the droplet surface. The latter also varies as the flow tube pressure is changed. In extensive experiments with H_2O_2 and SO_2, in which the pressure was varied from 2 to 50 torr with up to 70% added He or Ar, the pressure dependent gas mass transport and heterogeneous uptake rates were deconvoluted from one another. Figure 3 plots actual accommodation coefficients obtained by correcting observed uptake rates for gas diffusion limitations using parameters determined in the H2O2 and SO2 experiments.

The line in Figure 3 shows a simple Arrhenius fit to the observed temperature dependence. The curve in Figure 2 is a convolution of this Arrhenius dependence with gas phase diffusion to simulate the actual laboratory data. The Arrhenius fit is somewhat qualitative but does give the first indication of the temperature dependence of the gas/water accommodation process.

The $\gamma(0°C)$ and ΔE values obtained so far are summarized in Table 1. The negative ΔE for H_2O_2 and HNO_3 are consistent with attractive sticking of these molecules to the aqueous surface. The magnitude of ΔE in the 4-10 kcal/mole range is consistent with attractive well which is less than the solvation energy of these highly soluble species.

As listed in Table 1, we have also measured the N_2O_5 sticking coefficient to be 0.08 at 0°C. The HNO_3 and N_2O_5 results are consistent with the values $> 10^{-3}$ reported for these molecules on 200°K ice surfaces.

In experiments with pure water droplets, there is no indication that droplets freeze even upon supercooling down to -20°C. However, upon the addition of pseudomanas syringel, a naturally occurring bacterium that is known to indicate ice nucleation at -3 to -5°C, droplets freeze on a 10 millisec timescale when supercooled to -10°C. Freezing is detected via depolarization of a polarized He/Ne laser beam backward scattered from the ice particles. Preliminary experiments measured an uptake rate for HCl on to ice consistent with an accommodation coefficient of ~0.1. Uncertainties in the trace gas/stream interaction volume limit the precision of the gas/ice experiments to date, but the measured HCl uptake is consistent with that observed for other soluble gases on pure water droplets and with observations reported for ice coated surfaces (Molina et. al., 1987). Further experiments on ice particle streams are in progress.

We have also demonstrated that we can produce streams of aqueous sulfuric acid droplets up to 95% (by weight) H_2SO_4. Control of these streams is complicated by the fact that evaporation or condensation of water vapor from or to the droplets changes both the temperature and composition of the droplet surface. Preliminary experiments with HNO_3 indicate that for 50% H_2SO_4 surfaces, $\gamma(HNO_3)$ is 0.1. This is similar to the γ on pure water and is significantly larger than the $< 10^{-3}$ value typically for 95% H_2SO_4 surfaces. Further experiments are currently in progress to directly probe the range around 75% H_2SO_4 composition that is typical of stratospheric conditions.

References

Molina, M.J., T.L. Tso, L.T. Molina and F.C.Y. Wang, Science 238, 1253 (1987).

Tolbert, M.A., M.J. Rossi, R. Malhotra and D.M. Golden, Science 238, 1258 (1987).

Table 1 - Mass Accommodation Coefficients on Liquid Water Droplets

	$\gamma(0°C)$	ΔE (kcal/mole)
HNO_3	0.16	-10
H_2O_2	0.21	-4
N_2O_5	0.08	---
HCl on ice	~0.1	---

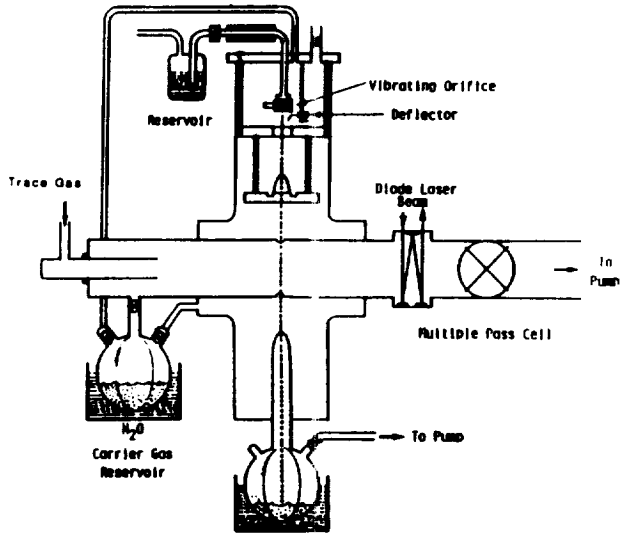

Figure 1. Experimental Apparatus for Mass Accomodation Coefficient Measurements

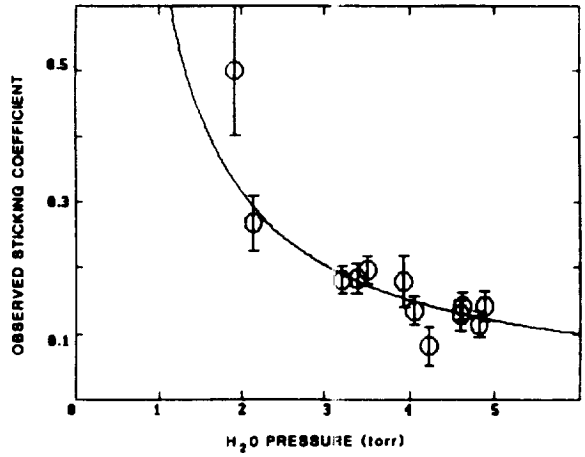

Figure 2. Observed γ Versus Water Vapor Pressure for HNO_3.

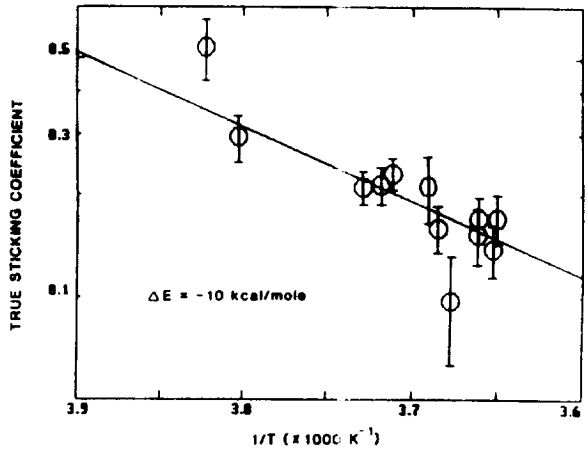

Figure 3. Semi-log Plot of Corrected Mass Accommodation Coefficient Versus 1/T.

157606

N89-14539

LABORATORY STUDIES OF STICKING COEFFICIENTS AND HETEROGENEOUS REACTIONS IMPORTANT IN THE STRATOSPHERE

Ming-Taun Leu

Jet propulsion Laboratory, California Institute of Technology, 4800 Oak Grove Drive, Pasadena, California 91109.

The discovery of ozone depletion during springtime in the Antarctic stratosphere has received wide spread attention. Both meteorological and chemical mechanisms have been used in attempts to explain this observation. The chemical theory focused on the chlorofluoromethanes released into the atmosphere. However, gas-phase, homogeneous reactions alone in the model can not adequately explain such a depletion. Heterogeneous reactions, such as:

(1)	$ClONO_2$	+	HCl	----->	Cl_2	+	HNO_3
(2)	$ClONO_2$	+	H_2O	----->	HOCl	+	HNO_3
(3)	N_2O_5	+	HCl	----->	$ClNO_2$	+	HNO_3
(4)	N_2O_5	+	H_2O	----->	2 HNO_3		

on ice surfaces could be important in the Antarctic stratosphere. Reactions (1)-(4) are thought to convert $ClONO_2$ and N_2O_5 into HNO_3 in the solid phase while Cl_2, HOCl, and $ClNO_2$ are released into the stratosphere as gas -phase products. The photolysis of Cl_2, HOCl, and $ClNO_2$, then produces active chlorine which subsequently removes ozone through several catalytic cycles, including the Cl_2O_2 mechanism. The polar stratospheric clouds are thought to consist of mixtures of water ice, nitric acid, and sulfuric acid. Condensation of HCl onto the PSC's could provide active surfaces for heterogeneous reactions, such as (1) and (3).

A fast flow reactor was used for investigating the sticking coefficients of the trace gases on ice. The diameter of the flow tube was 1.89 cm, and the length was 50 cm. The temperature of the flow tube was measured by a pair of thermocouples and its temperature was maintained at about 190-200 K by circulating cooled dry nitrogen through its outside jacket. The cooling jacket was further insulated by another exterior jacket which was evacuated by a mechanical pump. The pressure was monitored at the downstream end of the flow tube by means of a Baratron pressure meter. The ice surface was prepared by passing water vapor in helium carrier through an injector tube which was slowly moved along the length of the flow tube until a thin uniform ring was formed. Ice was prevented from forming in the injector tube by flowing dry nitrogen through a jacket which extended beyond its downstream end. The flow rate of water vapor was measured by monitoring the pressure and the temperature at the water reservoir and also monitoring the helium flow rate. The detection of the trace gases was performed by using an EMBA II

quadrupole mass spectrometer. We utilized the electron impact ionization method to monitor the parent peak or the fragmentation peaks of the gas molecules. For example, H_2O or HCl were detected by their parent peaks while $ClONO_2$ or N_2O_5 were measured by NO_2 ions.

Measurements of sticking coefficients for H_2O, HCl, Cl_2 and HNO_3 on ice and of reaction probabilities for reactions (1) and (2) have been summarized in a recent publication. Measured sticking coefficients are: 0.3 (+0.7,-0.1) for H_2O, 0.4 (+0.6,-0.4) for HCl, $< 1.0 \times 10^{-4}$ for Cl_2, and 0.3 (+0.7,-0.3) for HNO_3 at 200 K. The reaction probability of $ClONO_2$ on ice was found to be 0.06 ($\pm$0.03) while HOCl was observed as the sole product in the gas phase. In the presence of 0.015-0.071 mole fractions of HCl in ice, the reaction probability of $ClONO_2$ is greatly enhanced, approaching 0.27 (+0.73, -0.13) while molecular chlorine was found to be the major product in the gas phase. Another reaction product was nitric acid which remained in the solid phase.

In a preliminary investigation the reaction probability of N_2O_5 was found to be 2.8 ($\pm$1.1) $\times 10^{-2}$ on ice at 195 K and 3.4 ($\pm$1.4) $\times 10^{-2}$ with 0.015-0.040 mole fractions of HCl at 195 K. One of the reaction products, HNO_3, remained in the condensed phase. It should be noted that the yield of NO_2, a probable reaction product, was negligible in these N_2O_5 reactions. This work will be continued in the laboratory and the results will be presented at the Workshop.

In addition, similar reactions on sulfuric acid/water ice surfaces will be investigated because of their potential importance for the global stratosphere.

Acknowledgments. The research described in this paper was performed by the Jet Propulsion Laboratory, California Institute of Technology, under a contract with the National Aeronautics and Space Administration.

References:

1. J. C. Farman, B. G. Gardiner, and J. D. Shanklin, Nature, 315, 207 (1985).
2. M-T. Leu, Geophys. Res. Lett., 15, 17 (1988).
3. Geophysical Research letters, November Supplement (1986).
4. M. B. McElroy, R. J. Salawitch, S.C. Wofsy, and J. A. Logan, Nature, 321, 759 (1986).
5. L. T. Molina and M. J. Molina, J. Phys. Chem., 91, 433 (1987).
6. S. Solomon, R. R. Garcia, F. S. Rowland, and D. J. Wuebbles, Nature, 324, 755 (1986).
7. M. A. Tolbert, M. J. Rossi, R. Malhotra, and D. M. Golden, Science, 238, 1258 (1987).
8. M. J. Molina, T-L Tso, L. T. Molina, and F. C. Wang, Science, 238, 1253 (1987).

S37-45
157607

N89-14540

LIDAR OBSERVATIONS OF POLAR STRATOSPHERIC CLOUDS AT McMURDO, ANTARCTICA, DURING NOZE-2

Bruce M. Morley
SRI International
333 Ravenswood Ave.
Menlo Park, CA 94025

SRI International operated a dual wavelength (1.064 μm and .532 μm) aerosol lidar at McMurdo Station, Antarctica, as part of the National Ozone Expedition-2 (NOZE-2). The objective of the project was to map the vertical distributions of polar stratospheric clouds (PSCs), which are believed to play an important role in the destruction of ozone in the Antarctic spring. Altitude, thickness, homogeneity, and duration of PSC events as well as information on particle shape, size or number density will be very useful in determining the exact role of PSCs in ozone destruction. The lidar gives a direct measure of PSC density distributions, and when combined with measurements of other investigators, additional properties of PSCs can be estimated.

Lidar data were collected on 22 days between September 3 and October 5, and PSCs were observed on 16 of those days. A total of over 200 hours of lidar data were collected. The lidar system transmitted energy into the atmosphere at an infrared wavelength of 1.064 μm (500 mj) and at a green wavelength of 0.532 μm (200 mj) simultaneously, with a pulse repetition frequency up to 10 pulses per second. The backscattered light was collected by a 61 cm diameter telescope, optically filtered to remove background light, separated into infrared and green components, and focused onto an appropriate detector. Three channels were used for data collection. The output of a silicon avalanche photodiode used for detection of the infrared (1.064 μm) signals was logarithmically amplified to enhance the dynamic range of the lidar observations, and then digitized by a high speed analog-to-digital (A-D) converter (12-bit, 10 MHz). An average of 128 laser firings (a 30 second to 5 minute time period) was then recorded on 9-track magnetic tape. The green lidar optical returns were converted to electrical signals by a photomultiplier tube. The high gain of the PM tube necessitated gating the tube to prevent detector saturation from strong lower tropospheric backscatter signals.

During NOZE-2, the PM tube was normally gated on at a lidar range of approximately 10 km. An analog signal was taken from the anode of the tube, logarithmically amplified, and digitized with a high-speed averaging A-D converter (10 bit, 20 MHz). An average backscatter signature derived from 256 laser firings was then recorded on magnetic tape. The signal from the last dynode of the PM tube was used in a photon-counting data channel. Again, averages of 256 lidar signatures were written on the magnetic tape. Both A-D converters operated at a vertical resolution of 15 m, while the photon counter provided a vertical resolution of 150 m. A color display of all three signals was used

for real-time monitoring of the lidar performance and for providing information on aerosol distributions for operational purposes.

Figure 1 (presented here in black-and white) is an example of the real time display generated during data collection. The PM tube was gated on at about 10 km, and Rayleigh scattering can be seen in both the analog ("green") and in the photon counting channel ("blue") up to an altitude of 20 km. A PSC return feature is seen in both PM tube channels between 16 and 18 km. The 1.064 μm return signal ("red") shows Rayleigh scattering below 4 km and cirrus cloud backscatter between 4 and 8 km. No evidence of the PSCs is seen in the infrared return signal because of the reduced sensitivity of the infrared system.

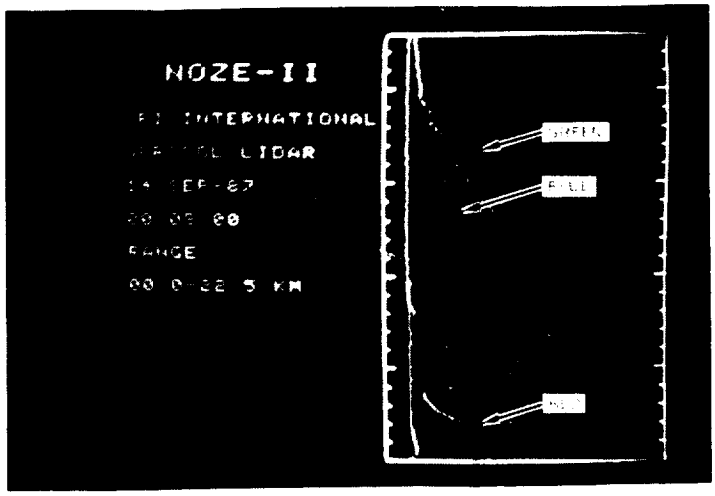

FIGURE 1 REAL-TIME DISPLAY WITH 1.064 μm RETURN (RED), 0.532 μm ANALOG RETURN (GREEN), AND 0.532 μm PHOTON COUNTING RETURN (BLUE)

Figure 2 is an example of PSC height/time distributions derived from 0.532 μm analog return signals displayed with a post-collection data processing program. The PSCs are seen as white bands between 12.5 and 14.5 km. The variability of the return signal strength and altitude is evident in this display. A short-lived layer of PSCs at 15.5 km centered at about 0100 local time is also of note.

The solid lines in Figure 3 represent an analysis of the photon counting signal in terms of relative backscatter (A) and scattering ratio (B) as functions of altitude. Scattering ratio is the total backscatter divided by Rayleigh backscatter, and is a parameter typically used to quantify lidar-detected stratospheric aerosol layers. The dashed line in (A) represents backscatter from a model Rayleigh atmosphere, and in (B) it represents the scattering ratio of a Rayleigh atmosphere (by definition equal to 1). The fine vertical structure seen in Figure 2 is not apparent in Figure 3 due to the 150 m range bins of the photon counting data channel.

More examples of PSC events will be presented in the formats of Figure 2 and Figure 3. Scattering ratios from the green analog data

channel will be presented. Estimates of infrared scattering ratios will be shown for cases where PSCs were detected in the 1.06 μm channel. These results are currently being analyzed in terms of PSC properties which are useful for modeling the stratospheric ozone depletion mechanism.

This work was sponsored by the National Science Foundation under Grant DPP-8617364.

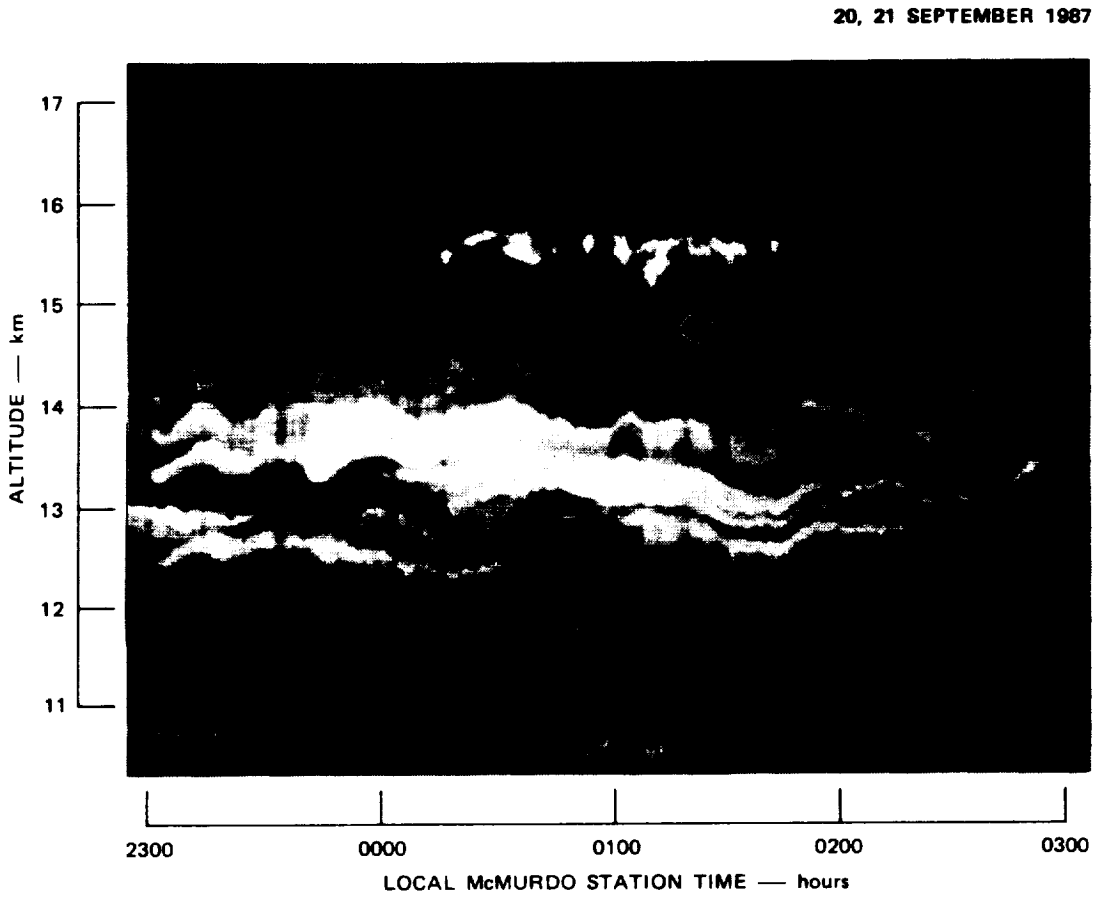

FIGURE 2 EXAMPLE OF HEIGHT/TIME POLAR STRATOSPHERE CLOUD STRUCTURE OBSERVED BY THE NOZE-2 LIDAR PROGRAM

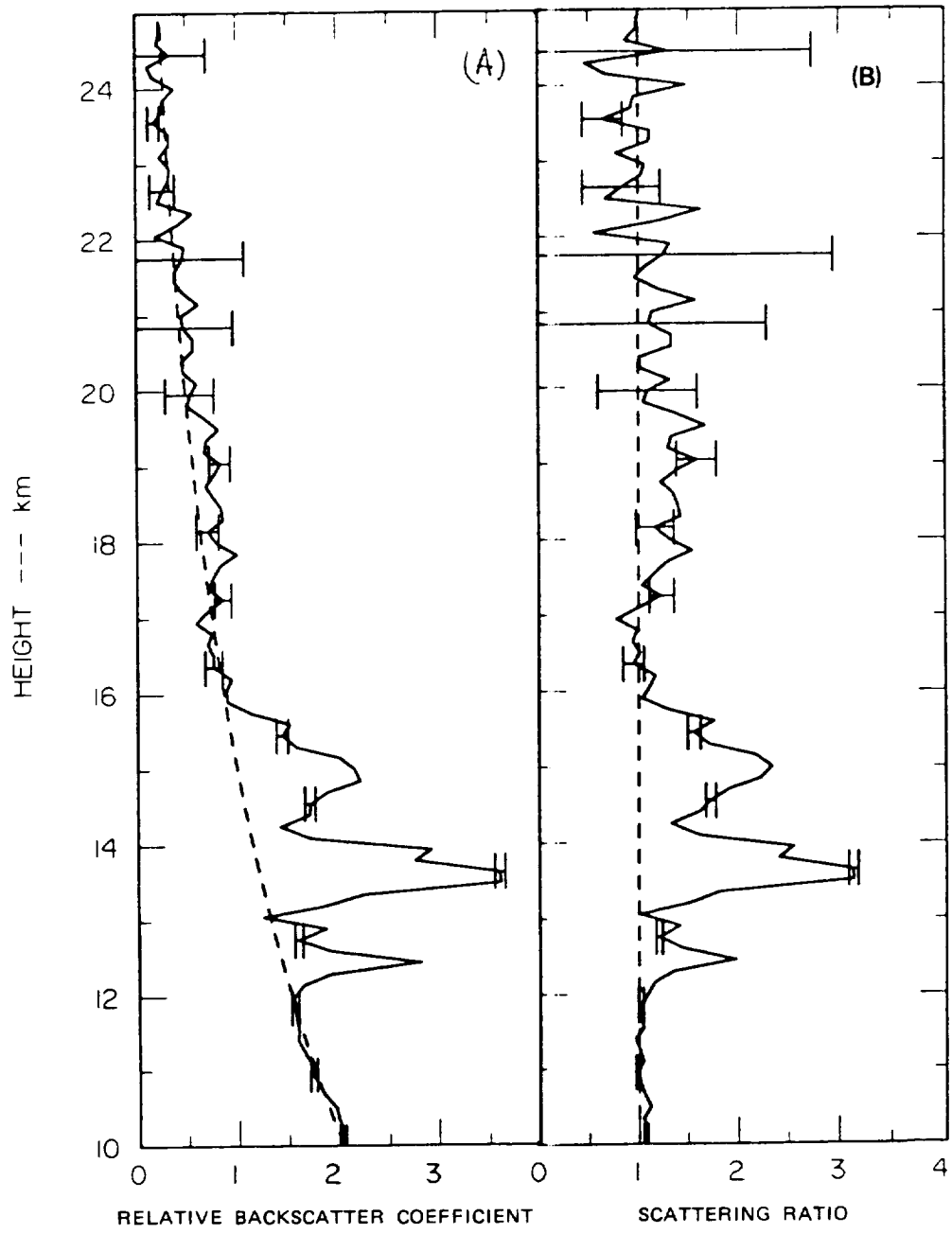

FIGURE 3 (A) LIDAR-MEASURED RELATIVE BACKSCATTER (SOLID LINE) AND RELATIVE RAYLEIGH MODEL BACKSCATTER (DASHED LINE), AND (B) LIDAR-MEASURED SCATTERING RATIO: McMURDO STATION, 21 SEPTEMBER 1987, 00300 LOCAL TIME.

OBSERVATIONS OF CONDENSATION NUCLEI IN THE 1987 AIRBORNE ANTARCTIC OZONE EXPERIMENT

by

J.C. Wilson[1], S.D. Smith[2], G.V. Ferry[3], M. Loewenstein[3]

[1]University of Denver
Department of Engineering
Denver, CO 80208

[2]Aerosystems
St. Paul, MN

[3]NASA Ames Research Center
Moffett Field, CA 94035

INTRODUCTION

The condensation nucleus counter (CNC) flown on the NASA ER-2 in the Airborne Antarctic Ozone Experiment provides a measurement of the number mixing ratio of particles which can be grown by exposure to supersaturated n-butyl alcohol vapor to diameters of a few microns. Such particles are referred to as condensation nuclei (CN). The ER-2 CNC was calibrated with aerosols of known size and concentration and was found to provide an accurate measure of the number concentration of particles larger than about 0.02 μm (Wilson et al. 1983). Since the number distribution of stratospheric aerosols is usually dominated by particles less than a few tenths of micron in diameter, the upper cutoff of the ER-2 CNC has not been determined experimentally. However, theory suggests that the sampling and counting efficiency should remain near one for particles as large as 1μm in diameter. Thus, the CN mixing ratio is usually a good measure of the mixing ratio of submicron particles.

The mixing ratio of CN is expressed as the number of particles per milligram of air (#/mg AIR). Measurements of CN together with observations of larger particles and trace species provide information on the processes affecting small particles and on the role they play in the dynamics of the antarctic stratospheric aerosol.

The ER-2 flights in the Airborne Antarctic Ozone Experiment consisted of flights from Punta Arenas, Chile (53 S lat) to approximately 72 S lat near the base of the Palmer peninsula as well as ferry flights from Moffett Field, CA to Punta Arenas and back. On most flights south of 53 S, the ER-2 profiled a range of altitudes around 72 S. These profiles were done in a region of the atmosphere where ClO concentrations were elevated and NOy and H_2O were depleted and are insitu measurements in the Antarctic Ozone Hole.

OBSERVED CN MIXING RATIOS AND POPULATIONS OF SUB .12μm PARTICLES

Profiles of CN mixing ratios measured at 8 N latitude (Panama) and 53 S latitude (Punta Arenas) are shown in Fig. 1. The values shown for 8 N are characteristic of those measured at 8 S in January 87 as well. Most of the CN mixing ratio profiles measured from August 12 to October 3, 1987 are plotted on Figure 2 where the solid line profiles were measured south of Puerto Montt(41 S). Figure 3 shows profiles similar to those measured at 53 S and 72 S in August and September 1987. Figure 2 confirms the impression provided by Figure 1 that CN mixing ratios at a given potential temperature were observed to be smaller south of 41 S. Figure 3 shows that the decrease continues for potential temperatures below about 400 K as one moves to 72 S. Above about 400 K at 72 S, increases in CN mixing ratio suggest an upper altitude source of small particles. When number concentration is plotted against ambient pressure, the variability is found to decrease. At 18 km pressure altitude almost all of the measured profiles show concentrations between 4 and 6 particles/cm^3.

Figure 4 shows the ratio of CN mixing ratio to the mixing ratio of particles with a diameter larger than 0.12μm measured with the PMS ASAS-X aerosol spectrometer. Small ratios occur when size distributions are dominated by particles larger than 0.12μm in diameter and large ratios occur when number distributions are dominated by smaller particles. Comparison of Figures 3 and 4 shows that small CN mixing ratios often occur when size distributions are dominated by particles larger than 0.12μm in diameter. For potential temperatures below 420 k, the ratios of CN to ASAS-X (ch 2 to 22) were usually smaller at 72 S than at 53 S.

RELATIONSHIP BETWEEN CN AND N_2O: CN SOURCES AND SINKS

The sources for N_2O are in the troposphere and it is destroyed at high altitude in the stratosphere. At the altitudes reached by the ER-2, the chemical lifetime of N_2O is long compared to the transport times and so N_2O serves as a tracer for tropospheric air. The profiles of N_2O measured at 72 S differ considerably from those measured at 53 S with lower values being observed at the same potential temperatures at 72 S. A scatter plots of CN vs N_2O for profiles measured at 53 S and 72 S are shown in Figure 5. For concentrations of N_2O above 180 ppbv, CN and N_2O show a positive correlation. In this region, the tropospheric source of CN dominates. For concentrations of N_2O below 130 ppbv, the correlation between CN and N_2O is reversed and a stratospheric source of CN causes the vertical gradient of CN mixing ratio to be reversed. This pattern is repeated on nearly all flights. Figure 6 contains all the N_2O-CN scatter data for Sep 20 and shows that the relation holds to about $\pm$25% for all potential temperatures encountered during the flight. The reversal of CN mixing ratio gradient occurs at about 18 km pressure altitude on Sep 20 at 72 S.

Hofmann et. al. (1988) report an increase of CN concentration with altitude above 20 km pressure altitude in the 1986 Ozone Hole and suggest that it is associated with subsiding air. The relationship between CN and N_2O shown in Figures 5 and 6 supports their supposition.

For N_2O values between 190 ppbv and 240 ppbv, Figure 5 shows that the profiles at 72 S and 53 S show the same relationship between CN and N_2O. A similar overlap occurs on many flights. The parcels involved in the overlap have quite different potential temperatures. Assume that the parcels started with similar makeup at the same potential temperature and that the parcel sampled at 72 S lowered its potential temperature by diabatic processes involving PSC's. Then using N_2O as a tracer, we conclude that the removal of CN in the process was not larger than the 30% scatter in the plot

REFERENCES

Wilson J.C., Hyun J.H., Blackshear E.D., *J. Geophys. Res., 88(6781-6785), 1983*

Hofmann, D.J., Rosen J.M., Harder J.W., *J. Geophys. Res., 93(665-676), 1988*

Figure 1.

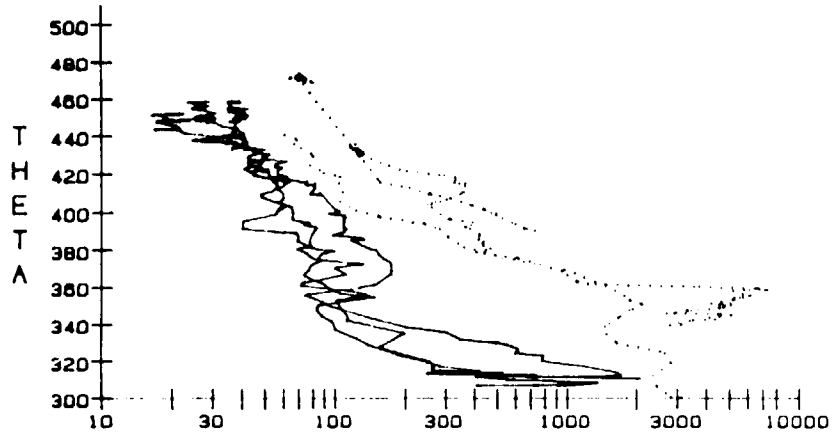

CNC MIXING RATIO, #/mg AIR

LINES: PROFILES FROM PUNTA ARENAS, SEP 87
DOTS: PROFILES FROM PANAMA, AUG 87 AND OCT 87

Figure 2.

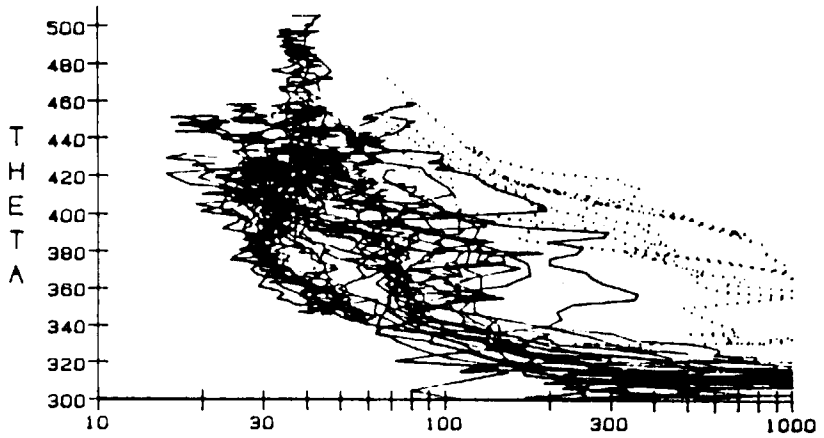

MIXING RATIO

SOLID LINES: SOUTH OF PUERTO MONTT
DOTS: PANAMA AND AMES

Figure 3.

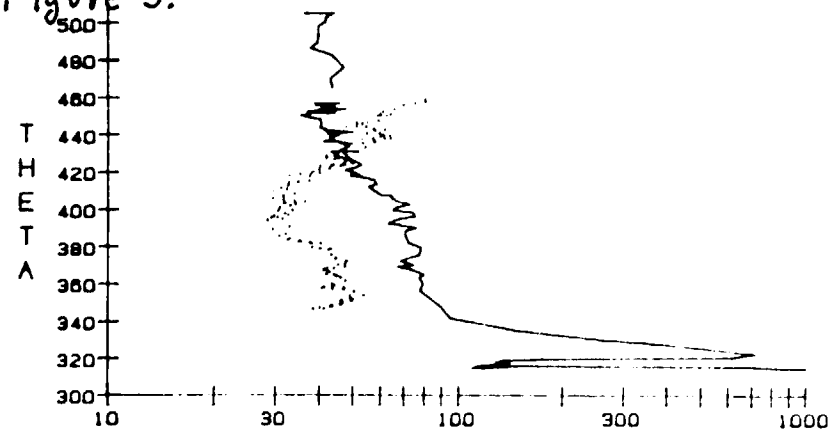

CNC MIXING RATIO, #/mg AIR

LINES: PROFILES FROM 53 S, 20 SEP 87
DOTS: PROFILES AT 72 S, 20 SEP 87

Figure 7.

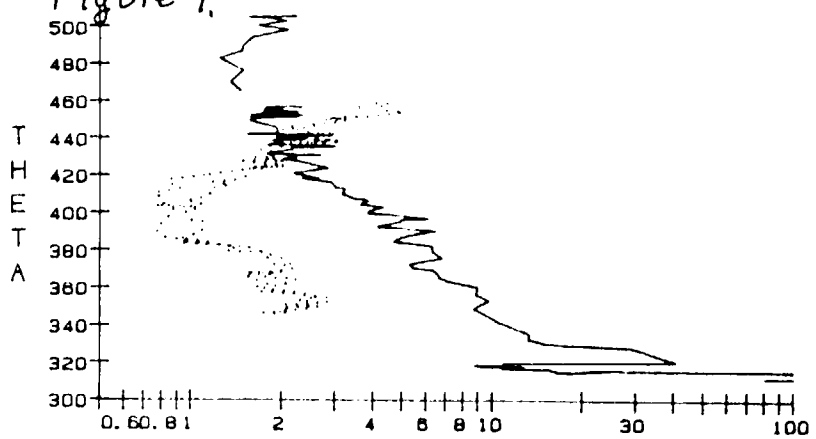

RATIO OF CN/ASAS-X

LINES: PROFILES FROM 53 S, 20 SEP 87
DOTS: PROFILES AT 72 S, 20 SEP 87

Figure 5.

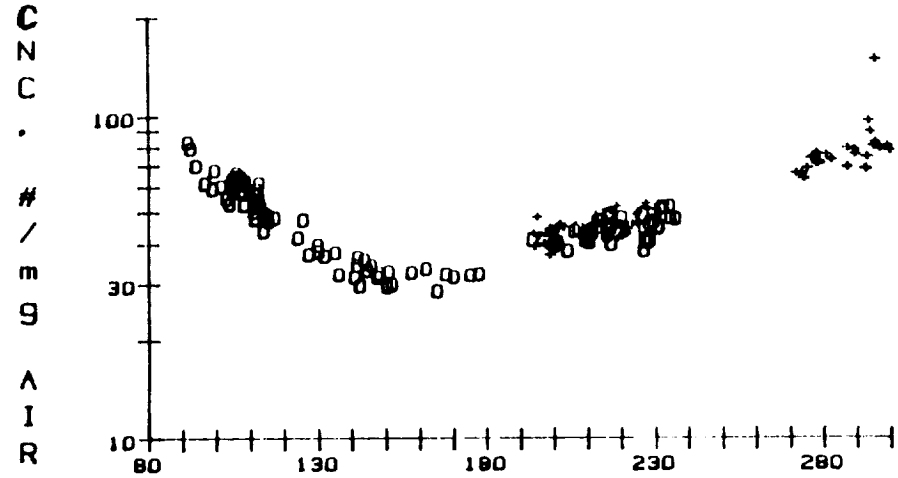

+: POINTS FROM PROFILE AT 53 S
O: POINTS FROM PROFILE AT 72 S

Figure 6.

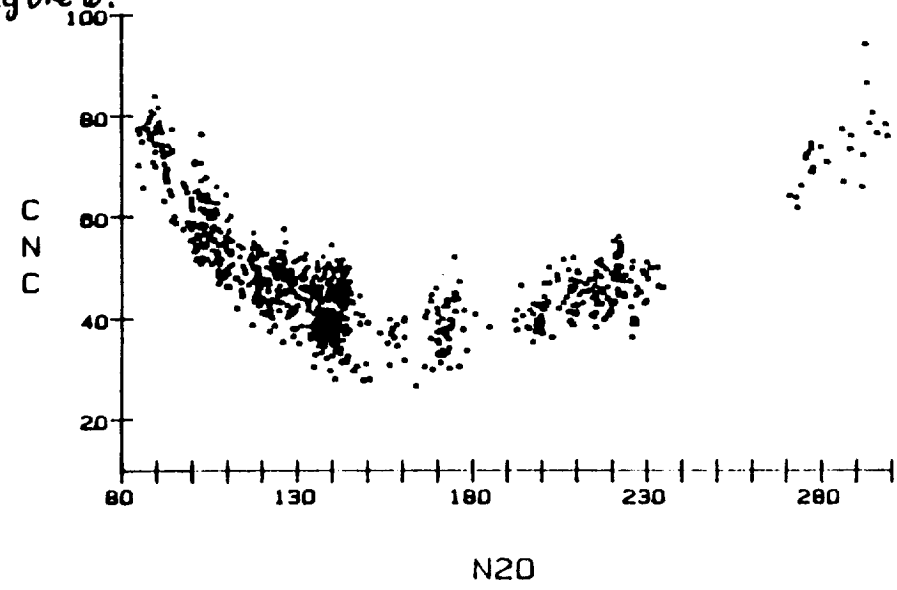

CN-N2O SCATTER PLOT FOR 20 SEP 87

SESSION IV - Remote Sensing of Trace Gases
Presiding, R. Turco, R & D Associates
Tuesday Afternoon, May 10, 1988

STRATOSPHERIC COLUMN NO2 MEASUREMENTS FROM THREE ANTARCTIC SITES

J.G.Keys and P.V.Johnston
Physics and Engineering Laboratory,DSIR
Lauder, Central Otago, New Zealand

The significance of stratospheric odd-nitrogen compounds in Antarctic ozone depletion studies has prompted an increase in our Antarctic activities since 1986. Although several species are being studied, work has concentrated on the acquisition of NO2 data. Ground-based measurements of stratospheric column NO2 have been made at Arrival Heights, Antarctica, since spring 1982, with some gaps in the data base. Additional data has been acquired since February 1986 at Pole Station and Halley Bay, thus providing a chain of stations across the continent.

The technique used is that of absorption spectroscopy in several wavelength regions, although here we only report on those measurements in the 430-450nm region where strongly structured absorption features due to NO2 are identified in scattered sunlight in the zenith sky. Operation of a moon-tracking system at Arrival Heights has provided some additional data during the polar night. Previous analyses have shown that the NO2 column observed from the ground is strongly influenced by the season, and by the location of the site with respect to that of the polar vortex. The column amount correlates strongly with stratospheric temperature at about 70 mbar. The present data set further illustrates these features, and demonstrates both the strengths and qualifications apparent in the technique.

Data are acquired over a range of solar zenith angles around dawn and dusk twilight, and plots of data taken at 90 degrees show the seasonal trends in the observed slant column. Figure 1 shows a composite data set for Arrival Heights for 1982-1987. In general the afternoon values are higher than in the morning because of release of NO2 from its overnight storage reservoir. It can be seen that there is a steady seasonal decline in NO2 in the autumn data, and a corresponding increase in spring, caused in the main by movement of NO2 to and from the polar night storage reservoirs, thought to be N2O5 and HNO3. It should be pointed out, however, that the large 90 degree slant column values are a consequence of enhanced absorption in the long path at twilight; and model calculations show that the enhancement factor, proportional to airmass, is also dependent on layer height. Our initial calculations suggest that the bulk of the NO2 layer in autumn is probably at a height of about 20km, whereas in spring it is located much higher, perhaps 30km. If the layer is rising during autumn, therefore, some reduction in the observed slant column of up to 25 percent could result,without any real change in the vertical column. Large quasi-cyclic variations in spring are the result of observing NO2 enriched air from lower latitudes as the vortex moves away from the site. A more detailed examination of the year by year plots shows

1) Onset, at about day 60, of conversion of NO2 to N2O5 as continuous daytime photolysis of NO3 first ceases, even though the layer is still continuously, but weakly, illuminated:

2) Rather uniform behaviour in autumn, but large differences in spring as planetary wave activity changes from year to year:

3) A suggestion in the 1987 data of a reduction in the diurnal variation of NO2, which may mean that more NOx is sequestered in HNO3 at the expense of N2O5:

4) Consistently low values of NO2 in spring 1987, evidently associated with the low temperatures that prevailed.

Figure 2 shows the combined data for Halley Bay, Pole Station and Arrival Heights for 1986. Because 90 degree data can only be obtained from Pole at the equinox, the Pole values have been extrapolated to 90 degrees, and are hence subject to some uncertainty. The data clearly show the response of the stations to the particular location of the polar vortex.

Figure 3 shows an interesting data set from Pole Station acquired near the 1987 autumn equinox. During the course of day 90/91 the solar zenith angle increases by only half a degree, but the data clearly show a diurnal variation of up to twenty percent in the slant column. We interpret this as the signature of a horizontal spatial gradient in NO2 seen in the slant column as the sun moves around the station at effectively constant solar zenith angle. Some of the variation may also be due to a spatial change in the effective height of the NO2 layer.

Acknowledgements:
We are indebted to staff of the British Antarctic Survey, of the GMCC group at NOAA, and of the New Zealand Antarctic Division, for their operation of equipment and logistic support for the programmes at Halley Bay, Pole Station and Arrival Heights; and to the US National Science Foundation for continued help. We also wish to acknowledge with gratitude the stratospheric temperature data provided by M E Gelman, of the NMC Climate Analysis Center, the help of Dr W A Matthews, and the technical assistance given by A Thomas of DSIR.

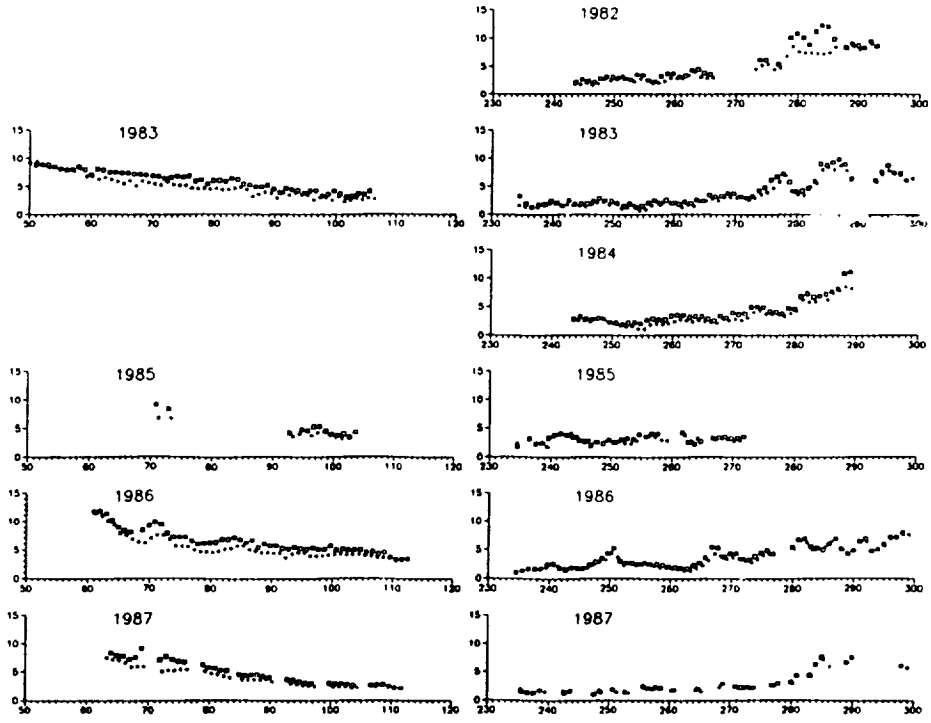

FIGURE 1: ARRIVAL HEIGHTS
SLANT COLUMN NO2(1E16 MOL CM-2)
1982-1987. AM(•), PM(•)

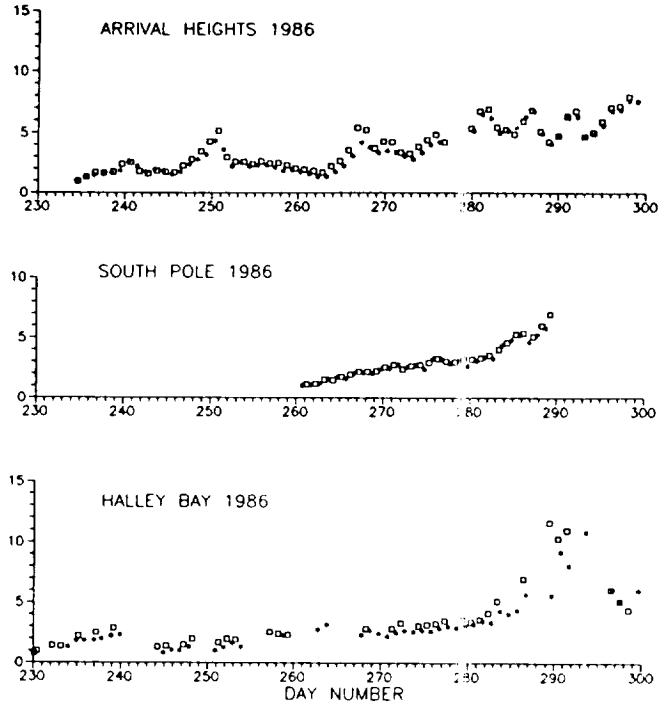

FIGURE 2: SLANT COLUMN NO2
(1E16 MOL CM-2)

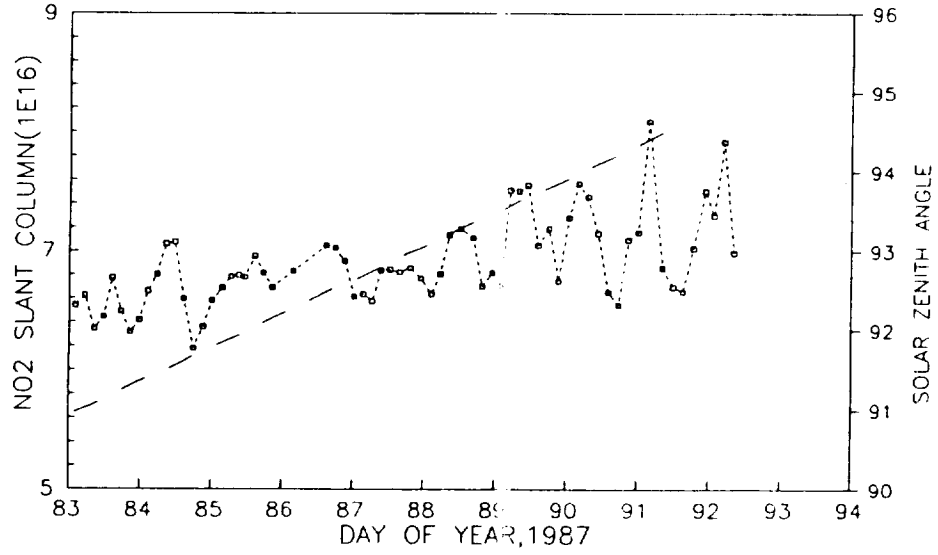

FIGURE 3: SOUTH POLE, ANTARCTICA
SLANT COLUMN NO2
3-HOUR AVERAGES

Ground-based measurements of O_3, NO_2, OClO, and BrO during the 1987 Antarctic ozone depletion event

R. W. Sanders, S. Solomon, M. A. Carroll, and A. L. Schmeltekopf

Aeronomy Laboratory, NOAA, Boulder, CO 80303

Near-ultraviolet absorption spectroscopy in the wavelength range from 330-370 nm was used to measure O_3, NO_2, OClO, and BrO at McMurdo Station (78S) during 1987. Visible absorption measurements of O_3, NO_2, and OClO were also obtained using the wavelength range from about 403-453 nm. These data are described and compared to observations obtained in 1986. It is shown that comparisons of observations in the two wavelength ranges provide a sensitive measure of the altitude where the bulk of atmospheric absorption takes place. The measurements indicate that the bulk of the NO_2 column abundance is located near 30 km, while those of OClO and O_3 are near 20 km. The measurements of NO_2 display a systematic increase during the month of September, probably reflecting the release of odd nitrogen from reservoirs formed earlier in the winter season. The measurements of OClO display a strong diurnal variation, with considerably higher values being obtained in the evening than those measured in the morning. The evening twilight OClO column abundances obtained in 1987 were notably larger than those in 1986, perhaps because stratospheric temperatures were colder, and associated heterogeneous chemistry may have been more intense. These observations provide important constraints on the coupled nitrogen-halogen chemistry of antarctic spring and its influence on the springtime antarctic ozone depletion. Observations of the evening twilight BrO abundance over McMurdo Station, Antarctica during austral spring, 1987 are described. The observed variation of the slant column abundance with increasing solar zenith angles suggests that most of the BrO is located near 15 km. The total vertical column abundance observed during one week of measurements yielded an average value of 2.5×10^{13} cm^{-2} assuming the room temperature absorption cross sections measured by Cox et al. [1]. These values are consistent with BrO mixing ratios of about 5-15 pptv distributed from 150 to 20 mb.

[1] Cox, R. A., D. W. Sheppard and M. P. Stevens, J. Photochem., *19*, 201, 1982.

ABSTRACT

Near UV Atmospheric Absorption Measurements From the DC-8 Aircraft During the 1987 Airborne Antarctic Ozone Experiment

A. Wahner*, R.O. Jakoubek*, A.R. Ravishankara, G.H. Mount, and A.L. Schmeltekopf.

Aeronomy Laboratory, NOAA/ERL, Boulder, CO 80303
*Cooperative Institute for Research in Environmental Science (CIRES), University of Colorado, Boulder, CO 80309

During the Airborne Antarctic Ozone Experiment from 28 August 1987 to 30 September 1987 near UV zenith scattered sky measurements were made over Antarctic from the NASA DC-8 aircraft using a 1/3 m spectrograph equipped with a diode-array detector. Scattered sky light data in the wavelength range 348 nm - 388 nm was spectrally analyzed for O_3, NO_2, $OC\ell O$, and BrO column abundances. Slant column abudances of O_3, NO_2, $OC\ell O$ and BrO were determined, using a computer algorithm of non-linear and linear least square correlation of Antarctic scattered sky spectra to laboratory absorption cross section data. Using measured vertical electrochemical sonde ozone profiles from Palmer, Halley Bay, and the South Pole Stations the slant columns of O_3 were converted into vertical column abundances. The vertical column amounts of NO_2, $OC\ell O$, and BrO were derived using vertical profiles calculated by a chemical model appropriate for Antarctica. NO_2 vertical column abundances show steep latitudinal decrease with increasing latitude for all 13 flights carried out during the mission. In the regions where NO_2 abudances are low, $OC\ell O$ and BrO were observed. The spatial and temporal vertical column abundances of these species will be discussed in the context of the chemistry and dynamics in the antarctic polar vortex during the austral spring.

Infrared measurements of column amounts of stratospheric constituents in the Antarctic winter, 1987

by
William G. Mankin and M. T. Coffey
*National Center for Atmospheric Research**
P. O. Box 3000, Boulder, Colorado 80307

The discovery by Farman *et al.* (1985) of recent large depletions of ozone in the Antarctic stratosphere in the austral spring has aroused great interest because of its serious potential consequences, as well as its surprising nature. An airborne expedition, including 21 experiments on two aircraft, was mounted from Punta Arenas, Chile, in August and September, 1987, to gather a wide range of data to understand the origins and implications of this phenomenon, known as the "ozone hole". As a part of this expedition, we flew a high resolution Fourier transform spectrometer on the DC-8, measuring the column amount of a number of trace gases above the flight altitude.

Infrared spectroscopy is a valuable technique for studying the chemistry of the stratosphere. It is a remote sensing technique, capable of operation on aircraft with ceilings below the region to be observed. Using the sun as a source for absorption spectroscopy allows high resolution and signal-to-noise, permitting detection of species at sub-ppb levels. The inherent spatial averaging of the technique focuses on large scale phenomena rather than small fluctuations. Perhaps its most valuable attribute is the ability to measure a number of species simultaneously, allowing study of the relationships of members of a family of chemical species. The principal disadvantages are the inability to measure some important species, especially free radicals, because of their low concentration, the limited ability to determine the vertical profile of concentration, and the sensitivity of retrieved columns to assumptions of the distribution of temperature and relative concentration.

Our instrument consists of an infrared window for admitting infrared radiation from the sun, a suntracker for directing the radiation into the spectrometer, a Michelson interferometer for separating the wavelengths and measuring the intensity, and a computer for collecting the data and storing it for analysis. The window is a disk of ZnSe 20 cm in diameter and 1.5 cm thick; it allows us to observe the sun over a range of zenith angles of 75 to 93° and azimuths of 80 to 100° relative to the aircraft heading. The suntracker has two axis control, frequency response from d.c. to about 10 Hz, and automatic gain control to correct for varying solar brightness as the sun sets or we encounter thin clouds. It maintains the solar image stable to about an arcmin even in the presence of moderate turbulence or clouds with visible optical depth less than 2.

The spectrometer is based on a commercial modulator. It uses plane mirrors and an air bearing for motion of the moving mirror. The maximum optical path difference is 16 cm, yielding an apodized resolution (FWHM) of 0.06 cm^{-1}. The output beam is focused on a field stop with diameter about 15 arcmin. This reduces the effect of any modulation of the signal by tracking errors. A bandpass filter selects the spectral region to be observed. A dual element "sandwich" detector measures the intensity; the elements are InSb for wavenumbers greater than 1900 cm^{-1}, and HgCdTe for lower

frequencies. The spectral region covered is 700-5000 cm^{-1} in several bands. A single spectrum requires 6 seconds to record. Typically 10 successive spectra are averaged for analysis.

A PDP-11/23+ computer controls the operation of the instrument and records the interferograms, housekeeping data, and the output of the aircraft navigation data system on magnetic tape. It includes a high speed array processor which allows transformation of interferograms to produce spectra allowing analysis and determination of column amounts of several species during the flight. This proved to be useful in determining when the observations were inside the region of reduced ozone in almost real time.

We made observations on two test flights from Ames Research Center, on ferry flights to and from Punta Arenas, and on ten flights over Antarctica. Three other flights, including one from Punta Arenas to Christchurch, N.Z., were made entirely in the dark. Most of the observation flights had one or more periods of typically half hour duration when the heading of the aircraft was selected to permit solar observations. In the course of the experiment, we obtained approximately 6440 spectra. These are distributed among the filters as shown in Table I.

Table I

Filter	Spectral Region	Number of Spectra	Molecules Measured
1	1900-3900 cm^{-1}	470	none
2	700-1850 cm^{-1}	660	O_3,CH_4,HNO_3
3	700-1340 cm^{-1}	1800	O_3,HNO_3,N_2O,CH_4,$ClONO_2$
4	2850-3100 cm^{-1}	1170	HCl, CH_4
5	1970-2420 cm^{-1}	540	CO, OCS, O_3
6	1500-1650 cm^{-1}	870	H_2O, NO_2
7	790-1070 cm^{-1}	30	none
8	4000-4500 cm^{-1}	610	HF
9	1760-1980 cm^{-1}	290	NO

For each molecule and spectral region used, a spectral line or group of lines was selected for analysis, based on strength and freedom from interference. For molecules such as HCl where the suitable lines are few and far apart, we used an equivalent width method of analysis (Coffey *et al.*, 1981), whereas for molecules such as ozone where there are many suitable lines, including spectral regions where the target molecule dominates the atmospheric absorption, the process of nonlinear least squares fitting of a calculated spectrum to the observed spectrum was employed (Niple *et al.*, 1980). The latter process is more laborious and computer intensive, but improves the precision by using more lines, including overlapping lines. Details of the analysis procedure will be published elsewhere. The spectroscopic parameters for the selected lines were taken form the AFGL compilation (Rothman *et al.*, 1987)

Both analysis methods require the calculation of the expected spectrum with a particular amount of the target gas, for comparison with the observed spectrum. The spectra are calculated by the Fourier technique of Mankin (1979). The calculations

require knowledge or assumption of the vertical distribution of the temperature, pressure, and absorber mixing ratio. This information is used at two stages: first, for the calculation of the absorption corresponding to a given amount of absorber along the line of sight, and second, for the conversion of the line of sight amount to a vertical column. While in the past, we have taken the shape of the mixing ratio curves from published vertical profiles (Coffey *et al.*, 1981), in the highly perturbed chemical region of Antarctica, the profiles are expected to be quite different than standard midlatitude profiles. For ozone, there are ozonesonde data from several stations which serve as a guide, but for the trace species, there is little information. Some information can be gained from the spectra if observations are made through the same air mass at different solar elevations. This experiment was, in fact, performed on September 24, when three sun runs were made in the vicinity of 80°S., 111°W. at sun angles around 0.75°, 2.84°, and 6.03°. We have used these data to adjust the mixing ratio profiles, and have used these profiles to reduce other observations within the vortex. The greatest uncertainty from this source occurs near the vortex boundary.

The precision of the results is good, particularly from the flights later in the mission after certain improvements in the operation were made. During the flight of September 21, a series of 40 successive spectra were recorded near 82°S. These were divided into groups of 10, averaged, and analyzed. The standard deviation in the ozone column retrieved from the four groups was less than 1% of the mean. The comparison of our ozone columns with those of TOMS and the JPL interferometer was also good (Margitan, this volume) The absolute accuracy is harder to estimate. The principal errors come from errors in the line parameters, errors in the assumed distribution of temperature and mixing ratio, and approximations made in the calculation of the synthetic spectra. These errors are estimated at 10% for ozone and somewhat greater for the trace gases.

In this paper, we present column results only from the flight of September 21; results from other flights are included in the accompanying paper. Figure 1 shows the deduced columns for ozone, HCl, and NO_2 deduced from the spectra, plotted as a function of latitude. It should be noted that there are many other factors varying as well as the latitude, but latitude seems to be the variable which most clearly provides a passage across the vortex boundary. It can be seen that south of 76°S., the column of ozone, HCl, and NO_2 all decrease markedly. The ratio of HCl to HF, normally about 5:1 in midlatitudes, approaches unity. Clearly the chemistry of chlorine and nitrogen are disturbed in the region of low ozone. While dynamical theories could perhaps explain a reduction of these three gases in the same region, since all are of stratospheric origin, it is difficult to see how any purely dynamical mechanism could produce the observed HCl:HF ratio, since the two gases have similar origins. A close look at other species to be reported as well as the correlation with other measurements, such as ClO (J. Anderson, private comm.) supports the conclusion that the ozone depletion is a result of chemical processes which deplete HCl and NO_x relative to the midlatitude situation.

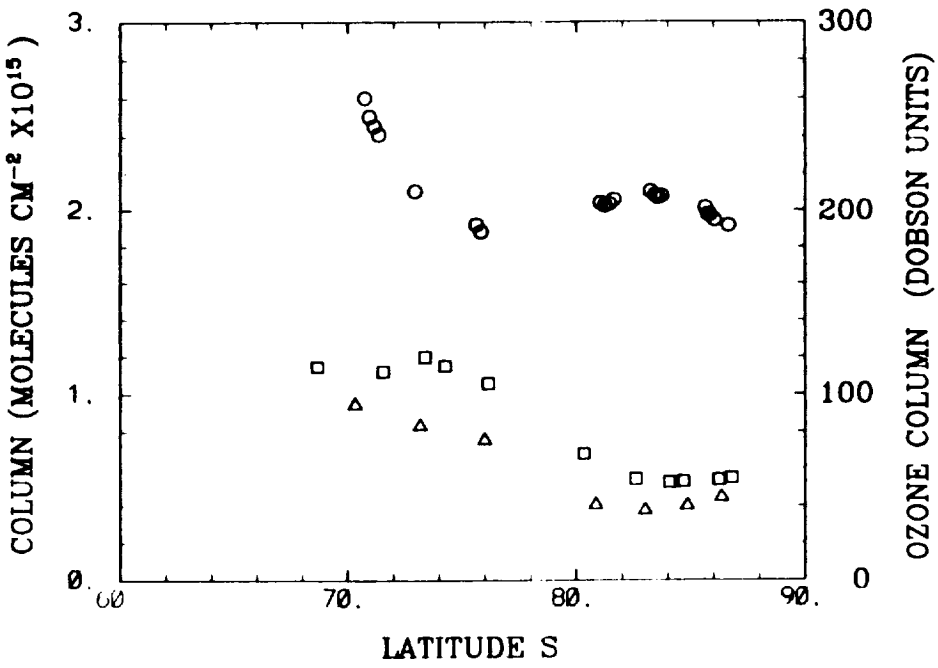

Figure 1. Latitudinal variation of observed columns of ozone, HCl, and NO_2 on September 21, 1987. The ordinate scale on the right refers to ozone, while the scale on the left refers to the other two molecules. o :ozone; □ HCl; △ :NO_2.

References

Coffey, M. T., W. G. Mankin, and A. Goldman, 1981: Simultaneous spectroscopic determination of the latitudinal, seasonal and diurnal variability of stratospheric N_2O, NO, NO_2 and HNO_3. *J. Geophys. Res., 86,* 733.

Farman, J.C., B.G. Gardiner, and J.D. Shanklin, 1985: Large losses of total ozone in Antarctica reveal seasonal ClO_x/NO_x interaction. *Nature, 315,* 207.

Mankin, W. G., 1979: Fourier transform method for calculating the transmittance of inhomogeneous atmospheres, *Appl. Opt., 18,* 3436.

Niple, E., W. G. Mankin, A. Goldman, D. Murcray, and F. Murcray, 1980: Stratospheric NO_2 and H_2O mixing ratio profiles from high resolution infrared solar spectrum using non linear least squares. *Geophys Res. Lett., 7,* 489.

Rothman, L.S., R.R. Gamache, A. Goldman, L.R. Brown, R.A. Toth, H.M. Pickett, R.L. Poynter, J.-M. Flaud, C. Camy-Peyret, A. Barbe, N. Husson, C.P. Rinsland, and M.A.H. Smith, 1987: The HITRAN database: 1986 edition. *Appl. Optics, 26,* 4058.

ABSTRACT

Infrared Aircraft Measurements of Stratospheric Composition over Antarctica during September 1987

G.C. Toon, C.B. Farmer, L.L. Lowes, P.W. Schaper, J.-F. Blavier and R.H. Norton
California Institute of Technology, Jet Propulsion Laboratory,
4800 Oak Grove Drive, Pasadena, CA 91109

The JPL Mark IV Interferometer recorded high resolution, infared solar spectra from the NASA DC-8 aircraft during flights over Antarctica in September 1987. The atmospheric absorption features in these spectra have been analyzed to determine the overburdens of O_3, NO, NO_2, HNO_3, $ClONO_2$, HCl, HF, CH_4, N_2O, CO, H_2O and CFC-12. The spectra were obtained at latitudes which ranged between 64°S and 86°S, allowing the composition in the interior of the polar vortex to be compared with that at the edge. The figure summarizes the latitude dependence observed for NO, NO_2, HNO_3, $ClONO_2$, HCl and HF. the solid lines South of 65°S are derived from the ensemble of Antarctic measurements. The values at 30°S were observed on the ferry flight from New Zealand to Hawaii. The dashed lines connecting the two have been interpolated across the region for which we have no measurements. The chemically perturbed region is seen to consist of a "collar" of high HNO_3 and $ClONO_2$ surrounding a "core" in which the overburdens of these and of HCl and NO_2 are very low. Clear increases in the overburdens of HF and HNO_3 were observed during the course of September in the vortex core. HCl and NO_2 exhibited smaller, less significant increases. The overburdens of the tropospheric source gases, N_2O, CH_4, CF_2Cl_2, CO and H_2O, were observed to be much smaller over Antarctica than at mid-latitudes. This, together with the fact that HF over Antarctica was more than double its mid-latitude value, suggests that downwelling has occurred.

SUMMARY OF LATITUDE VARIATIONS
OF STRATOSPHERIC TRACE GASES

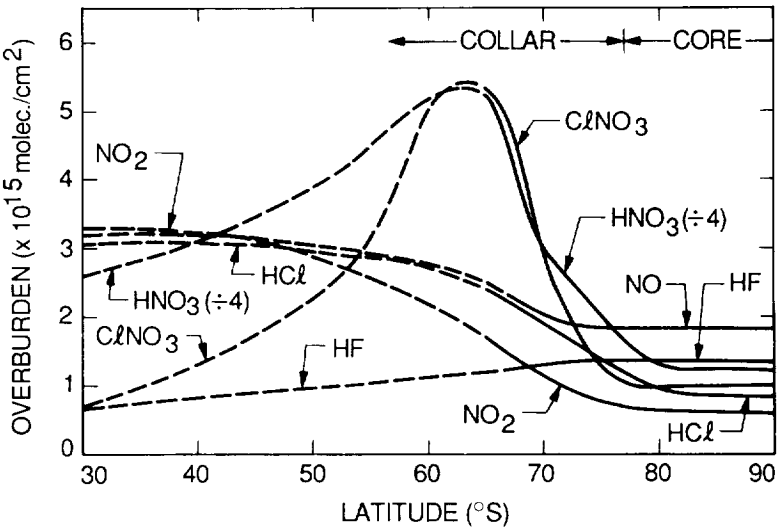

Infrared Measurements in the Spring 1987 Ozone Hole

F. J. Murcray, D. G. Murcray, A. Goldman
Physics Department
University of Denver
Denver, Colorado

J. G. Keys, W. A. Matthews
Physics and Engineering Laboratory, Lauder
Department of Scientific and Industrial Reasearch
Central Otago, New Zealand

Solar spectra were recorded from Arrival Heights (McMurdo), Antartica, with the University of Denver FTIR system (.02 cm^{-1} apodized resolution) during the austral spring of 1987. Spectra were recorded on 22 days from September 13 through October 28. The instrument was setup with 2 detectors for simultaneous operation in 2 wavelength regions: 750-1250 cm^{-1} (HgCdTe) and 2700-3100 cm^{-1} (InSb). Several stratospheric gases have measurable absorptions in these regions including HCl, HNO_3, O_3, $ClONO_2$, and NO_2. The system is equipped with an automatic solar tracking system and records data on tape cartridges. A portable personal computer allows Fourier transforming and initial processing of some of the data.

The equipment and personnel arrived during WINFLY in late August. Although the equipment was operational in early September, the weather prevented observations until September 13. Data were taken during clear periods until the drive mechanism failed after the run on October 28.

The HNO_3 gas column amount shows large variations, but no apparent correlation with stratospheric temperature. The HCl column shows a steady increase from 0.9 x 10^{15} molecules/cm^2

on September 13 to 1.5 x 10^{15} on October 6. McMurdo moved out of the polar vortex for a few days, and the HCl column jumped to 2.9 x 10^{15} by October 11. Although McMurdo moved back under the vortex, the HCl continued to increase, reaching 3.4 x 10^{15} at the end of the period.

Quantitative Observations of the Behavior of Anomalous Low Altitude ClO in the Antarctic Spring Stratosphere, 1987

R.L.de Zafra, M.Jaramillo, J.Barrett, L.Emmons, P.Solomon, and A.Parrish*
State University of New York, Stony Brook, N.Y.
*also at Millitech Corp, S.Deerfield, Mass.

During the second National Ozone Expedition we carried out ground-based observations at McMurdo Station Antarctica which resulted in a second season's measurement of abnormally large amounts of chlorine monoxide in the antarctic spring stratosphere. Our original measurements of 1986, in which the presence of this anomalous layer was first discovered (R.L.de Zafra, et al. 1987 and P.Solomon, et al., 1987), were limited in low altitude recovery of the ClO mixing ratio profile by the restrictions of the spectral bandwidth (256 MHz) which was used to measure the pressure-broadened ClO emission line shape. Our 1987 measurements were marked by the use of twice the spectral bandpass employed the previous year, and allow a better characterization of the ClO mixing ratio profile in the critical altitude range 18-25 km. In-situ aircraft measurements of ClO made over the Palmer Peninsula during August and September of 1987 by Anderson, et al. effectively determined the important question of the ClO mixing ratio profile at altitudes inaccessible to our technique, below ~18 to 18.5 km. These flights did not penetrate further than 72°S, however, (vs 78°S for McMurdo) and were thus limited to coverage near the outer boundaries of the region of severest ozone depletion over Antarctica in 1987, did not reach an altitude convincingly above that of the peak mixing ratio for ClO, and were not able to make significant observations of the diurnal variation of ClO. The two techniques, and the body of data recovered by each, thus complement one another in producing a full picture of the anomalous ClO layer intimately connected with the region of antarctic springtime ozone depletion. In this talk we shall present an analysis of the mixing ratio profile from ~18 to 45 km, the diurnal behavior, and briefly comment on the secular change in ClO over McMurdo Station during September and early October 1987.

The 1987 Antarctic spring vortex was markedly more regular in shape and more closely centered on the pole than in 1986, or in fact during other recent years. Stratospheric temperatures were also significantly and consistently lower at the stratopause than in 1986 (Hofmann, et al, private communication) and ozone depletion was more severe than ever before recorded. Conditions at ground level at McMurdo were rather less stable than in 1986, however, and observations were hampered by more frequent storms and by generally higher tropospheric opacity due to higher ground temperatures and greater water vapor content. Our observations for 1987 are consequently of shorter overall duration - from September 8 to October 13 - and more frequently interupted or rendered of poorer quality by marginal observing conditions than in 1986. We shall concentrate our attention here on data taken over the period Sept. 20-24 for a detailed discussion of the mixing ratio profile, the peak mixing ratio for ClO, and the diurnal behavior. Some conclusions will be drawn with respect to the secular trend during the period from Sept.8 to Oct.13, using data in blocks averaged over several days each.

We employ high-resolution spectral measurements of the pressure broadened line shape and intensity of the 278 GHz (1.1 mm) rotational emission line of ClO, using a cryogenically cooled mm-wave heterodyne receiver coupled to a filterbank spectrometer having 512 contiguous channels of 1 MHz bandwidth each.

The pressure-broadening coefficient for the 278 GHz line of ClO is about 3 MHz/mb (hwhm for a Lorentzian lineshape) so that well-resolved line shapes can be measured over an altitude range of ~17 to 45 km (or ~80 to 1 mb, with respect to the antarctic pressure profile). The sum of emission line intensities over all contributing stratospheric layers yields a pressure-broadened non-Lorentzian line shape which can be deconvolved against measured pressure and temperature profiles to recover a mixing ratio profile for ClO or any other detected species. The accuracy with which this can be achieved depends critically on the signal/noise ratio of the data, and also varies with altitude and with the actual mixing ratio profile. Discussion of the accuracy with which mixing ratio profiles may be retrieved from our 1987 data, for the prevailing conditions, is covered in a companion paper at this workshop (P. Solomon, et al.).

Deconvolutions are carried out by a modified Chahine-Twomey algorithm, in which an initial mixing ratio profile is iteratively modified to yield successively better fits between the resulting synthesized line shape and the experimental data. This proceedure decreases rapidly in sensitivity at low (<~18 km) and high (>~45 km) altitudes: for this reason, we have chosen to assume an upper limit of 0.3 ppbv for the ClO mixing ratio at 15 km, in approximate agreement with in situ ER-2 aircraft measurements, to assist in achieving a reasonable lower altitude profile for the work presented in this paper. The assumption of one-third this value at 15 km has a negligible effect in altering the resultant retrieved profiles. Above 15 km, the profiles are determined by the deconvolution process. The effect of choosing different initial profile shapes between 15 and 25 km on the final retrieved profile has also been explored and is discussed elsewhere (P.Solomon, et al., this workshop): to summarize, maximum mixing ratio and the altitude at which it occurs are altered by no more than 20% and 10% respectively by the use of initial mixing ratio profiles differing by as much as a factor of 5.

Our result for the mid-day mixing ratio profile for the period Sept.20-24 is shown in Fig.1b, retrieved from the emission lineshape shown in Fig.1a. The mixing ratio profile is strongly separated into two distinct layers, a 'normal' high altitude component peaking around 37 km, and an anomalous low altitude layer never seen at tropical or mid latitudes, and exhibiting a mixing ratio in excess of 100 times that normally found (Brune, et al., 1988) at mid latitudes in this altitude range . This anomalous low altitude component is responsible for the broad wings in the lineshape of Fig.1a.

We find the peak mixing ratio to be 1.8 (+.5,-.9) parts per billion by volume and to occur at an altitude of 19 $\pm$ 1 km. The vertical column of ClO from 15 to 27 km derived from the profile of Fig.1b is 2.1 $\pm$ 0.5 x $10^{15}/cm^2$. The error margins quoted here are intended to include both uncertainties in intensity calibration (~12 %) and deconvolution accuracy.

The low altitude component shows a strong diurnal dependence, as exhibited in Fig.2, where data for Sept.20-24 has been averaged and binned in 2-hour time blocks starting 2 hours before dawn (defined at 20 km) and ending 6 hours after sunset. (The smooth curves fitted to the data are synthesized from mixing ratio profiles obtained by deconvolution for the mid-day intervals and by trial lineshape fitting for the remaining intervals ,where diminishing S/N ratios provide less reliable deconvolution results.) The high altitude component of ClO is seen to persist throughout the night (about 8 hours duration) with diminished intensity, while the low altitude component appears to drop below the level of detectability by sunset and does not detectably reappear until the time interval 2-4 hours after sunrise, after which it shows a very rapid increase to midday.

In Fig.3 we exhibit a time progression of mixing-ratio profiles consistent

with the synthesized lineshapes (smooth curves) of Fig.2. In this plot, the vertical lines mark the midpoints of the two-hour time intervals into which the data was binned. (But note that the mid-day block, as in Fig.2, contains all data taken at least 6 hours after sunrise and at least six hours before sunset. This block is ~ 4 hours in length). In Fig. 4, the integrated vertical column density obtained from the profiles of Fig.3 between 15 and 27 km are shown as a function of time. The error bars reflect the range of values obtained from mixing ratio profiles giving equally good fits (within a chosen quality factor) to the lineshape measurements of Fig.2. Meaningful models of antarctic chlorine chemistry must meet the constraints imposed by these observations. These results are in qualitive agreement with recent diurnal modeling reported by Salawitch, et al.(1988), but do not allow any clear choice between various BrO and ClO reactions proposed in that work.

References:

Brune,W.H., E.M. Weinstock, and J.G.Anderson, "Midlatitude ClO Below 22 km Altitude: Measurements with a New Aircraft-Borne Instrument", Geophys. Res. Letters, 15, 144-147, 1988.

de Zafra,R.L., M.Jaramillo, A.Parrish, P.Solomon, B.Connor, and J.Barrett, "High Concentrations of Chlorine Monoxide at Low Altitudes in the Antarctic Spring Stratosphere: Diurnal Variation", Nature, 328, 408-411, 1987.

Salawitch,R.J., S.C.Wofsy, and M.B.McElroy, "Chemistry of OClO in the Antarctic Stratosphere: Implications for Bromine", Planet. Space Sci., Feb.1988.

Solomon,P.M., B.Connor, R.L.de Zafra, A.Parrish, J.Barrett, and M.Jaramillo, "High Concentrations of Chlorine Monoxide at Low Altitudes in the Antarctic Spring Stratosphere: Secular Variation", Nature, 328, 411-413, 1987.

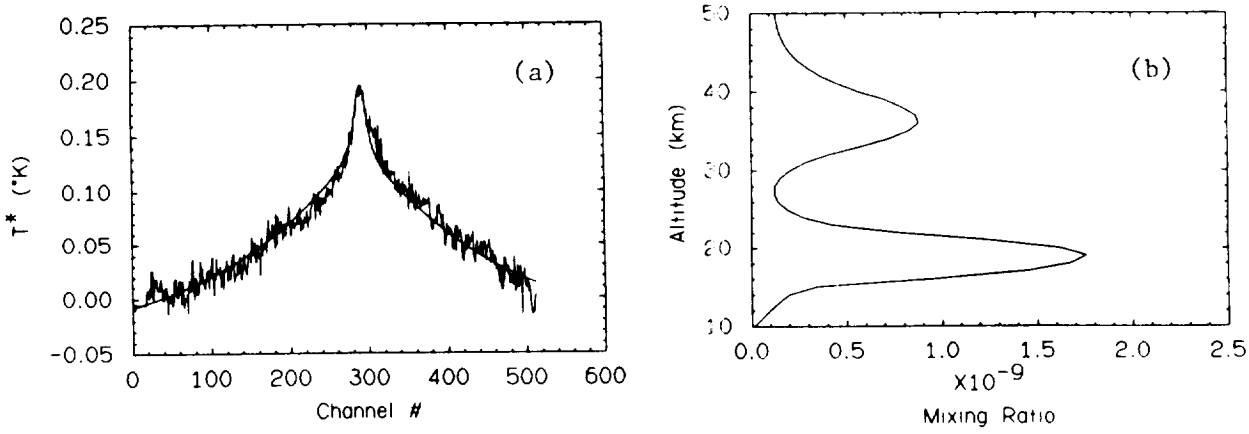

Fig.1 a) Midday ClO signal for the period 9/20-24/87. Abscissa is in channel number, at 1 MHz/channel, ordinate is in degrees equivalent radiative temperature. Smooth curve is synthesized lineshape given by mixing ratio profile in (b). b) Mixing ratio profile obtained by deconvolution from data in (a).

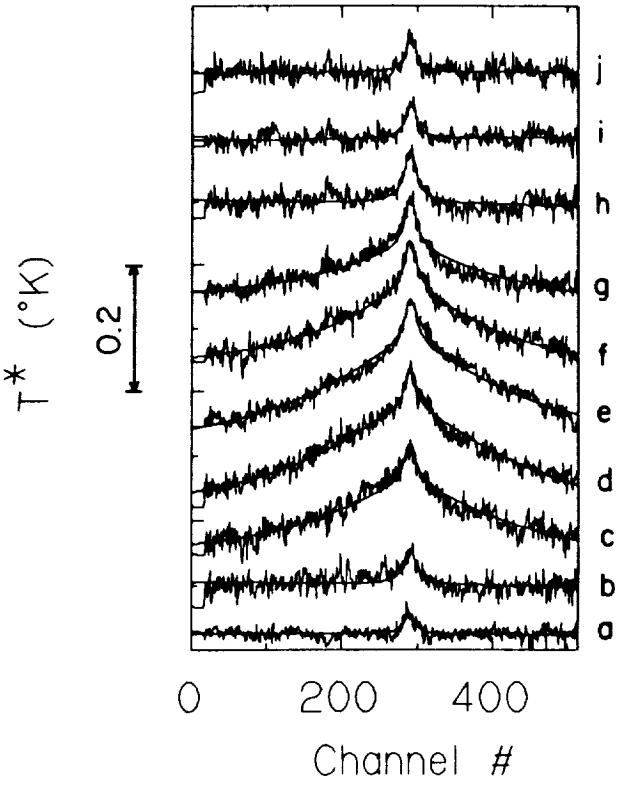

Fig.2. Data from 9/20-24/88 averaged into two-hour time bins counting forward from dawn and backward from sunset. "a" is -2 to 0 hrs before dawn, "b" is 0 to 2 hrs after dawn, etc. "h" is sunset to 2 hrs before, "g" is -4 to -2 hrs from sunset, etc. "e" is midday block ~ 4 hrs long, starting 6 hrs post-dawn and ending 6 hrs pre-sunset (dawn and sunset at 20 km). Smooth curves are synthesized linefits generated from recovered vertical profiles.

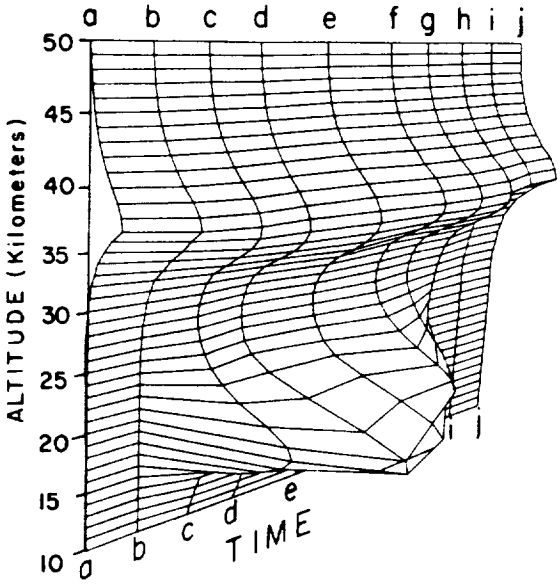

Fig.3 Time evolution of vertical mixing ratio profiles recovered from data. Same profiles generate linefits of Fig.2.

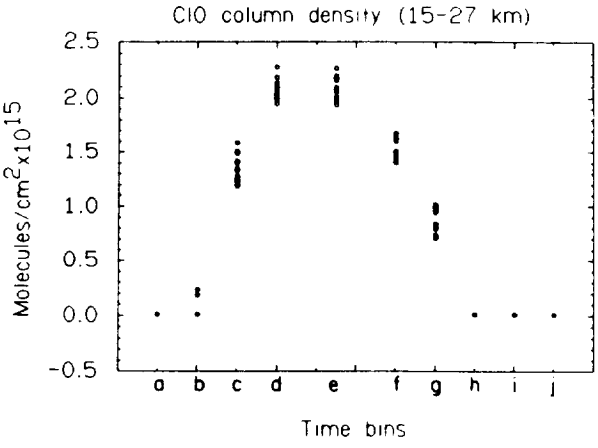

Fig.4 Integrated column densities of lower altitude components of ClO, obtained from recovered mixing ratio profiles for time-bins of Fig. 2. Range of points represent results from various deconvolutions meeting the same criterion of quality-of-fit to data.

DAYTIME *ClO* OVER McMURDO IN SEPTEMBER 1987: ALTITUDE PROFILE RETRIEVAL ACCURACY

J.Barrett,P.Solomon, M.Jaramillo, R.deZafra, A.Parrish*, and L.Emmons
State University of New York, Stony Brook, NY
*also at Millitech Corp., South Deerfield, MA

During the 1987 National Ozone Expedition, mm-wave emission line spectra of the 278.6 GHz rotational stratospheric *ClO* were observed at McMurdo Station, Antarctica (deZafra *et al.*, these proceedings). The results confirm the 1986 discovery (deZafra *et al.*, *Nature* **328**, 408, 1987; Solomon *et al.*, *Nature* **328**, 411, 1987) of a lower stratospheric layer with ~100 times the normal amount of *ClO*; our 1987 observations, made with a spectrometer bandwidth twice that used in 1986, make possible a more accurate retrieval of the altitude profile of the low altitude component of stratospheric *ClO* from the pressure broadened line shape, down to ~16 km. The accuracy of the altitude profile retrievals is discussed, using the "daytime" (09:30 to 19:30, local time) data from 20 to 24 September, 1987 as an example. The signal strength averaged over this "daytime" period is ~85% of the midday peak value. We also discuss the rate of ozone depletion implied by the observed *ClO* densities.

Figures 1 & 2 show the derived *ClO* profile in units of mixing ratio and number density respectively. For the initial guess at the altitude profile required by the deconvolution algorithm, we used a constant 0.5 ppbv at altitudes above 18 km. Below 18 km, we assumed that the *ClO* mixing ratio declined rapidly as found in the *in situ* aircraft measurements (NASA Press Release, October, 1987) over the Palmer Peninsula during August and September, 1987.

The distribution is bimodal with maxima at 19 km and at about 36 km. The uncertainty in the derived profile is much greater for the upper stratospheric *ClO*, which depends on the intensities over narrow frequency intervals near the line center, while the lower stratospheric mixing ratio depends on intensities averaged over wide frequency intervals in the spectral line wings. In this paper we will focus on the lower stratosphere, which is the location of the Antarctic ozone depletion.

The sources of error include 1) system calibration, 2) statistical noise in the data, 3) baseline curvature due to variations in instrumental response across the spectrum, 4) the effect of the initial guess on the retrieved profile and 5) the bias introduced by the retrieval technique.

1) The instrumental calibration has an uncertainty of ±12%. Since this results in an uncertainty in the overall scaling of the profile which is independent of altitude, we have not included it in the error bars in Figures 1 & 2.

2) The largest errors, particularly in the upper stratosphere, are from the statistical noise in the spectral line data. Monte Carlo tests of the retrieval algorithm were carried out to determine the magnitude of the expected errors. The noise-free spectral line shape that

would be observed if our derived altitude profile were the actual ClO profile was calculated. Gaussian noise at the same level as that in our data was then added to this line shape, and the result fed into the deconvolution algorithm to produce an output profile. This was done many times, with different noise spectra added, producing an ensemble of output profiles. Figure 3 shows the the two profiles from this ensemble which give the extreme high and low values of the ClO mixing ratio at 20 km. This ensemble was analyzed statistically, and the error bars in Figures 1 & 2 represent plus and minus twice the standard deviation (95% confidence interval) obtained in this analysis.

3) As can be seen in Figure 4, the spectral line appears symmetrical with little evidence of baseline curvature. It is possible to derive altitude profiles using only the low frequency or only the high frequency side of the line. These are shown in Figure 5, along with the profile derived using the whole line (which also appeared in Figure 1). The differences are very small for the lower stratosphere, consistent with those expected just from differing statistical noise in the two sides of the spectrum.

4) We have found that within a wide range of initial guesses at constant mixing ratio (0.1 to 1.0 ppbv from 16 to 50 km), the retrieved profile varied only slightly and the possible errors were small compared to those from statistical noise. The effect of the fixed ClO mixing ratio below 15 km is also small, providing that the true mixing ratio at 14 km is less than that of the peak.

5) In interpreting the altitude profile we note that the retrieval cannot recover any small scale layering in the ClO profile. We have carried out Monte Carlo tests to determine the accuracy with which the retrieval algorithm can recover model altitude profiles of varying width from the corresponding spectral line shapes with noise added; these show that if the layer is at least 6 km thick (full width at half maximum), the thickness will be successfully recovered. We find that the ClO layer over McMurdo has half of the peak mixing ratio at 16 and 23 km or a thickness of 7 km. (see Figure 1).

In the lower stratosphere, the peak daytime ClO mixing ratio is 1.55 ± 0.3 ppbv, centered at an altitude of 19 ± 1 km, falling to half peak at 16 and 23 km, and falling below 0.3 ppbv above 24 km. Thus, during the day, a half of the available chlorine is in the active form, ClO. For the purposes of determining the ozone depletion rate due to chlorine it is more convenient to look at the ClO density profile in Figure 2. This shows a layer centered at 18 km, with a peak density of $[ClO] = 2.9 \times 10^9\ cm^{-3}$, and extending from 22 km at the top down to about 15 km. The altitude of this layer corresponds very closely to the altitude range of ozone depletion found above McMurdo during the same time period (Hofmann *et al.*, Preprint, January, 1988), which shows strong ozone depletion extending from 15 to 22 km.

These very high ClO densities are favorable for a depletion mechanism which depends on the square of the ClO density (Molina and Molina, *J. Phys. Chem.* **91**, 433, 1986). In this mechanism the rate limiting step is the formation of the ClO dimer through the reaction:

$$ClO + ClO + M \rightarrow Cl_2O_2 + M$$

If we assume that the preferred destruction channels of Cl_2O_2 release two free chlorine atoms, either by photodissociation or thermal decomposition, then the rate of ozone destruction is twice the rate of formation of the ClO dimer. Letting $t_{1/2}$ be the ozone half

life, K be the rate constant for the dimer formation and $MR(O_3)$ the mixing ratio of ozone,

$$t_{1/2} = \frac{0.69\, MR(O_3)}{2\, K\, [ClO]^2}$$

Using $K = 6.1 \times 10^{-32}\ cm^6 s^{-1}$ (Hayman *et al.*, *GRL* **13**, 1347, 1986), $[ClO] = 2.9 \times 10^9\ cm^{-3}$ and $MR(O_3) = 1.5 \times 10^{-6}$ gives $t_{1/2} = 1.0 \times 10^6$ seconds. Since these numbers are representative of the twelve hours of daylight, the actual time scale for the ozone depletion is

$$t_{1/2} = 23\ days$$

This time scale is also in approximate agreement with observed rate of ozone depletion.

These *ClO* observations thus demonstrate that both the altitude and rate of ozone depletion can be accounted for by chlorine acting through the *ClO* dimer mechanism.

Figure 1. 20 – 24 SEPT, 1987. AVERAGE DAYTIME ClO.

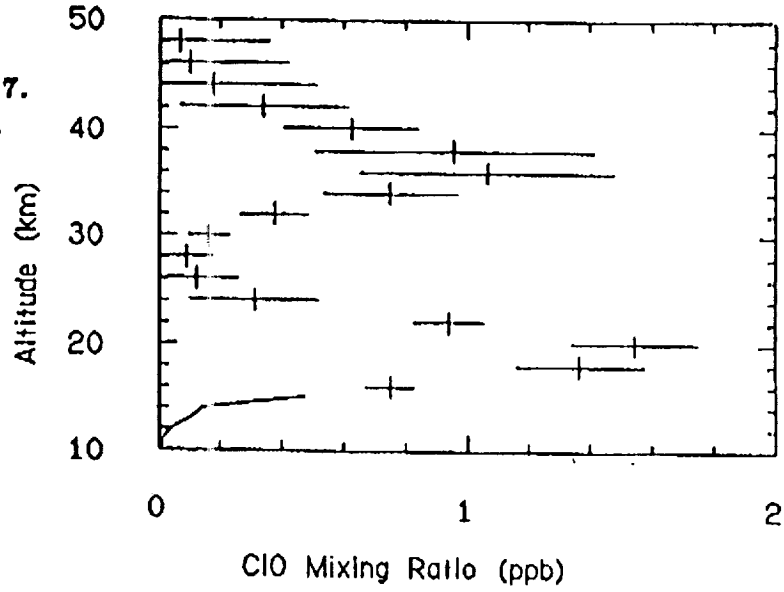

Figure 2. 20 – 24 SEPT, 1987. AVERAGE DAYTIME ClO.

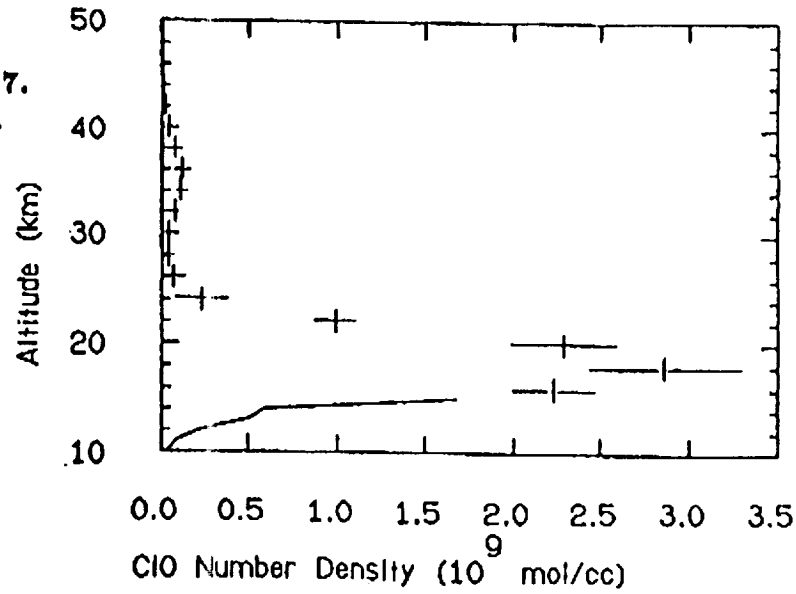

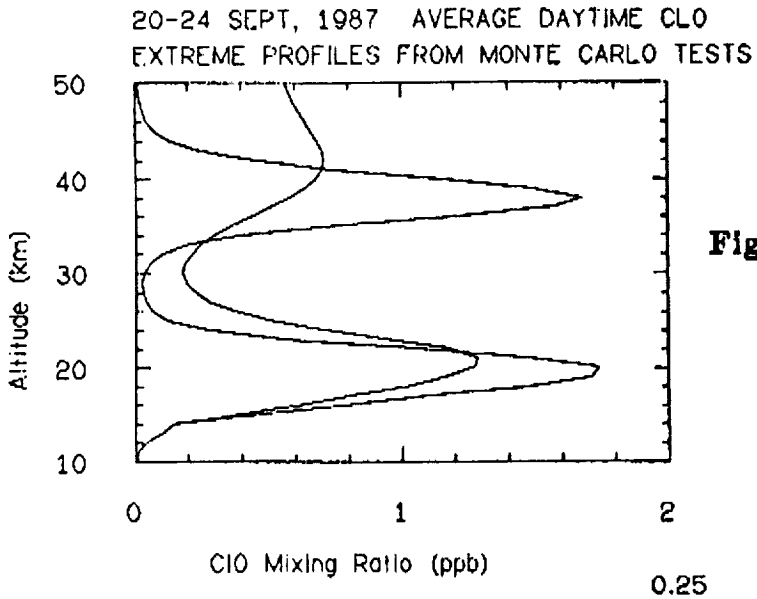

Figure 3.

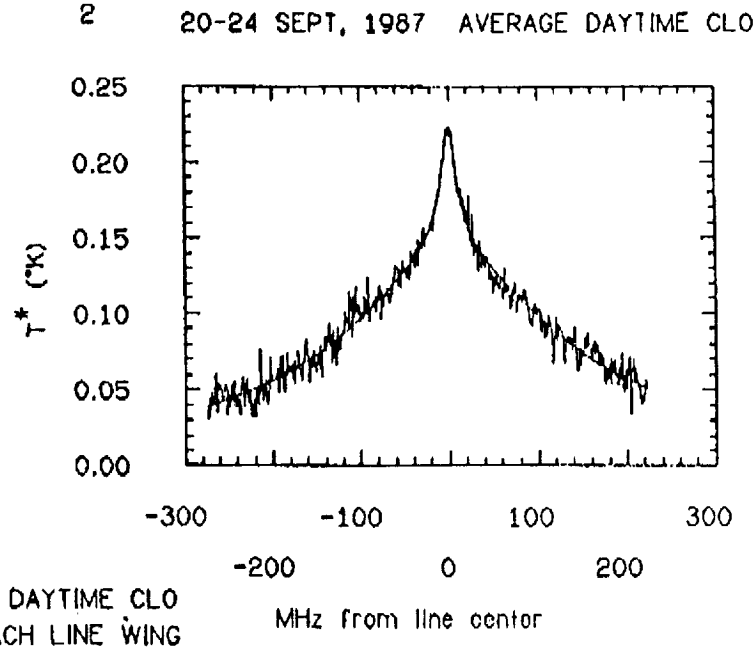

Figure 4.

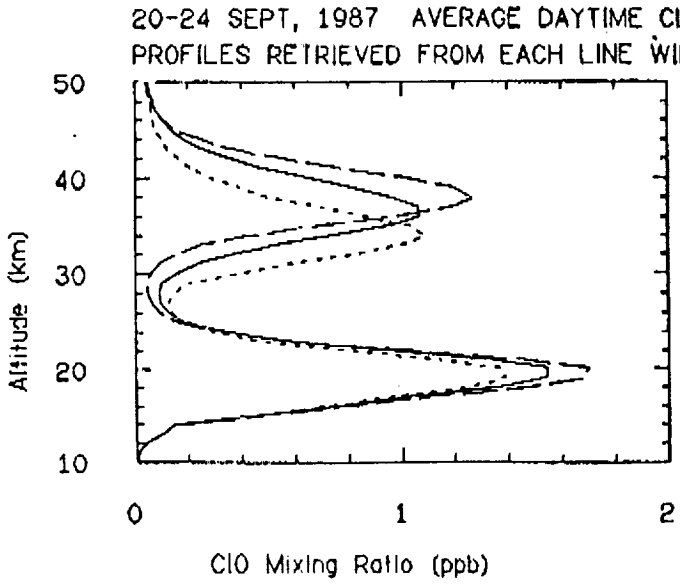

Figure 5. Profiles recovered from full spectrum (solid line), low frequency side only (dashed line) and high frequency side only (dotted line).

An FTIR Spectrometer for Remote Measurements of Atmospheric Composition

C.B. Farmer, P.W. Schaper, G.C. Toon, J.-F. Blavier,
G. Mohler and D. Petterson, Jet Propulsion Laboratory,
California Institute of Technology, Pasadena, California 91109

Abstract

The JPL Mark IV interferometer, an infrared Michelson interferometer, was built specifically for recording high resolution solar absorption spectra from remote ground-based sites, aircraft and from stratospheric balloons. The instrument is double-passed, with one fixed and one moving corner reflector, allowing up to 200-cm of optical path difference (corresponding to an unapodised spectral resolution of 0.003 cm^{-1}). The carriage which holds the moving reflector is driven by a flexible nut riding on a lead screw. This arrangement, together with the double-passed optical scheme, makes the instrument resistant to the effects of mechanical distortion and shock.

The spectral range of the instrument is covered by two liquid nitrogen-cooled detectors: an InSb photodiode is used for the shorter wavelengths (1.8-5.5 μm, 1,800-5,500 cm^{-1}) and a HgCdTe photoconductor for the range (5.5-15 μm 650-1,800 cm^{-1}). For a single spectrum of 0.01 cm^{-1} resolution, which requires a scan time of 105 seconds, the signal/noise ratio is typically 800:1 over the entire wavelength range.

Temporal and spatial distribution of stratospheric trace gases over Antarctica in August and September, 1987

by
M. T. Coffey and William G. Mankin
*National Center for Atmospheric Research**
P. O. Box 3000, Boulder, Colorado 80307

There have been a large number of suggestions made concerning the origin of the Antarctic "ozone hole" since its discovery by Farman *et al.* (1985); these have included suggestions that it is related to changes in polar meteorology, changes in stratospheric chemistry, or changes in the solar input, or combinations of these effects. Supporting or refuting these theories requires a wide variety of data for comparison with the predictions. In August and September, 1987, a field observation expedition was made over Antarctica from a base in Punta Arenas, Chile. Two aircraft, an ER-2 with *in-situ* instruments flew at altitudes up to 18 km measuring ozone, water, ClO, BrO, NO_x, particles, and meteorological parameters in the ozone layer. A DC-8 flew at altitudes of 10-12 km, below the ozone layer, using remote sensing instruments for measuring composition and aerosol content of the ozone layer, as well as *in-situ* instruments for measuring composition at aircraft altitudes.

The observation of a number of chemical species and their correlation with each other and with meteorological parameters gives a useful set of data for comparison with various theories. Infrared spectroscopy is a particularly valuable observational technique for this purpose as it can measure with good sensitivity and time resolution and can measure a large number of chemical species simultaneously. Two high resolution infrared spectrometers were among the instrument complement on the DC-8. Our experiment, described in greater detail in the accompanying paper, enabled us to determine the total column above the flight aircraft of ozone, water, methane, nitrous oxide, nitric oxide, nitrogen dioxide, nitric acid, hydrochloric acid, hydrofluoric acid, chlorine nitrate, and several other species. Many of these were measured nearly in real time. Plots of the geographical variation of these species on various flights enables us to see how the concentration of these constituents varies inside and outside the vortex, as well as to see the temporal development of their concentration during the late winter and early spring. It is especially interesting to look for changes after mid-September, when the stratosphere began to warm above the temperatures for condensation of water and nitric acid at stratospheric concentrations.

Figure 1 shows samples of our data for three chemical species for two days late in the mission. We shall show similar results for other observed species throughout the whole mission, along with midlatitude results for comparison. The correlation of these measurements with the meteorological situation will be considered.

**The National Center for Atmospheric Research is sponsored by the National Science Foundation.*

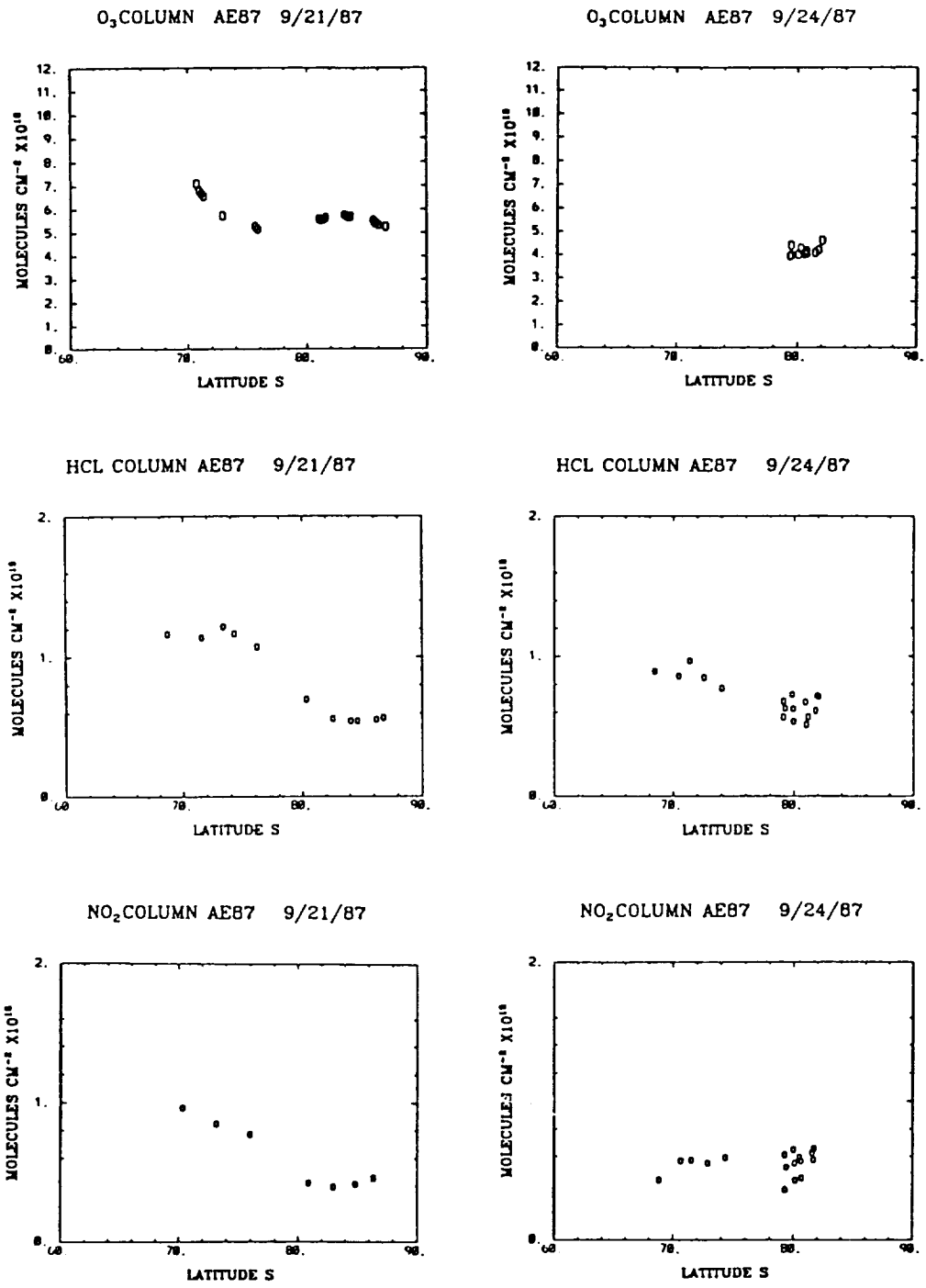

Figure 1. Latitudinal variation of ozone, hydrochloric acid, and nitrogen oxide above the DC-8 flight altitude on 21 September and 24 September, 1987.

Reference

Farman, J.C., B.G. Gardiner, and J.D. Shanklin, 1985: Large losses of total ozone in Antarctica reveal seasonal ClO_x/NO_x interaction. *Nature, 315,* 207.

N89-14552

MEASUREMENTS OF OZONE IN THE ANTARCTIC REGION DURING AUGUST AND SEPTEMBER OF 1987

Walter L. Starr and James F. Vedder
NASA Ames Research Center
Moffett Field, California

Mixing ratios are presented for ozone in the austral polar atmosphere during August and September of 1987. Since the mid-1970's, there has been a continuing decrease in the total column abundance of ozone over Antarctica during the late winter and early spring. This reduction now amounts to about one-half of the historical October mean. The recent discovery of this phenomenon has stimulated several theoretical and experimental efforts to understand the mechanisms responsible for the reduction. The results presented here are derived from an ultraviolet ozone photometer designed and built by NASA Ames Research Center and installed on NASA's multi-instrumented, high-altitude ER-2 aircraft. This aircraft carrying 14 instruments participated in a major effort to penetrate the region of depletion. Data were gathered between latitudes of 53° and 72° south at pressure altitudes (U.S. Standard Atmoshere) up to 21 km in a series of 12 flights from Punta Arenas, Chile, over the Palmer Peninsula. Additional data were obtained between latitudes of 37° north and 53° south on the 3 flight legs required to reach Punta Arenas from Moffett Field, California, and on the same return legs to Moffett Field. The photometer is located on the aft section of the main instrument bay of the aircraft. The air inlet probe protrudes into the airstream at a location on the right side of the aircraft close to the instrument. The sampled airflow is driven by the dynamic pressure generated by the aircraft's motion and is vented just aft of the inlet. The information required for the calculation of the mixing ratio for ozone is stored in battery backed RAM each second throughout a flight. The pressure altitude, total air temperature, and Mach number are also recorded by this instrument. A typical flight profile consisted of a southbound path on the 428° K potential temperature surface, a descent to a pressure altitude of 13.7 km, a climb to 460° K surface, and return on this surface. The mixing ratios for ozone at pressure altitudes above 15 km in the southern part of the flights were significantly lower than values outside the polar vortex. The observed ozone mixing ratios indicate the effects of chemistry as well as the effects of the stratospheric polar vortex. Examples of the distributions of ozone mixing ratios as a function of altitude, latitude, or time and the relationships to temperature and other trace gases are presented.

Observations of the diurnal variations of BrO and OClO at McMurdo Station, Antarctica (78S)

S. Solomon[1], R. W. Sanders[2], M. A. Carroll[1], and A. L. Schmeltekopf[1]

[1] Aeronomy Laboratory, NOAA, Boulder, CO 80303

[2]Cooperative Institute for Research in Environmental Science (CIRES), University of Colorado, Boulder, CO 80309

Observations of the diurnal variations of OClO and BrO during austral spring, 1987 using long-path visible and near-ultraviolet absorption spectroscopy are presented and compared to simplified model calculations. It is shown that care must be taken to compare model calculations and measurements along the line of sight of the instrument. Evening twilight observations of OClO are shown to be broadly consistent with current photochemical schemes, assuming ClO and BrO levels near 50 mb of about 0.5 ppbv and 7 pptv, respectively, throughout the observing period from late August to mid-October. Nighttime observations of OClO obtained using the moon as a light source display evidence for growth through the night in late-August, but not in late-September. Further, the observed morning twilight OClO abundances are in agreement with model calculations in late August, but generally fall below in late September and October. Observations of BrO in mid-September systematically show far greater evening twilight than morning twilight abundances. It is shown that the diurnal variations of BrO and OClO in mid-September and October can be explained by formation of the $BrONO_2$ reservoir species at night, although other reservoir species with comparably long lifetimes could also explain the observations. If formation of $BrONO_2$ is the correct explanation for these data, the observations suggest that NO_2 levels in the antarctic lower stratosphere are on the order of a few pptv or less in late August, a few tens of pptv in mid-September, and a few hundred pptv in October. Constraints on the coupled nitrogen-halogen chemistry of the austral spring season revealed by the observed diurnal variability of OClO and BrO will be discussed.

SESSION V - In-Situ Measurements of Chemical Species and Their Interpretation - A
Presiding, S. Solomon, NOAA/Aeronomy Laboratory
Wednesday Morning, May 11, 1988

IN SITU OBSERVATIONS OF *ClO* IN THE ANTARCTIC: EVIDENCE FOR CHLORINE CATALYZED DESTRUCTION OF OZONE

J.G. Anderson and W.H. Brune
Department of Chemistry
and
Department of Earth and Planetary Science
Harvard University
Cambridge, MA 02138

M.J. Proffitt
NOAA Aeronomy Laboratory
325 Broadway
Boulder, CO 80302

W. Starr and K.R. Chan
NASA Ames Research Center
Mountain View, CA 94043

Results from a series of twelve ER-2 aircraft flights into the Antarctic polar vortex are summarized. These in situ data define the spatial and temporal distribution of *ClO* as the aircraft flew at an altitude of ~ 18 km from Punta Arenas (54°S latitude) to the base of the Palmer Peninsula (72°S latitude), executed a rapid descent to ~ 13 km, turned north and climbed back to ~ 18 km, returning to Punta Arenas. A general pattern in the *ClO* distribution is reported: mixing ratios of approximately 10 ppt are found at altitude in the vicinity of 55°S increasing to 50 ppt at 60°S. In the vicinity of 65°S latitude a steep gradient in the *ClO* mixing ratio is observed. At a fixed potential temperature, the *ClO* mixing ratio through this sharp transition increases by an order of magnitude within a very few degrees of latitude, thus defining the edge of a "chemical containment vessel." From the edge of that containment vessel to the southern extension of the flights, 72°S, a dome of slowly increasing *ClO* best describes the distribution. Peak mixing ratios at 18

km at the southern extension of the flight track increased to 1.2 ppbv by 22 September. This corresponds to approximately 500 times the ClO mixing ratio observed at comparable altitudes at midlatitude.

At the southernmost extent of the aircraft trajectories ($\sim$ 72°S latitude) the vertical scan revealed the following gradient in ClO mixing ratio with potential temperature: 1.2 ppbv @ 450°K, 1.0 ppbv @ 440°K, 0.9 ppbv @ 430°K, 0.8 ppbv @ 420°K, 0.7 ppbv @ 410°K, 0.5 ppbv @ 400°K, 0.4 ppbv @ 390°K, 0.3 ppbv @ 380°K, 0.25 ppbv @ 370°K, 0.2 ppbv @ 360°K, 0.1 ppbv @ 350°K.

It is demonstrated using data from the first flights (17, 18 and 23 August) that in the region of high ClO, poleward of the containment vessel wall, ozone emerges from the austral polar night largely unperturbed, with little distinction between concentration observed inside (poleward) and outside (equatorward) of the chemical containment vessel wall. During the first three weeks of September, this condition alters dramatically such that by the flight of 16 September, ozone has dropped by a factor of two within the chemical containment vessel with further erosion occurring to the end of the mission on 22 September. Through the wall of the containment vessel which clearly defines the spatial transition from unperturbed ozone (and low ClO) equatorward to dramatically reduced ozone (and high ClO) poleward of the vessel wall, both ozone and ClO execute large fluctuations in mixing ratio (a factor of 2 to 3) on surfaces of constant potential temperature and in all cases these fluctuations are strongly negatively correlated.

Based upon observed concentrations of ClO as a function of latitude, altitude and time, the rate of ozone removal based on the dimerization mechanism

$$ClO + ClO \rightarrow ClOOCl$$

$$ClOOCl + h\nu \rightarrow Cl + ClOO$$

$$ClOO + M \rightarrow Cl + O_2 + M$$

$$\underline{2 \times (Cl + O_3 \rightarrow ClO + O_2)}$$

$$Net: \quad 2O_3 \rightarrow 3O_2$$

is compared with the observed rate of ozone disappearance. The rate determining step is taken to be $ClO + ClO \rightarrow ClOOCl$ with a rate of

$$d[O_3]/dt = 2k^{III}[M][ClO]^2$$

A radiative transfer model is used to calculate the "waveform" of ClO as a function of solar zenith angle which is then normalized to the observed concentration of $[ClO]$ to determine

$$\Delta O_3 = 2 \int k^{III}[M][ClO]^2 dt$$

for each day from early August through the end of the mission. Comparison between (1) the rate determining step in the above catalytic cycle based on observed $[ClO]$ and (2) the observed rate of ozone loss at the 450°K, 440°K, 430°K, 420°K, 410°K, 400°K, 390°K, 380°K, 370°K and 360°K potential temperature surfaces demonstrates that, within experimental uncertainty, the observed rate of ozone loss is consistent with the rate limiting step from the 450°K surface to below the 400°K surface.

We conclude the following:

1. ClO concentrations define the edge of a chemical containment vessel which mimics the position of the Antarctic polar votex.
2. Within this containment vessel, ClO concentrations reach 500 times those found at comparable altitudes at midlatitude. Altitude profile at the southern end of the flight trajectories show that the ClO mixing ratio is very steep.
3. Ozone emerges from the austral polar night largely unperturbed. However, within the chemical containment vessel during the first three weeks of September, ozone drops by a factor of two to three such that a strong anticorrelation develops between ClO and O_3 through the wall of the containment vessel.
4. The observed rate of ozone disappearance equals, within experimental uncertainty, the rate limiting step of the ClO-ClO dimer catalytic cycle based on observed concentrations of ClO.

Measurements of NO and total reactive odd-nitrogen, NOy, in the Antarctic Stratosphere

by

D. W. Fahey [1], D. M. Murphy [1,3], C. S. Eubank [1,3],

G. V. Ferry [2], K. R. Chan [2], M. K. W. Ko [4]

[1] Aeronomy Laboratory
National Oceanic and Atmospheric Administration
325 Broadway
Boulder, Colorado 80303

[2] Ames Research Center
National Aeronautics and Space Administration
Moffett Field, California 94035

Cooperative Institute for Research in Environmental Sciences
University of Colorado
Boulder, Colorado 80309

[4] Atmospheric and Environmental Research, Inc.
840 Memorial Drive
Cambridge, MA 02139

Measurements of NO and total reactive nitrogen, NOy, were made as part of the Airborne Antarctic Ozone Experiment conducted in Punta Arenas, Chile during August and September 1987. The total reactive nitrogen reservoir includes the species NO, NO2, NO3, N2O5, HNO3, and CLONO2. The instrument was located on board the NASA ER-2 aircraft which conducted twelve flights over the Antarctic continent reaching altitudes of 18 km at 72 S latitude. The NOy technique utilized the conversion of component NOy species to NO on a gold catalyst and the subsequent detection of NO by the chemiluminescence reaction of NO with ozone. Since the inlet sample line is heated and the catalyst operates at 300 C, NOy incorporated in aerosols evaporates and is converted to NO. NO was measured on two separate flights by removing the catalyst from the sample inlet line.

The NOy values between 15 - 20 km pressure altitude and between 53 and 64 S latitude were in the range 8 - 12 parts per billion by volume(ppbv). The corresponding NO values were between 0.1 and 0.2 ppbv. These values are in reasonable accord with the results of 2-D models that are zonally symmetric and incorporate only homogeneous chemistry.

At latitudes near 64 S, large latitude gradients of NO and NOy were often found. When the aerosol NOy component was low, NOy values dropped to the range of 0.5 - 4 ppbv within several degrees of latitude. NO values declined similarly to levels below the detection limit of ~0.03 ppbv. In addition, the altitude gradient of NOy was small at the highest latitudes between 15 and 20 km. The latitude region > 64 S is the center of the polar vortex and the region of perturbed chemistry as defined by the observed ClO levels.

The discussion of the results will address low NOy levels as evidence of the systematic removal of NOy from the stratosphere, the partitioning of residual NOy in the vortex between HNO3 and ClONO2, and calculations of the steady state between NO, O3, and ClO used to determine the abundance of NO2 and ClONO2 inside and outside the vortex.

MIXING RATIOS OF TRACE GASES IN THE AUSTRAL POLAR ATMOSPHERE DURING AUGUST AND SEPTEMBER OF 1987

James F. Vedder
National Aeronautics and Space Administration
Moffett Field, California

Leroy E. Heidt, Walter H. Pollock, Bruce E. Henry, & Richard A. Lueb
National Center for Atmospheric Research
Boulder, Colorado

Mixing ratios are presented for a number of long-lived trace gases in the austral polar atmosphere during August and September of 1987. The recent discovery of a 12-year trend of increasing depletion of ozone over the Antarctic Continent in the spring of each year led to numerous theoretical interpretations and several scientific expeditions to the region. The results herein were obtained as part of a major effort involving penetration of the region of depletion by NASA's multi-instrumented aircraft. One of the 14 instruments on the high-altitude ER-2 aircraft collected pressurized air samples between latitudes of 53° and 72° south at pressure altitudes up to 21 km in a series of 12 flights from Punta Arenas, Chile, over the Palmer Peninsula. The sampling system, located in the nose section of the ER-2, has an inlet tube in the free airstream, a metal-bellows air pump, and 14 specially treated 1.6 l stainless-steel canisters for containing the pressurized air at 350 kPa. A programmable controller activated by a switch in the cockpit operated the sampling system according to a schedule selected prior to the flight. A typical flight profile consisted of a southbound path on the 428° K potential temperature surface, a descent to a pressure altitude of 13.7km, a climb to the 460° K surface, and return on this surface. The location of and the time interval between samples was determined by the scientific goals of a flight. Mixing ratios for the trace gases were obtained from gas chromatographic analyses of the pressurized air samples. Additional samples were obtained between latitudes of 42° and 53° south on arrival from Puerto Montt, Chile, on August 15 and on departure to Puerto Montt on September 29. Of the species measured, the mixing ratios for CH_4, CO, N_2O, CF_2Cl_2, $CFCl_3$, CH_3CCl_3, CCl_4, and $C_2F_3Cl_3$ are reported here. Significant changes appear in the mixing ratios along the flight tracks on constant potential temperature surfaces. Changes also occur from flight to flight. Values for samples at the higher altitudes in the southern part of the flights are significantly lower than values from mid latitudes. The variations in mixing ratios of these trace gases indicate the presence, motion, and history of various air masses in the austral polar atmosphere. The influence of the stratospheric polar vortex on the distributions is evident. Relationships between these trace species and the gases and physical parameters measured by others will be discussed.

Southern Hemispheric Nitrous Oxide measurements obtained during the 1987 Airborne Antarctic Ozone Experiment

J.R. Podolske, M. Loewenstein, S.E. Strahan, and K.L. Chan

Nitrous Oxide (N2O) is a valuable tool for detecting air motions in the lower stratosphere. It is well mixed in the troposphere, and falls off with altitude in the stratosphere due to photolysis and reaction with O(1D). N2O vertical profiles have been measured over the last decade by aircraft and balloon instruments, and its global distribution is fairly well characterized. The chemical lifetime of N2O is about 150 years, which makes it an excellent dynamical tracer of air motion on the time scale of the ozone depletion event. For these reasons its was chosen to help test whether dynamical theories of ozone loss over Antarctica were plausible, particularly the theory that upwelling ozone-poor air from the troposhere was replacing ozone-rich stratospheric air.

The N2O measurements were made with the Airborne Tunable Laser Absorption Spectrometer (ATLAS) aboard the NASA ER-2 aircraft. The detection technique involves measuring the differential absorption of the IR laser radiation as it is rapidly scanned over an N2O absorption feature. Originally designed to measure CO, ATLAS was modified to measure N2O for this project. For the AAOE mission, the instrument was capable of making measurements with a 1 ppb sensitivity, 1 second response time, over an altitude range of 10 to 20 kilometers.

The AAOE mission consisted of a series of 12 flights from Punta Arenas (53S) into the polar vortex (approximately 72S) at which time a vertical profile from 65 to 45 km and back was performed. In addition a series of transit flights between 38N to 53S were made to get broader latitudinal coverage.

Comparison of the observed profiles inside the vortex with N2O profiles obtained by balloon flights during the austral summer showed that an overall subsidence had occurred during the winter of about 5-6km. Also, over the course of the mission (mid-August to late September), no trend in the N2O vertical profile, either upward or downward, was discernable, eliminating the possibility that upwelling was the cause of the observed ozone decrease. Throughout the mission, significant latitudinal gradients of N2O on isentropic surfaces were observed. These will prove useful in understanding the extent of lateral mixing air into and out of the vortex. An average N2O distribution for austral winter-spring will be presented.

N89-14558

"OBSERVATIONAL RESULTS OF MICROWAVE TEMPERATURE PROFILE MEASUREMENTS FROM THE AIRBORNE ANTARCTIC OZONE EXPERIMENT"

Bruce L. Gary
Jet Propulsion Laboratory; California Institute of Technology

INTRODUCTION

The Microwave Temperature Profiler, MTP, is installed on NASA's ER-2 aircraft. MTP measures profiles of air temperature versus altitude. Temperatures are obtained every 13.7 seconds for 15 altitudes in an altitude region that is approximately 5 km thick (at high flight levels). MTP is a passive microwave radiometer, operating at the frequencies 57.3 and 58.8 GHz. Thermal emission from oxygen molecules provides the signal that is converted to air temperature. MTP is unique, in that it is the only airborne instrument of its kind.

The MTP instrument was used during the Airborne Antarctic Ozone Experiment, AAOE, to enable "potential vorticity" to be measured along the flight track. Other uses for the MTP data have become apparent. The most intriguing unexpected use is the detection and characterization of mountain waves that were encountered during flights over the Palmer Peninsula. These and other observations will be described.

ALTITUDE TEMPERATURE PROFILES

The MTP's basic observational product is air temperature at 15 altitudes every 13.7 seconds, as illustrated below:

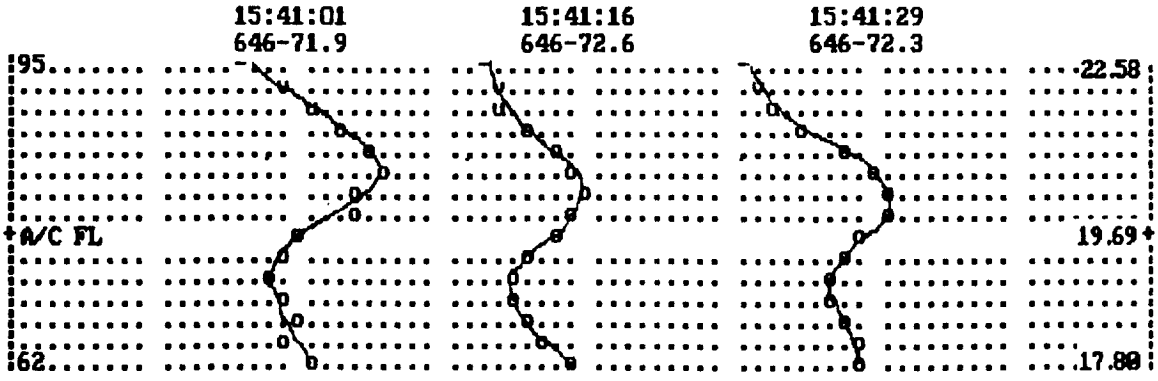

Figure 1. A sequence of 3 altitude temperature profiles.

The above profiles were taken during level flight at 64,600 feet (pressure altitude). The temperature scale is 0.25 K/column. The altitude scale extends from 6200 feet below to 9500 feet above flight level. Pressure altitudes, in km, are shown on the right. Below the time blocks are flight level (in units of 100 feet) and outside air temperature [degC]. This figure shows that the aircraft is flying within an inversion layer that is 5000 feet thick and is about 1.4 degC warmer at the top than at the bottom. Slow changes in inversion layer properties are evident.

LAPSE RATE AND POTENTIAL VORTICITY

From the altitude temperature profiles it is possible to calculate lapse rate, dT/dz, by comparing temperatures at altitudes above and below flight level. This parameter can be converted to potential temperature lapse rate, d(theta)/d(pressure), using standard equations. Potential temperature is defined as: theta = T*(1000mb/pressure)^.286, where T is air temperature [K]. Potential vorticity is the product of potential temperature lapse rate and horizontal wind gradient (to first order). The ER-2's Meteorology Measurement System, MMS, measures wind vector versus time. Combining observations of MTP and MMS thus enables potential vorticity to be calculated. Potential vorticity is a conservative property of air parcels on suitably short timescales; hence, it can be used as a constraint on scenarios for the recent history of air parcels.

An inspection of potential temperature lapse rate versus latitude, for flights which penetrated into the volume of air with high chlorine monoxide and low ozone, failed to show a noticeable change at the boundary. An analysis described elsewhere (Hartmann et al, 1988), which uses the MMS and MTP combined data sets for a calculation of potential vorticity versus latitude, does show a correlation with penetration into the ozone hole.

POTENTIAL TEMPERATURE CROSS-SECTIONS

Each altitude temperature profile can be converted to a profile of potential temperature. Interpolations can be made for deriving altitudes of potential temperature surfaces. A time series of such potential temperature surface altitudes can be used to create "potential temperature cross-sections."

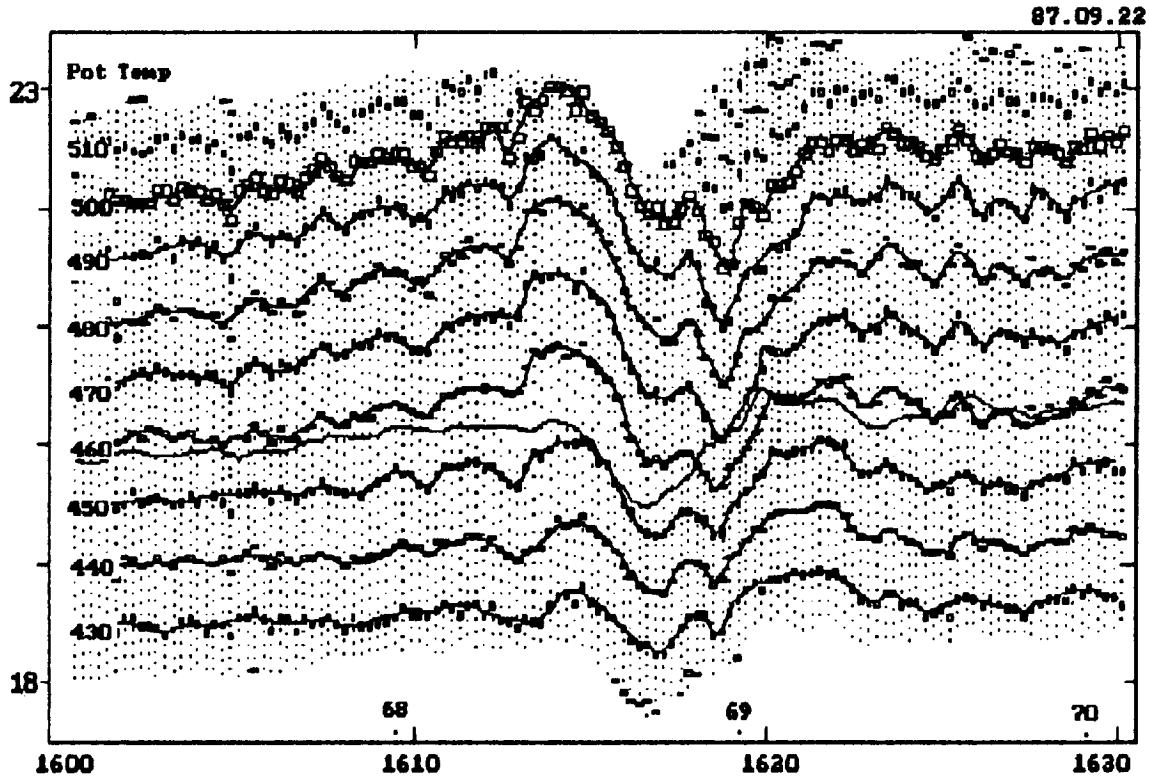

Figure 2. Potential temperature cross-section for a mountain wave encounter, 1987 September 22. Altitude [km] is indicated on the left, UT times below.

In the above figure the pressure altitudes for selected potential temperatures are plotted with coded symbols. The 500 K altitudes are plotted with large squares. Hand-fitted lines are shown for potential temperature surfaces at 10 K intervals. The extra trace, at about 20 km (or 457 K), is the ER-2's flight level. Note the flight level excursions, at 1615 to 1620 UT, caused by down- and up-drafts.

MOUNTAIN WAVE ENCOUNTERS

Potential temperature cross-sections show "waves" of some amplitude and period almost all the time. Generally, wave amplitudes are less than 200 meters, peak-to-peak, and their wavelengths are longer than 100 km. On 12 occasions waves were encountered that differed in 3 ways: they had higher amplitudes (200 to 1200 meters), much shorter wavelengths (typically 20 km), and they existed at all altitudes sampled (18 to 23 km, typically).

An analysis of the location of the aircraft when these high amplitude, short period waves were encountered shows that they always occurred over the Palmer Peninsula. An analysis was made of the likelihood of encountering these waves for each of the regions where several overflights occurred. The waves were encountered at the south end of Palmer Peninsula 64% of the time. The northern half of the peninsula had an encounter probability of 30%. Flights were not made near the eastern edge of the peninsula because the pilots noted wave clouds in those regions.

On 3 consecutive flights, September 20, 21 and 22, a short period wave group was encountered at approximately the same location on both the outbound and inbound legs of the flight. Presumably this was the "same" wave that persisted for at least 3 days. It may have lasted longer, since the 22nd was the last flight over the Palmer Peninsula.

It is reasonable to conclude, based on the strong correlation of high amplitude waves of short period with underlying topography, that the entire Palmer peninsula was producing mountain waves; and that the mountain wave production rate was ranged from at least 30% at the north end to at least 64% at the south end.

It is noteworthy that these waves extended from the lowest altitudes sampled by the MTP instrument to the highest. Figure 2 shows the highest amplitude wave encountered, and it's amplitude is 1.2 km at the highest altitudes. Mountain wave theory predicts that wave amplitude should increase with altitude in accordance with the reciprocal of the square root of air pressure. On average, the waves encountered over Palmer Peninsula obey this relationship.

IMPLICATIONS FOR OZONE HOLE

Mountain waves that propagate into the polar vortex may have implications for the formation of the ozone hole. Upward excursions of air parcels lead to a brief cooling. This can begin the process of cloud formation. It is important to determine how much additional formation of polar stratospheric cloud (PSC) material is possible by the passage of air parcels through a mountain wave pattern that endures for long periods. Other mountain wave effects have been suggested, such as a speeding up of the vortex, and a consequent cooling of large air volumes (which in turn might add to PSC production).

N89-14559

PHOTOCHEMICAL TRAJECTORY MODELLING STUDIES OF THE 1987 ANTARCTIC SPRING VORTEX

J. Austin, R.L. Jones and D.S. McKenna

Meteorological Office,
London Road,
Bracknell,
Berks.,
RG12 2SZ.

Simulations of Antarctic ozone photochemistry performed using a photochemical model integrated along air parcel trajectories are described. This type of model has a major advantage at high latitudes of being able to simulate correctly the complex interaction between photolysis and temperature fields, which, because of the polar night cannot be represented accurately in a zonally averaged framework. Isentropic air parcel trajectories were computed using Meteorological Office global model analyses and forecast fields from positions along the ER2 flight paths during the Airborne Antarctic Ozone Experiment in Austral Spring 1987. A photochemical model is integrated along these trajectories using the aircraft observations to initialise constituent concentrations. The model was adapted from Austin et al. (1987a) and includes additional reactions of the ClO dimer and also bromine reactions, which are thought to play a significant role in Antarctica (McElroy et al., 1986 ; Molina and Molina, 1987). The model also includes heterogeneous reactions (Solomon et al., 1986) which are invoked when the air parcel passes through a polar stratospheric cloud (PSC). The existence of a PSC is determined throughout the course of the model integration from the parcel temperature and the saturated vapour pressure of water over an assumed H_2O/HNO_3 mixture (Toon et al., 1986). The air parcel temperature is used to determine the saturated vapour pressure of HNO_3 over the same mixture. Mixing ratios which exceed saturation result in condensation of the excess in the model and hence lead to a reduction of the amount of gas phase NO_y available for chemical reaction.

In the paper, modelled and observed constituent concentrations outside and within the chemically perturbed region of the vortex are compared. Figure 1 shows examples of 6 day trajectories starting on 4 Sept 1987, at latitudes 58S and 72S. The arrows denote the date at 0GMT and the crosses indicate the locations of PSCs encountered along the trajectory. Note that only the more poleward air parcel experienced a PSC in the model. Figures 2 and 3 show selected species from the chemical model for the two trajectories as functions of time. The integrations have identical initialisations, for comparison purposes, and correspond to species concentrations measured in the chemically perturbed region of the vortex. Results from the more poleward trajectory show that in the model, the heterogeneous reactions cause the ClO concentration to become elevated to levels comparable to that observed within the chemically perturbed region from the ER2, and to produce a substantial O_3 depletion of over 1% per day largely through the ClO dimer destruction cycle. However, for the trajectory starting at 58S (nominally outside the chemically perturbed region) the O_3 concentration levels off after only 4 days of integration, despite the initial conditions being favourable for O_3 depletion.

Further integrations over 80 day trajectories from 1 Aug 1987 are presented in which the net O_3 destroying potential of the perturbed

chemical region is assessed for different conditions. The importance of the level of denitrification and of the frequency of PSCs in determining the net O_3 depletion is emphasised. Results indicate that given suitable initial partitioning of the chlorine species, ClO concentrations can increase during the model integration as observed throughout the AAOE. The extent to which this is consistent with other (column) observations is assessed.

References:

Austin et al. Q.J.R.M.S 113, 361-392, 1987.

McElroy et al. Nature 321, 759-762, 1986.

Molina and Molina J.Phys.Chem 91, 433-436, 1987.

Solomon et al. Nature 321, 755-758, 1986.

Toon et al. Geophys.Res.Lett., 13, 1284-1287, 1987.

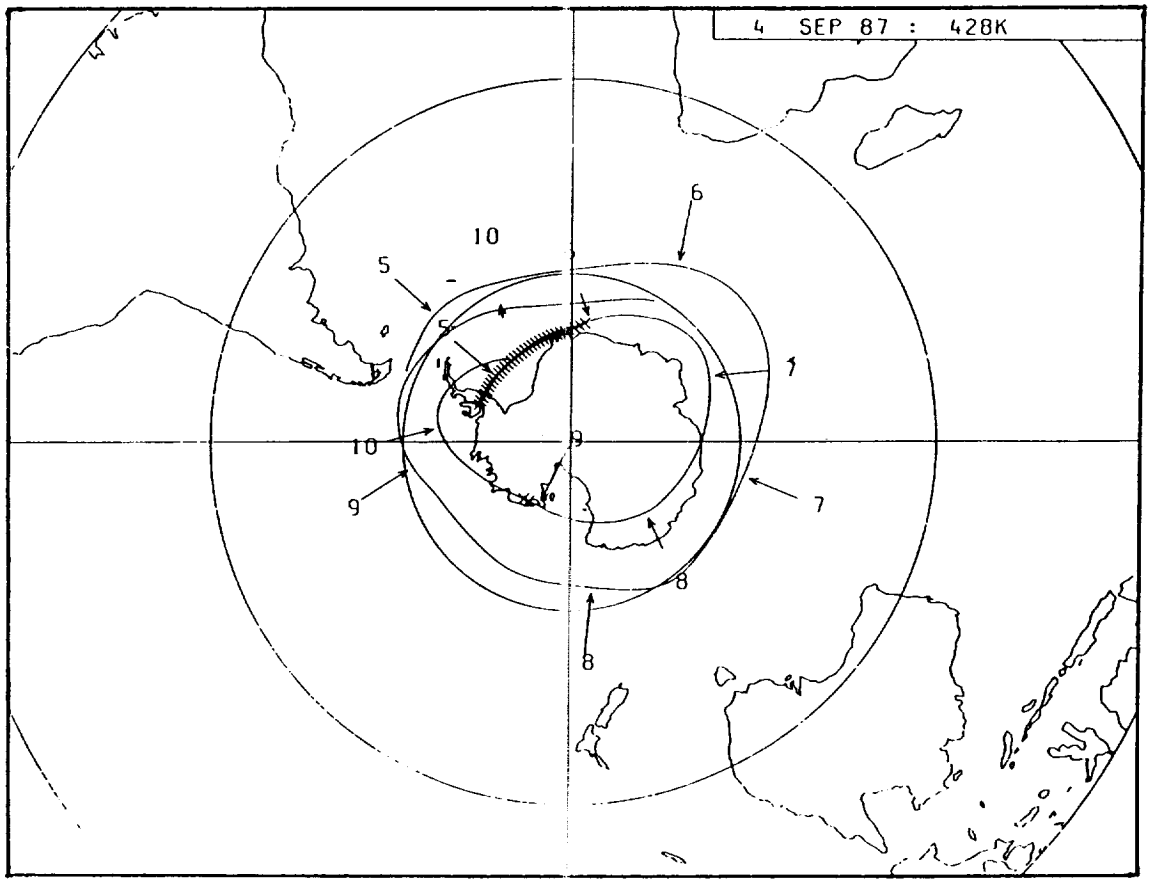

Figure 1 6 day isentropic trajectories calculated from UK Meteorological Office global model analyses initialised on 4 Sept. 1987.. Regions of the trajectories in PSCs are denoted by crosses

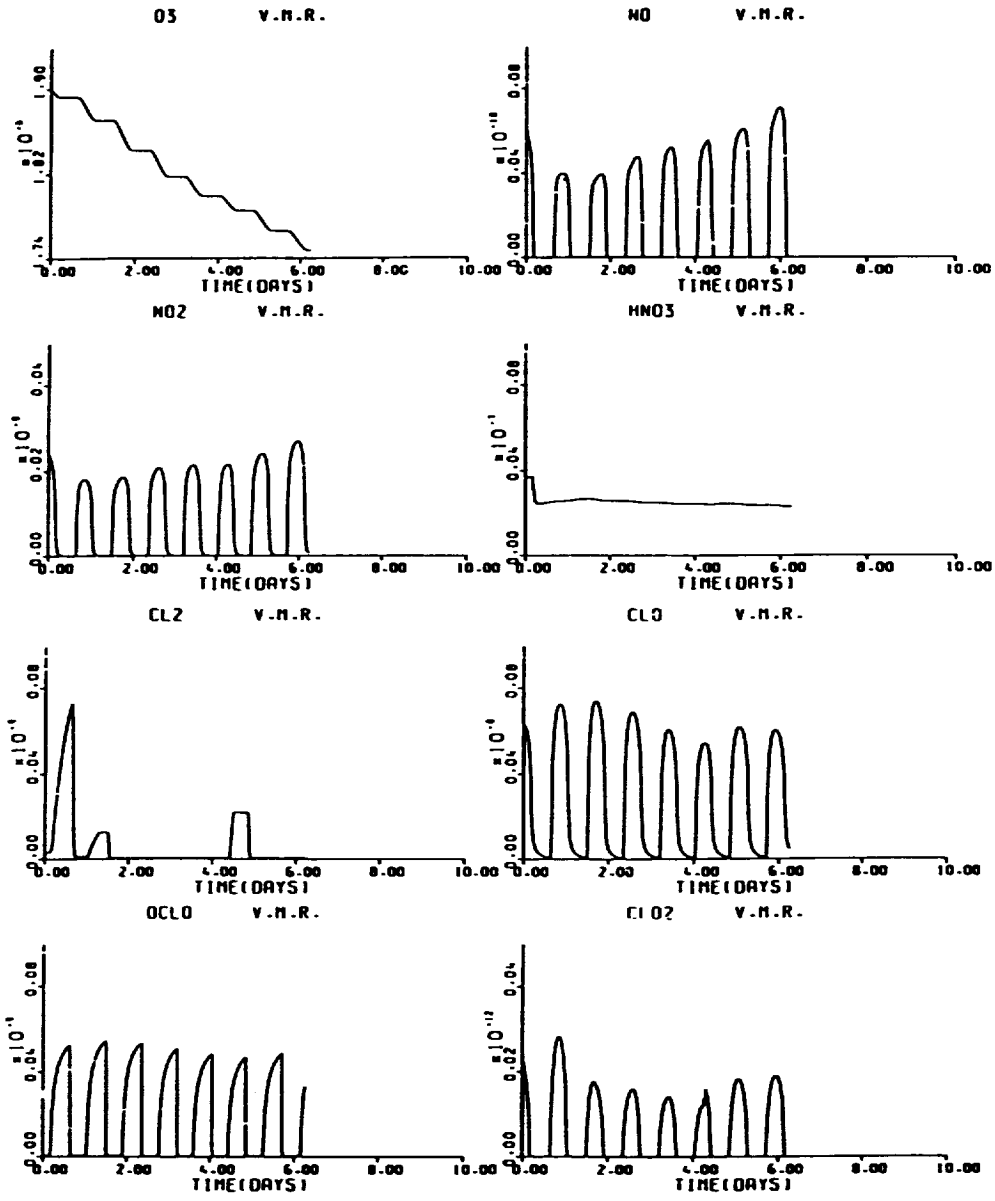

Figure 2 Calculated time variation of selected chemicals from the model run initialised at 72S (inside the chemically perturbed region).

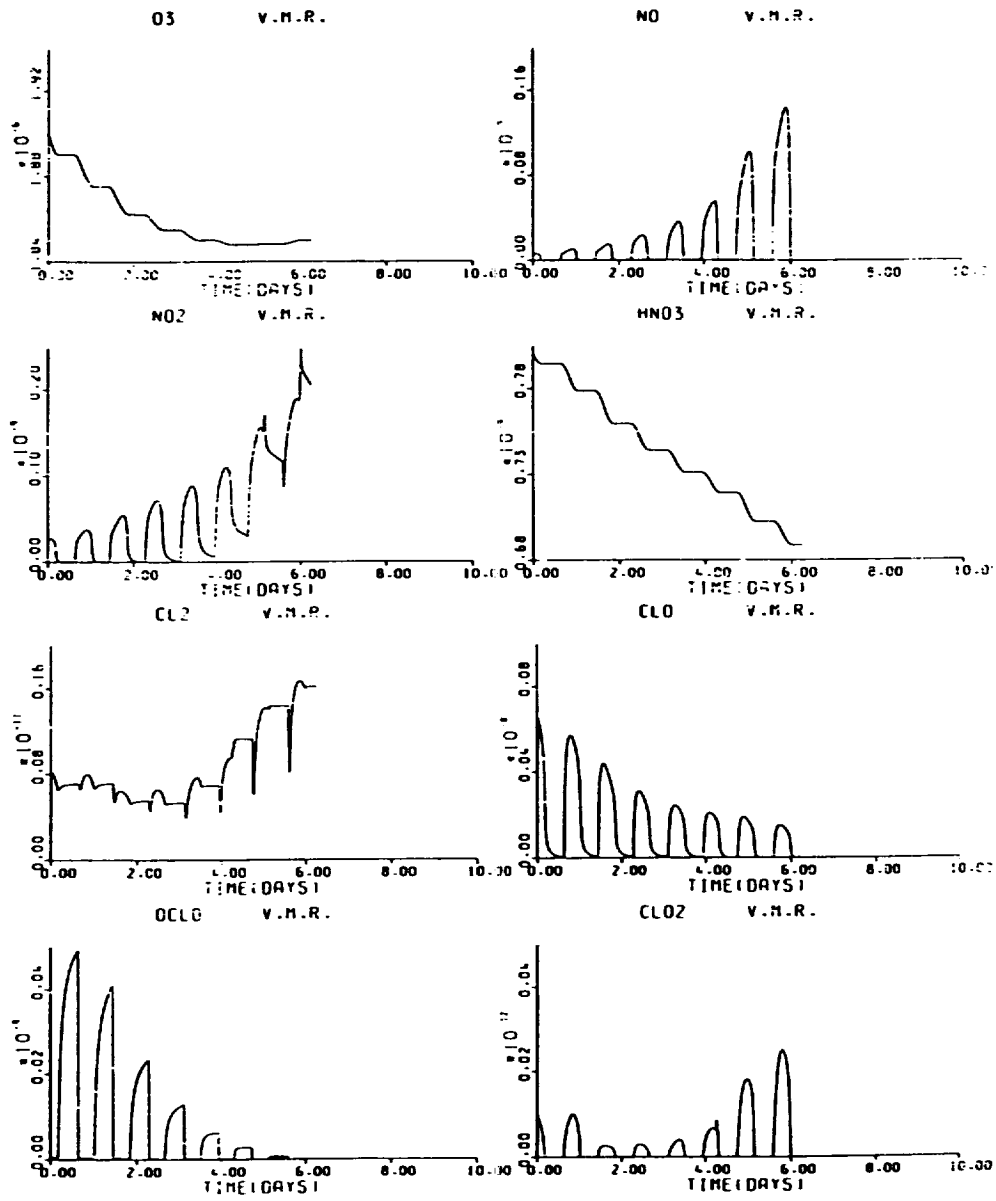

Figure 3 Calculated time variation of selected chemicals from the model run initialised at 58S (outside the chemically perturbed region).

Temperature and Horizontal Wind Measurements on the ER-2 Aircraft during the 1987 Airborne Antarctic Ozone Experiment

K. Roland Chan, Stan G. Scott, T. Paul Bui
NASA, Ames Research Center, Moffett Field, California

Stuart W. Bowen
San Jose State University, San Jose, California

and
Jon Day
I.M.I. Incorporated, Palo Alto, California

Abstract

The NASA ER-2 aircraft is equipped with special instrumentation to provide accurate in-situ measurement of the atmospheric state variables during flight. The Meteorological Measurement System (MMS) on the ER-2 aircraft is briefly described. Since the meteorological pararmeters (temperature, pressure, and wind vector) are extensively used by other ER-2 experimenters for data processing and interpretation, the accuracy and resolution of each of these parameters are assessed and discussed.

During the 1987 Airborne Antarctic Ozone Experiment (AAOE) mission, the ER-2 aircraft was stationed at Punta Arenas, Chile (53 S, 72 W), and successfully flew over Antarctica on 12 occasions between August 17 and September 22, 1987. On each of the 12 flights, the ER-2 aircraft flight plan was to take off at approximately the same local time, fly southward at a near constant potential temperature surface, descend and ascend at the southernmost terminus at about 72 S over Antarctica, and return northward at either the same or a different constant potential temperature surface.

The measurements of the MMS experiment during the AAOE mission are presented. MMS data are organized to provide a composite view of the polar atmosphere, which is characterized by frigid temperatures and high zonal winds. Altitudinal variations of the temperature measurement (during takeoff/landing at Punta Arenas and during descent/ascent at the southern terminus) and latitudinal variations of the zonal wind (on near constant potential temperature surfaces) are emphasized and discussed.

Trace Gas Measurements From Whole Air Samples Collected Over the Antarctic Continent

L. E. Heidt,† J. F. Vedder,* W. H. Pollock,† B. E. Henry,† and R. A. Lueb†

ABSTRACT

Whole air samples collected aboard both the NASA DC-8 and ER-2 aircraft as part of the Airborne Antarctic Ozone Experiment (AAOE) were analyzed in a field laboratory set up at Punta Arenas, Chile, in August and September, 1987. Mixing ratios obtained from gas chromatographic analyses of these samples are presented for N_2O, $CFCl_3$, CF_2Cl_2, $C_2F_3Cl_3$, CH_3CCl_3, CCl_4, CH_4, and CO. Variations in the mixing ratios of these gases along the individual flight paths of the aircraft are used as tracers to indicate the history of air masses over and near the Antarctic continent.[a]

† National Center for Atmospheric Research

* NASA Ames Research Center

[a] Data analysis is still underway; this abstract will be expanded upon completion. For this reason we would prefer a poster session.

The Meteorological Measurement System on the NASA ER-2 Aircraft

Stan G. Scott, T. Paul Bui, K. Roland Chan
NASA, Ames Research Center, Moffett Field, California

and
Stuart W. Bowen
San Jose State University, San Jose, California

Abstract

A Meteorological Measurement System (MMS) was designed for the high-altitude ER-2 aircraft (NASA 706). Through dedicated instrumentation installed on the aircraft and repeated calibrations, the MMS provides accurate in-situ measurements of free-stream pressure, temperature, and the wind vector. The MMS experiment has participated in two major high-altitude scientific expeditions, the Stratosphere-Troposphere Exchange Project (STEP) based in northern Australia and the Airborne Antarctic Ozone Experiment (AAOE) based in southern Chile.

Key MMS subsystems are described. The MMS consists of a dedicated inertial navigation system (INS), a radome differential pressure system, a data acquisition system, and air data instrumentation.

The MMS incorporates a high-resolution INS (Litton LTN-72RH model), which is specially configured and is updated at 25 Hz. The differential pressure system, consisting of two sets of pressure ports and transducers, is installed in the ER-2 radome to provide sensitive measurements of the airflow angles (angle of attack and angle of sideslip). The data acquisition system was designed to meet aircraft requirements of compactness and light weight (2 cu. ft, 50 lb) and for MMS requirements to sample, control, process, and store 45 parameters (some redundant) at a sampling rate up to 10 Hz. The MMS data are stored both in a tape recorder (20 MB) and a hermatically-sealed winchester hard disc (10 MB). Special and redundant instrumentation for temperature and pressure measurements were also installed on the aircraft.

The operational software was written in MC68000 assembly language to facilitate preflight checkout, inflight sampling (currently operating at a 5-Hz sampling rate), quick postflight download, and operating utilites. The software package must accommodate various modes of MMS data: analog and digital, serial and parallel, synchronous and asynchronous. The application software was developed in FORTRAN for data conversion, processing, analysis, diagnostics, and graphic presentation.

THE PLANNING AND EXECUTION OF ER-2 AND DC-8 AIRCRAFT FLIGHTS OVER ANTARCTICA, AUGUST AND SEPTEMBER, 1987

A.F. Tuck
NOAA Aeronomy Laboratory, 325 Broadway, Boulder, CO 80303-3328

R.T. Watson
NASA Headquarters, Washington, DC 20546

E.P. Gordon
NASA Ames Research Center, Moffett Field, CA 94035

J.J. Margitan
NASA Headquarters, Washington, DC 20546

The questions addressed by the mission are stated. The selection of the payload to provide answers is given. The reasons for the flight profiles flown are laid out, and the crucial role of meteorological forecasts, both standard and special, is explained. A short directory of each aircraft mission is presented, with a diagram of the flight track relative to the TOMS ozone map for the day.

SESSION VI - In-Situ Measurements of Chemical Species and Their Interpretation - B
Presiding, M. McIntyre, University of Cambridge
Wednesday Afternoon, May 11, 1988

SYNOPTIC AND CHEMICAL EVOLUTION OF THE ANTARCTIC VORTEX IN WINTER AND SPRING, 1987

A.F. Tuck
NOAA Aeronomy Laboratory, 325 Broadway, Boulder, CO 80303-3328
(and other authors/affiliations)

It is demonstrated that the dynamical evolution of the vortex at least up to 50 mb is dominated by synoptic scales in the troposphere. In particular, there is a clear response when poleward extension of tropospheric anticyclones from latitudes of 40°-50°S to 70°-80°S occurs. This response is evident in isentropic potential vorticity maps, TOMS ozone fields and SAM II polar stratospheric clouds.

An important feature of the high latitude southern hemisphere lower stratosphere is a transition at potential temperatures in the 390-400K range. This transition, the "vortopause", is clearly marked in aircraft profiles of O_3, H_2O, N_2O and ClO at latitudes 68°-72°S near the Antarctic peninsula, and also over Punta Arenas (53°S). The transition is evident in meteorological cross-sections of potential vorticity and potential temperature; above it, the isopleths are more closely spaced than below it.

The aircraft measurements of H_2O, O_3, NO_y, N_2O, ClO, and whole air data are examined in "material coordinates", θ and P_θ, backed up by trajectory analysis. The evolution of the chemical mixing ratios is examined in these coordinates as a function of time from mid-August to late September. Conclusions are drawn about the rates of change and their causes.

The meteorological and aircraft data are examined for evidence of the following kinds of motion with respect to the vortex: ingress of air aloft, subsidence, peeling off of air to lower latitudes, and folding of the vortopause.

Conclusions are presented regarding the evidence for a chemical sink of ozone above and below θ = 400K, and whether the vortex has a mass flow through it, or if the chemical sink operates on a fixed mass of air. Implications for mid-latitudes are briefly considered in the light of the conclusions.

DEHYDRATION IN THE LOWER ANTARCTIC STRATOSPHERE IN LATE WINTER AND SPRING

K.K. Kelly, A.F. Tuck, D.W. Fahey
NOAA Aeronomy Laboratory, 325 Broadway, Boulder, CO 80303-3328

M.H. Proffitt, D.M. Murphy
NOAA Aeronomy Laboratory and CIRES, 325 Broadway, Boulder, CO 80303-3328

R.L. Jones, D.S. McKenna
Meteorological Office, United Kingdom

L.E. Heidt
National Center for Atmospheric Research, Boulder, CO 80307

G.V. Ferry, M. Loewenstein, J.R. Podolske, and K.R. Chan
NASA Ames Research Center, Moffett Field, CA 94035

The history of minimum temperatures at 50 and 70 mb is examined from NMC, UK Met O and ECMWF analyses. MSU channel 24 data are similarly inspected. South Pole sonde data are used to calculate saturation humidity mixing ratio as a function of altitude and time throughout 1987. Saturation with respect to ice could be maintained for water mixing ratios of 3.5 ppmv for a period of about 80 days from mid-June to mid-September. Dehydration to mixing ratios of 1 ppmv or less was possible sporadically.

Data from the ER-2 flights between 53°S and 72°S are used in conjunction with particle size measurements and air parcel trajectories to demonstrate the dehydration occurring over Antarctica. Water mixing ratios at the latitude of Punta Arenas (53°S), in conjunction with tracer measurements and trajectory analysis, show that at potential temperatures from about 325 to 400K, the dryness (< 3ppmv) had its origin over Antarctica rather than in the tropics.

Water mixing ratios within the Antarctic vortex varied from 1.5 to 3.8 ppmv, with a strong isentropic gradient being evident in the region of high potential vorticity gradients.

TEMPORAL TRENDS AND TRANSPORT WITHIN AND AROUND THE ANTARCTIC POLAR VORTEX DURING THE FORMATION OF THE 1987 ANTARCTIC OZONE HOLE

M.H. Proffitt, J.A. Powell
NOAA Aeronomy Laboratory and CIRES, 325 Broadway, Boulder, CO 80303-3328

A.F. Tuck, D.W. Fahey, K.K. Kelly
NOAA Aeronomy Laboratory, Boulder, CO 80303-3328

M. Loewenstein, J.R. Podolske, and K.R. Chan
NASA Ames Research Center, Moffett Field, CA 94035

During the 1987 Airborne Antarctic Ozone Experiment an ER-2 high altitude aircraft made twelve flights out of Punta Arenas, Chile (53°S, 71°W) into the Antarctic polar vortex. The aircraft was fitted with fast response instruments for in-situ measurements of many trace species including O_3, ClO, BrO, NO_y, NO, H_2O and N_2O. Grab samples of long-lived tracers were also taken and a scanning microwave radiometer measured temperatures above and below the aircraft. Temperature, pressure, and wind measurements were also made on the flight tracks. Most of these flights were flown to 72°S, at a constant potential temperature, followed by a dip to a lower altitude and again assuming a sometimes different potential temperature for the return leg. The potential temperature chosen was 425K (17 to 18 km) on 12 of the flight legs, and 5 of the flight legs were flown at 450K (18 to 19 km). The remaining 7 legs of the 12 flights were not flown on constant potential temperature surfaces.

Tracer data have been analyzed for temporal trends. Data from the ascents out of Punta Arenas, the constant potential temperature flight legs, and the dips within the vortex are used to compare tracer values inside and outside the vortex, both with respect to constant potential temperature and constant N_2O. The time trend during the one-month period of August 23 through September 22, 1987, shows that ozone decreased by 50% or more at altitudes from 15 to 19 km. This trend is evident whether analyzed with respect to constant potential temperature or constant N_2O. The trend analysis for ozone outside the vortex shows no downward trend during this period. The analysis for N_2O at a constant potential temperature indicates no significant trend either inside or outside the vortex; however, a decrease in N_2O with an increase in latitude is evident. Small scale and large scale correlations between different trace species have also been examined. These correlations and the changes in O_3 and N_2O relative to the polar jet will be discussed as they relate to isentropic and diabatic transport of air within and around the Antarctic polar vortex.

Small Scale Structure and Mixing at the Edge of the Antarctic Vortex

D.M. Murphy, A.F. Tuck, K.K. Kelly, M. Loewenstein, J.R. Podolske, S.E. Strahan, and K.R. Chan

Small scale correlations and patterns in the chemical tracers measured from the NASA ER-2 aircraft in the 1987 AAOE campaign can be used to investigate the structure of the edge of the polar vortex and the chemically perturbed region within it. Examples of several types of transport processes can be found in the data.

Since ClO and O_3 have similar vertical gradients and opposite horizontal gradients near the chemically perturbed region, the correlation between ClO and O_3 can be used to study the extent of horizontal transport at the edge of the chemically perturbed region. Horizontal transport dominates the correlation for a latitude band up to 4 degrees on each side of the boundary. This implies a transition zone containing a substantial fraction of the mass of the total polar vortex. Similar horizontal transport can be seen in other tracers as well. It has not been possible to distinguish reversible transport from irreversible mixing.

One manifestation of the horizontal transport is that the edge of the chemically perturbed region is often layered rather than a vertical "curtain." This can be seen from the frequent reversed vertical gradients of nitrous oxide, caused by air with high nitrous oxide overlapping layers with lower mixing ratios.

Water and nitrous oxide are positively correlated within the chemically perturbed region. This is the opposite sign to the correlation in the unperturbed stratosphere. The extent of the positive correlation is too great to be attributed solely to horizontal mixing. Instead, it is hypothesized that dehydration and descent are closely connected on a small scale, possibly due to radiative cooling of the clouds that also cause ice to fall to lower altitudes.

Polar Ozone Workshop Abstract

"Transport into the South Polar Vortex in Early Spring"

D. Hartmann
University of Washington,

L. Heidt
National Center for Atmospheric Research.

M. Lowenstein, J. Podolske, W.Starr and J. Vedder,
NASA Ames Research Center

Estimates of the mean circulation and diffusive transport of ozone and other species into the antarctic polar vortex during the spring of 1987 are made using data from the Airborne Antarctic Ozone Experiment. Measurements of long-lived tracers of tropospheric origin remained relatively constant at the levels of the maximum rate of decline of ozone during September. At lower levels in the stratosphere some evidence exists to support intrusions of tropospheric or low latitude air. Given the distribution in latitude and height of these tracers measured from the ER-2 aircraft, it can be inferred that the Lagrangian or diabatic mean circulation was zero or downward over Antarctica during the period of the ozone decline. The observation of a decline in ozone therefore requries a photochemical sink for ozone.

The magnitude of the required photochemical sink must be sufficient to offset the transport of ozone into the polar region and produce the observed decline. Quasi-isentropic mixing and downward motion are coupled and are difficult to estimate from a single tracer. The full suite of measured tracers and auxiliary information are brought together to provide an estimate of the rate at which air is cycled through the polar vortex during spring. Estimates of large-scale transport of potential vorticity and ozone from previous years are generally consistent with the data from the airborne experiment in suggesting a relatively slow rate of mass flow through the polar vortex in the lower stratosphere during September.

.5 45
157635

N89-14568

The Evolution of AAOE Observed Constituents with the Polar Vortex

M. R. Schoeberl[1], L. Lait[2], P. A. Newman[3], R. Martin[3]

M. Loewenstein[4], J. Podolske[4]

J. Anderson[5], and

M. Proffitt[6]

One of the difficulties in determining constituent trends from the ER-2 flight data is the large amount of day to day variability generated by the motion of the polar vortex. To reduce this variability, the observations have been transformed into the conservative (Lagrangian) reference frames consisting of the coordinate pairs, potential temperature (PT) and potential vorticity (PV), or PT and N_2O. The requirement of only two independent coordinates rests on the assumption that constituent distributions and their chemical processes are nearly zonal in that coordinate system. Flight data is used everywhere for these transformation except for potential vorticity. Potential vorticity is determined from level flight segments, and NMC PV values during flight dives and takeoffs are combined with flight data in a smooth fashion.

Once the data has been transformed into the conservative reference frames, least square linear fits are used to determine trends. Using the (PT, N_2O) transformation O_3 is shown to decrease on the 440K surface within the polar vortex at a rate of about .06 ppm/day over the mission period. Despite the general reduction in measurement variance this technique produces, a significant degree of variance is still present near the "ClO wall" due to the finite resolution of (PT, N_2O) coordinate transform processes.

Using the (PT, PV) transformations and all of the flight data composited together, constituent distributions over a substantial region can be estimated and then back transformed using the (PT, PV) distribution for any day as derived from global and/or flight meteorological fields. The result is a rather complete picture of the Austral polar vortex chemical structure and its evolution. Sample reconstructions are shown for ClO, O_3 and N_2O on 9/20/87 in the enclosed figure.

[1]NASA/GSFC, Greenbelt, MD 20771
[2]NRC NASA/GSFC, Greenbelt, MD 20771
[3]Applied Research Corporation, 8201 Corporate Dr., Landover, MD 20785
[4]Harvard University, Cambridge, MA
[5]NASA/Ames, Moffett Field, CA
[6]NOAA Aeronomy Lab, Boulder, CO

Figure Caption

Reconstruction of the N_2O, ClO, and O_3 distributions using the (PT, PV) compositing method. The left hand figures show the constituent observations using a gray scale. The fluctuating solid line is the flight track. The faint dashed lines show the NMC potential temperature at 65°W for the day, and the faint solid lines are isopleths of potential vorticity computed from NMC. The heavy solid lines show NMC zonal winds. The right hand figure shows the reconstructed fields using both flight and NMC potential vorticity and flight winds. The reconstructions use all the data from 12 flights. Agreement with the observations is good, but sharper features (e.g. the ClO wall) are washed out to some extent. Reconstructions have been performed for each flight day and the day after the last flight, 9/23/88.

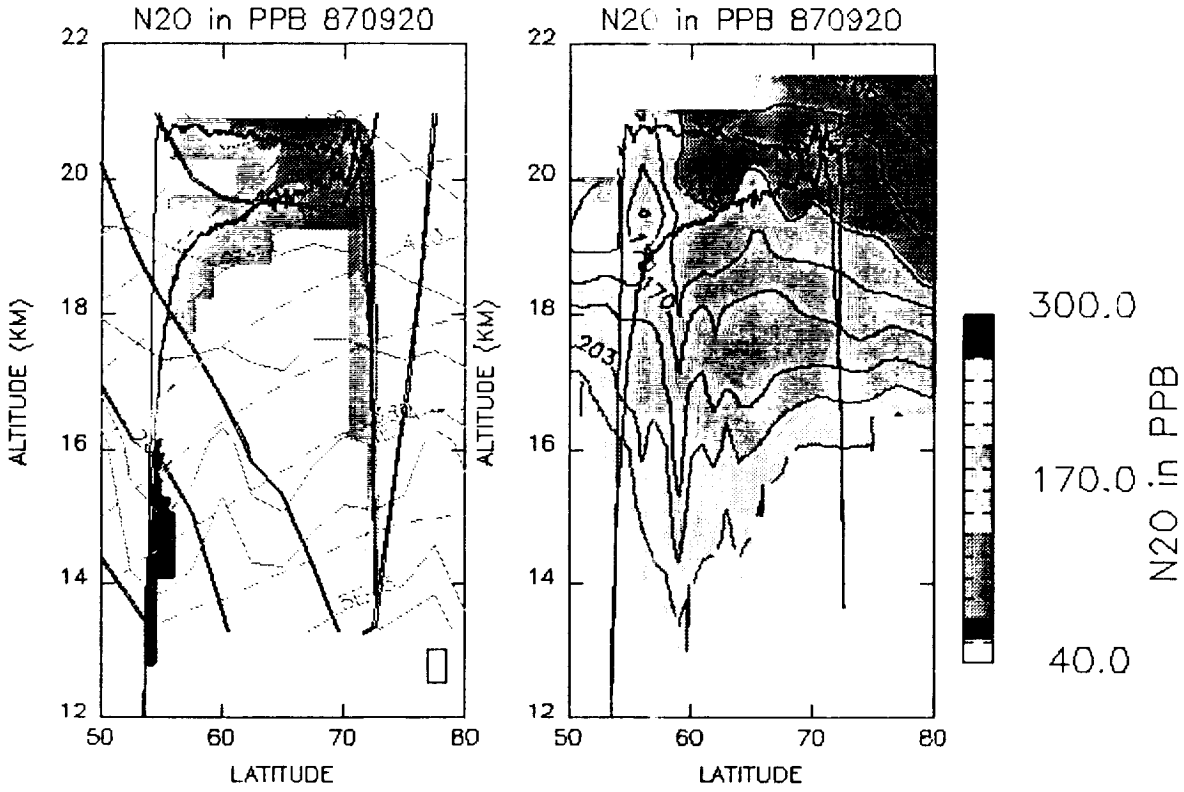

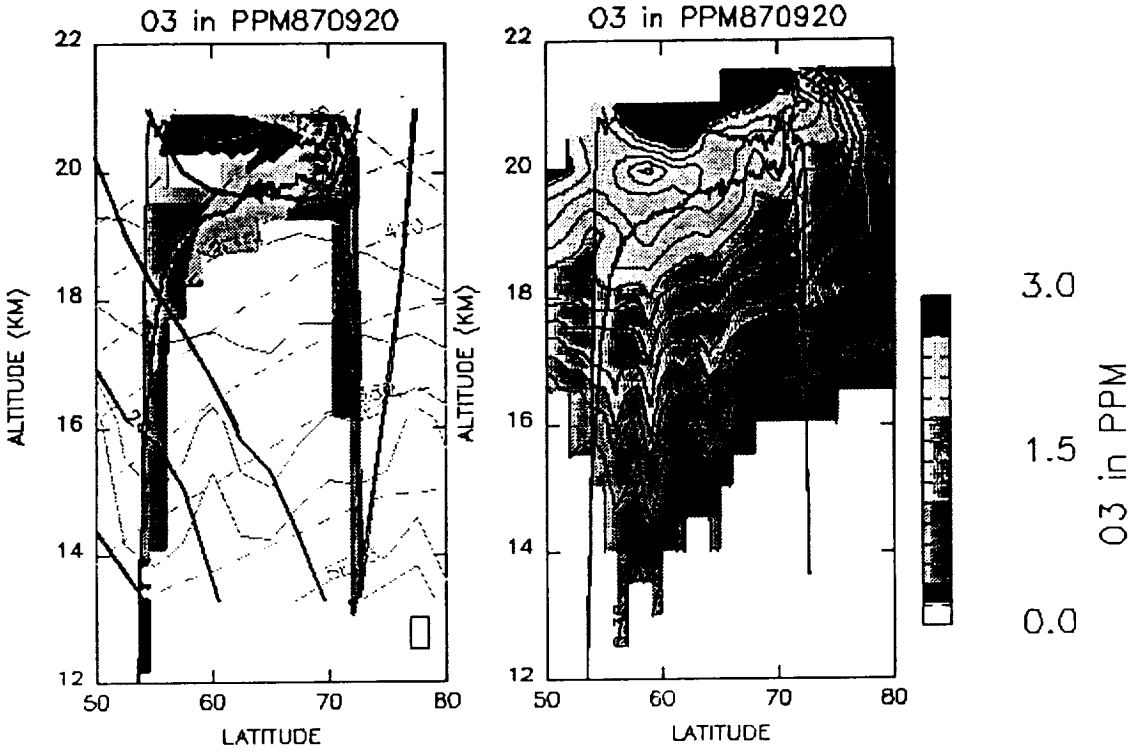

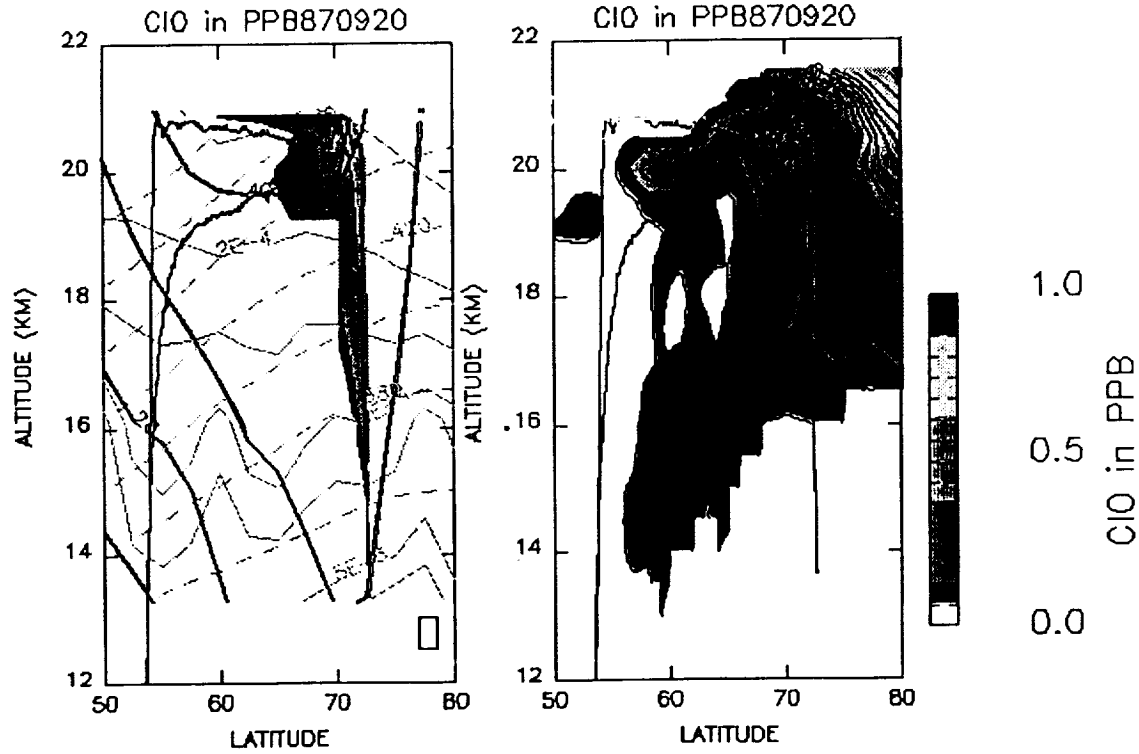

PHOTOCHEMICAL MODELING OF THE ANTARCTIC STRATOSPHERE: OBSERVATIONAL CONSTRAINTS FROM THE AIRBORNE ANTARCTIC OZONE EXPERIMENT AND IMPLICATIONS FOR OZONE BEHAVIOR

Jose M. Rodriguez
Nien Dak Sze
Malcolm K. W. Ko

Atmospheric and Environmental Research, Inc.
840 Memorial Dr.
Cambridge, MA 02139 USA
617-547-6207

The rapid decrease in O_3 column densities observed during antarctic spring has been attributed to several chemical mechanisms involving nitrogen, bromine, or chlorine species, to dynamical mechanisms, or to a combination of the above. Chlorine-related theories, in particular, predict greatly elevated concentrations of $C\ell O$ and $OC\ell O$ and suppressed abundances of NO_2 below 22 km. The heterogeneous reactions and phase transitions proposed by these theories could also impact the concentrations of $HC\ell$, $C\ell NO_3$ and HNO_3 in this region. Observations of the above species have been carried out from the ground by the National Ozone Expedition (NOZE-I, 1986, and NOZE-II, 1987), and from aircrafts by the Airborne Antarctic Ozone Experiment (AAOE) during the austral spring of 1987. Observations of aerosol concentrations, size distribution and backscattering ratio from AAOE, and of aerosol extinction coefficients from the SAM-II satellite can also be used to deduce the altitude and temporal behavior of surfaces which catalyze heterogenous mechanisms. All these observations provide important constraints on the photochemical processes suggested for the spring antarctic stratosphere.

Results are presented for the concentrations and time development of key trace gases in the antarctic stratosphere, utilizing the AER photochemical model. This model includes complete gas-phase photochemistry, as well as the heterogeneous reactions:

$$C\ell NO_3 + HC\ell\ (ice) \longrightarrow C\ell_2 + HNO_3\ (ice) \quad (1)$$

$$C\ell NO_3 + H_2O\ (ice) \longrightarrow HOC\ell + HNO_3\ (ice) \quad (2)$$

$$N_2O_5 + HC\ell\ (ice) \longrightarrow C\ell NO_2 + HNO_3\ (ice) \quad (3)$$

$$N_2O_5 + H_2O\ (ice) \longrightarrow 2HNO_3\ (ice) \quad (4).$$

Heterogeneous chemistry is parameterized in terms of surface concentrations of aerosols, collision frequencies between gas molecules and aerosol surfaces, concentrations of $HC\ell/H_2O$ in the frozen particles, and probability of reaction

per collision (γ). Values of γ are taken from the latest laboratory measurements. The heterogeneous chemistry and phase transitions are assumed to occur between 12 and 22 km. The behavior of trace species at higher altitudes is calculated by the AER 2-D model without heterogeneous chemistry. Calculations are performed for solar illumination conditions typical of 60°, 70°, and 80° S, from July 15 to October 31.

The final products of heterogeneous processing by reactions (1)-(4) are very sensitive to the adopted initial concentrations of NO_x ($NO + NO_2 + C\ell NO_3 + 2xN_2O_5$), to the adopted rates of (1) - (4), and to the degree of illumination during the processing. We consider four cases representing different initial conditions for NO_x, and different rates for the heterogeneous processing. These cases illustrate different possibilities for the behavior of antarctic trace species, given the existing uncertainties and the constraints placed by available observations. We have concentrated on the following measurements from AAOE: 1) column densities of $HC\ell$, NO_2, HNO_3 and $C\ell NO_3$ by the infra-red spectrometers aboard the DC-8 aircraft; 2) local densities of NOY ($NO_x + HNO_3$) measured aboard the ER-2 aircraft; 3) local densities of $C\ell O$ measured aboard the ER-2; 4) local densities of ozone measured aboard the ER-2; 5) column densities of ozone from the TOMS instrument.

Comparison of calculations and observations indicate the following:

- The observed column densities of HNO_3 are consistent with mixing ratios of about 2.5 ppbv below 18 km near 70°, and of 1.5 ppbv deeper into the vortex. These values are also consistent with the ER-2 NOY measurement.
- Calculated column abundances of NO_2 are about 50% larger than observations. Since calculations indicate that most of this NO_2 is located above 22 km for the denitrified conditions of antarctic spring, resolution of this discrepancy requires more careful consideration of modeling and measurements in this region.
- The calculated column densities of $HC\ell$ are generally consistent with the low values observed, particularly if heterogeneous processing occurs throughout the month of September.
- Processing by (1) - (4) can yield substantial amounts of chlorine nitrate during August if initial NO_x concentrations during winter were of order 2 ppbv at 18 km. Negligible amounts of $C\ell NO_3$ would be produced if initial

NO_x abundances were a factor of two smaller. The high column densities of $C\ell NO_3$ observed during September could be an indication of $C\ell NO_3$ formation through reaction with NO_2 from photolysis of nitric acid during this month, or that large amounts of $C\ell NO_3$ present in August are not converted to active chlorine.

- Processing by (1) - (4) yields mixing ratios of $C\ell O$ between 0.4 and 1.1 ppbv at 18 km during the early half of September.
- The decrease in local ozone densities observed by the AAOE instruments can be explained by chlorine-mediated catalytic cycles above 15 km. The $C\ell_2O_2$ cycle contributes about 80% of the calculated reduction, if we adopt currently accepted values for the formation and photolysis rates of $C\ell_2O_2$, and assume that the photolysis produces molecular oxygen. Since there are still uncertainties in the above, these conclusions are dependent on future resolution of these issues.
- The calculated behavior of $C\ell O$ after the end of the AAOE mission depends crucially on the amount of HNO_3, its photolysis rate, and the assumed duration of heterogeneous chemistry.
- The calculated reduction in column ozone between August and October ranges from 40 to 110 Dobson units in the four cases considered, depending on the assumed concentrations of NO_x, HNO_3, and the temporal extent of heterogeneous chemistry. Observations of $C\ell O$ during late September and October would further constrain the above estimates.
- Calculated reductions in column ozone at different levels of chlorine exhibit a non-linear behavior. The calculated reduction accelerates for chlorine levels comparable to the adopted initial NO_x abundances during winter. Since these abundances also control the amount of processed $HC\ell$, the deepening of the ozone hole slows down for higher levels of chlorine in the future. Details of this behavior, however, are sensitive to the adopted HNO_3 concentrations and rates of heterogeneous reactions, particularly of (2).

Decending Motion of Particle and its Effect on Ozone Hole Chemistry

Y. Iwasaka

Water Research Institute, Nagoya University, Chikusa-ku, Nagoya 464 JAPAN

Abstract

The descending motion of particles which grow up to a few micrometer under the cold winter Antarctic stratosphere is also important process to accerelate the effect of heterogeneous reactions on ozone hole formations.

1. Introduction

In the winter Antarctic stratosphere, a lot of particulate matter was formed under very cold temperature which decreases to lower than -85° C at Syowa Station (69° 00'S, 39° 35'E) (e.g., Iwasaka et al., 1985; Iwasaka., 1986). Some investigators suggested that the surface of particulate mattercould act as an effective chemical reaction site for ozone-destruction chemical reaction series (e.g., Solomon et a., 1985). It was suggested that the excellent correlation of total ozone content with 100 mb surface temperature during Antarctic spring could be explained if the effect of the heterogeneous chemical reactions including the aerosols was taken into consideration (e.g., Iwasaka and Kondoh, 1987).

Most of previous investigations decsribing the effect of the particles on chemical reactions payed their attention to the surface area of particles or chemical composition of particles but not the effect of particle descending motion.

The possibility of particle descending in the winter Antarctic stratosphere was suggested on the basis of eye-observation of stratospheric clouds (Stanford, 1973) and lidar measurements (Iwasaka, 1986). McCormick et al.(1985) suggested that the descending motion of the Antarctic aerosol layer observed by SAM II could be associated with a downward air motion. Iwasaka (1986) suggested that the descending motion of the layer was capable when particles grew to a few micron size aerosols. The particle descending motion is imporatnt process controlling the redistribution of the chemical species relating 'ozone hole'

Combination of particle growth, evaporation of particle, chemical adsorption, and particle settling can play as sink or source of chemical species, and it strongly depends on a stratospheric temperature distribution.

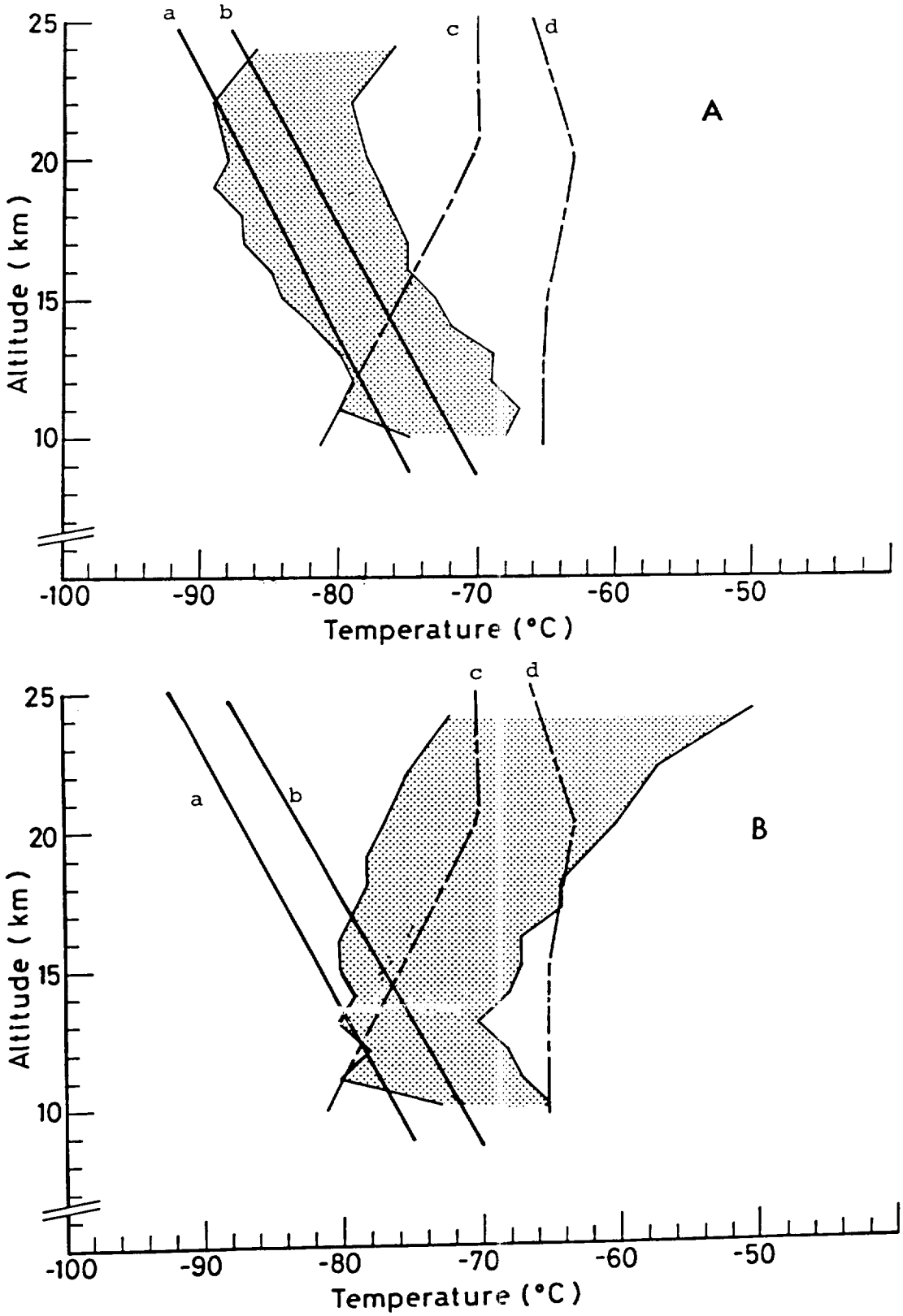

Fig. 1, The shaded area means the observed temperature rangeat Syowa Station (69° S, 40° E) in July 1983 (a) and in September (b). Curve a and b are frost point temperature of pure water. Curve c and d are frost point of HNO_3-H_2O (50% weight) crystal.

2. Particle Growth

Following points are essential for heterogeneous reactions controlling 'Ozone Hole' ;

1) What kind of gases are used to produce the particulate matter ?

2) What kind of reactions can take place on the surface of particles ? and What is surface area ?

3) Is there the possibility of particle descending motion ?

Steele et al. (1983) and Iwasaka (1986) discussed growth of ice crystal particle from pre-existing sulfuric acid droplet. In their model, the main gas used to increase particulate matter was water vapor. However, the lidar measurements additionally showed meaningful time delay between particulate content increase and depolarization ratio increase (Iwasaka, 1986). Toon et al. (1986), and Crutzen and Arnold (1986) suggested the possibility that nitric acid vapor condense to solid state $HNO_3 \cdot 3H_2O$ particles. According to Cruzten and Arnold (1986) the condensation can start at higher temperature (205 + 5° K) than the frost point of water vapor at about 100mb.

Importance of the point 1) is easily understood comparing the amount of gas used to form particles with the remaining gas content. For water vapor, about 10% to 40% of water would be in solid (or liquid) state during the most developed phase of PSC's event. For HNO_3 the ratio of the amount of particulate matter phase will be extremely larger than the case of water vapor. Cruzten and Arnold (1986) emphasized that the depletion of HNO_3 alowed a rapid rise of hydroxyl radical consentrations as the cycle of reactions

$$OH + NO_2 \rightarrow HNO_3 \quad \text{and} \quad HNO_3 + OH \rightarrow H_2O + NO_2$$

do no longer operate.

The potential influence of surface reactions depends on the surface area of particles,

In Fig. 1, temperature distribution measured in winter at Syowa Station is compared with the frost point temperatures of water and mixture of HNO_3-H_2O (50% weight mixture). These curves suggest that particle production is active near 15km for water vaour, and above about 15km for HNO_3 particles in mid winter.

3. Descending motion of particles

The descending motion of aerosol layer was observed during winter by a lidar at Syowa Station. The particle size would be about a few micrometer or larger than it if the descending motion was due to a gravitational sedimentation (Iwasaka, 1986). As shown in Fig. 1, the condition of super saturation was not always satisfied for pure water vapor or nitric acid vapor even in mid-winter if the density profiles in mid-latitudes is assumed. Therefore the particle which settles to the region of $P < P_D$, where P and P_D are partial pressure of water vapor (or nitric acid vapor) and saturation

pressure of the vapor respectively, evaporates the gases condensed in the particles there.

Iwasaka and Kondoh (1987) showed that ozone depletion rate was largest near 15km and the second peak was near 10km and lower than it. The heights of these active ozone loss region do not correspond to the regio where particle production rate is large and apparently is lower. In Fig. 2, schematic picture showing the particle sedimentation effect is given. The desending motion of particles to the region where evaporation rate is high seems to accerelates the production rate of Cl_2 and ClOH near the tropopause.

4. Summary

The particle descending motion is one possible process which causes ozone loss near the tropopause in Antarctic spring. However, particle size distribution has not been measured yet. The particle settle is important redistribution process of chemical constituents contained in particles. To understand the particle settle effects on 'Ozone Hole', informations on the size distribution and the chemical composition of particles are desired.

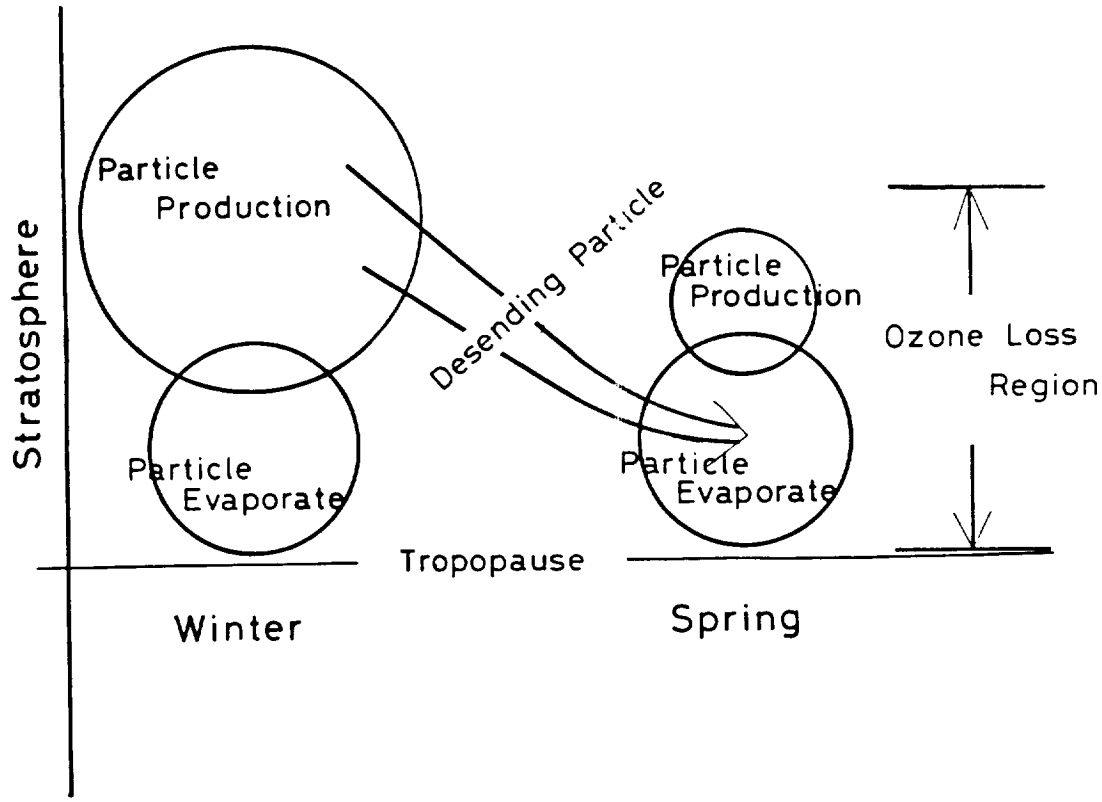

Fig. 2, The particles grow at the region where large super saturation occures in winter descendes to the region where evaporation from particles is active in spring.

SESSION VII - Arctic Measurements
Presiding, I. Isaksen, University of Oslo
Thursday Morning, May 12, 1988

VARIATIONS OF TOTAL OZONE IN THE NORTH POLAR REGION AS SEEN BY TOMS

Richard S. Stolarski
Arlin J. Krueger

NASA Goddard Space Flight Center
Laboratory for Atmospheres
Greenbelt, MD 20771
USA

Data from the TOMS instrument has been used to follow the course of development of the Antarctic ozone springtime minimum since 1979. This paper addresses the question of possible north polar region changes which might be deduced from the nine years of TOMS measurements of total ozone. Total ozone is a much more variable quantity in the northern hemisphere than in the southern hemisphere. This makes the search for trends more difficult and the interpretation of results more uncertain. We have examined the nine-year time series of TOMS data at high latitudes in the northern hemisphere. Because the TOMS measurements have drifted by 3-4% with respect to closely colocated Dobson measurements, we have chosen in this study to adopt the Dobson normalization and adjust the TOMS measurements accordingly. The accompanying figure shows a simple difference between the last two years of the TOMS record, 1986 and 1987, and the first two years of the record, 1979 and 1980. The difference is shown in percent as a function of latitude and time of year. The Antarctic springtime decrease is clearly seen, as well as a smaller change which extends to about 50 degrees south latitude at all seasons. Changes in the northern hemisphere are less dramatic and are concentrated near the polar night where solar zenith angles are very large. These data are now being examined in more detail and updated results will be presented at the Workshop.

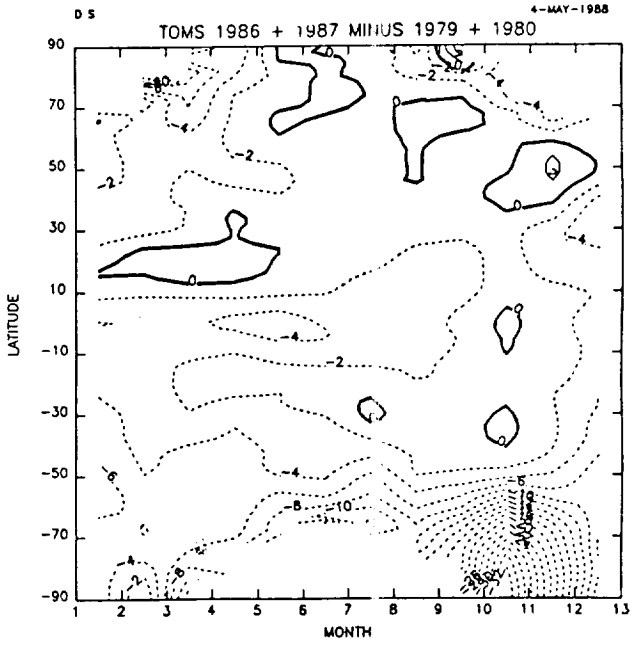

N89-14572

ABSTRACT FOR MEETING ON POLAR OZONE, ASPEN, COLORADO, MAY 9-13, 1988

WINTER-TIME LOSSES OF OZONE IN HIGH NORTHERN LATITUDES

Neil Harris, University of California, Irvine
F.S. Rowland, University of California, Irvine
Rumen Bojkov, Atmospheric Environment Service, Canada
Peter Bloomfield, North Carolina State University

Total column ozone data over the past 22-30 years from ground-based Dobson and filter ozonometer stations between 30°N and 80°N have been analyzed for residual trends remaining after allowance for the known geophysical variations corresponding to: (a) the yearly change of seasons; (b) the quasi-biennial oscillation; and (c) the 11-year solar sunspot cycle. Examination of the data from several ground stations between 45°N and 55°N indicated a seasonal difference in the long-term ozone series, with statistically significant losses in several winter months. Accordingly, the data from individual stations were analyzed with multiple regression analysis, seeking trends on a monthly basis after allowance for the known geophysical cycles. Previous statistical analyses have been conducted as tests of one-dimensional model calculations which do not show any differences with the seasons, and which therefore any trend toward change in ozone concentrations is expressed in a yearly trend without seasonal variation. Such a model is inappropriate for calculations with a data set which exhibits a pronounced tendency toward seasonal differences in the trends. Comparisons with model calculations then require two-dimensional models into which seasonal and latitudinal differences can readily be programmed.

Multiple regressions have been calculated for the ozone data from about 30 individual Dobson stations, and for latitudinal band averages covering four latitude ranges from 30°N to 80°N. Table 1 shows the magnitude of the residual linear trends for individual months that correspond to ozone changes in these bands since 1969 after allowance for the QBO, solar cycle and seasonal effects. The correlation of ozone change with the QBO is known to be dependent upon latitude and this conclusion is confirmed with the sign change in Table 1. The ozone response to the solar cycle is as large as 2%, minimum to maximum. The residual linear trends show a measurable decrease in the annual average total column ozone of 1.7% to 3.0% in all latitude bands from 30°N to 80°N from 1969 to 1986. The decreases are largest during the winter months (2.3% to 6.2%) of December through March, and contrast with smaller changes (+ 0.4% to - 2.1%) in the summer months of June through August.

The winter/summer differences are especially large in the two most northerly bands in Table 1, with winter-time losses appreciably larger than can be explained by model calculations. An obvious possibility is that the winter-time losses are enhanced through heterogeneous chemical processes analogous to those found in the Antarctic ozone hole. The time distribution of such effects would be quite different in the Arctic because of the difference in meteorology. In contrast to the tight polar vortex in the south which effectively retains the same air over Antarctica all winter long, the Arctic air masses tend to

pass through the polar night and back into sunlight again. Any chemical effects causing ozone depletion in the Arctic winter air would therefore be distributed over a much larger total volume of air than in the constricted Antarctic; the much lesser abundance of polar stratospheric clouds in the north, and the shorter exposure time of individual air masses to the polar night, may substantially reduce the total amount of ozone depletion induced by such stratospheric chemical reactions.

The typical set of Dobson data from a station north of 30°N shows a much larger standard deviation for the monthly average values during winter months than in the summer. Treatment of such data with a multiple regression requiring that all months have the same trend over time for changes in total ozone emphasizes the less-noisy summer data, and down-weights the noisier wintertime measurements. The chief consequence of this statistical circumstance is that the yearly trend values calculated for a particular set of data show significantly smaller trends than given by the average of the monthly trends, as also shown in Table 1.

Table 1

Coefficients of Multiple Regression Statistical Analysis of Re-analyzed Dobson Measurements of Total Ozone Concentrations Collected into Latitudinal Band Averages. (Data are expressed in total percent changes for the period 1969-1986.)

	Latitude Band			
Month	60-80°N	53-64°N	40-52°N	30-39°N
January	- 7.4 ± 2.4	- 8.3 ± 2.2	- 2.6 ± 2.1	- 2.2 ± 1.5
February	- 8.9 ± 3.7	- 6.7 ± 2.8	- 5.0 ± 2.2	- 1.2 ± 1.9
March	- 3.2 ± 1.6	- 4.0 ± 1.4	- 5.6 ± 2.3	- 3.5 ± 1.9
April	- 1.8 ± 1.6	- 2.0 ± 1.4	- 2.5 ± 1.7	- 1.7 ± 1.3
May	- 2.9 ± 1.1	- 2.1 ± 1.2	- 1.3 ± 1.1	- 1.7 ± 0.9
June	+ 0.2 ± 0.9	+ 1.1 ± 0.9	- 1.8 ± 1.0	- 3.3 ± 1.0
July	- 0.7 ± 1.0	+ 0.0 ± 1.1	- 2.2 ± 1.0	- 1.3 ± 1.0
August	+ 0.1 ± 1.0	+ 0.2 ± 1.2	- 2.4 ± 1.0	- 1.0 ± 1.0
September	- 0.3 ± 1.1	+ 0.2 ± 1.1	- 2.9 ± 1.0	- 1.0 ± 0.9
October	- 0.6 ± 1.8	- 1.1 ± 1.2	- 1.5 ± 1.5	- 0.9 ± 0.8
November	+ 1.3 ± 2.1	+ 1.5 ± 1.8	- 2.4 ± 1.3	- 0.1 ± 0.8
December	- 5.4 ± 2.9	- 5.8 ± 2.3	- 5.5 ± 1.7	- 2.1 ± 1.1
Annual Average	- 2.7 ± 0.9	- 2.3 ± 0.7	- 3.0 ± 0.8	- 1.7 ± 0.7
Winter Average	- 6.2 ± 1.9	- 6.2 ± 1.5	- 4.7 ± 1.5	- 2.3 ± 1.3
Summer Average	- 0.1 ± 0.9	+ 0.4 ± 0.8	- 2.1 ± 0.7	- 1.9 ± 0.8
QBO*	- 2.2 ± 0.6	- 2.0 ± 0.6	- 1.3 ± 0.6	+ 1.9 ± 0.6
Solar*	+ 2.0 ± 0.6	+ 1.8 ± 0.6	+ 0.8 ± 0.7	+ 0.1 ± 0.6

* Percent changes per cycle, minimum-to-maximum. All uncertainties are expressed with one sigma statistical significance.

Average of Monthly Ozone Trends in Dobson Units per year and Percent change in 17 Years:

- 0.57±0.20	- 0.52±0.16	- 0.63±0.17	- 0.32±0.14
- 2.7±0.9	- 2.3±0.7	- 3.0±0.8	- 1.7±0.7

Uniform Trend in Ozone Change Assumed throughout the year, in Dobson Units per year and in Percent Change in 17 years):

(- 0.17±0.15)	(- 0.14±0.13)	(- 0.47±0.13)	(- 0.17±0.11)
(- 0.8±0.7)	(- 0.7±0.6)	(- 2.3±0.7)	(- 0.9±0.6)

Polar Ozone Workshop, Aspen
May 9 - 13, 1988

Observations of stratospheric source gas profiles during the Arctic winter

U. Schmidt, R. Bauer, G. Kulessa, E. Klein, and B. Schubert

Kernforschungsanlage Jülich, Institut für Atmosphärische Chemie
P.O. Box 1913, D-5170 Jülich, FRG

An international campaign was performed at ESRANGE rocket base, near Kiruna, Sweden (68°N) from January 4 to February 15 in order to investigate the Chemistry of Ozone in the Polar Stratosphere (CHEOPS). Within the framework of this campaign two sets of large stratospheric air samples were collected by means of a balloon borne cryogenic air sampler. The two balloons were launched on February 1, and February 10, 1988. At present the samples are analyzed in our laboratory for their contents of several long lived trace gases such as CH_4, N_2O, H_2, CO_2, CO and the major halocarbons CH_3Cl, $CFCl_3$, CF_2Cl_2, CCl_4, CH_3CCl_3, $C_2F_3Cl_3$.

The vertical profiles derived from these samples will be presented and compared with previous observations made in February 1987. The data will be discussed in view of the dynamical evolution of the arctic polar vortex during this winter.

To be presented at the "Polar Ozone" Workshop
at Aspen, 9-13 May, 1988

ROCKET- AND AIRCRAFT-BORNE TRACE GAS MEASUREMENTS IN THE WINTER POLAR STRATOSPHERE

F. Arnold, O. Möhler, K. Pfeilsticker and H. Ziereis
Max-Planck-Institut für Kernphysik
P.O. Box 103980, D-6900 Heidelberg, F.R. Germany

In January and February 1987 we have performed stratospheric rocket- and aircraft-borne trace gas measurements in the North Polar region using ACIMS (Active Chemical Ionisation Mass Spectrometry) and PACIMS (PAssive Chemical Ionisation Mass Spectrometry) instruments. The rocket was launched at Esrange (European Sounding Rocket Launching Range) (68° N, 21° E, Northern Sweden) and the twin-jet research aircraft operated by the DFVLR (Deutsche Forschungs- und Versuchsanstalt für Luft- und Raumfahrt) and equipped with our mass spectrometer laboratory was stationed at Kiruna airport. Various stratospheric trace gases were measured including also nitric acid, sulfuric acid, non-methane hydrocarbons (acetone, hydrogen cyanide, acetonitrile, methanol etc.), and ambient cluster ions.

The experimental data will be presented and possible implications for polar stratospheric ozone will be discussed.

IN SITU OBSERVATIONS OF *ClO* IN THE WINTERTIME NORTHERN HEMISPHERE: ER-2 AIRCRAFT RESULTS FROM 21°N TO 61°N LATITUDE

W.H. Brune, D.W. Toohey, and J.G. Anderson
Department of Chemistry
and
Department of Earth and Planetary Science
Harvard University
Cambridge, MA 02138
and
E.F. Danielsen and W. Starr
NASA Ames Research Center
Mountain View, CA 94043

We report here measurements of lower stratospheric *ClO* taken during a NASA ER-2 flight between Moffett Field, CA (37°N, 122°W) and Great Slave Lake, Canada (61°N, 116°W) on 13 February 1988. Northbound, the aircraft was flown at ~ 20 km altitude from 39°N to 56°N, at 18 km from there to 58°N, in a descent to 15 km at 60°N, and in a rise and turn at the northernmost point. The southbound leg was flown in a gradual climb from 20 km to 21.5 km. On this day, the central position of the Arctic polar vortex, as determined by an NMC analysis of heights and temperatures at the 50 mb and 70 mb levels, was approximately (79°N, 100°W). Because the vortex was located on the North American side of the pole, the aircraft was able to reach a point slightly inside the maximum horizontal wind region where wind speeds were (80 - 90) knots.

The general pattern for the observed *ClO* is that it increased with both latitude and altitude, and attained a maximum of ~ 55 pptv at 61°N latitude and 20.5 km altitude. This value is ~ 20 times smaller than the maxima observed over Antarctica, but is comparable to those seen just outside the "chemical containment vessel" located inside the Antarctic Polar vortex. On the other hand, in a comparison with northern midlatitude data taken on

this and three other February flights, ClO mixing ratios observed north of 55°N latitude are 2 to 5 times larger at all flight altitudes (15 - 20 km). We will discuss possible reasons for this enhancement over midlatitude and consider the evidence for whether or not the instruments sampled Arctic polar vortex air.

A second feature of the data is the strong positive correlation between ClO and O_3 during the entire flight. This relationship holds for all observable spatial scales and at all altitudes. A negative correlation, as observed first over Antarctica on 16 September 1987, implies photochemical loss of ozone and is not expected to occur in the air sampled during this flight. With ClO at $\sim$ 60 pptv, the chlorine photochemical mechanisms proposed for the Antarctic ozone hole are too slow to reduce ozone in the course of a few months.

Three other flights were made on 12 February, 16 February, and 19 February. On 12 February, night-to-day transitions of ClO and BrO were measured; day-to-night transitions were measured on 16 February. The aircraft was flown northward to $\sim$ 47°N and back for both flights. The 19 February flight was directed south to 21°N latitude in an altitude "sawtooth" pattern — allowing us to establish a coarse grid of ClO and BrO with respect to altitude between 17 and 21 km and latitude between 21°N and 61°N.

Visible and Near-Ultraviolet Spectroscopy at Thule AFB (76.5°N) from January 28-February 15, 1988

G. H. MOUNT[1], R. W. SANDERS[2], R. O. JAKOUBEK[2], A. L. SCHMELTEKOPF[1], and S. SOLOMON[1]

[1]Aeronomy Laboratory, National Oceanic and Atmospheric Administration, Boulder, CO

[2]Cooperative Institute for Research in Environmental Sciences (CIRES), University of Colorado, Boulder, CO

Near-ultraviolet and visible spectrographs identical to those employed at McMurdo Station, Antarctica (77.8S) during the austral spring seasons of 1986 and 1987 were used to study the stratosphere above Thule, Greenland (76.5N) during early spring, 1988. Observations were carried out both at night using the direct moon as a light source, and during the day by collecting the scattered light from the zenith sky when solar zenith angles were less than about 94.5 degrees. Excellent meteorological conditions prevailed both in the troposphere and stratosphere during this observing program at Thule. Surface weather was extremely clear over most of the period, facilitating measurements of the direct light from the moon. The lower stratospheric arctic polar vortex was located very near Thule throughout the observing period, and temperatures at the 30 mbar level were typically below -80C above Thule, according to the National Meteorological Center daily analyses. Thus conditions were favorable for polar stratospheric cloud formation above Thule.

Total column ozone abundances were about 350-400 Dobson units, and did not suggest a clear temporal trend over the observing period. Stratospheric nitrogen dioxide measurements were complicated by the presence of a large component of tropospheric pollution on many occasions. Stratospheric nitrogen dioxide could be identified on most days using the absorption in the scattered light from the zenith sky, which greatly enhances the stratospheric airmass while suppressing the tropospheric contribution. These measurements suggest that the total vertical column abundance of nitrogen dioxide present over Thule in February was extremely low, sometimes as low as 3×10^{14} cm^{-2}. The abundance of nitrogen dioxide increased systematically from about 3×10^{14} in late January to 1.0×10^{15} cm^{-2} in mid-February, perhaps because of photolysis of N_2O_5 in the upper part of the stratosphere, near 25-35 km.

Spectra obtained using the moon as a light source on the nights of February 2 through February 7 have been analyzed for OClO. Preliminary results suggest a small but measurable vertical column abundance of OClO, around 3×10^{13} cm^{-2} on the night of February 3, for example. Measurements of OClO in Antarctica during late August, 1987 suggest a much larger value of about 2.3×10^{14} cm^{-2}, while photochemical model calculations employing purely

homogeneous chemistry (no heterogeneous polar stratospheric cloud chemistry) imply a nighttime OClO abundance of only about 5.0×10^{12} cm^{-2}. Thus the observed Antarctic abundances of OClO are about fifty times greater than model calculations neglecting heterogeneous chemistry, while the Thule measurements are about six times greater than such models. This limited series of measurements therefore suggests that significant enhancements of reactive chlorine radicals are present in the Arctic vortex, albeit to a much less extent than in the Antarctic. The possible implications of this suite of measurements for the depletion of Arctic ozone will be explored.

OZONE AND NITROGEN DIOXIDE GROUND BASED MONITORING BY ZENITH SKY VISIBLE SPECTROMETRY IN ARTIC AND ANTARCTIC

J.P. POMMEREAU AND F. GOUTAIL
Service d'Aéronomie du CNRS
91371 - Verrières le Buisson - FRANCE

Unattended diode array spectrometers have been designed for ground based stratospheric trace species monitoring by zenith sky visible spectrometry. Measurements are performed with a 1.0 nm resolution between 290 nm and 590 nm in order to allow simultaneous evaluations of column densities of ozone, nitrogen dioxide . Field tests have shown that the species can be monitored with a precision of ± 2 Dobson for the first and $\pm 2.10^{15}$ mol./cm^2 for the second, although the absolute accuracy of the method is limited by the error of the estimation of the atmospheric optical path of the scattered light.Two identical instruments have been set-up in January 1988, one in Antarctica at Dumont d'Urville (66 S, 140 E) which will be operated all along the year and an other one in the Arctic at Esrange at Kiruna (68 N; 22 E) which will stay up to the final warming of spring 1988. The data are processed in real time at both stations. O_3 and NO_2 columns are transmitted together with surface and stratospheric temperature and winds. They are also recorded for further treatment and search for OClO and BrO.

Only one month of data from Antartica is available at the moment (figure 1). Obtained during polar summer they cannot show more than stable columns of O_3 and NO_2 and for the last species, the build up of its diurnal variation.

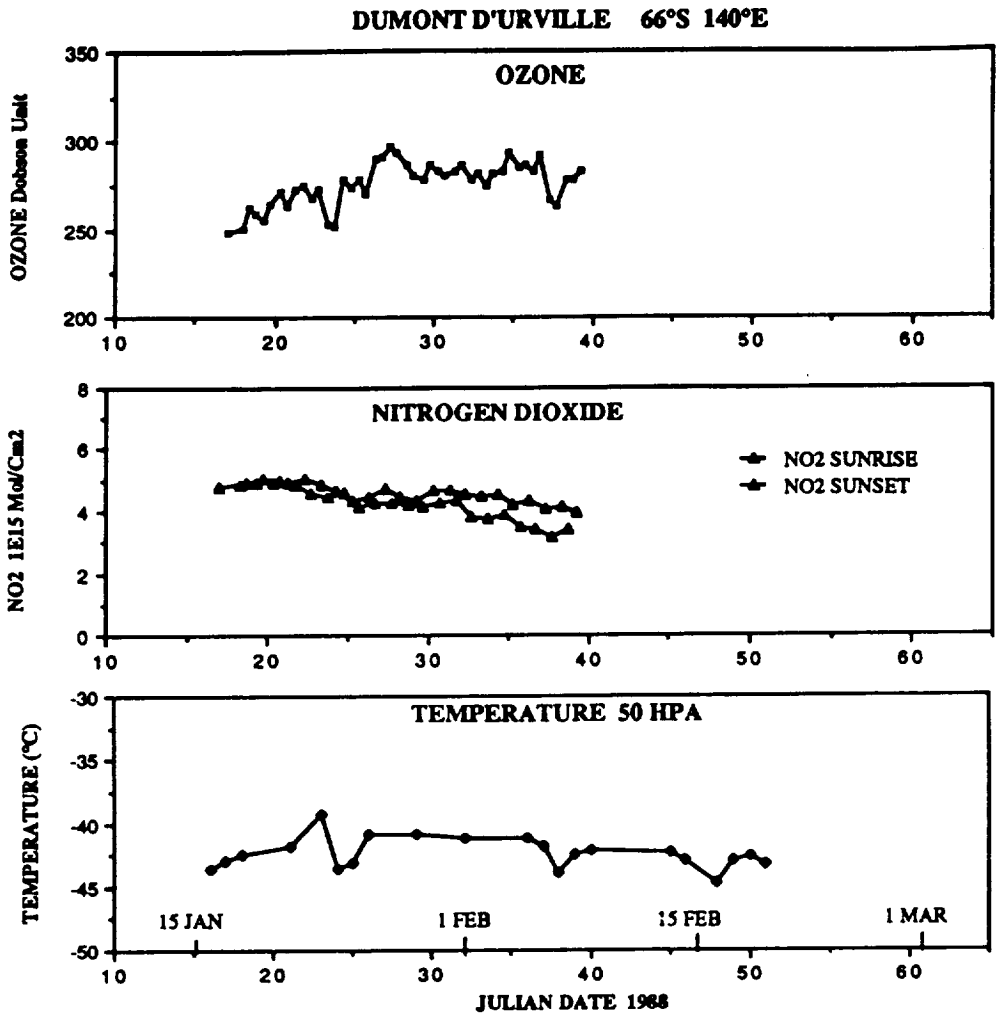

FIGURE 1

The Artic instrument began its measurements on January 16 and is still running as the exceptionnal stratospheric winter 1987-88 continues (figure 2). Ozone was observed to increase slowly in average from 300 DU to 390 DU untill mid February afterwards large variations are present, the lowest columns being correlated with the polar vortex approaching Northern Scandinavia. Nitrogen dioxide is found to vary considerably at Kiruna. Although the station is located 2000 km north of the major industrial and urban European areas, large pollution episodes were found at several circonstances. They occur when the surface wind is directed from S-SE to SW. Observed columns, that is vertical columns if the species is tropospheric, reached values as high as 1.5 10^{17} $mol.cm^{-2}$. Making the difference between polluted and clear periods is not always straight forward. If only those situations where the surface wind is outside the polluted sector are kept, then NO_2 appears to be strongly correlated with temperature at 30 mb.

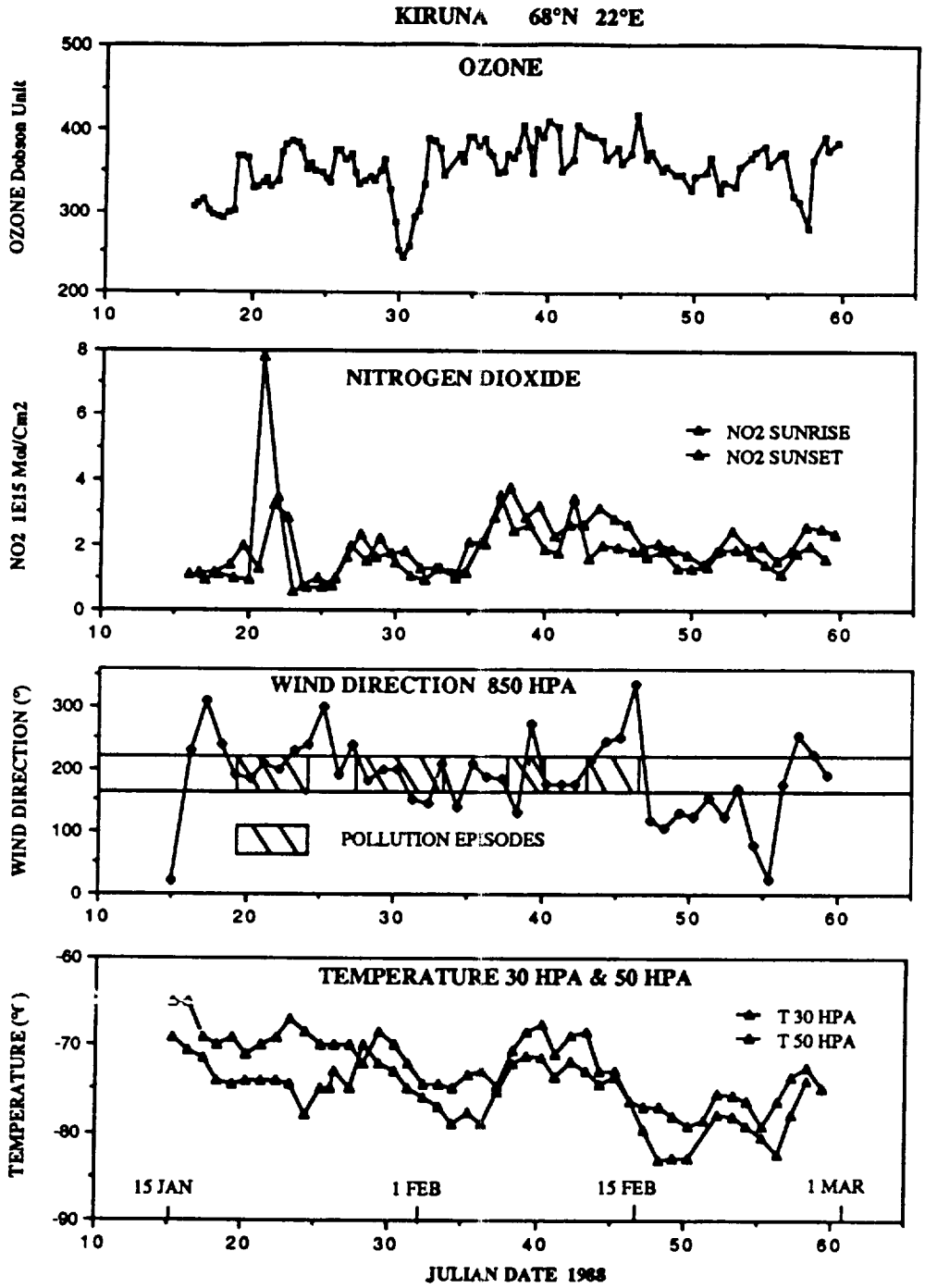

FIGURE 2

For the lowest temperature (-82°C), the column is reduced to values below 1.10^{15} $mol.cm^{-2}$. The diurnal cycle totally absent in January is still very small by the end of February although the sun culminates at 76° at noon. Its amplitude covaries with stratospheric temperature. Measurement will follow on, the data recorded will be reprocessed and we expect to present a complete picture of the evolution of both NO_2 and O_3 up to the final spring warming.

CANOZE MEASUREMENTS OF THE ARCTIC OZONE HOLE

W.F.J. Evans, J.B. Kerr and H. Fast
Atmospheric Environment Service
4905 Dufferin Street
Downsview, Ontario, Canada
M3H 5T4

Abstract

In CANOZE 1 (Canadian Ozone Experiment), a series of 20 ozone profile measurements were made in April, 1986 from Alert at 82.5 N. CANOZE is the Canadian program for study of the Arctic winter ozone layer.

In CANOZE 2, ozone profile measurements were made at Saskatoon, Edmonton, Churchill and Resolute during February and March, 1987 with ECC ozonesondes. Ground based measurements of column ozone, nitrogen dioxide and hydrochloric acid were conducted at Saskatoon. Two STRATOPROBE balloon flights were conducted on February 26 and March 19, 1987. Two aerosol flights were conducted by the University of Wyoming. The overall results of this study will be reported and compared with the NOZE findings. The results from CANOZE 3 in 1988, will also be discussed.

The appearance of the Antarctic ozone hole, which was reported in 1985, has led many scientists to speculate on the cause. It is natural to expect that a similar phenomenon will occur in the northern hemisphere since there is a cold polar vortex formed in the winter just as in the southern hemisphere. The phenomenon may be different and more difficult to research because of the higher level of planetary wave activity and the presence of stratospheric warmings. The Antarctic is a continent surrounded by oceans whereas the Arctic is an ocean surrounded by continents. It has been pointed out that the Antarctic has much colder temperatures than the Arctic; although the spring temperature is warmer in the Arctic, this is not true during December and January when the northern vortex forms and temperatures below - 80°C are frequent. The Antarctic ozone hole has been associated with the polar stratospheric clouds through heterogeneous reactions. Polar stratospheric clouds have also been observed in the northern vortex during December. Weisburd[1] (1986) has reported on work by Heath, which indicated the presence of a developing ozone hole in the northern hemisphere from an annual analysis of SBUV satellite data, apparently located over Spitzbergen in late winter; this hole is only about a third as deep and a third as large in area. In conclusion, it is not unreasonable to expect the formation of an ozone crater in the northern hemisphere. Based on these expectations we have been conducting a search for a similar crater in the Arctic, using our Canadian network of ozone monitoring stations (Evans[2], 1987).

A modest study was conducted from Alert, 82.5 N, in conjunction with the AGASP2 project. This work consisted of a series of ECC ozonesondes from March 31 to April 23, 1986 to study the Arctic tropospheric ozone profile in spring.

In the upper altitudes of these profiles, there were layers of depleted ozone similar to those reported by Hofmann et al.[3] (1987) from McMurdo under the Antarctic ozone hole. These depleted layers were found at 100 mb and 160 mb, about 50 mb lower than in the Antarctic. This is understandable since the tropopause was 50 mb lower in the Arctic than in the Antarctic at McMurdo. These profiles are supplemented by our regular soundings from Resolute, Churchill and Goose Bay. The layers of depleted ozone are also apparent on these station profiles at the appropriate times. In order to assist the interpretation of these findings, the TOMS data for this period were processed into imagery and examined. A shallow crater in the ozone field was found over Alert on April 13. Subsequent examination of the TOMS imagery revealed that a large crater had existed in the ozone field from mid-January until April with a maximum extent in mid-March. This hole had an area about one half of the Antarctic hole and was not as deep. The ozone crater had amounts of over 500 DU in the rim and values below 225 DU in the floor of the crater.

An ozonesonde profile from a station near the floor of the crater in mid-March showed that the ozone profile was depleted from 10 km up to 15 km, an observation similar to the measurements of Kohmyr[4] (1988) from South Pole station in mid-October, 1986 in the floor of the crater. This was in marked contrast to the ozone profile from Resolute in mid-March in the rim of the crater. Again, there is a 5 km shift in altitude when comparing with the profiles in the southern hemisphere hole. The total ozone was 550 DU in the Resolute profile in the rim and 255 DU in the floor from the ozonesonde profile from northern Europe. The corresponding values in the Antarctic crater were 400 DU for the rim and 155 DU in the floor in 1986.

A more expanded program of ozone layer measurements was conducted in 1987. As well as ozone profile measurements from the four Canadian stations at Edmonton, Churchill, Resolute and Goose Bay, a special program was conducted from Saskatoon. This consisted of ground based measurements of ozone and nitrogen dioxide, ozonesonde profile measurements and STRATOPROBE balloon flights. In addition, special ground based measurements with a modified Brewer spectrometer were conducted from Alert from March 12 to March 31 to search for chlorine dioxide.

Later analysis of the TOMS imagery showed that, unfortunately, no ozone hole or crater structure was present in spring, 1987. However, depleted layers were found in the ozone profiles from Saskatoon, Churchill and Resolute during March, 1987; these appeared to be similar to the depleted layers reported by Hofmann et al.[3] (1987) from the Antarctic during September, 1986. Thus, the crater mechanism may have been operating earlier in 1987, but the hole was probably destroyed by stratospheric warmings which took place in February and March.

The STRATOPROBE balloon flights were conducted on February 26 and March 19, 1987 from 52 N at a time when the vortex was nearby over northern Hudson Bay. In particular on February 26, the air at 30 mb had been in darkness for 2 weeks as it came from over the pole. The nitric acid profile showed greatly enhanced amounts of nitric acid with a layer maximum mixing ratio of 15 ppbv peaked at 20 km. Chlorine nitrate was also enhanced by a factor of 2 over summer values at the same latitude. Moderate amounts of nitrogen dioxide and N_2O_5 were observed.

In 1988, as part of CANOZE 3, STRATOPROBE balloon flights were conducted from Saskatchewan on January 27 and on February 13. A new light-weight infrared instrument was developed and test flown. A science flight was successfully conducted from Alert (82.5 N) on March 9, 1988 when the vortex was close to Alert; a good measurement of the profile of nitric acid was obtained.

Overall, the Arctic spring ozone layer exhibits many of the features of the Antarctic ozone phenomenon, although there is obviously not a hole present every year. The Arctic ozone field in March, 1986 demonstrated many similarities to the Antarctic ozone hole. The TOMS imagery showed a crater structure in the ozone field similar to the Antarctic crater in October. Depleted layers of ozone were found in the profiles around 15 km, very similar to those reported from McMurdo. Enhanced levels of nitric acid were measured in air which had earlier been in the vortex. The TOMS imagery for March 1987 did not show an ozone crater, but will be examined for an ozone crater in February and March, 1988, the target date for the CANOZE 3 project.

Acknowledgements

We would like to thank the staff of the Experimental Studies Division for their expert contributions to the measurements. Scientific Instruments Limited provided the launch service and support.

References

1. Weisburd, S., One Ozone Hole Returns, Another is Found, Science News, 130, #14, p 215 (1986).

2. Evans, W.F.J., Depletion in the Arctic and Antarctic Ozone Holes, M-13-24, p 871, Abstracts of the IUGG/IAMAP Meetings, August 1987, Vancouver.

3. Hofmann, D.J., J.W. Harder, S.R. Rolf and J.M. Rosen, Balloon-borne Observations of the Development and Vertical Structure of the Antarctic Ozone Hole in 1986, Nature, 326, 59-62 (1987).

4. Komhyr, W.R., Oltmans, S.J. and Grass, R.D., Atmospheric Ozone at South Pole, Antarctica, J. Geophys. Res., 93, xx-yy (1988).

BREWER SPECTROPHOTOMETER MEASUREMENTS IN THE CANADIAN ARCTIC

J.B. Kerr and W.F.J. Evans
Atmospheric Environment Service
4905 Dufferin Street
Downsview, Ontario, Canada
M3H 5T4

Abstract

In the winters of 1987 and 1988 we have conducted measurements with the Brewer Spectrophotometer at Alert (82.5 N) and Resolute (74.5N). The measurements were conducted as part of our Canadian Program to search for an Arctic Ozone Hole (CANOZE).

Ozone measurements were conducted in the months of December, January and February using the moon as a light source.

The total ozone measurements will be compared with ozonesonde profiles, from ECC sondes, flown once per week from Alert and Resolute.

A modified Brewer Spectrophotometer was used in a special study to search for chlorine dioxide at Alert in March 1987.

Ground based observations at Saskatoon in February and at Alert in March 1987 failed to detect any measureable chlorine dioxide. Interference from another absorbing gas, which we speculate may be nitrous acid, prevented the measurements at the low levels of chlorine dioxide detected in the southern hemisphere by Solomon et al.[1] (1987).

Reference

1. Solomon, S., G.H. Mount, R.W. Sanders and A.L. Schmeltekopf, Visible Spectroscopy at McMurdo Station, Antarctica, 2, Observations of OClO, J. Geophys. Res., 92, 8329-8338 (1987).

ABSTRACT

Ozone Measurements During Wintertime in the Arctic . Comparison with Recent Measurements at the Same Places are made. Here the 30 hPa. Temperatures are shown .

To be presented as POSTER

Søren H.H. Larsen
Department of Physics, University of Oslo,
P.O.Box 1048 Blindern,
0316 OSLO 3, Norway.

Moon measurements made at Tromsø and at Spitzbergen, 70 and 78 deg. north, back in the fifties have been re-evaluated. One has to take into account that the wedge calibration will change when the focussed image of the moon on the inlet slit is used. A correction was later decided to be used after several experiments in Dobsons Laboratory in Oxford. The absorption coefficients have been changed since the observations were taken and evaluated the first time. The re-evaluated ozone values have been plotted, in one diagram for Spitzbergen, and in one for Tromsø. The zonal mean value for ozone is given as a reference.

Ozone measurements from the winter season 1985/86 and 1986/87 made at the same places are presented. Here the daylight measurements are incorporated and also TIROS satellite data from single point data retrieval are given. The two winter seasons were very different. In the first we had a late final stratospheric warming, and in the other we had a early final stratospheric warming. This can be seen from the 30 millibar temperatures, provided by Barbara Naujokat, and plotted in the diagrams. Again the zonal mean values of ozone are given as reference.
Diagrams with ozone and 30 hPa. temperatures for the same seasons, from Oslo, are also presented.

C-41

SPRINGTIME SURFACE OZONE FLUCTUATIONS AT HIGH ARCTIC LATITUDES AND THEIR POSSIBLE RELATIONSHIP TO ATMOSPHERIC BROMINE

Samuel J. Oltmans[1], Patrick J. Sheridan[2], Russell C. Schnell[3], and John W. Winchester[4]

[1]NOAA/Geophysical Monitoring for Climatic Change, Boulder, Colorado 80303
[2]National Research Council Associate, NOAA/GMCC, Boulder, CO 80303
[3]CIRES, University of Colorado, Boulder, CO 80309
[4]Florida State University, Tallahassee, FL 32306-3048

At high Arctic stations such as Barrow, Alaska, springtime near-surface ozone amounts fluctuate between the highest and lowest values seen during the course of the year (Oltmans, 1981). Episodes when the surface ozone concentration is essentially zero last up to several days during this time of year (Fig. 1). In the Arctic Gas and Aerosol Sampling Program (AGASP-I and AGASP-II) in 1983 and 1986, it was found that ozone concentrations often showed a very steep gradient in altitude with very low values near the surface (Herbert et al., 1988; Bridgman et al., 1988). The cold temperatures, and snow-covered ground make it unlikely that the surface itself would rapidly destroy significant amounts of ozone.

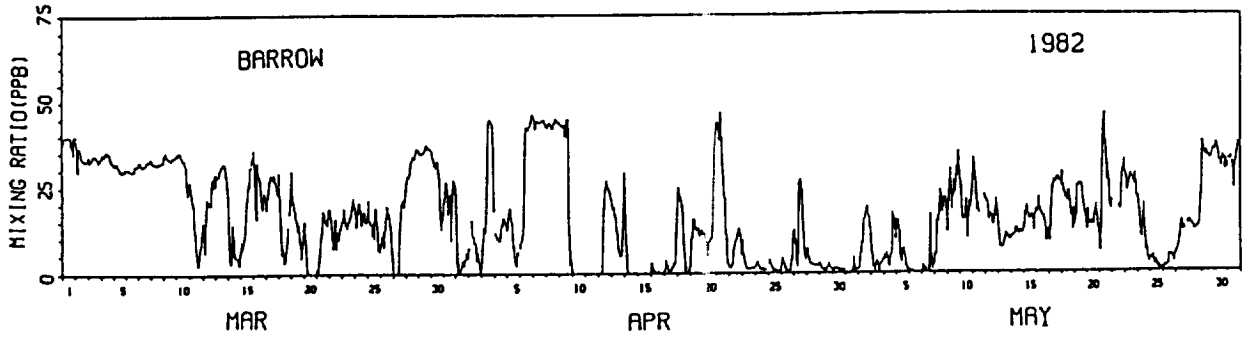

Fig. 1. Hourly surface ozone concentrations at Barrow for Mar-May 1982 showing large fluctuations and periods of near-zero values.

Fifteen years of ozone observations near the surface at Barrow, Alaska (71°N, 157°W) show (Fig. 2) a late autumn and winter maximum, a sharp springtime drop; a modest recovery to a secondary maximum in June; a small dip during the summer; followed by rising concentrations during autumn. Although ozone concentrations in Fig. 2 show a great deal of variability which ranges in scale from days to years, the pattern described above is in evidence each year. A very similar pattern is seen in the ozonesonde record at Resolute, NWT (75°N) for observations near the surface. Such a seasonal pattern is unique to the high Arctic and is not seen at other relatively high latitutde stations (e.g. Churchill at 59°N) outside the Arctic Basin. Ozonesonde observations at both Barrow and Resolute show that this behavior is confined to the boundary layer.

The AGASP aircraft measurements that found low ozone concentrations in the lowest layers of the troposphere also found that filterable excess bromine (the amount of bromine in excess of the sea salt component) in samples collected wholly or partially beneath the temperature inversion had higher bromine concentrations than other tropospheric samples. Of the four lowest ozone minimum concentrations, three of them were associated with the highest bromine enrichments. Surface measurements of excess filterable bromine at Barrow (Berg et al., 1983) show a strong seasonal dependence with values rising dramatically early in March, then declin-

ing in May. The concentration of organic bromine gases such as bromoform (Fig. 3) rise sharply during the winter, and then begin to decline after March with winter and early spring values at least three times greater than the summer minimum (Cicerone et al., 1988). Recently Barrie et al. (1988) found that at Alert, NWT (82°N), ozone mixing ratios during April 1986 were anticorrelated at a level of better than 0.95 with filterable bromine concentrations.

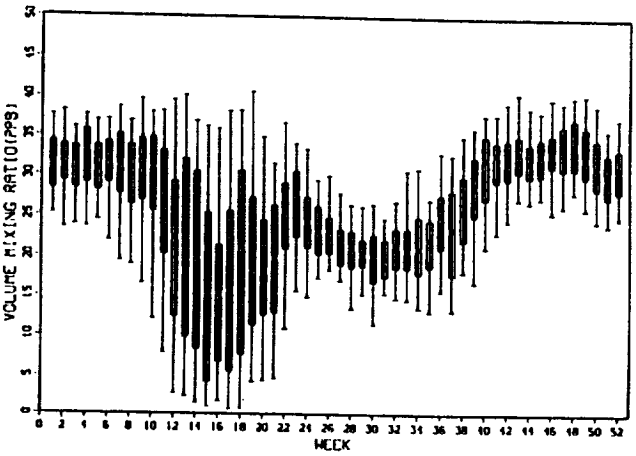

Fig. 2. The seasonal variation of ozone at Barrow, AK for 1973-1986. Box and whisker plots at weekly intervals are from daily means. The median (dot), the upper and lower quartiles (ends of the box) and upper and lower 5 percentiles (ends of lines are shown.

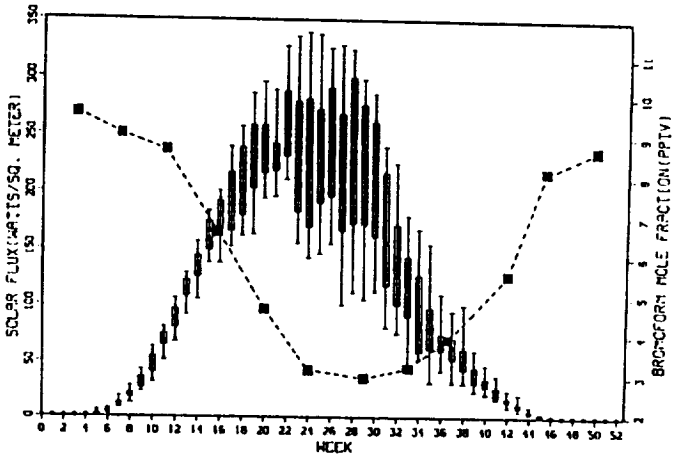

Fig. 3. Total global flux of solar radiation at Barrow for 1976-1983, with box and whisker plots as in Fig. 2 and mean monthly bromoform mole fraction (from Cicerone et al., 1988).

The critical link between the presence of organic bromine gases and the large fluctuations in ozone near the surface is the appearance of sunlight in the spring. In early March at Barrow, the total global flux of solar radiation (Fig. 3) begins a rapid rise. March and April appear to be months with a number of days having relatively clear skies. Although the radiative input continues to climb through May, there is an increasing amount of cloudiness as 24-hour daylight approaches. If solar radiation is an important factor, then more northerly stations should show a later appearance of the spring peak in filterable bromine. This indeed does appear to be the case from data presented by Sturges and Barrie (1988) from stations ranging in latitude from 70°N to 82°N.

The springtime minimum in the seasonal cycle of surface ozone concentrations at high arctic latitudes appears to be linked to the destruction of ozone in the boundary layer by reactions with bromine compounds (Wofsy, 1975; Barrie et al., 1988). Organic bromine compounds emitted from the predominatly ice-covered ocean appear to react with ozone in the presence of adequate sunlight to destroy ozone and produce filterable bromine particles. During stable periods, bromine compounds appear to produce a rapid and thorough destruction of the ozone as seen in the Barrow surface ozone record. Simultaneous measurements of filterable bromine and ozone at the surface were made at Barrow during the spring of 1986. The broad features of the relationship between filterable bromine enrichment and ozone mixing ratio are shown in Fig. 4. A 60-hour running mean has been applied to these data to smooth out small scale fluctuations. Although the correlation is a modest -0.64 between these two quantities, there is a clear tendency for high bromide values to be associated with low ozone concentrations and vice versa. The long

series of ozone measurements combined with measurements of filterable bromine, bromine gases and solar insolation show that the pattern seen in 1986 is found each year at Barrow. Data from aircraft and from a number of other locations suggest that this is an important process over a broad region of the Arctic Basin.

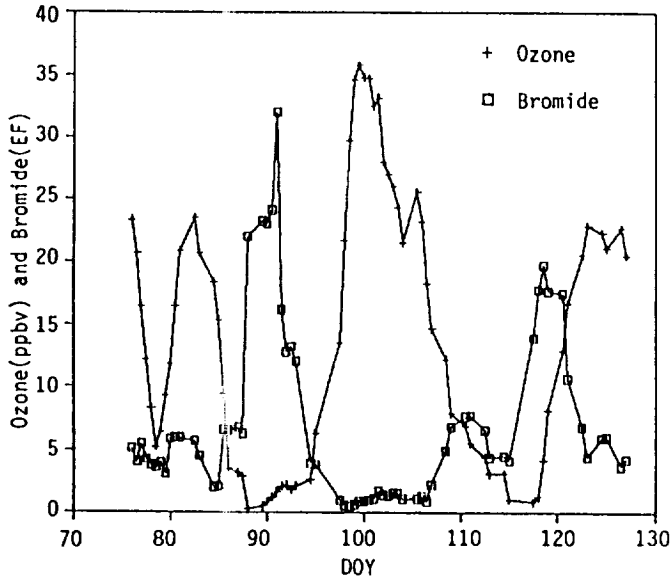

Fig. 4. Surface ozone mixing ratio (+) and filterable bromine enrichment factor (□) during Spring 1986 at Barrow, AK.

REFERENCES

1. Barrie, L. A., J. W. Bottenheim, R. C. Schnell, P. J. Crutzen, and R. A. Rasmussen. Ozone destruction and phtochemical reactions at polar sunrise in the lower arctic atmosphere, *Nature*, in press 1988.
2. Berg, W. W., P. O. Sperry, K. A. Rahn, and E. S. Gladney (1983). Atmospheric bromine in the Arctic, *J. Geophys. Res.*, **88**, 6719-6736.
3. Bridgman, H. A., R. C. Schnell, G. A. Herbert, B. A. Bodhaine, and S. J. Oltmans (1988). Meteorology and haze structure during AGASP-II, part 2: Canadian Arctic flights, 13-16 April 1986, *J. Atmos. Chem.*, in press 1988.
4. Cicerone, R. J., L. E. Heidt, and W. H. Pollock. Measurements of atmospheric methyl bromide (CH_3Br) and bromoform ($CHBr_3$). *J. Geophys. Res*, in press 1988.
5. Herbert, G. A., R. C. Schnell, H. A. Bridgman, B. A. Bodhaine, S. J. Oltmans, and G. E. Shaw. Meteorology and haze structure during AGASP-II, part I: Alaskan Arctic flights, 2-10 April, 1986. *J. Atmos. Chem.*, in press 1988.
6. Oltmans, S. J. (1981). Surface ozone measurements in clean air. *J. Geophys. Res.*, **86**, 1174-1180.
7. Sturges, W. T., and L. A. Barrie (1988). Halogens in Arctic aerosols. *Atmos. Env.*, in press 1988.
8. Wofsy, S. C., M. B. McElroy, and Y. L. Yung (1975). The chemistry of atmospheric bromine. *Geophys. Res Lett.*, **2**, 215-218.

-79 4-
157649

N89 - 14582

Airborne Measurements of Tropospheric Ozone Destruction and Particulate Bromide Formation in the Arctic

CU508845 NJ920144 WF835154

Russell C. Schnell[1], Patrick J. Sheridan[2], Richard E. Peterson[3] and S.J. Oltmans[4]
[1]CIRES, University of Colorado, Boulder, CO 80309
[2]NRC Research Associate, NOAA/GMCC, Boulder, CO 80303
[3]Chemistry Department, University of Washington, Seattle, WA 98195
[4]NOAA/GMCC, Boulder, CO 80303

Aircraft profiles of 0_3 concentrations over the Arctic ice pack in spring exhibit a depletion of 0_3 beneath the surface temperature inversion. One such profile from the NOAA WP-3D Arctic Gas and Aerosol Sampling Program (AGASP) flights in April, 1986 north of Alert, NWT (YLT, 82.5°N) is shown in Figure 1. The gradient of 0_3 across the temperature inversion, which is essentially a step function from tropospheric values (35-40 ppbv) to 0, is somewhat masked by a 1-minute running mean applied to the data.

Barrie et al. (1988) have presented evidence that 0_3 destruction beneath the Arctic temperature inversion is the result of a photochemical reaction between gaseous Br compounds and 0_3 to produce particulate Br aerosol. They note that in springtime, 0_3 at the Alert Baseline Station regularly decreases from 30-40 ppbv to near 0 over the period of a few hours to a day. At the same time, there is a production of particulate Br with a near 1.0 anti-correlation to 0_3 concentration. Surface concentrations of bromoform in the Arctic exhibit a rapid decrease following polar sunrise (Cicerone et al., 1988).

AGASP aircraft measurements of filterable bromine particulates in the Arctic (March-April, 1983 and 1986) are shown in Figure 2. The greatest concentrations of Br aerosol (shown as enrichment factors relative to Na in seawater, EFBR (Na)) were observed in samples collected beneath the surface temperature inversion over ice. Samples collected at the same altitude over open ocean (off Spitzbergen) labeled "Marine" did not exhibit similar Br enrichments.

A second region of particulate Br enrichment was observed in the lower stratosphere, which regularly descends to below 500 mb (5.5 km) in the high Arctic. The NOAA WP-3D flew in the stratosphere on all AGASP flights and occasionally measured 0_3 concentrations in excess of 300 ppbv.

AGASP aircraft gas flask measurements (Berg et al., 1984) show that both bromoform and methylene bromide concentrations decrease with altitude in the troposphere but increase in the lower stratosphere as shown in Figure 3. Bromoform and methylene bromide over the ocean (symbol M) do not exhibit higher concentrations beneath the temperature inversion as they do over ice.

It is yet to be determined if any relationship exists between the relatively high concentrations of bromine gases in the stratosphere and the associated elevated bromide concentrations. If the same tropospheric bromine-ozone photochemistry were to occur in the lower stratosphere as in the troposphere, one might speculate that stratospheric ozone is being similarly eroded at its lower boundary.

References

Barrie, L.A., J.W. Bottenheim, R.C. Schnell, P.J. Crutzen, and R.A. Rasmussen. Ozone destruction and photochemical reactions at polar summer in the lower Arctic atmosphere. *Nature*, (in press), 1988.

Berg, W.W., L.E. Heidt, W. Pollock, P.D. Sperry and R.J. Cicerone, Brominated organic species in the Arctic atmosphere. *Geophys. Res. Lett. 11*, 429-432, 1984.

Cicerone, R.J., L.E. Heidt, and W.H. Pollock. Measurements of atmospheric methyl bromide (CH_3 Br) and bromoform ($CHBr_3$). *J. Geophys. Res.*, (in press), 1988.

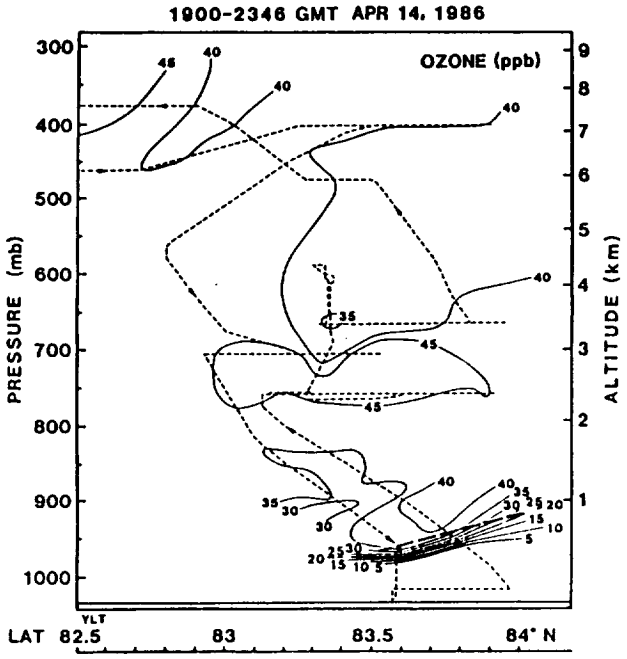

Figure 1. Cross-section of ozone concentrations upwind of Alert, NWT (82.5 °N) on April 14, 1986. The thick-dashed line indicates the base of the surface temperature inversion and the thin-dashed lines plot the aircraft flight track. The depleted ozone below the surface temperature inversion is evident.

AIRCRAFT FILTER DATA FROM THE 1983 AND 1986 AGASP MISSIONS

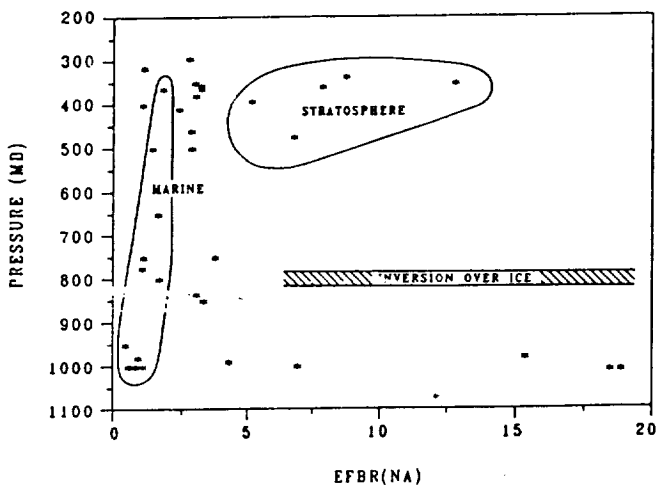

Figure 2. Aerosol filter data from the Arctic showing enrichments of filterable bromine relative to seawater. High concentrations of bromide particulates were present over ice beneath the surface temperature inversion and in the lower stratosphere. There were no bromide enrichments over the open ocean (MARINE) at any altitude.

BROMINATED ORGANIC SPECIES IN THE ARCTIC ATMOSPHERE

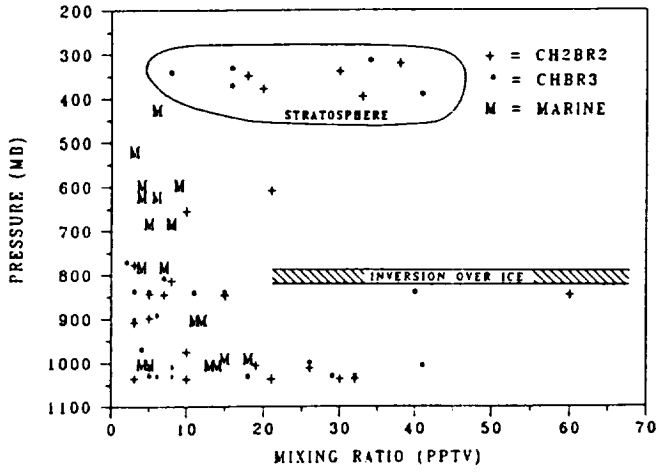

Figure 3. Concentrations of the gases bromoform ($CHBr_3$) and methylene bromide (CH_2Br_2) in the high Arctic. Samples indicated by M were collected over the open ocean. Higher gas concentrations in the lower troposphere and the lower stratosphere are in evidence.

IN SITU OBSERVATIONS OF *BrO* OVER ANTARCTICA: ER-2 AIRCRAFT RESULTS FROM 54°S to 72°S LATITUDE

W.H. Brune and J.G. Anderson
Department of Chemistry
and
Department of Earth and Planetary Science
Harvard University
Cambridge, MA 02138

Bromine monoxide was observed in situ at ~ 18 km altitude during nine flights of the NASA ER-2 aircraft from Punta Arenas, Chile (54° latitude) to 72°S latitude over the Palmer Peninsula, Antarctica. The first flight for the *BrO* detection system was on 28 August. We report here the results from the flights over Antarctica and from the ferry flights from Punta Arenas to Moffett Field, California (37°N latitude).

Bromine monoxide is a major component of the total inorganic bromine abundance throughout the lower stratosphere because homogeneous bromine photochemistry partitions inorganic bromine into basically only two species *BrO* and $BrONO_2$. How much of the total inorganic bromine content, which is thought to be (5 - 15) pptv, is *BrO* depends strongly on the NO_2 abundance in the air parcel. Inside the antarctic polar vortex, where NO_2 is low, *BrO* should be essentially the only inorganic bromine species. A measurement of *BrO*, however, may not be an accurate measure of the total inorganic bromine because the heterogeneous chemistry of bromine, which is virtually unknown, may act to reduce or redistribute bromine.

A key question concerning *BrO*, then, is how it is distributed with respect to the "chemical containment vessel" defined by elevated *ClO* mixing ratios. This question is answered with greatest statistical significance if the data are averaged into five regions:

outside the vessel, aircraft heading south; inside the vessel on the same potential temperature surface; in the "dive" region; inside the vessel on a given potential temperature surface, aircraft heading north; and outside the vessel on the same surface. The result is that the *BrO* distribution inside the "chemical containment vessel" was different from that found outside. Inside, the *BrO* mixing ratio was (5.0 ± 1.1) pptv between the 400 K and 460 K potential temperature surfaces, decreasing only slightly with potential temperature, and was less than 3.6 pptv below the 400 K surface. The abundance of *BrO* inside the "chemical containment vessel" showed no discernible temporal trend during the course of the nine flights. Outside the vessel, the *BrO* mixing ratio was (4.7 ± 1.3) pptv near the 450 K surface, but decreased to (2.8 ± 1.0) pptv near the 420 K surface. Bromine monoxide was clearly enhanced in the "chemical containment vessel", and the average enhancement was a factor of 1.7 ± 0.8. This difference was greatest near the 420 K potential temperature surface, and was almost negligible near the 450 K surface.

Away from the south polar region, the *BrO* mixing ratio was (1.0 - 3.0) pptv at latitudes between 45°S and 37°N and potential temperatures between 435 K and 500 K (18.5 km and 20.7 km altitude). These data were taken on the ferry flights north on 29 September, and 1 and 3 October. Unlike *ClO* which was ~ 500 times larger inside the antarctic polar vortex than at midlatitudes, *BrO* was less than five times larger inside the vortex than on comparable potential temperature surfaces at lower latitudes.

omit

SESSION VIII - Dynamical Simulations
Presiding, J. Pyle, University of Cambridge
Thursday Afternoon, May 12, 1988

The QBO and Interannual Variation in Total Ozone

L.R. Lait[1], M.R. Schoeberl[2], P.A. Newman[3], and R.S. Stolarski[2]

I. QBO modulation of the spring ozone decline rate

Introduction

Garcia and Solomon (1987) have noted that the October monthly mean minimum total ozone amounts south of 30S were modulated by a quasibiennial oscillation (QBO) signal. The precise mechanism behind this effect, however, is unclear. Is the modulation brought about by the circulation-produced QBO signal in the ozone concentration itself, or does the temperature QBO modulate the formation of polar stratospheric clouds (PSCs), leading to changes in the chemically induced Antarctic spring ozone decline rate? Or is some other phenomenon involved?

To investigate the means through which the QBO effect occurs, a series of correlation studies has been made between polar ozone and the QBO signal in ozone and temperature.

Analysis and results

It seems likely that variations in polar ozone would be more directly affected by the QBO in the Southern midlatitudes than by the tropical QBO. Therefore, quasibiennial signals from 66 S to the equator were extracted by digital filtering zonally averaged daily TOMS maps and NMC layer mean temperature fields. To better establish the link between these filtered data and the tropical QBO, both a narrow bandwidth filter (designed to isolate the QBO) and a broad bandwidth filter (retaining most signals with periods longer than the annual cycle) were used. The filtered data were correlated with the 30 and 50 mb winds over Singapore. Total ozone between 15 and 50 S and the 50-30 mb layer mean temperatures between 30 and 50 S are strongly anticorrelated with the 30 mb Singapore winds.

To obtain a picture of the evolution in time of the ozone within the polar vortex, daily minima poleward of 30 S were extracted from gridded TOMS data. The resulting time series was smoothed, and the spring decline rate for each year was determined by a linear least squares fit from September 1 to October 5. As shown in Figure 1, the decline rate shows an overall increase in magnitude from 1979 to 1987 but fluctuates with a period of about two years.

The filtered zonal mean total ozone is highly correlated with the polar ozone decline rate anomalies in the Southern midlatitudes and anticorrelated with the tropical QBO (Figure 2). The NMC 30-50 mb layer mean temperatures show similar results.

If the decline rates and the October mean ozone values were modulated directly by a QBO in the ozone superimposed on the overall decline, the slope of the midlatitude QBO should be associated with a decline rate deviation of the same sign. In fact, however, the two are poorly correlated; moreover, the slopes of the QBO signal for August-September (at most 0.03 DU/day) are too small to account for the decline rate deviations (about 0.4 DU/day). An alternative explanation is that a QBO in the temperature modulates the formation of PSCs, thereby affecting the rate of chemical destruction of ozone over the pole. This hypothesis seems better to account for the observed deviations in the decline rate, but cannot be proven from this data set.

1. NRC/NASA/GSFC, Greenbelt, MD 20771
2. NASA/GSFC, Greenbelt, MD 20771
3. Applied Research Corporation, 8201 Corporate Dr., Landover, MD 20785

Such a QBO signal in the temperature may be due to a direct circulation similar to that described for lower latitudes by Plumb and Bell (1982) and Plumb (1984), or it may be the result of a QBO modulation of midlatitude eddy activity (Holton and Tan, 1982; Dunkerton, 1988; Newman and Randel, 1988).

The sensitivity of the spring Antarctic decline rate to the QBO (whatever the precise mechanism) and the fact that the decline rate anomalies are a significant fraction of the decline rate itself indicates how strongly the Antarctic depletion can be modified by midlatitude processes. Thus, while the basic ozone depletion mechanism appears to be chemical, the overall chemistry is apparently highly sensitive to the dynamics of the Austral winter stratosphere.

II. The dilution effect

It has been suggested (M. Ko, personal communication) that, upon breakup of the polar vortex in the Southern late spring, subsequent transport and mixing of its depleted-ozone air could result in lower ozone levels at other latitudes (the dilution effect).

Zonal mean TOMS data from 1979 to 1987 have been averaged over months bracketing the Antactic ozone depletion event and differenced in an effort to separate such an effect from an overall secular decline or instrument drift. If the high ozone region just outside the polar vortex is reduced by the dilution effect, one would expect such differences to be positive over the vortex and negative over the high-ozone region, with an overall decrease from year to year. Figure 3 shows the December-September difference as a function of latitude and year. Some weak evidence for the dilution effect can be seen, but a large QBO signal in the data tends to obscure straightforward interpretation.

Figure Captions.

1. August-September decline rates of the daily map minimum in total ozone for each year (solid line), with their linear least squares fit (dashed line).

2. Correlation coefficient versus latitude of ozone decline rate deviations with zonal mean total ozone, filtered to extract the QBO. Dotted line is the correlation of the decline rate deviations with the rate of change of filtered zonal mean total ozone.

3. December-September difference of monthly mean zonally averaged total ozone for each year.

References

Dunkerton, T. J., Body Force Circulation and the Antarctic Ozone Minimum, *J. Atmos. Sci.*, **45**, 427-438, 1988.

Garcia, R. R. and S. Solomon, A possible relationship between interannual variability in Antarctic ozone and the quasi-biennial oscillation, *Geophys. Res. Lett.*, **14**, 848-851, 1987.

Holton, J. R. and H. C. Tan, The quasi-biennial oscillation in the Northern Hemisphere lower stratosphere, *J. Meteor. Soc. Japan*, **60**, 140-148, 1982.

Newman, P. A. and W. J. Randel, Coherent ozone-dynamical changes during the Southern Hemisphere spring, 1979-1986, submitted to *J. Geophys. Res.*, 1988.

Plumb, R. A., The quasi-biennial oscillation, in *Dynamics of the Middle Stratosphere*, edited by J.R. Holton and T. Matsuno, pp. 217-251, Terra Scientific Pub. Co., Tokyo, 1984.

Plumb, R. A. and R. C. Bell, A model of the quasi-biennial oscillation on an equatorial beta plane, *Quart. J. Roy. Meteor. Soc.*, **108**, 335-352, 1982.

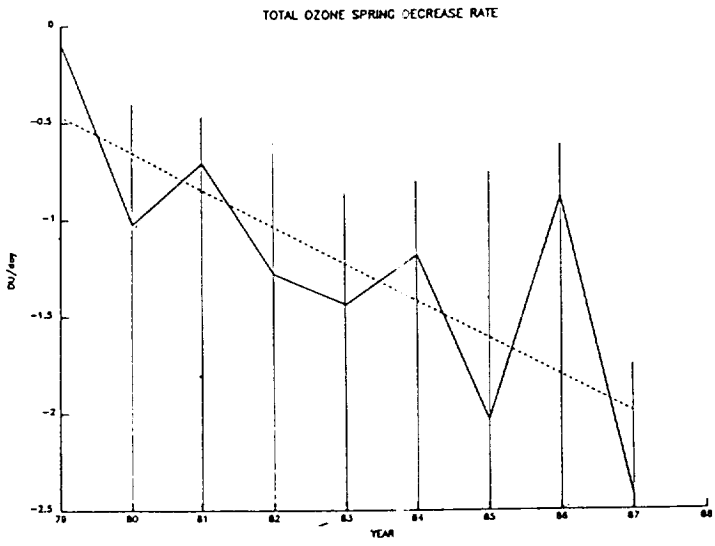

Figure 1.

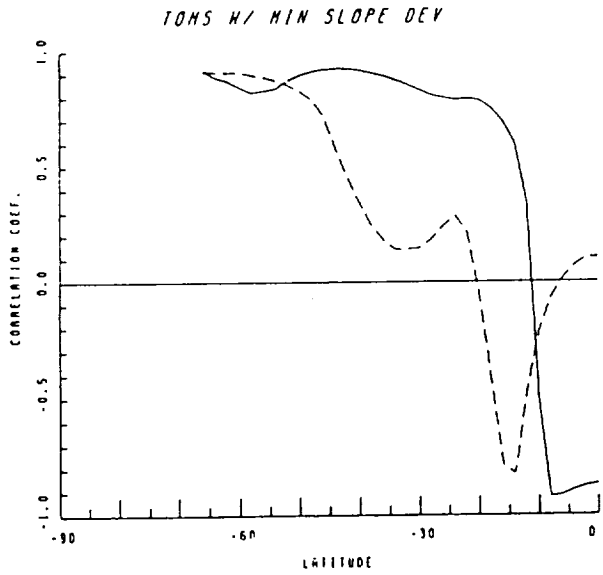

Figure 2.

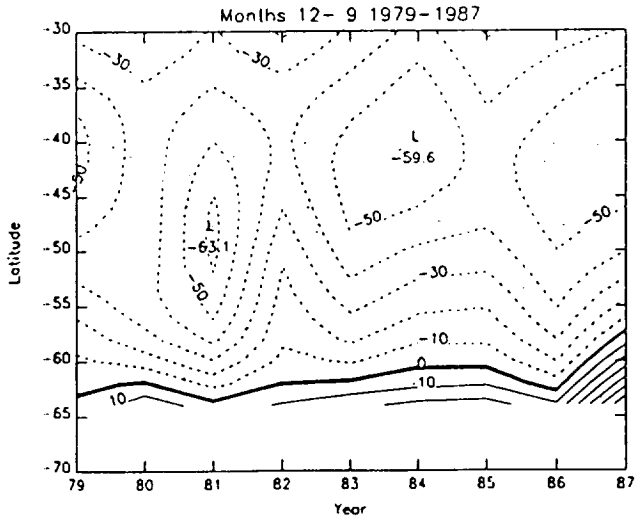

Figure 3.

N89-14585

Antarctic Ozone Decrease: Possible Impact on the Seasonal and Latitudinal Distribution of Total Ozone as Simulated by a 2-D Model

Malcolm K. W. Ko, Nien-Dak Sze, Debra K. Weisenstein and Jose M. Rodriguez

Atmospheric and Environmental Research, Inc.
840, Memorial Drive,
Cambridge, Ma 02139

Satellite borne instruments (TOMS and SBUV) show that total column ozone has decreased by more than 5% in the neighborhood of 60°S at all seasons since 1979. This is considerably larger than the decrease calculated by 2-D models which take into account solar flux variation and increases of trace gas concentrations over the same period. The meteorological conditions (warmer temperature and the apparent lack of polar stratospheric clouds) at these latitudes do not seem to favor heterogeneous chemistry as the direct cause for the observed ozone reduction. A mechanism involving the seasonal transport of ozone-poor air mass from within the polar vortex to lower latitudes (the so-called 'dilution effect') is proposed as a possible explanation for the observed year-round ozone reduction in regions away from the vortex.

Observations indicated that the column content of O_3 within the antarctic polar vortex decreases by about 50% during the austral spring. This amount corresponds to about 4% of the global content of O_3. Following the break down of the vortex in October, the O_3 content in the region is observed to recover within a few weeks. Given that the photochemical replacement time of O_3 at such latitude is estimated to be longer than a season below 25 km, the rapid filling-in of the O_3 hole can only be achieved by transport of O_3 from the mid-latitude region and mixing of air masses between the two regions. The assumption that spring O_3 decrease within the vortex is due to removal by photochemical processes raises the question of whether the subsequent redistribution of O_3 to fill the hole can affect the global O_3 content on a year long basis.

The extent and the persistence of the global impact will partially depend on the ability of the atmosphere to compensate for the antarctic loss by photochemical adjustment. The photochemical replacement time for O_3 in the upper stratosphere is a few days, i. e. the concentration of O_3 in the upper stratosphere would recover to its normal value within a few days if the O_3 were perturbed. Thus, if the O_3-poor air is exported to and replaced by O_3-rich air imported from the upper stratosphere, the impact on global content should be minimum. However, if the O_3 hole is to be filled by mixing with air from the lower stratosphere, where the photochemical replacement time ranges from a few months to a year, the photochemical compensation may not be complete within the year before the recurrence of the O_3 hole in the next spring. Using a 2-D model, we show that dilution could contribute to a year-round decrease of O_3 outside the polar vortex.

Although present 2-D models are not designed to simulate the formation and evolution of the polar vortex, they can be used to assess the global impact of the O_3 redistribution on a seasonal time scale. We modify the circulation in the 2-D model to simulate the vortex by preventing exchange of air across the boundary of the vortex between 14 and 22 km from mid-April to the end of October. Instead of actually putting in detailed heterogeneous chemistry to simulate the O_3 removal, we simply remove an additional amount of O_3 within the vortex right during the time the barrier is in place.

Our model results showed that

- the dilution effect could be a major contributing factor to the observed year-round decrease of total O_3 between 40°S - 60°S. The impact is, however, small for latitudes north of 30 S.
- the time constant of ozone associated with the dilution effect is relatively short, of order 1 year. This means that the dilution impact is essentially non-accumulative.
- the magnitude of the O_3 change is sensitive to the value of Kyy adopted in the model calculation.

Polar Ozone Workshop, 9-13 May, 1988, Aspen, Colorado

GLOBAL IMPACT OF THE ANTARCTIC OZONE HOLE: SIMULATIONS WITH A 3-D CHEMICAL TRANSPORT MODEL

Michael J. Prather (NASA/Goddard Institute for Space Studies, 2880 Broadway, New York, NY 10025) and
María M. García (Dept. of Applied Physics & Nuclear Engineering, Columbia U., New York, NY)

A study of the Antarctic ozone hole has been made with a 3-D chemical transport model using linearized photochemistry for ozone based on observed distributions. The tracer model uses the winds and convection from the GISS general circulation model (8° × 10° × 23 layers). A 3-year control run of the ozone distribution is compared with the observed climatology. In two experiments, a hypothetical Antarctic ozone "hole" is induced on October 1 and on November 1; the tracer model is integrated for 1 year with the standard, linearized chemistry. The initial depletion, 90% of the O_3 poleward of 70°S between 25 and 180 mbar, amounts to about 5% of the total O_3 in the Southern Hemisphere. As the vortex breaks down and the "hole" is dispersed, significant depletions to column ozone, of order 10 D.U., occur as far north as 36°S during Austral summer. One year later, about 25% of the original depletion remains, mostly below 100 mbar and poleward of 30°S. Details of the calculations will be shown, along with a budget analysis showing the fraction of the "hole" filled in by photochemistry versus that transported into the troposphere.

Table. Dobson Map of the Dispersion of an Antarctic Ozone Hole: Initialized November 1

(Units are negative D.U. relative to control climatology)

lat.	Nov1	Dec1	Jan1	Feb1	Mar1	Apr1	May1	Jun1	Jul1	Aug1	Sep1	Oct1	Nov1
4S	0	0	0	0	0	0	0	0	0	0	0	0	0
12S	0	0	0	0	0	0	0	0	0	0	0	0	0
20S	0	0	0	1	1	1	0	0	0	0	0	0	0
28S	0	0	2	2	2	2	2	2	2	2	2	2	2
36S	0	1	4	6	6	7	6	7	6	6	5	5	4
44S	0	7	11	11	11	11	10	10	9	8	7	6	5
52S	0	17	20	16	16	14	14	12	10	9	8	7	6
60S	0	31	26	22	19	17	16	13	12	9	9	7	6
68S	0	46	29	27	21	20	18	16	13	12	10	8	7
76S	242	59	33	28	22	20	19	17	15	13	11	9	7
84S	235	109	60	33	29	25	19	18	16	15	12	10	7
90S	212	160	88	42	33	29	14	15	18	16	11	9	7

Diagnostic Studies of the 1987 Antarctic Spring Vortex: Studies relating to the Airborne Antarctic Ozone Experiment (1987) employing the UK Meteorological Office Global Analysis.

Austin, J., Jones, R.L. and McKenna, D.S.
Meteorological Office,
London Road,
Bracknell.
Berks.,
RG12 2SZ

Dynamical fields from the UK Meteorological Office global forecast model were used throughout the 1987 Airborne Antarctic Ozone Experiment (AAOE) for flight planning and diagnostic studies. In this paper several studies based on the Meteorological Office global analysis (resolution 1.5 deg lat x 1.875 deg long, Lyne et al) are described. The wind and temperature data derived form the model analysis are compared with observations made from both the DCB and the ER-2, and an assessment of the model performance given. Derived quantities such as potential vorticity and potential temperature are calculated independently from both aircraft and model data and discrepancies due to the neglect of terms in the expression for potential vorticity and to errors in the model data will be discussed.

The composition of the vortex as indicated by some of the constituents observed by the ER-2 showed regions of reversal of latitudinal mixing ratio gradients near the southern extreme of the ER-2 flight track (725). It has been suggested that this structure could be indicative of a 'trough' or 'annulus' in the concentration fields of these constituents. However maps of potential vorticity are presented (see Fig 1) which show that this structure is consistent with distortions in the vortex on the scale of hundreds of km.

During the AAOE, there were several occasions when the column O3 as seen by the total ozone mapping spectrometer (TOMS) decreased by the order of 50 Dobson units over a 24-hr period. Model data valid for the time of these occurrences are used to argue that this phenomenon results from reversible differential advection of air from different levels and that a large proportion of the column deficit can be attributed to the poleward advection of air between 100-200 mb. Furthermore, it will be shown that the advection results from the poleward extension of a surface ridge.

Finally model data along the DCB flight tracks are presented which indicate the presence of structures in the model flow, which in certain respects are characteristic of tropopause folds. Air parcel trajectories are presented which indicate large irreversible equatorward excursions for some air parcels which originate in the vicinity of a fold (see Fig 2). The possible mass transfer associated with these events is estimated and the overall significance of this transport mechanism to the ozone budget of the southern hemisphere discussed.

References.

Lyne, W.H., Little, C.T., Dumelow, R.K., Bell, R.S. Met. O. 11 Technical Note No. 18: 'The Operational Data Assimilation Scheme.'

Figures.

1. Potential Vorticity on the 428K Isentropic Surface. Valid for 18Z 04/09/87.
2. Trajectories on the 340K isentropic surface.

UK MET OFFICE COARSE MESH DATA FOR ANTARTIC OZONE EXPERIMENT
POTENTIAL VORTICITY(M**2.K/KG.S)*10**6(SOLID) AND PRESSURE(MB)(BROKEN)
VALID AT 12Z ON 4/9/1987 DAY 247 DATA TIME 12Z ON 4/9/1987 DAY 247
LEVEL:428.0K

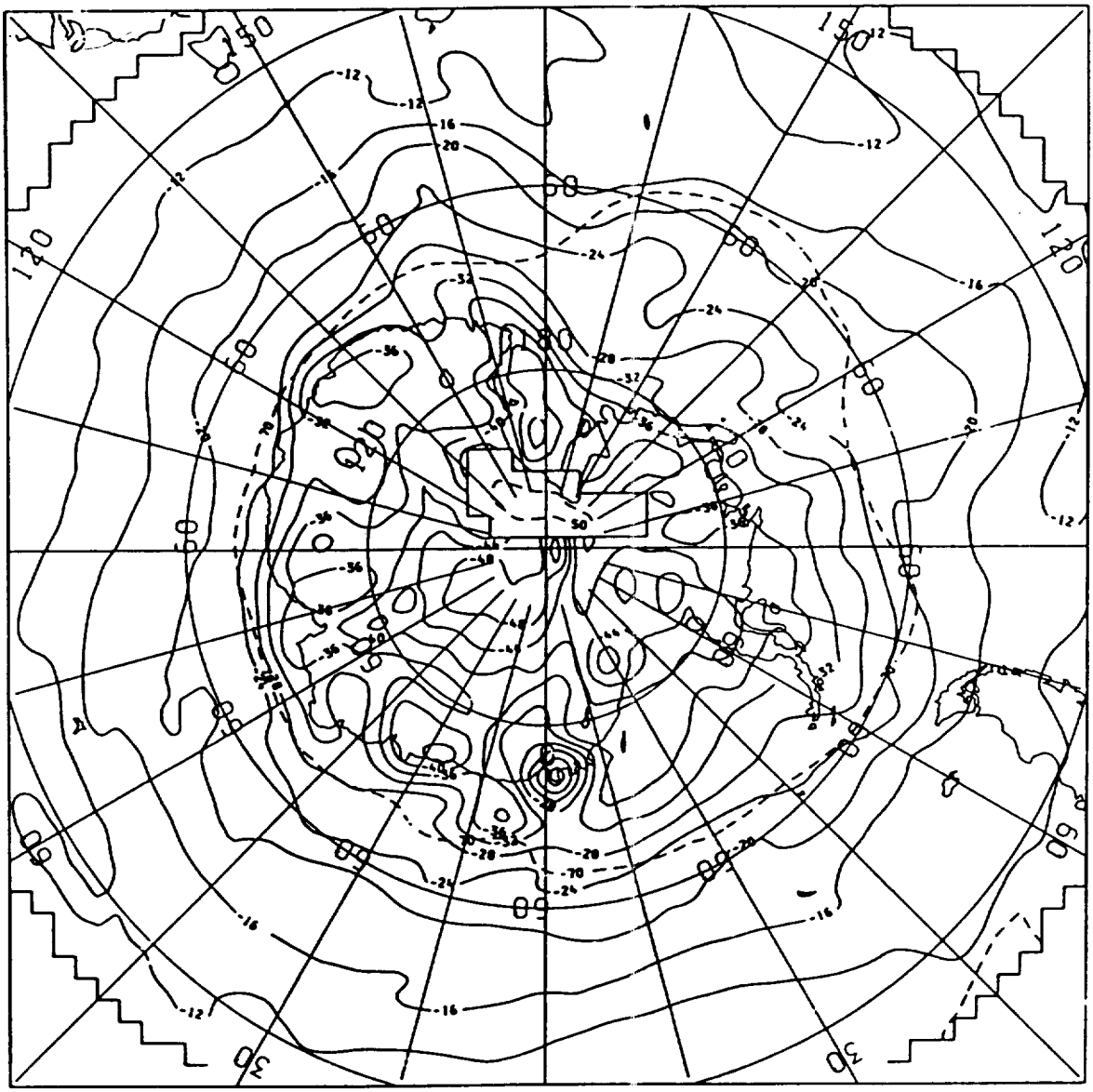

UK MET OFFICE COARSE MESH DATA FOR MINI HOLE ANALYSIS
FORWARD TRAJECTORIES ARROWHEADS EVERY: 12 HRS
FROM 12Z ON 5/9/87 DAY 248 TO 14Z ON 13/9/87 DAY 256
LEVEL:340.0 K GROUP: 1

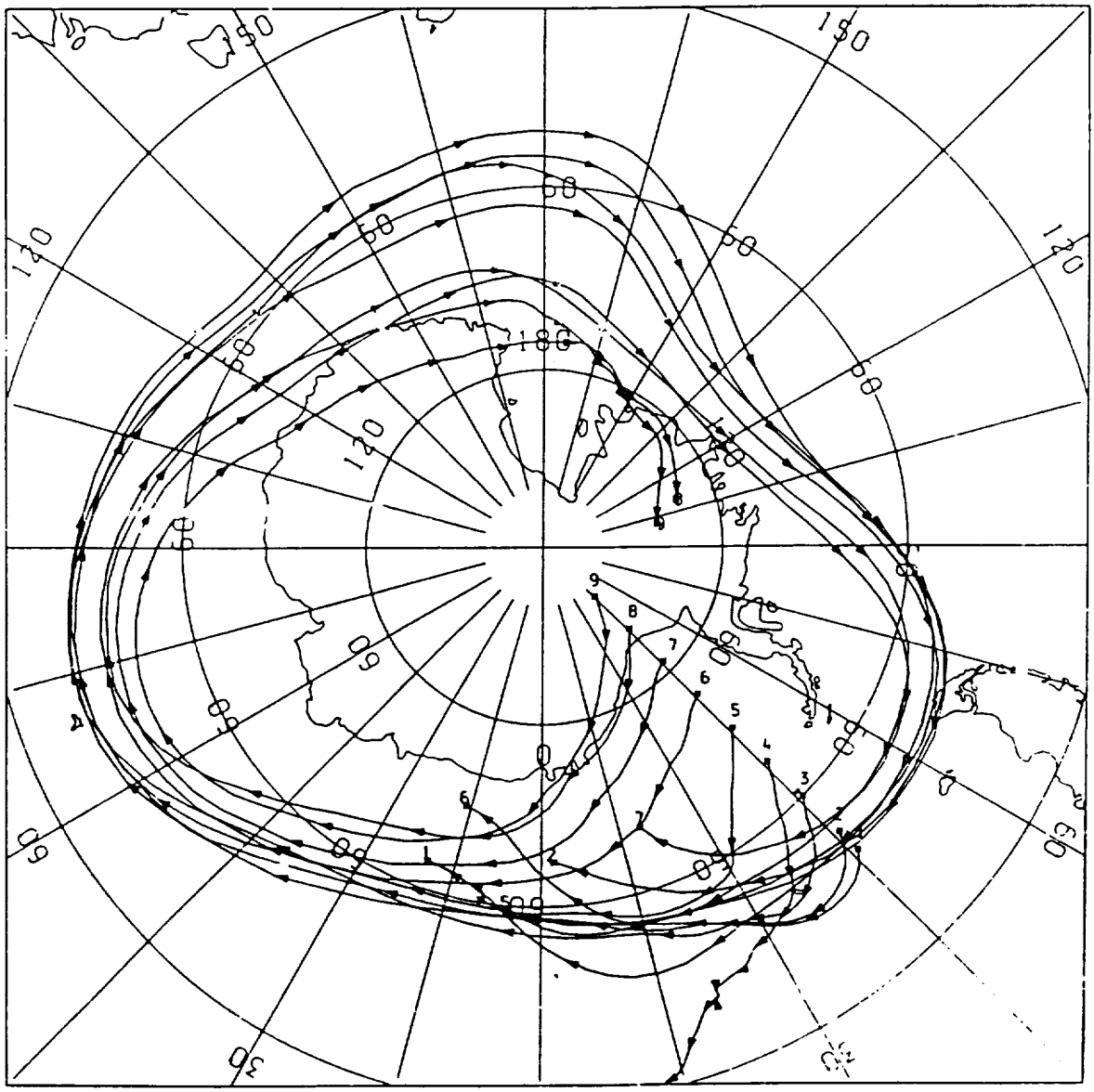

N89-14588

157655

22 February 1988

Abstract For Snowmass Polar Ozone Workshop (suggested oral presentation)

Polar Vortex Dynamics

Michael McIntyre

Department of Applied Mathematics and Theoretical Physics
Silver Street, Cambridge, England CB3 9EW.

Recent work with high resolution, one-layer numerical models of fluid flows resembling those in the real stratosphere has suggested that:

1. The interiors of strong cyclonic vortices like the Antarctic polar vortex may be almost completely isolated laterally from their surroundings - perhaps even completely isolated, under some circumstances;

2. By contrast, material near the edge of such an isolated region can easily be 'eroded' (or mixed one-sidedly) into the surrounding region;

3. The erosion characteristically produces extremely steep gradients in isentropic distributions of potential vorticity (PV) and of other tracers, possibly down to horizontal length scales of a few kilometres only. Such length scales may occur both at the edge of the main polar vortex and in smaller features outside it, such as thin filamentary structures, produced by the erosion process.

These results (for more details see Juckes and McIntyre 1987, '88) seem likely to be relevant to the Antarctic ozone problem. For example, point 1 would be especially relevant if it were turn out that the chemistry of the ozone hole is sensitive to 'contamination' e.g. from nitric oxides that might enter the polar vortex from outside. Point 3 might be relevant to the interpretation of high-resolution tracer observations. It is important to ask, therefore, to what extent the qualitative features just listed might carry over to the real stratospheric vortex and its surroundings.

Several modelling studies are currently in progress at Cambridge, involving work by D.G.Dritschel, P.H.Haynes, and W.A.Norton, using the computing resources of the U.K. Universities' Global Atmospheric Modelling Project. These aim to go beyond the earlier work and establish a hierarchy of models that will thoroughly test the robustness of the foregoing conclusions. Results to date will be reported on, including, it is hoped, some high resolution, fully three-dimensional, baroclinic polar-vortex simulations. Further details are given in two posters by Dritschel and Haynes submitted concurrently with this presentation.

One interesting result is a tendency for isentropic distributions of PV to exhibit a particularly steep 'cliff' at the outermost edge of the main vortex. This feature appears highly characteristic of the erosion process, at least when the vortex is disturbed mainly from outside, or by a planetary-scale wave only, as in model simulations to date. However, the real Antarctic vortex might be significantly stirred within its interior as well, making the isolated core region more nearly homogeneous than it might otherwise be, a circumstance that would also have chemical implications. A possible mechanism is stirring by the action of anticyclonic, tropopause-level PV anomalies associated with the observed "mini-holes" in column ozone, if and when these move underneath the main vortex. Such anomalies could induce synoptic-scale circulations in the air within the isolated vortex core above them, without requiring any material transport across the edge higher up, eg on the 420K isentropic surface.

The prediction of thin filaments and steep gradients (point 3) is physically reasonable; there is no reason to suppose that the real atmosphere has any pre-existing 'eddy diffusivity', like the artificial eddy diffusivities used in numerical models, that would smooth such features. These features are part of the physical mechanism that causes what might appear in a coarse-grain statistical description to be an 'eddy diffusivity'.

Indeed, the one-sided nature of 'erosion' of material from the edge of a strong vortex revealed by the numerical models provides a typical illustration of how deceptive the standard idea of 'mixing' and 'eddy diffusion' can be. It is always possible, of course, to define an eddy viscosity or tracer diffusivity by dividing an eddy flux by some mean gradient, but this idea may draw attention away from the fact that such quantities exhibit an extreme degree of spatio-temporal inhomogeneity in many naturally-occurring fluid flows. For instance as one crosses the edge into the polar vortex the eddy diffusivity must drop suddenly to zero, or to extremely small values, insofar as it can be defined usefully at all. It may rise again as one crosses into the interior.

From a theoretical-dynamics point of view one of the most striking aspects of flows like these is a tendency to exhibit a mixture of 'wavelike' and 'turbulent' characteristics in closely adjacent or overlapping regions. The distortions of the (edge of the) main polar vortex are an example of 'Rossby waves', and the surrounding region an example of two-dimensional turbulence or, in this context, 'Rossby-wave surf'. The interacting regions -- a sort of highly inhomogeneous 'wave-turbulence jigsaw puzzle'-- poses one of the biggest challenges facing dynamicists today. Results from the Antarctic may provide some unique clues to the solution of this puzzle, and hence an opportunity to make fundamental advances in dynamics as well as chemistry.

References

Juckes, M.N. and McIntyre, M.E., 1987: A high resolution, one-layer model of breaking planetary waves in the stratosphere.

Nature, 328 590-596,

Juckes, M.N. and McIntyre, M.E., 1988: Barotropic simulations of breaking planetary waves and vortex erosion in the stratosphere.

Q. J. Roy. Meteorol. Sol., to be submitted

Evolution of the Antarctic Polar Vortex in Spring: Response of a GCM to a Prescribed Antarctic Ozone Hole

B.A. Boville, J.T. Kiehl and B.P. Briegleb

National Center for Atmospheric Research*
P.O. Box 3000, Boulder, CO 80307

1. Introduction:

This study examines the possible effect of the Antartic ozone hole on the evolution of the polar vortex during late winter and spring using a general circulation model (GCM). The GCM is a version of the NCAR Community Climate Model whose domain extends from the surface to the mesosphere and is similar to that described in Boville and Randel (1986). Ozone is not a predicted variable in the model. A zonally averaged ozone distribution is specified as a function of latitude, pressure and month for the radiation parameterization. Rather than explicitly address reasons for the formation of the ozone hole, we postulate its existence and ask what effect it has on the subsequent evolution of the vortex.

The evolution of the model without an ozone hole is compared against observations in order to establish the credibility (or lack thereof) of the simulations. The change in the evolution of the vortex when an ozone hole is imposed is then discussed.

2. Experiments

A control and an ozone hole experiment are discussed here. Each experiment has been integrated through 4 separate realizations of Austral spring beginning in early August and ending in early January. The control experiment used an ozone distribution based on observations prior to the development of the ozone hole. In the ozone hole experiment, the ozone mixing ratios were altered poleward of 50°S based on the total column ozone observations in Stolarski and Schoeberl (1986) and the vertical column observations in Solomon et al. (1986).

Ozone mixing ratios for the fifteenth of each month are specified in the model and daily values are obtained by linear interpolation. The September and October values were altered in the ozone hole experiment. Thus, the hole develops from August 16 to September 15 then deepens slightly until October 15. The hole is gone on November 15 regardless of the state of the vortex.

The control experiment was integrated for 20 months beginning on May 1 to obtain two realizations of Austral spring. Ozone hole experiments were started in early August of

---

*The National Center for Atmospheric Research is sponsored by the National Science Foundation.

each year. The other two realizations of each experiment were obtained by perturbing the original experiments in early August. This methodology results in 4 separate realizations for relatively modest cost.

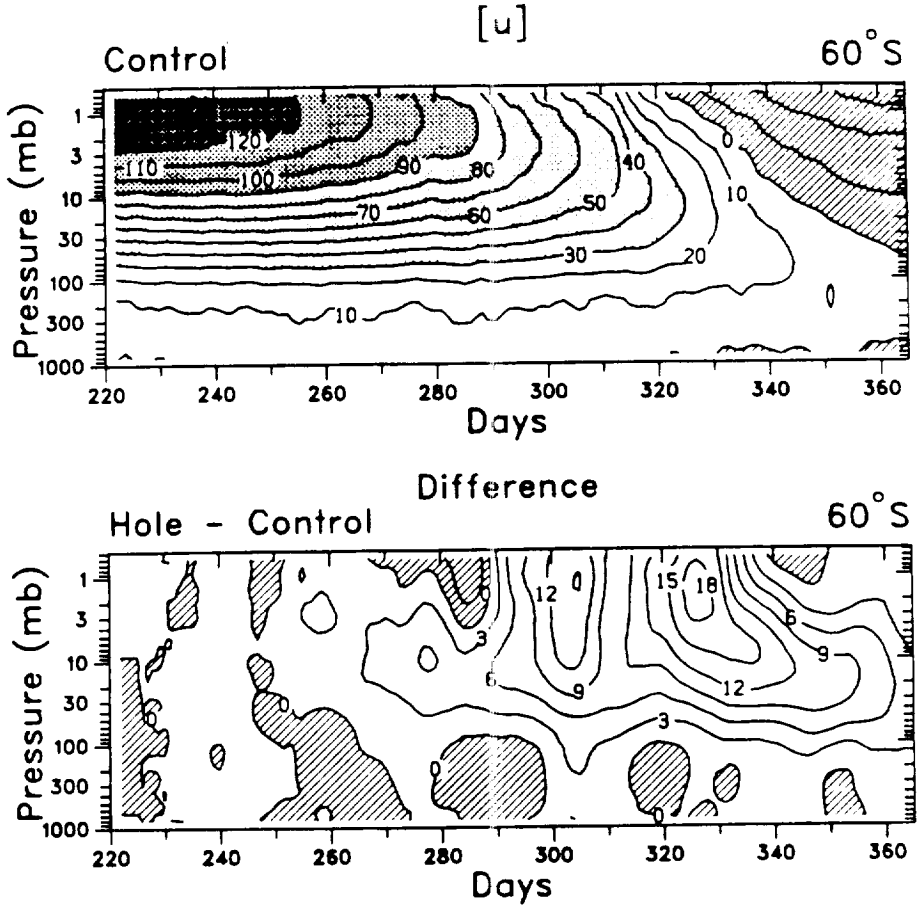

Figure 1. Time - pressure section of the zonally averaged zonal wind (ms^{-1}) at 60°S for the control simulation and the difference between the ozone hole and control simulations. Hatched region indicates negative values. Day numbers refer to day of the year (day 220 is August 8).

3. Results

The time evolution of the zonal wind is shown in Fig. 1 as a function of pressure and in Fig. 2 as a function of latitude. Ensemble means for the 4 realizations are shown. The polar night jet in the control simulation is stronger than observed during late winter, particularly at upper levels. At 10 mb and below the agreement with observations is much better (e.g. Randel, 1987) in late winter. The observed downward and poleward shift of the jet core through late winter and early spring can be found in the control simulation but is both too weak and too late. Note that this shift is the result of errosion of the jet at upper levels and low latitudes, not an acceleration at lower levels and higher latitudes. There appears to be insufficient dynamical forcing of the simulated polar vortex in early spring, resulting in an unrealistic persistence of the westerlies into December.

Imposing an ozone hole in September (days 244-273) and October (days 274-304) results in a colder and more stable vortex with a correspondingly stronger jet. Although the imposed ozone hole is gone by November 15, the lower stratospheric wind are almost 5 ms^{-1} stronger in the ozone hole simulation at the end of December. The large positive differences in November at upper levels in Fig. 1 result from a delay of about 10 days in the descent of the jet core in the ozone hole experiment compared to the control and a similar delay in the transition to easterlies. Below 10 mb the delay in the transition to easterlies is even longer, about 2 weeks. Westerlies persist until the end of December in the ozone hole simulation, although they are very weak.

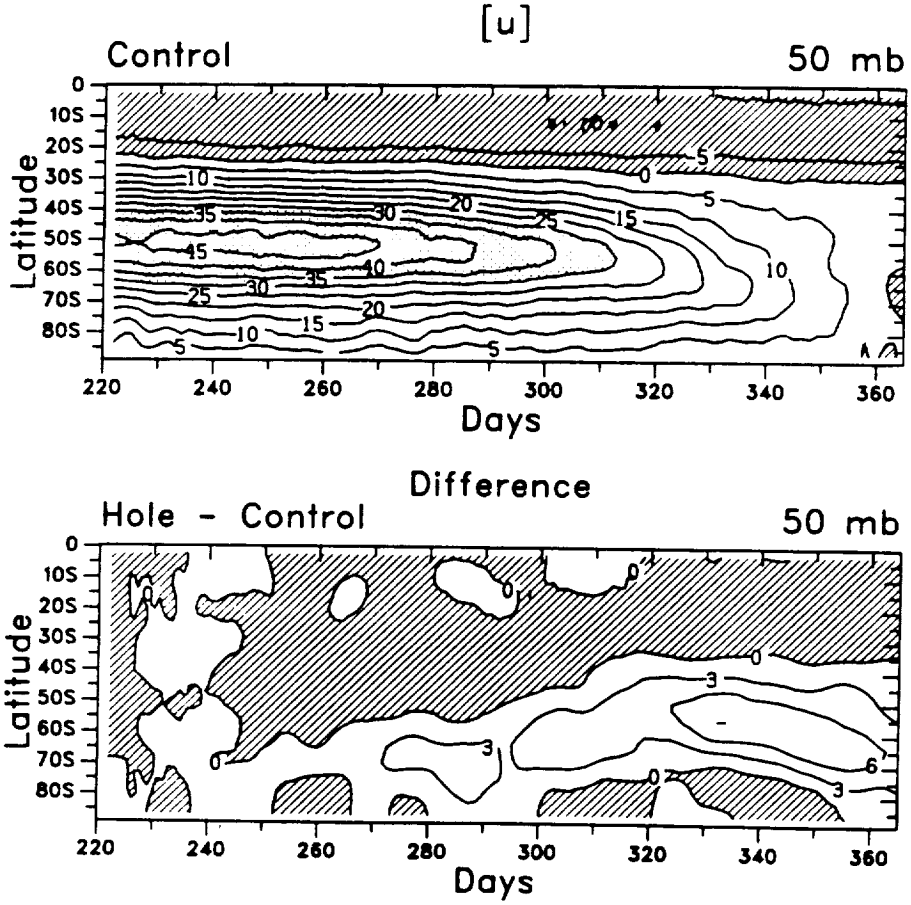

Figure 2. As in Fig. 1 except that a time - latitude section is shown at 50 mb.

4. Summary

The GCM results indicate that the presence of an ozone hole in September and October should result in a colder and more persistent polar vortex. This prediction is independent of the source of the hole, since the hole was simply imposed in the model. Whether a similar change in the persistence of the vortex can be observed in the atmosphere is uncertain. Even the control simulation of the GCM has weak dynamical forcing resulting in an overly persistent vortex. The stronger dynamical forcing present in the atmosphere in spring could swamp the tendency of the ozone hole to make the vortex persist longer.

References

Boville B.A., and W.J. Randel, 1986: Observations and simulation of the variability of stratosphere and troposphere in January. *J. Atmos. Sci.*, **43**, 3015–3034.

Randel, W.J. 1987: Global atmospheric circulation statistics, 1000–1 mb. NCAR Tech Note, NCAR/TN-295+STR, 245 pp.

Stolarski, R.S., and Schoeberl, M.R., 1986: Further interpretation of satellite measurements of Antarctic total ozone. *Geophys. Res. Lett.*, **13**, 1210–1212.

Solomon, S., Garcia, R.R., Rowland, F.S. and Wuebbles, D.J., 1986: On the depletion of Antarctic ozone. *Nature*, **321**, 755–758.

POLAR OZONE WORKSHOP
May 9–13, 1988

Theoretical Study of Polar and Global Ozone Changes Using a Coupled Radiative-Dynamical 2-D Model

by
H. Yang, K. K. Tung and E. Olaguar
Department of Mathematics and Computer Science
Clarkson University, Potsdam, N.Y.

ABSTRACT

Our existing 2-D model has recently been updated to incorporates ozone-temperature feedbacks with more comprehensive radiative transfer calculations and more detailed temperature data input. We attempt to address the following issues:

(a) Given the observed temperature changes for the past eight years, quantitatively how much ozone change can be produced by the dynamical effect of the temperature change over the Arctic and Antarctic?

(b) How much of the reported change in globally averaged ozone can be accounted for by temperature changes?

(c) The role of the diabatic circulation changes in the lower stratosphere in determining the timing of the polar spring maximum and minimum.

(d) The role of the seasonal change in the diabatic circulation in causing the fall minimum over the Arctic and the Antarctic.

Comparison of the Poleward Transport of Ozone in the Northern and Southern Hemispheres

by

Marvin A. Geller and Mao-Fou Wu
Laboratory for Atmospheres
NASA Goddard Space Flight Center
Greenbelt, Maryland 20771
and
Eric R. Nash
Applied Research Corporation
Landover, Maryland 20785

ABSTRACT

Six and one-half years of NOAA/NMC gridded SBUV ozone data and temperature data are used to extend Geller et al.'s (1988) study comparing the transport of ozone to high latitudes in the Northern and Southern Hemispheres. In this earlier study, it was pointed out that the poleward transport of ozone varies annually in the Northern Hemisphere but has a marked semiannual behavior in the Southern Hemisphere. This earlier study covered the period from December 1978 to November 1982. Two and one-half additional years have now been analyzed so that the analysis now extends to July 1986. With this extended data set, the maximum rate of

increase in total ozone is seen to occur in January in the Northern Hemisphere for all of the years investigated. In the Southern Hemisphere, the maximum rate of increase is seen in September for almost all of the years with a secondary maximum in the rate of increase in total ozone often being seen during the March-April period. The nature of the seasonal variation in total ozone is found to be much more variable in the Southern hemishere than in the Northern Hemisphere.

Wave number one dominates the planetary wave contributions to the poleward transport of ozone in both hemispheres. The amplitude of planetary wave number one also is seen to undergo an annual variation in the Northern Hemisphere and a semiannual variation in the Southern Hemisphere as opposed to wave number two which shows more of an annual variation in both hemispheres.

The computed poleward ozone transports will be shown for this six and one-half year period to see the relation between it and the rate of change of ozone at high latitudes on daily, seasonal, and year-to-year time scales.

REFERENCES

Geller, M. A., M.-F. Wu, and E. R. Nash, 1988: Satellite data analysis of ozone differences in the Northern and Southern Hemispheres. To appear in Pure Appl. Geophys.

Radiative Aspects of Antarctic Ozone Hole in 1985

H.Akiyoshi, M.Fujiwara and M.Uryu

Department of Physics, Faculty of Science,
Kyushu University, Fukuoka 812, Japan

In order to investigate the radiative heating effects of aerosols during September-October,1985, at Antarctica, we have solved the radiative transfer equation using one dimensional model, which includes the absorption of solar energy by water vapor, carbon dioxide, ozone and aerosols, the thermal emission and absorption by the above species and in addition, Rayleigh and Mie scattering, and the surface scattering effects. In this calculation, we have used data of ozone density, water vapor density and aerosol extinction at 0.385, 0.453, 0.525 and 1.02μm in the stratosphere obtained by SAGE II satellite and meteorological data from NOAA. The SAGE II data have been supplied by Dr.McCormick, NASA LRC.

Our results show that the Antarctic stratosphere is nearly in radiative equilibrium during that period, if the effects of aerosols are excluded (Figure 1). It is also shown that the heating effects of aerosols are too small to cause effective upward motions, in spite that some ambiguous parameters such as aerosol composition, the size distribution and so on are chosen so that they magnify the effects (Figure 2). As to the parameter dependences of our results will be also discussed.

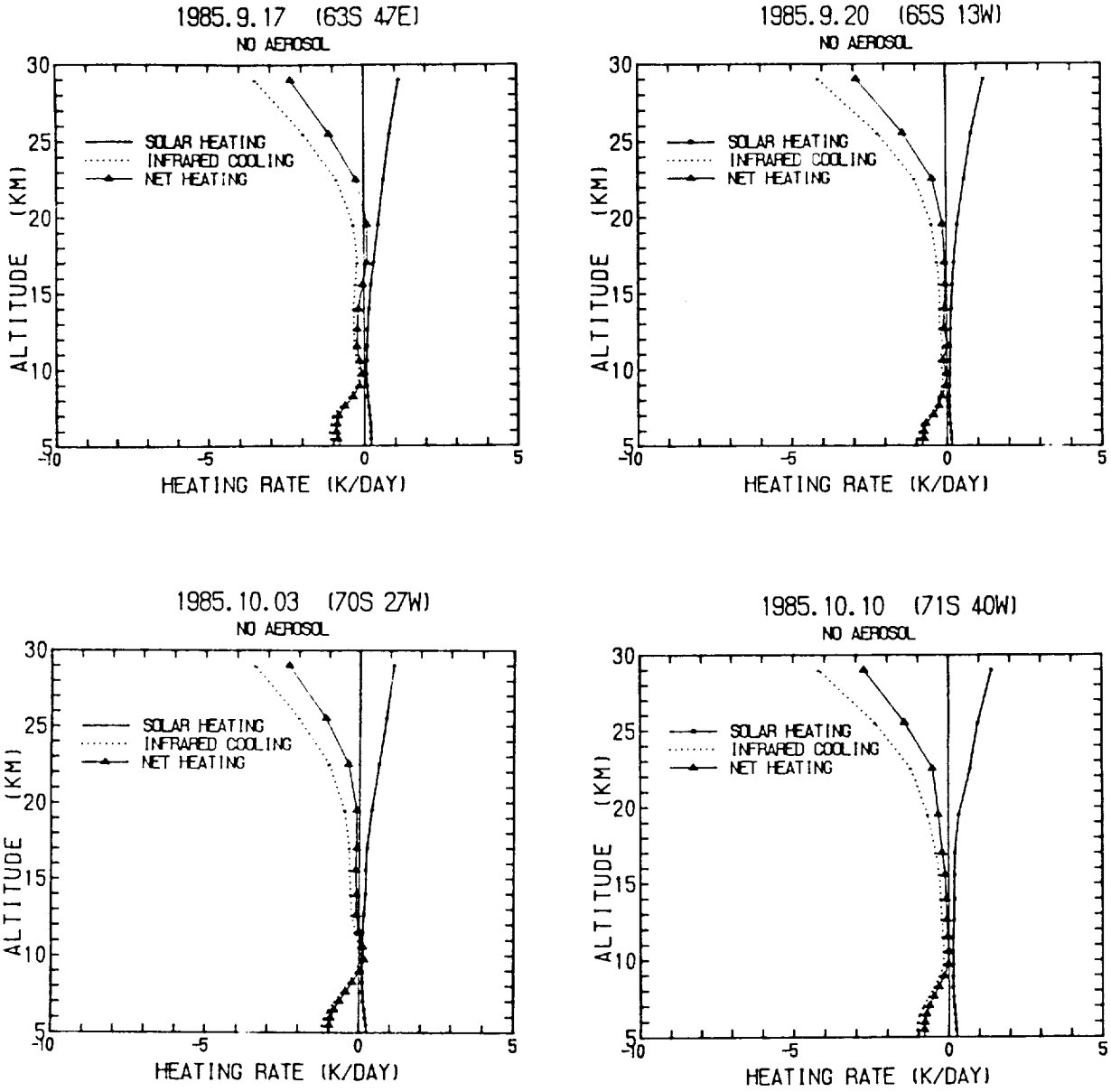

Figure 1

Day average heating rate without aerosols. Solid line, dotted line and triangle show solar heating thermal cooling and net heating, respectively.

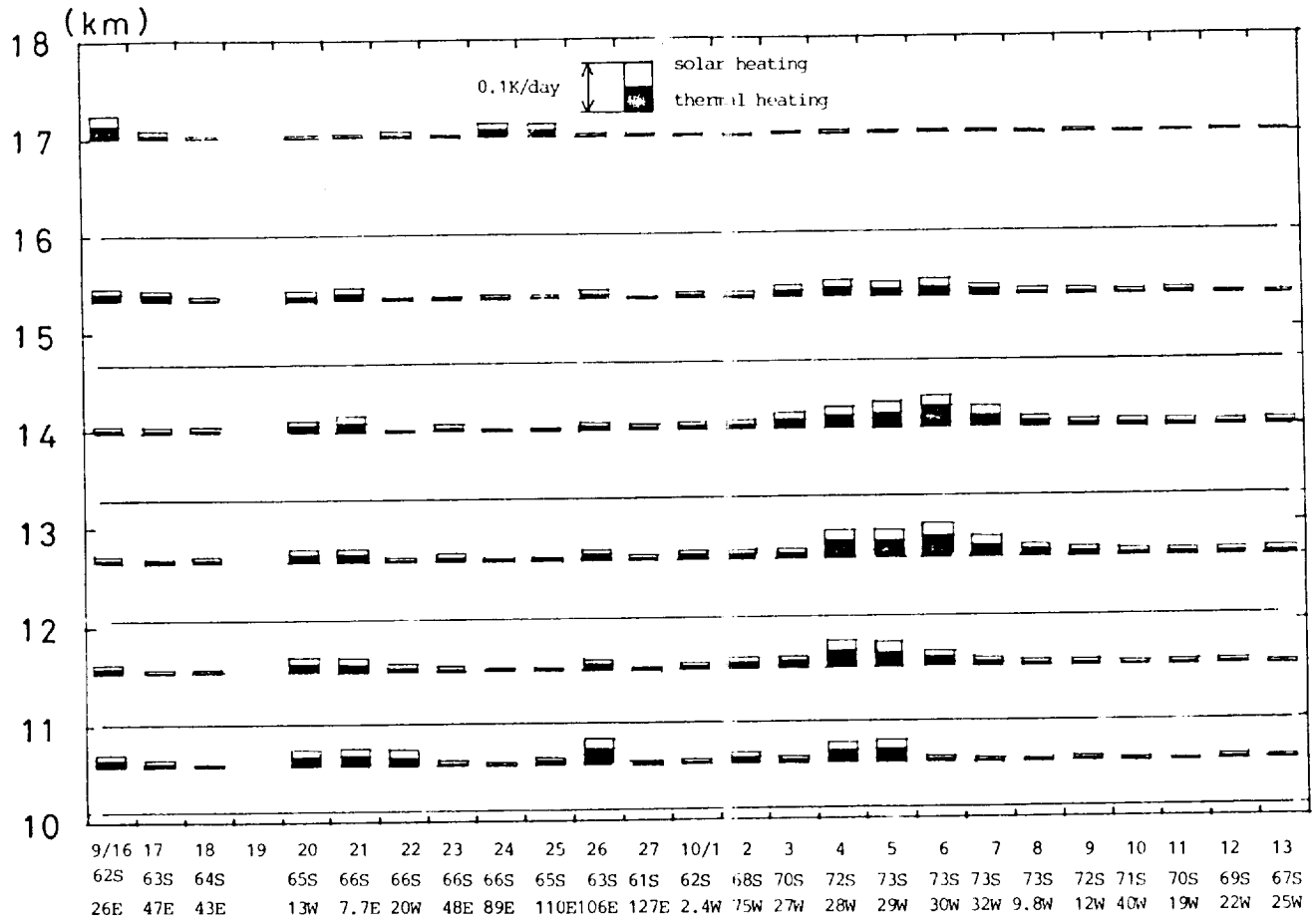

Figure 2

Additional heating rate due to aerosols, i.e., (heating rate including radiative effects of aerosols) minus (heating rate without them). The heating rate due to the absorption of solar energy is shown by white, and the thermal heating is shown by black. Aerosols can heat the atmosphere even in thermal spectrum region, because of the low ambient temperature in this height range. Dates, latitudes and longitudes of the data used in this calculation are indicated in abscissa. The size of heating, 0.1 K/day, is also shown.

22 February 1988

On the origin of steep edges and filaments in vorticity and potential vorticity fields.

D.G. Dritschel (DAMTP, Silver St., Cambridge, CB3 9EW, England)

High-resolution numerical calculations are shown which capture the fundamental process responsible for the intensification of vorticity gradients in an isolated vortex subject to externally imposed disturbances. Imposition of almost any weak strain or shear field--we concentrate of "large-scale" fields having no spatial scale selectivity--succeeds in stripping away the relatively weak vorticity at the edge of the vortex and leaves it with gradients four to six orders of magnitude greater than in the initial state. Calculations displaying such enormous gradients have never been reported previously, because of the artificial eddy diffusivities that always limit such gradients in standard numerical models. The present calculations, which have no such limitations, have been made possible by the development of a novel and robust new numerical technique for vortex dynamics called "contour surgery".

High-resolution dynamical modelling of the Antarctic stratospheric vortex.

P.H. Haynes (AMTP, Silver St., Cambridge, CB3 9EW, England)

Progress is reported on the high-resolution three-dimensional numerical simulation of flows characteristic of the Antarctic wintertime stratosphere. The numerical model is a modified version of the Reading University sigma-coordinate spectral model, used previously for tropospheric studies. Physical parametrizations are kept to a minimum in order to concentrate as much computing power as possible on simulating details of the dynamical processes. The major question addressed is whether the features observed in recent high-resolution two-dimensional simulations - namely (i) the formation of a sharp edge to the vortex (seen in the potential vorticity field), (ii) the survival of the polar vortex in a material entity, and (iii) the formation of small-scale eddies rough the break-up of tongues of high potential vorticity drawn out from the polar vortex - are realised in three-dimensional simulations.

S92-75
15166

N89-14595

Simultation of the Transport of Halogen Species from the Equatorial and Mid-Latitude Stratosphere to the Polar Stratosphere in a Two-Dimensional Model

Yuk L. Yung, R.L. Shia*, M. Allen**, R.W. Zurek**, D. Crisp**, and J.S. Wen** (*California Institute of Technology, Pasadena, CA 91125; **Jet Propulsion Laboratory, 4800 Oak Grove Drive, Pasadena, CA 91109)*

The bulk of O_3 destruction in the Antarctic stratosphere takes place in the lower stratosphere between 15 and 25 km. Both O_3 and the halogen reservoir species have their origins in the higher altitude region (20-30 km) in the equatorial and mid-latitude stratosphere. Using the Caltech-JPL two-dimensional residual circulation model, we investigate the growth of stratospheric halogen due to the increase of $CFCl_3$ and CF_2Cl_2.

The model has 18 latitudes (pole to pole) and 40 vertical layers (0 to 80 km). It was run from 1972 to 1988, with $CFCl_3$ and CF_2Cl_2 specified at the lower boundary

$$F_{11}(t) = 96.5 + 9.0 \times t \quad ,$$
$$F_{12}(t) = 162.7 + 15.3 \times t \quad ,$$

where the mixing ratio is given in pptv and t is in years since 1972.

Preliminary conclusions are:

(a) Between 1976 and 1987 the column abundance of HF at 45 N increased by 6 x 10^{14}cm^{-2} (see Fig. 1a) compared with an observed increase of 4 x 10^{14}cm^{-2} (Zander *et al.*, 1987a).

(b) In the same period the column abundance of HCl at 45°N increased by 9 x 10^{14}cm^{-2} (See Fig. 1c), compared with an observed increase of 7 x 10^{14}cm^{-2} (Zander *et al.*, 1987b; Farmer, 1988 private communication).

(c) The corresponding increases in HF and HCl at 85 S are 1.4 x 10^{15} and 1.7 x 10^{15} cm^{-2} respectively.

(d) The increase of free fluorine (F_x) and free chlorine (Cl_x) occurs above 25 km at midlatitudes, but occurs much deeper in the atmosphere at 85 S. (see Fig. 2).

References:

Zander, R., G. Roland, L. Delbouille, A. Sauval, C.B. Farmer and R.H. Norton, 1987a. Monitoring of the integrated column of hydrogen fluoride above Jungfraujoch Station since 1977 - the HF/HCl column ratio. *J. Atmos. Chem.* 5, 385-394.

Zander, R., G. Roland, L. Delbouille, A. Sauval, C.B. Farmer and R.H. Norton, 1987b. Column abundance and the long-term trend of hydrogen chloride (HCl) above the Jungfraujoch Station. *J. Atmos. Chem.* 5, 395-404.

Figure Caption:

Fig. 1a. Column abundance of HF at 45 N due to increase of $CFCl_3$ and CF_2Cl_2 in the atmosphere.
Fig. 1b. Same as Fig. 1a, for 85 S.
Fig. 1c,d. Same as Fig. 1a,b for HCl.
Fig. 2a. Vertical profile of F_x at 45 N and 85 S in Jan 1987 derived from $CFCl_3$ and CF_2Cl_2.
Fig. 2b. Same as Fig. 2a, for October 1987.
Fig. 2c, d. Same as Fig 2a,b for Cl_x.

a
45 N.
COL. DEN. OF HF(10^{15}/CM^2)
YEAR
b
45 N.
COL. DEN. OF HCL(10^{15}/CM^2)
YEAR
c
85 S.
COL. DEN. OF HF(10^{15}/CM^2)
YEAR
d
85 S.
COL. DEN. OF HCL(10^{15}/CM^2)
YEAR

Fig. 1

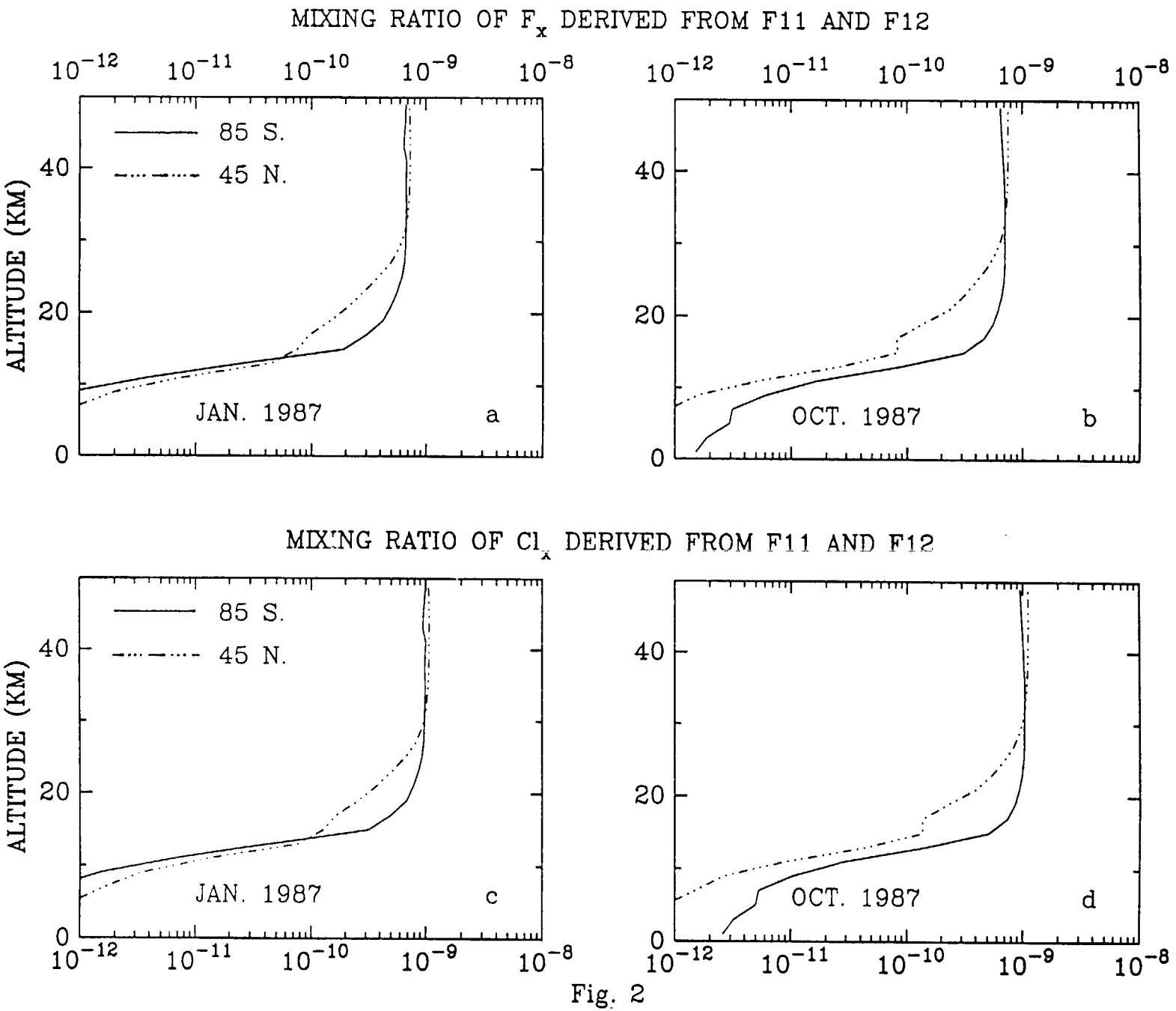
MIXING RATIO OF F_x DERIVED FROM F11 AND F12
10^{-12} 10^{-11} 10^{-10} 10^{-9} 10^{-8}
85 S.
45 N.
ALTITUDE (KM)
0
20
40
JAN. 1987
a
OCT. 1987
b
MIXING RATIO OF Cl_x DERIVED FROM F11 AND F12
c
d

Fig. 2

A Two Dimensional Model of the Quasi Biennial Oscillation of Ozone

L.J.Gray, Rutherford Appleton Laboratory, Chilton, Didcot, Oxon., U.K.,
J.A.Pyle, Physical Chemistry Department, Cambridge University, Cambridge U.K.

ABSTRACT. The largest amplitudes of the observed Quasi Biennial Oscillation (QBO) in column ozone are found in high latitudes and this must be taken into account in any explanation of the increased depletion of ozone in the southern polar spring during the 1980's. A QBO in zonal wind, temperature and column ozone has been successfully modelled in a two dimensional dynamical/chemical model by the introduction of a parametrization scheme to model the transfer of momentum to the zonal flow associated with the damping of vertically propagating Kelvin and Rossby-Gravity waves. The largest anomalies in column ozone of approximately 20 DU are present at high latitudes. The equatorial ozone QBO is out of phase with the mid- and high latitude ozone QBO, in good agreement with observations.

1 Introduction

The presence of a quasi-biennial oscillation (QBO) in zonal winds, temperature and column ozone in the equatorial stratosphere is well known (Reed 1960, Veryand and Ebdon 1961, Wallace 1973, Angell and Korshover 1978, Coy 1979, Tolson 1981, Hasebe 1983, Naujokat 1986). The largest amplitudes of the ozone QBO, however, are found in high latitudes and this must be allowed for in any explanation of the increasing depletion of ozone in the southern polar spring during the 1980's (Bojkov 1986, Garcia and Solomon 1987). We describe a simulation of the QBO in a two-dimensional model which extends from pole to pole and includes a comprehensive photochemical scheme. We are therefore able to investigate the effects of the equatorial QBO on the extra-tropical dynamics of the model and the relationship between the dynamical QBO and the distribution of ozone.

2 The Model

The two-dimensional model of Harwood and Pyle (1975,1977,1980) was employed in the study. The model configuration is essentially the same as that employed by Gray and Pyle (1987a), hereafter referred to as GP, except that the improved 'wide-band' radiation scheme developed by Haigh (1984) has been used. This has resulted in a much deeper and stronger Hadley circulation in the equatorial lower stratosphere. (Note that, in this respect the present model differs from that described by Gray and Pyle 1987b). The parametrization scheme to model the Semi-Annual Oscillation (SAO) developed in GP was retained in the present runs but the gravity wave breaking parametrization was omitted.

The zonal wind QBO has been modelled by including the momentum deposition associated with thermally dissipating Kelvin and Rossby-Gravity waves. A WKB approximation is used to derive an expression for the mean flow acceleration: $\frac{d\bar{u}}{dt} = Aexp(\frac{z-z_0}{H})R(z)exp(-P(z))$ where $R(z) = \frac{\alpha(z)N}{k(\bar{u}-c)^2}$ and $P(z) = \int_{z_0}^{z} R(z')dz'$ (Lindzen and Holton 1968). A is the vertical momentum flux at z_0 (=16 km), $\alpha(z)$ is the thermal damping rate, N is the Brunt-Vaisala frequency and k is the zonal wavenumber. The equation was solved with parameter values appropriate to the Kelvin and Rossby-Gravity waves shown in the table below. Note that two Kelvin waves were forced which were identical apart from their phase speeds. The mean flow acceleration associated with the faster phase speed c=60 ms^{-1} occurs at higher levels in the modelled atmosphere and gives rise to the westerly phase of the SAO. The damping of the waves has been restricted to thermal damping, as in the SAO parametrization of GP; above 30 km the damping rate $\alpha(z)$ was chosen to be the 'slow' damping rate of Dunkerton (1979) which peaks at approximately $2x10^{-6}$ s^{-1} at 50 km; below this level a constant value of $0.35x10^{-6}$ s^{-1} was specified. Although no mechanical damping was explicitly employed in the QBO parametrization scheme, the model includes a vertical diffusion operating on the model wind fields with a constant value of k_{zz} = 1.0

m^2s^{-1} at all latitudes and heights. A gaussian distribution about the equator was applied to the forcing associated with the two types of waves, with an e-folding width $Y_L = (\frac{2\nu}{k\beta})^{\frac{1}{2}}$ for the Kelvin waves and $Y_L = (\frac{2\nu}{\beta(\frac{\rho}{\nu}-k)})^{\frac{1}{2}}$ for the Rossby-Gravity waves where $\frac{\rho}{\nu} = c$ (Holton 1975). All other symbols have their usual meaning and an overbar denotes a zonal average. The parametrized forcing associated with the Kelvin and the Rossy-Gravity waves were both present at all times of the modelled year.

	Kelvin Wave		Rossby-Gravity Wave
Zonal wavenumber	1		4
phase speed (ms^{-1})	+25	+60	-25
A, amplitude of vertical momentum flux at z_0 (m^2s^{-1})	2.5 x 10^{-3}	3.5 x 10^{-3}	15.0 x 10^{-3}

3 The QBO in Zonal Wind

The time-height section of the zonal wind at the equator from a model run that included both the QBO and SAO parametrizations is shown in figure 1. Four periods of the QBO are evident. The semi-annual oscillation is dominant above 35 km and the QBO is the dominant signal between 10 and 30 km, in good agreement with observational data. Both phases of the QBO exhibit a gradual descent with time (at an average rate of just over 1 km per month); the amplitude of the modelled QBO is a maximum at approximately 25 km where the winds vary between 20 ms^{-1} and -18 ms^{-1}. Thermal wind balance is maintained against thermal dissipation in the model by the development of a meridional circulation with adiabatic heating (cooling) in the cold (warm) region associated with upward (downward) motion (Reed 1964, Plumb and Bell 1982). Therefore, the direction of the induced circulation depends upon the phase of the QBO. During a westerly (easterly) phase descending (ascending) motion is present at the equator, just below the level of maximum wind shear, with rising (sinking) motion at mid-latitudes. The direct forcing of the zonal wind in the model due to the damping of vertically propagating equatorial waves is restricted to latitudes less than about 20 degrees from the equator; however, changes to the modelled atmosphere, particularly in the amount of the ozone column, occur further poleward of this as a result of the induced meridional circulation.

4 The QBO in Ozone

Observations of large ozone reductions in high southern latitudes during Spring (Farman et al., 1985) make the understanding of the latitudinal variation of the ozone QBO particularly important. Garcia and Solomon (1987), for example, have speculated that the QBO is relevant to the understanding of the temporal variation of the springtime column ozone in southern polar latitudes during the 1980's.

The photochemical time constant of ozone decreases with increasing altitude and generally, at any given height, with decreasing latitude. With a lifetime of hours in the upper stratosphere ozone is expected to be close to its steady state value. On the other hand, the ozone concentration in the polar lower stratosphere can be far from its equilibrium value since the photochemical time scale is long in that region and dynamics exerts a major influence. Between these two regions is a portion of the atmosphere where dynamical and photochemical time scales are roughly comparable. It is the morphology of this transition region that defines the ozone budget and distribution. The strength of the lower stratosphere circulation is a crucial parameter in a successful model simulation of the ozone distribution.

Figure 2 shows the time-series of ozone anomaly from the model run (the monthly mean has been subtracted from each point). A prominent QBO signal is present at all latitudes. The largest anomaly is in high latitudes, reaching 20 Dobson Units in some cases. A phase reversal is present at approximately 20 degrees latitude so that high latitude anomalies are out of phase with the equatorial anomalies. There is no evidence for in-situ photochemical control of the high latitude ozone anomaly. This is not suprising given that the photochemical constant of ozone is long there. None of the radicals involved in ozone photochemistry, including OH, HO_2, NO and NO_2, show significant biennial variations in high latitudes.

The overall behaviour of the modelled ozone QBO compares favourably with the zonally averaged observations of the QBO derived by Hasebe (1983) using SBUV data. In agreement with observations the positive ozone anomalies occur at approximately the same time as the westerly phase of the equatorial zonal wind QBO at 50 mb (see figure 2).

The modelled QBO in column ozone arises as a result of the interaction of dynamics and photochemistry in the following sequence of events. The equatorial zonal wind QBO give rise to a rising and sinking motion at the equator as already described. Hence, during a westerly phase the strength of the equatorial ascent of the Hadley cell is reduced and during an easterly phase it is enhanced. During an easterly phase the enhanced upward motion lowers the ozone column by reducing the lower stratosphere mixing ratios, since the mixing ratio profile increases with altitude; conversely, during a westerly phase downward motion increases the ozone column by advecting higher mixing ratios into a region where the photochemical lifetime is long. Thus during a westerly (easterly) phase a positive (negative) equatorial ozone anomaly will result.

The induced circulation is also responsible for the high latitude QBO in ozone. During a westerly phase of the QBO the induced downward motion at the equator implies an upward motion in the subtropics which opposes the Hadley circulation. The latitudinal extent of the induced circulation is restricted to the subtropics, however (Plumb 1982), so that it cannot directly transfer an ozone anomaly to high latitudes. Nevertheless, the descending arm of the Hadley cell extends to mid-latitudes and crosses the transition region from photochemical to dynamical control of the ozone distribution. Hence, for example, a suppression of the strength of the Hadley circulation during a westerly phase of the QBO results in a negative anomaly in mid-latitudes (not just in the subtropics). The ozone anomaly is then transferred further poleward by eddy motions (this is opposed by the mean motion and hence the distribution of ozone at high latitudes is determined by the balance between eddy and mean motion - see for example, Harwood and Pyle (1977) and Haigh (1984)).

The high latitude column ozone anomaly maxima in the two hemispheres of the run are displaced by several months; they tend to occur in spring/early summer and coincide with the column ozone maxima. This compares well with observations and arises in the model because the phase of the modelled QBO in column ozone tends to reverse during April/May of each year. Because of the direction of the mean circulation in the following months the ozone anomaly is immediately evident in the southern hemisphere mid-latitudes and this is then transferred to higher latitudes via eddy transfer (which is strongest in winter months). The corresponding anomaly maximum does not occur in the northern hemisphere until six months later when the direction of the mean circulation has reversed in direction.

References

Angell, J.K. and J. Korshover, 1978. Mon. Weather Rev., 106, 725.
Bojkov, R.D., 1986. Geophys. Res. Lett., 13, 1236.
Coy, L. 1979, J. Atmos. Sci., 35, 174.
Farman, J.C., B.G. Gardiner, and J.D. Shanklin, 1985. Nature, 315, 207.
Garcia, R.R. and S.Solomon, 1987. Geophys. Res. Lett, 14, 848.
Gray, L.J. and J.A. Pyle, 1987a. Quart. J. Roy. Met. Soc., 113, 635.
Gray, L.J. and J.A. Pyle, 1987b. in Transport Processes in the Middle Atmosphere, eds G. Visconti and R.Garcia, p.b. Reidel.
Haigh, J.D., 1984. Quart. J. Roy. Met. Soc.,110, 167.
Harwood, R.S. and J.A. Pyle, 1975. Quart. J. Roy. Met. Soc., 101, 723.
Harwood, R.S. and J.A. Pyle, 1977. Quart. J. Roy. Met. Soc., 103, 319.
Harwood, R.S. and J.A. Pyle, 1980. Quart. J. Roy. Met. Soc., 106, 395.
Hasebe, F., 1983. J. Geophys. Res., 88, 6819.
Holton, J.R. 1972. An Introduction to Dynamic Meteorology. pb Academic Press.
Lindzen, R.S. and J.R. Holton 1968. J. Atmos. Sci., 30, 513.
Naujokat, B. 1986. J. Atmos. Sci., 43, 1873.
Plumb, R.A. 1982. J. Atmos. Sci., 39, 983.
Plumb, R.A. and R.C. Bell, 1982. Quart. J. Roy. Met. Soc., 108, 313.
Reed, R.J. 1960. Paper presented at the 40th anniversary meeting of the Amer. Met. Soc. Boston.
Reed, R.J. 1964. Quart. J. Roy. Met. Soc., 90, 441.
Tolson, R.H. 1981. J. Geophys. Res., 86, 7312.
Veryand, R.G. and Ebdon, R.A. 1961. Meteor. Mag., 90, 125.
Wallace, J.M. 1973. Rev. Geophys. Space Phys., 11, 191.

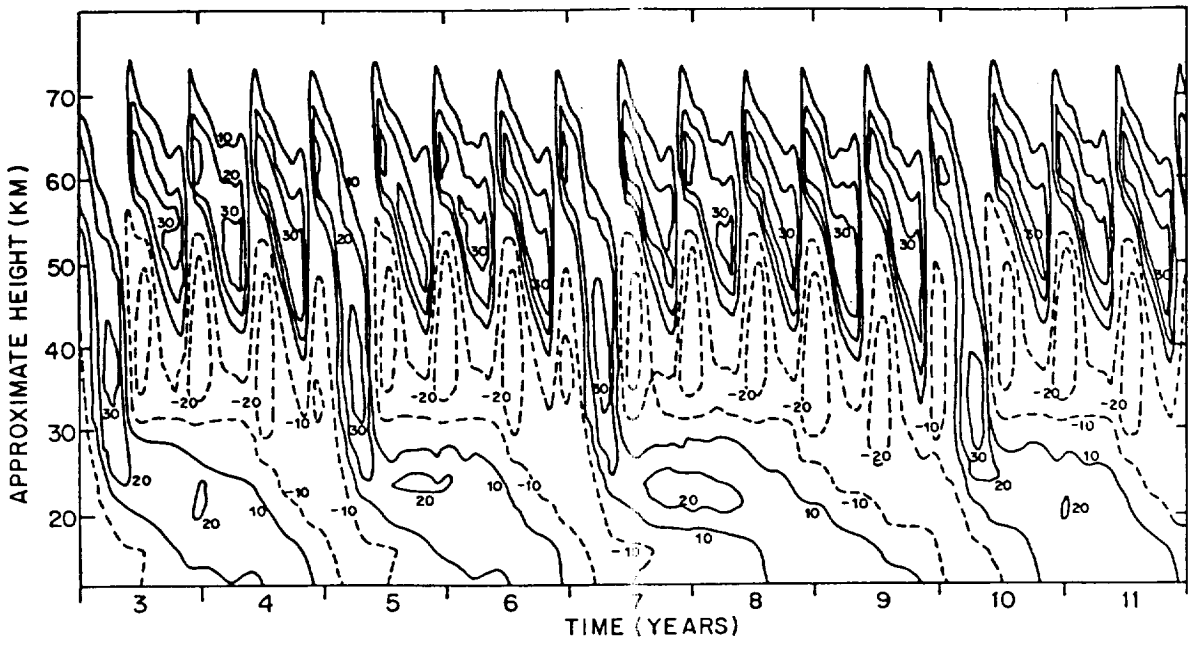

Figure 1: Time-height section of zonal winds (ms^{-1}) at the equator

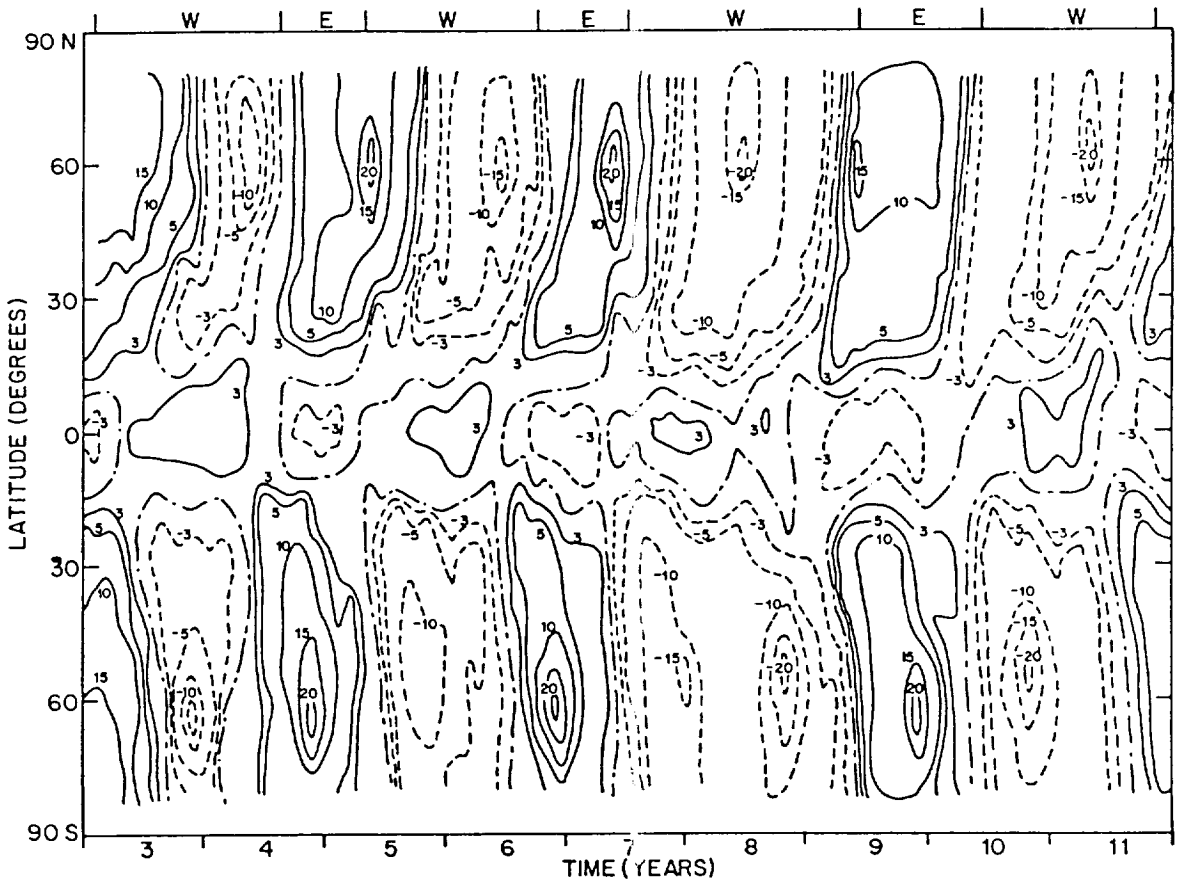

Figure 2: Latitude-time section of column ozone anomaly (Dobson Units). The monthly mean has been subtracted from each point. The direction of the equatorial wind at 50mb is also indicated.

Use of operational analyses to study the dynamics of troposphere-stratosphere interactions in polar regions

David A. Salstein and Richard D. Rosen
Atmospheric and Environmental Research, Inc., Cambridge, MA 02139

Alvin J. Miller
NOAA/NWS/Climate Analysis Center, Washington, DC 20233

1. Introduction

Operational analyses produced by large weather centers have been used in the past to monitor various aspects of the general circulation as well as address dynamical questions. Concerns about the problems with these analysis fields in the high southern latitudes have been expressed (Trenberth and Olson, 1988), however, so that calculations of dynamic processes with such fields might be compromised.

For a number of years we have been monitoring National Meteorological Center (NMC) analyses at 100 millibars because it is the level from which stratospheric analyses are built. In particular, we have closely examined the pressure-work term at that level which is an important parameter related to the forcing of the stratosphere by the troposphere. Rapid fluctuations typically seen in this quantity during the months of July-November, and similarly noted by Randel et al. (1987) may raise some concern about the quality of the analyses. We have investigated the behavior of the term mainly responsible for these variations, namely the eddy flux of heat, and furthermore have corroborated the presence of these variations in contemporaneous analyses produced by the European Centre for Medium Range Forecasts (ECMWF).

2. Evaluation of the pressure-work and eddy heat flux terms with operational analyses

The vertical transfer of eddy kinetics energy across a level in the atmosphere by means of boundary stresses $[\omega^* z^*]$, where ω is vertical velocity, z geopotential, brackets zonal mean and asterisk departure therefrom, can be written after a number of assumptions including the geostrophic approximation, as follows (Miller and Johnson, 1970):

$$[\omega^* z^*] \approx \frac{f}{g} (\partial[\theta]/\partial p)^{-1} \cdot [u] \cdot [v^* \theta^*] \qquad (1)$$

In this term, closely related to one component of the Eliassen-Palm (1960) flux, θ is potential temperature, u and v zonal and meridional wind, p pressure, f Coriolis parameter and g acceleration of gravity. The daily integrals of $[\omega^* z^*]$ at 100 mb between 20° and 90°S, calculated from NMC global analyses for 1986, which are similar in character to earlier years, are displayed in Figure 1. The presence of large fluctuations, peaking in the June-November period, raise the possibility that there were considerable problems with the analyses.

Of the multipliers on the right side of (1) we have isolated the erratic behavior in $[\omega^* z^*]$ to the eddy heat flux term, $[v^* \theta^*]$ in the vicinity of 55°-70°S, which can be seen in the time-latitude display in Figure 2. During this part of the year $[v^* \theta^*]$ is rather quiescent at most other latitudes. Similar displays of the zonal mean zonal winds [u] and the stability parameter $\partial[\theta]/\partial p$ reveal fairly steady behavior, incapable of producing the fluctuations in Figure 1.

As one means of checking the accuracy of the $[v^* \theta^*]$ variations, we acquired grid-point analyses from the ECMWF, and evaluated the same heat flux term at 5° latitude intervals in this region. The comparison of the NMC- and ECMWF-derived

parameters is displayed in Figure 3. For the months of July-November 1986, there is good agreement of the heat flux parameters from the two centers, offering a measure of confidence in the reality of these fluctuations. Although most of the raw data going into each center's assimilation are identical, there are substantial differences in the analysis and forecast components of the two centers. Therefore such strong agreement between the two analyses would be unlikely if the NMC heat fluxes were simply erroneous. Indeed the agreement between NMC and ECMWF fields in the high southern latitudes, at least for zonal winds, has been improving in recent years (Rosen et al. 1987).

3. Vertical and longitudinal structure of eddy heat fluxes

We have evaluated the $[v^*\theta^*]$ term at other pressure levels to examine the vertical structure of this quantity in high latitudes. Plots of this quantity (not shown) reveal that the fluctuations exist at the 50-mb level and they are present down into the troposphere as low as the 300-mb level, however, decreasing in amplitude with decreasing altitude.

We used the ECMWF analyses to investigate the longitudinal structure of the eddy heat fluxes, $v^*\theta^*$. Eastward propogating features are clearly evident, as is shown, for example, in Figure 4 for 65°S. Here, we observe that, for example, between September and November, anomalies in this heat flux travel eastward, at a rate of approximately 5-10 ms^{-1}. No particular longitudinal origin of these fluctuations is apparent, indicating that these features do not result from erroneous observations at fixed sites.

4. Conclusions

We have demonstrated that fluctuations in standing eddy heat fluxes, related to the forcing of the stratosphere by the troposphere, agree in two largely independent meteorological analyses. We believe, therefore, that these fluctuations are mostly real. Further work must be performed to determine the dynamical causes and consequences of these fluctuations, of course, but for now it is reassuring at least to find that the data sets available to pursue such work are appropriate for this purpose.

5. Acknowledgments

We thank T.M. Wood of AER for ably performing all the programming tasks. The work at AER was supported by NOAA under contract number 50-DGNW-7-00101.

6. References

Eliassen, A. and E. Palm, 1960: On the transfer of energy in stationary mountain waves. Geof. Publ. Geoph. Norv., 22, 1-23.

Miller, A.J. and K.W. Johnson, 1970: On the interaction between the stratosphere and troposphere during the warming of December 1967-January 1968. Quart. J. R. Met. Soc., 96, 24-31.

Randel, W.J., D.E. Stevens, and John L. Stanford, 1987: A study of planetary waves in the southern winter troposphere and stratosphere. Part II: Life cycles. J. Atmos. Sci., 44, 936-949.

Rosen, R.D., D.A. Salstein, A.J. Miller and K. Arpe, 1987: Accuracy of atmospheric angular momentum estimates from operational analyses. Mon. Wea. Rev., 115, 1628-1639.

Trenberth, K.E. and J.G. Olson, 1988: Evaluation of NMC global analyses. NCAR Technical Note TN-299+STR, 82 pp.

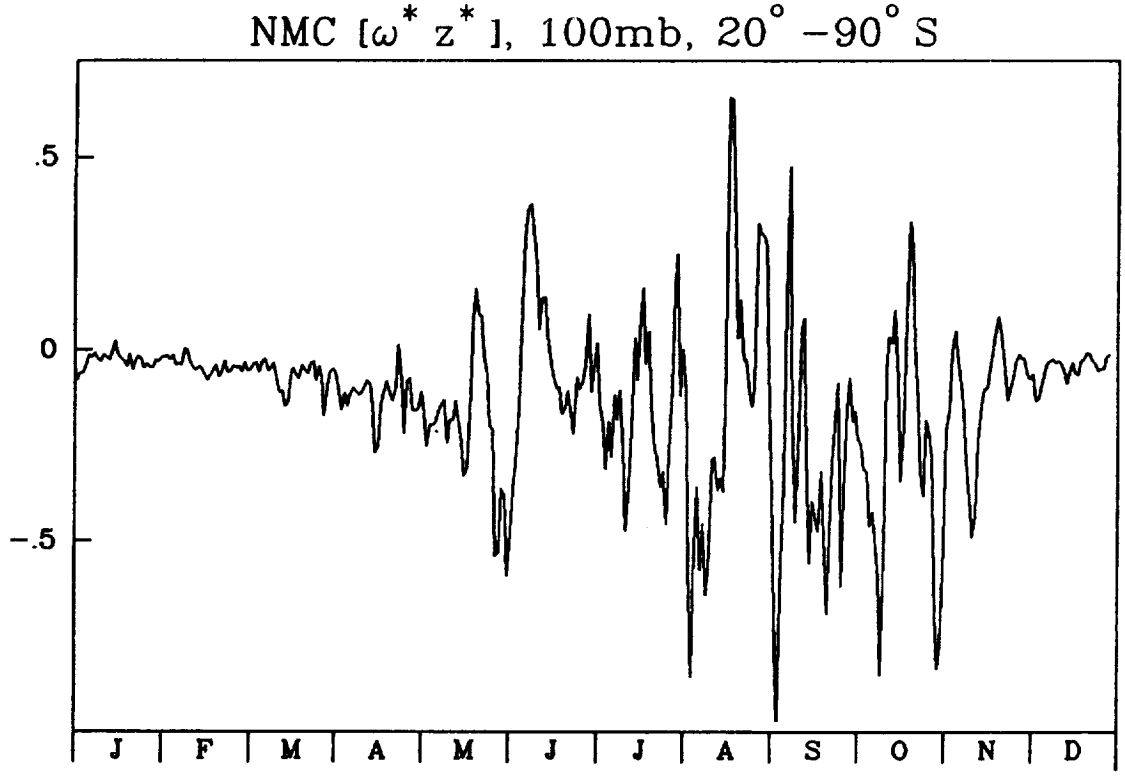

Fig. 1 Daily values of the pressure-work term from NMC analyses at 100 mb integrated between 20° and 90°S during 1986. Units are Wm^{-2}.

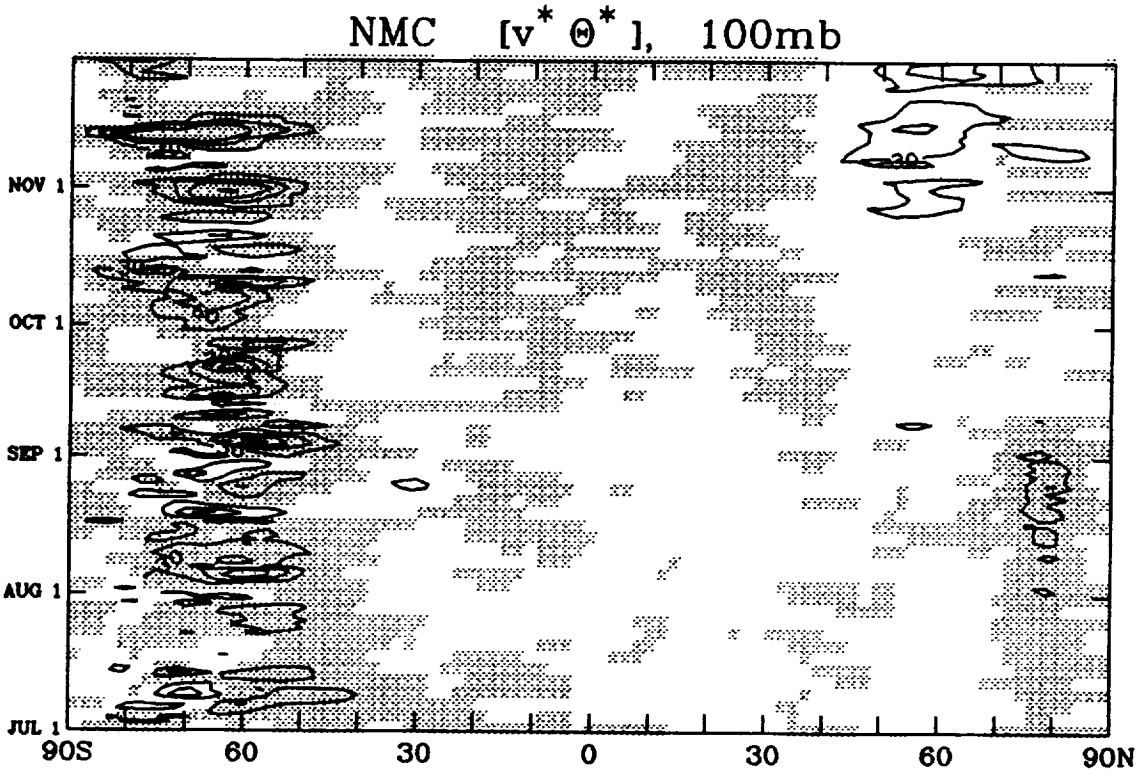

Fig. 2 Daily zonal means of eddy fluxes of heat at 100 mb from NMC analyses from pole to pole during July-November 1986. Negative values are shaded. Contours are 30 ms^{-1} °K, with 0 contours not plotted.

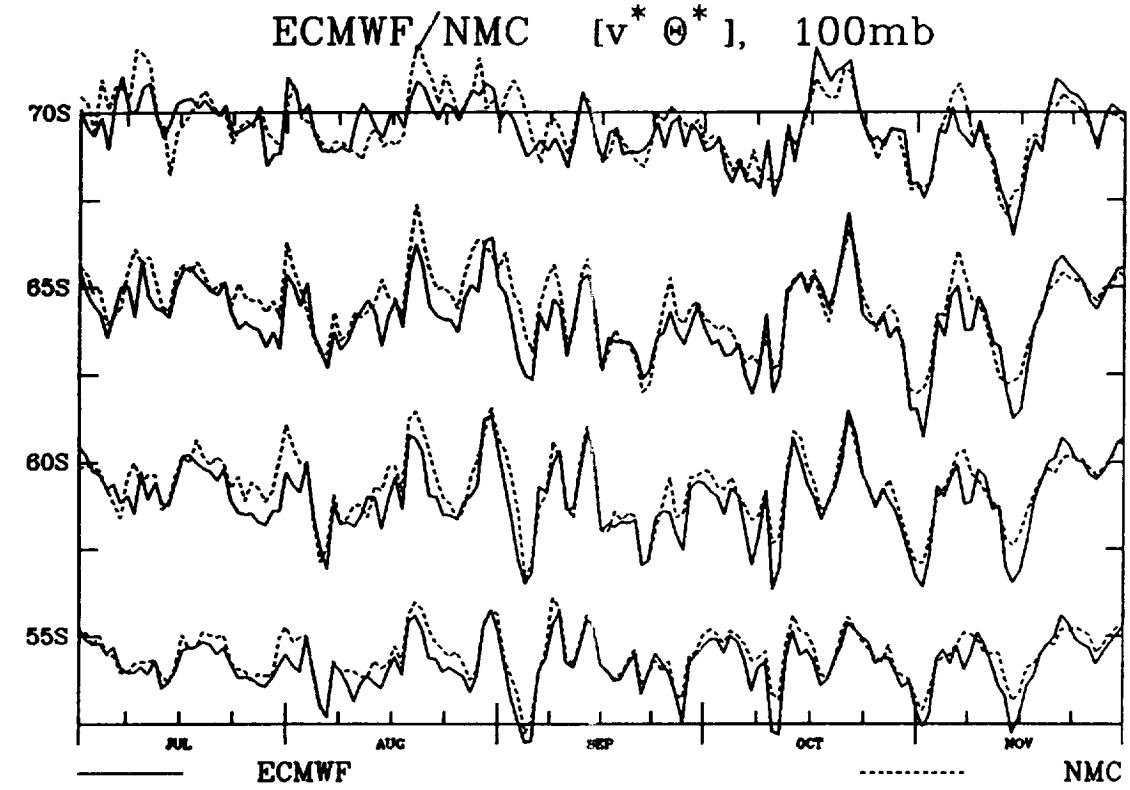

Fig. 3 Daily zonal means of eddy fluxes of heat at 100 mb from ECMWF and NMC analyses at 55°, 60°, 65° and 70°S during July-November 1986. Spacing between tick marks on the ordinate is 100 ms^{-1} °K.

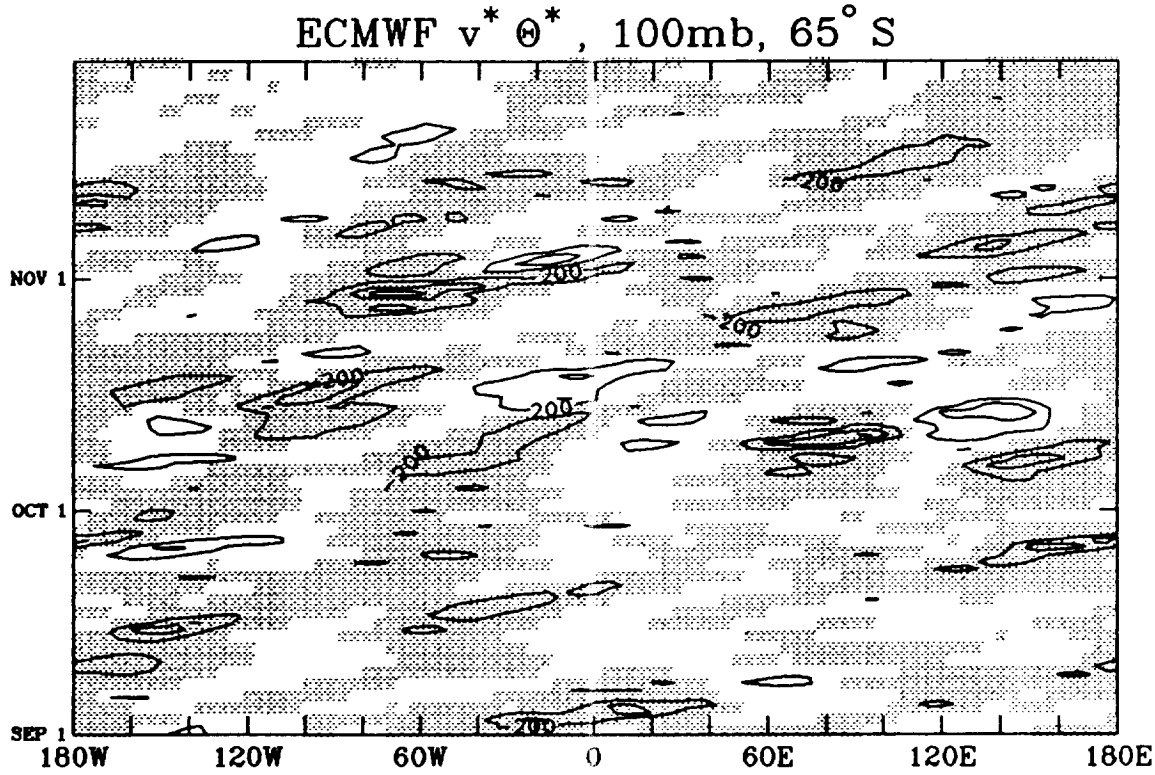

Fig. 4 Daily eddy heat fluxes at 100 mb from ECMWF analyses at 65°S every 5° in longitude during September-November 1986. Negative values are shaded. Contours are 200 ms^{-1} °K with 0 contours not plotted.

SESSION IX - Chemistry and Chemical Modeling
Presiding, M. Kurylo, National Bureau of Standards
Friday Morning, May 13, 1988

POLAR OZONE WORKSHOP
May 9-13, 1988
Snowmass in Aspen, Colorado

ABSTRACT

CHEMISTRY OF CHLORINATED SPECIES IN THE ANTARCTIC STRATOSPHERE

Mario J. Molina, Tai-Ly Tso and Frank C.-Y. Wang
Jet Propulsion Laboratory
Pasadena, California 91109

The chemistry of Cl_2O_2, the chlorine monoxide dimer, has been further investigated in order to better assess its potential role in catalytic ozone destruction cycles. The dimer has been generated in a flow system, in the 200-250K temperature range, by using ozone and chlorine atoms as ClO precursors. The Cl-atoms are produced by a microwave discharge of either Cl_2, or of F_2 with subsequent addition of HCl. With this later scheme the dimer can be generated in the absence of Cl_2.

The FTIR spectra of the products clearly indicates the presence of two isomers, in agreement with our earlier results (J. Phys. Chem., 91, 433, 1987). None of the observed IR bands can be attributed to a ClO-OClO adduct, since they all appear in the absence of any detectable amount of OClO.

The dimer decomposes readily on surfaces yielding Cl_2 and O_2 as final products, even at temperatures low enough to rule out significant dissociation back to the monomer. In our flow system these product

species are monitored by absorption spectroscopy in the vacuum ultraviolet. We are currently carrying out these experiments in the presence of water-ice surfaces, in an attempt to predict the behavior of the dimer under Antarctic stratospheric conditions.

We have also continued our studies of the physical chemistry of the $HCl-HNO_3$-water/ice system. We developed a high sensitivity technique to monitor HCl vapor in the presence of water, by optical absorption in the vacuum ultraviolet, in order to directly determine the vapor pressures and the phase diagram of the system under conditions appropriate to the Antarctic stratosphere. One of the major experimental difficulties is the preparation and characterization of a suitable homogeneous solid phase. The monohydrate of nitric acid has a relatively low affinity for HCl, but this affinity increases rapidly as the water content in the solid crystals increases.

It is likely that the particles in the polar stratospheric clouds will have a relatively dilute nitric acid outer layer, even if the core is the nitric acid monohydrate, since the particles are in equilibrium with the ambient water vapor, which is present initially at levels of a few parts per million.

ABSTRACT

POLAR OZONE WORKSHOP
May 9-13, 1988
Snowmass in Aspen, Colorado

STUDIES OF ClO AND BrO REACTIONS IMPORTANT IN THE POLAR STRATOSPHERE: KINETICS AND MECHANISM OF THE ClO + BrO AND ClO + ClO REACTIONS

Randall R. Friedl and Stanley P. Sander
Chemical Kinetics and Photochemistry Group
Jet Propulsion Laboratory
California Institute of Technology
Pasadena, California 91109

A. Introduction

The reactions,

$$BrO + ClO \rightarrow Br + ClOO \quad (1a)$$
$$\rightarrow Br + OClO \quad (1b)$$
$$\rightarrow BrCl + O_2 \quad (1c)$$

and

$$ClO + ClO \rightarrow Cl + ClOO \quad (2a)$$
$$\rightarrow Cl + OClO \quad (2b)$$
$$\rightarrow Cl_2 + O_2 \quad (2c)$$
$$\rightarrow (ClO)_2 \quad (2d)$$

have assumed new importance in explaining the unusual springtime depletion of ozone observed in the Antarctic stratosphere. The mechanisms of these reactions involve the formation of metastable intermediates which subsequently decompose through several energetically allowed product channels. The resulting pressure and temperature phenomenology is complex, providing the motivation to study these reactions using both the discharge flow - mass spectrometric and flash photolysis - ultraviolet absorption techniques. These methods have also been used to explore aspects of the kinetics and spectroscopy of the ClO dimer.

B. Mass Spectrometric Studies of ClO + BrO and $(ClO)_2$

As part of a comprehensive study of the ClO + BrO reaction, kinetic and product determinations were performed at 1 torr total pressure in a temperature controlled discharge flow apparatus. Mass spectrometric detection was employed with continuous sampling of the flow tube through a three stage beam inlet system coupled to a quadrupole mass filter using electron impact ionization.

Kinetic studies were carried out under pseudo first-order conditions in excess ClO. In order to avoid possible regeneration of BrO within the reaction zone, radical sources were employed that did not use O_3, in particular O + Br_2 (excess) → BrO and Cl(excess) + Cl_2O → ClO. Possible depletion of BrO in the reaction zone by Cl atoms, generated in the ClO source and from both ClO +

ClO and BrO + ClO, was avoided by insuring fast conversion of Cl atoms to BrCl with excess Br_2. The results of these kinetics experiments reveal that the ClO + BrO reaction, like many of the halogen monoxide self reactions, displays a negative temperature dependence as shown in Figure 1.

Product yields were determined from four distinct sets of experiments. The first set employed conditions identical to those used for kinetic determinations. Simultaneous measurements of OClO and BrO were obtained, revealing that the channel yielding OClO constitutes a significant fraction of the overall reaction. The second set of experiments also employed conditions similar to those used for kinetic runs with the exception that the O atoms were generated using isotopically labelled molecular oxygen ($^{36}O_2$). In these experiments the production of $^{34}O_2$ was monitored simultaneously with the decay of $Br^{18}O$, providing a measure of the combined yield of the Cl atom and BrCl producing channels. A third set of measurements, which employed a ClO source of Cl + OClO(excess) and which focussed on detection of BrCl, measured the same two channels as did the second set. The results of these two sets were consistent with one another and with the conclusion of the first set of experiments. Results from the third set of experiments also strongly suggested that the reaction of Br with $(ClO)_2$ rapidly forms BrCl. In the fourth set of experiments, the channel forming BrCl was isolated by the addition of large amounts of O_3 to the flow tube. In these experiments the BrCl channel constituted the only loss mechanism for BrO. The results derived from this last series of experiments have important implications for the diurnal behavior of OClO in Antarctica as well as for reinterpretation of several previous studies of ClO_x + BrO_x reactions.

During the investigation of the ClO + BrO reaction it was discovered that under certain ClO source conditions a signal could be detected at m/e 102. This peak has tentatively been assigned to the ClO dimer. A temperature controlled, high pressure source region has subsequently been interfaced to the discharge flow - mass spectrometer system. We have successfully optimized ClO dimer production in this source and are in the process of characterizing the kinetic behavior of this species in the presence of O_3, OClO, and various atomic species.

C. Flash Photolysis Studies of BrO and ClO Reactions

Reactions 1 and 2 were studied using the flash photolysis - ultraviolet absorption technique. For the study of reaction 1, BrO and ClO were produced by rapid reactions following the broad-band photolysis of Br_2 - Cl_2O mixtures. BrO and ClO were simultaneously monitored by long-path absorption. In order to avoid some of the difficulties encountered in previous studies of this reaction, ClO was produced in excess over BrO, and conditions were chosen such that the secondary regeneration of BrO was negligible. From the analysis of first-order BrO decays, rate constants for reaction 1 were obtained over the temperature range 220-400 K and pressure range 50-700 torr. The temperature dependence of the yield of OClO from reaction 1 was determined using a novel time-resolved diode array spectrometer. Calibrated ultraviolet absorption spectra for both BrO and ClO were obtained between 220 and 400 K in order to interpret the kinetic and product studies of reaction 1. For the first time, determinations were made of the rate constant temperature dependence for the reaction

$$Br + Cl_2O \rightarrow BrCl + ClO$$

and of quantum yields for the photolysis of Cl_2O, i.e.

$$Cl_2O + h\nu \rightarrow Cl + ClO \qquad \Phi_1$$
$$\rightarrow O + Cl_2 \qquad \Phi_2$$

Kinetic and spectroscopic studies of the ClO + ClO reaction were also carried out using this technique. The pressure and temperature dependences of the termolecular channel forming the ClO dimer were determined, and reaction products were studied using the gated diode-array spectrometer.

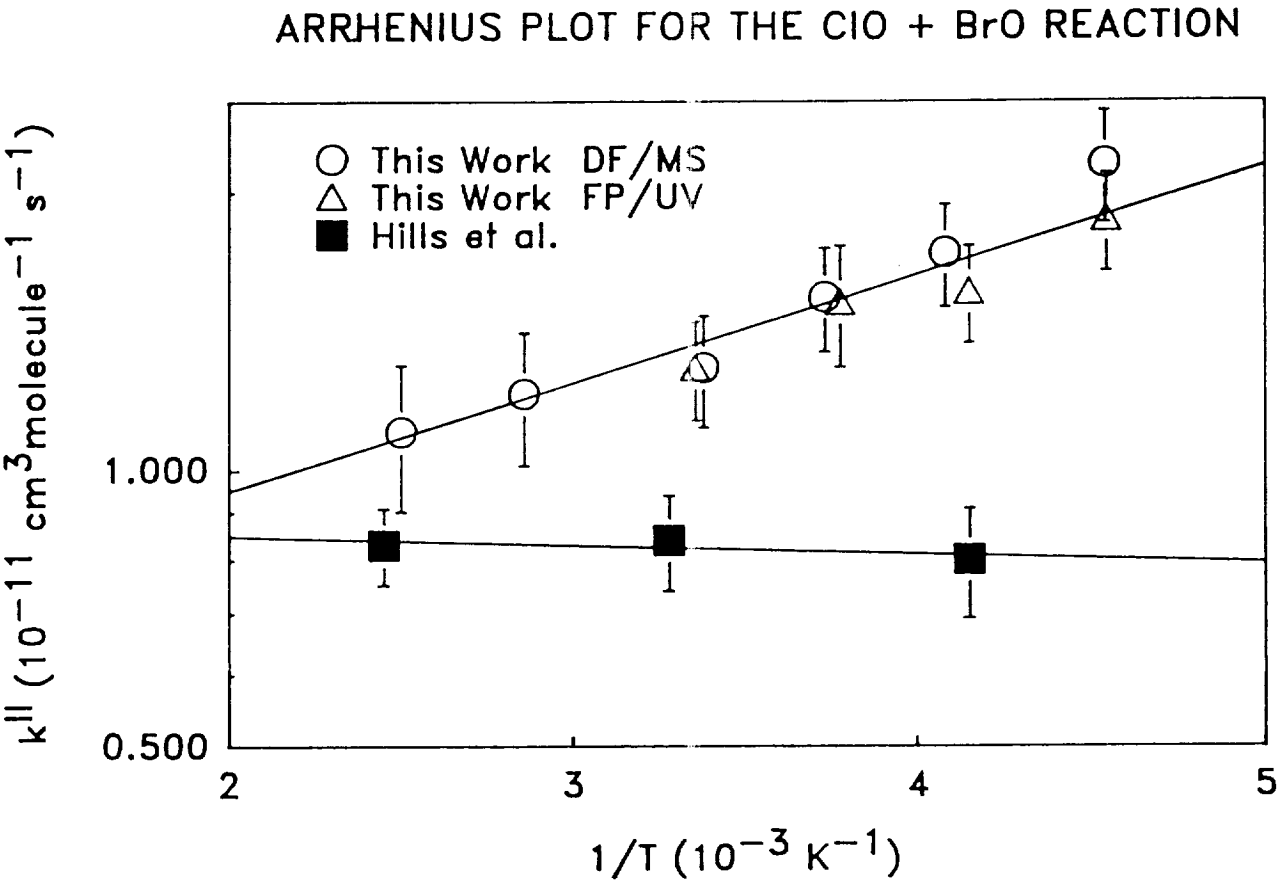

Figure 1. Temperature dependence of the BrO + ClO rate constant from this study and from Hills et al. (1987). DF/MS = Discharge Flow/Mass Spectroscopy, FP/UV= Flash Photolysis/Ultraviolet Absorption.

STABILITY AND PHOTOCHEMISTRY OF ClO DIMERS FORMED AT LOW TEMPERATURE IN THE GAS PHASE

by R.A. Cox and G.D. Hayman

Engineering Sciences Division,
Harwell Laboratory,
Didcot, Oxon. OX11 ORA
UK

Abstract

The recent observations of elevated concentrations of the ClO radical in the austral spring over Antarctica have implicated catalytic destruction by chlorine in the large depletions seen in the total ozone column. One of the chemical theories consistent with an elevated concentration of the ClO is a catalytic cycle involving the formation of the ClO dimer through the association reaction:

$$ClO + ClO = Cl_2O_2 \quad (1)$$

and the photolysis of the dimer to give the active Cl species necessary for O_3 depletion.

$$Cl_2O_2 + h\nu = Cl + ClOO \quad (2)$$

$$ClOO\ (+ M) = Cl + O_2 \quad (\text{fast})\ (3)$$

In the present paper we report experimental studies designed to characterise the dimer of ClO formed by the association reaction (1) at low temperatures. ClO was produced by static photolysis of several different precursor systems: $Cl_2 + O_3$; $Cl_2 + Cl_2O_2$; $OClO + Cl_2O$, O_2 or N_2. The reaction products were investigated by photodiode array spectroscopy in the U.V. region, which allowed the time dependence of Cl_2, Cl_2O, ClO, OClO, O_3 and other absorbing molecules to be determined.

Fig. 1 shows product spectra recorded in three different ClO precursor systems at 233K. Spectra 1a and 1b were obtained using the reactions of $Cl + O_3$ and $Cl + Cl_2O$ as a source of ClO. These appear to be associated with the major product of the ClO + ClO reaction in the temperature range 200-273K, which we believe to be the dimer Cl_2O_2. The absorption scales with $[ClO]^2$ and becomes more stable as temperature decreases. By means of mass balance a value of $(6.4 \pm 0.6) \times 10^{-18}$ cm^2 molecule was obtained for the cross-section at the peak of absorption at 245 nm. By observation of the temperature dependence of the concentration ratio $[Cl_2O_2]/[ClO]^2$, an expression is obtained for the equilibrium constant for reaction (1):

$$K_1 = (4.2 \pm 0.3) \times 10^{-30}.T.\exp(8720 \pm 360)/T)\,cm^3\ molecule^{-1}$$

Fig. 2 shows a Van't Hoff plot of the resultant values of K which

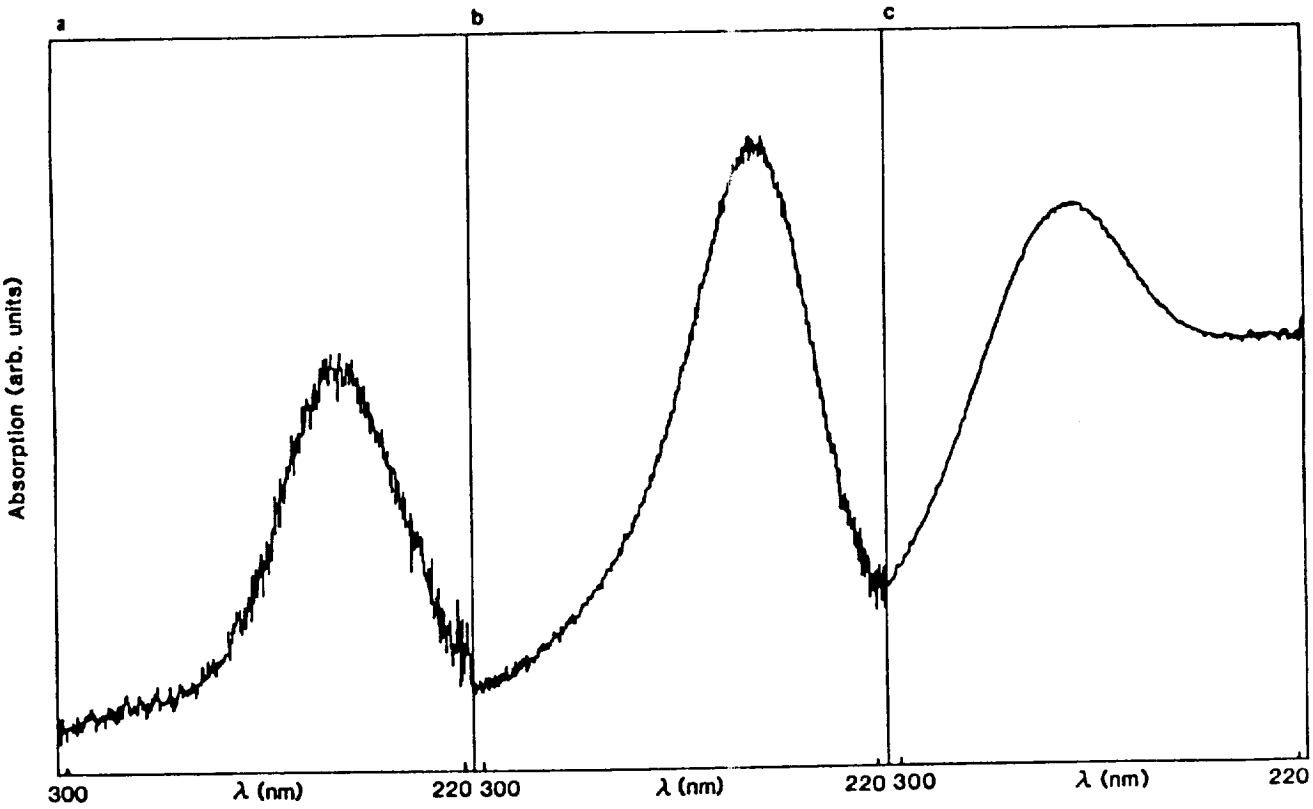

Fig. 1 - Residual absorptions seen in the photolysis of (a) $Cl_2/O_3/N_2$ mixtures (b) $Cl_2/Cl_2O/N_2$ mixtures (c) $OClO/Cl_2O/N_2$ mixtures

allow dermination of $\Delta H_1 = -72.5 \pm 3.0$ kJ mol^{-1} and $\Delta S_1 = -144 \pm 11$ J $mol^{-1}K^{-1}$

The third spectrum in Fig. 1 was obtained when the photolysis of a $OClO - Cl_2O - N_2$ mixture was used to make ClO:

$$OClO + h\nu = ClO + O \quad (4)$$

$$O + Cl_2O = 2ClO \quad (5)$$

The spectrum, which could also be produced in $OClO - O_2$ and $OClO - N_2$ photolysis systems at low temperature, differs significantly from that obtained in the systems without OClO present. At higher temperatures and longer reaction times the spectrum changed shape to give an absorption bearing a strong resemblance to that assigned to Cl_2O_2. The absorbance at short reaction times scaled approximately with the product [OClO] x [ClO] indicating the formation of an adduct, Cl_2O_3, via reaction of OClO with ClO. The Van't Hoff plot of the equilibrium

$$ClO + OClO = Cl_2O_3 \quad (6)$$

constants calculated on this basis at three temperatures in the range

233-273K is shown in Fig. 2.

The following thermochemical quantities were derived for reaction (6):

$$\Delta H_6 = -68.1 \pm 2.6 \text{ kJ mol}^{-1} \quad ; \quad \Delta S_6 = -165 \pm 10 \text{ kJ.mol}^{-1}\text{K}^{-1}$$

We have also made a preliminary investigation of the photolysis of the Cl_2O_2 dimer, using light at 254 nm, close to the absorption maximum.[2] Our results indicate that the major photolysis channel is reaction (2) producing a Cl atom and a ClOO peroxy radical, as suggested for the proposed catalytic cycle for O_3 removal in the antarctic stratosphere. This suggests that the 'stable' form of Cl_2O_2 that we observe is of a peroxy type structure : Cl-O-O-Cl. This is consistent with theoretical calculations of the geometry and structure of the possible ClO dimers.

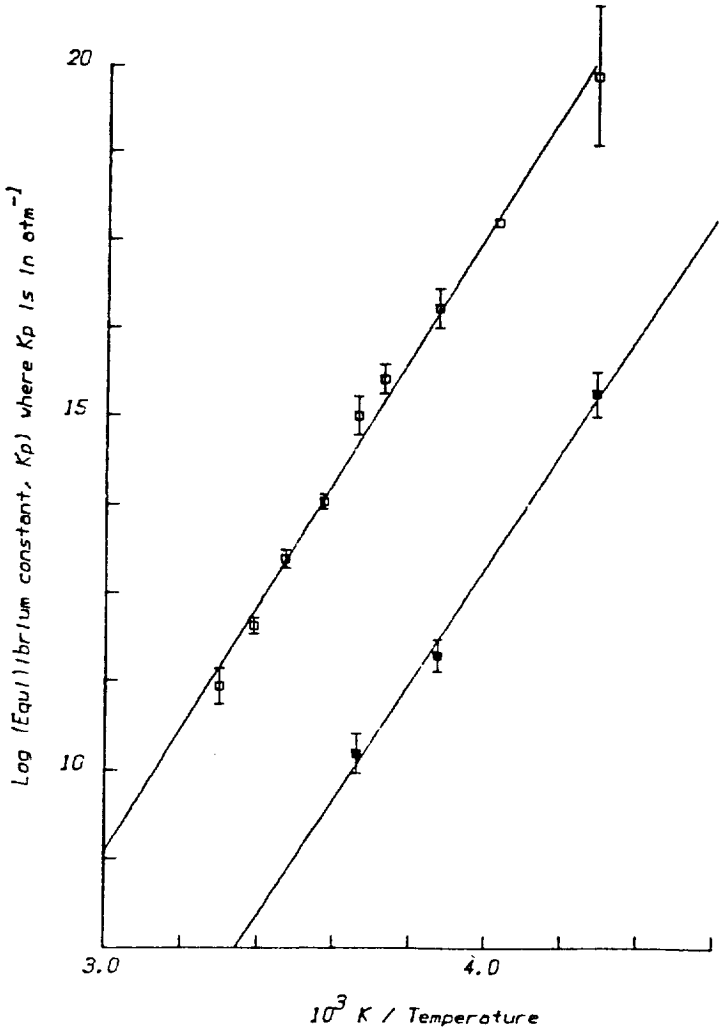

Fig. 2 - A Van't Hoff plot of $\log_e K_p$ against T^{-1} for the equilirbia: ClO + ClO = Cl_2O_2 (upper plot) and ClO + OClO = Cl_2O_3 (lower plot).

MEASUREMENTS OF THE ClO RADICAL VIBRATIONAL BAND INTENSITY AND THE ClO + ClO + M REACTION PRODUCT

James B. Burkholder, John J. Orlando, Philip D. Hammer, and Carleton J. Howard, NOAA Aeronomy Laboratory, R/E/AL2, 325 Broadway, Boulder, Colorado 80303 and Cooperative Institute for Research in Environmental Sciences University of Colorado, Boulder, Colorado and Aaron Goldman, Department of Physics, University of Denver, Denver, Colorado 80208

There is considerable interest in the kinetics and concentrations of free radicals in the stratosphere. Chlorine monoxide is a critically important radical because of its role in catalytic cycles for ozone depletion. Depletion occurs under a wide variety of conditions including the Antarctic spring when unusual mechanisms such as the BrO_x/ClO_x, ClO dimer (Cl_2O_2), and ClO_x/HO_x cycles are suggested to operate. Infrared spectroscopy is one of the methods used to measure ClO in the stratosphere [Menzies 1979 and 1983; Mumma et al. 1983]. To aid the quantification of such infrared measurements we have measured the ClO ground state fundamental band intensity.

The high ClO concentrations and the low stratospheric temperatures found in the Antarctic increase the liklihood of Cl_2O_2 formation and possible ozone destruction through the ClO dimer cycle. Little is currently known about the chemistry and photochemistry of Cl_2O_2. We have therefore studied the ClO + ClO + M reaction product to characterize the Cl_2O_2 infrared and UV absorption spectra.

The ClO band intensity and ClO + ClO + M reaction product measurements are made using a flow tube reactor coupled to a fast flow multipass

absorption cell. The absorption cell is optically coupled to a high resolution Fourier transform spectrometer (FTS) (Bomem, Model DA3.002) for infrared absorption measurements. A UV spectrometer is also optically coupled to the absorption cell for simultaneous UV absorption measurements on the gas sample.

ClO v = 0 - 1 Band Intensity Measurement

The ClO radical infrared line intensities were first measured by Rogowski et al. [1978] and Margolis et al. [1978] using tunable diode laser spectroscopy. The results from these two experiments are in good agreement and give a ClO v = 0 -1 band intensity of S = 11.8 ± 2 $cm^{-2}atm^{-1}$ at 298 K. This band intensity value and all subsequent band intensity values discussed include contributions from both chlorine isotopes and electronic spin states. A subsequent Herman Wallis analysis of data from our laboratory [Burkholder et al. 1987] gave S = 11.3 ± 2.0 cm^{-2} atm^{-1} in good agreement with the experimental values. Kostiuk et al. [1986] using infrared laser heterodyne spectroscopy to monitor ClO have recently reported a ClO band intensity of S = 4.9 $cm^{-2}atm^{-1}$ at 298 K, about a factor of 2.4 lower than the other measurements.

The discrepancy among the ClO band intensity measurements is significant and has a direct effect on the interpretation of quantitative atmospheric and laboratory infrared ClO measurements. In order to resolve this discrepancy we measured the v = 0 -1 band intensity of the ClO radical using directly calibrated [ClO]. The ClO spectra were recorded at 0.004 cm^{-1} resolution over the ClO concentration range 4 $x10^{12}$ to 1.4 $x10^{13}$ molecule cm^{-3} using two different chemical sources of ClO, Cl + O_3 and NO + OClO. Spectra were recorded at a total pressure of ≤ 0.4 torr, M = He. A sample ClO spectrum recorded during these measurements is shown in figure 1.

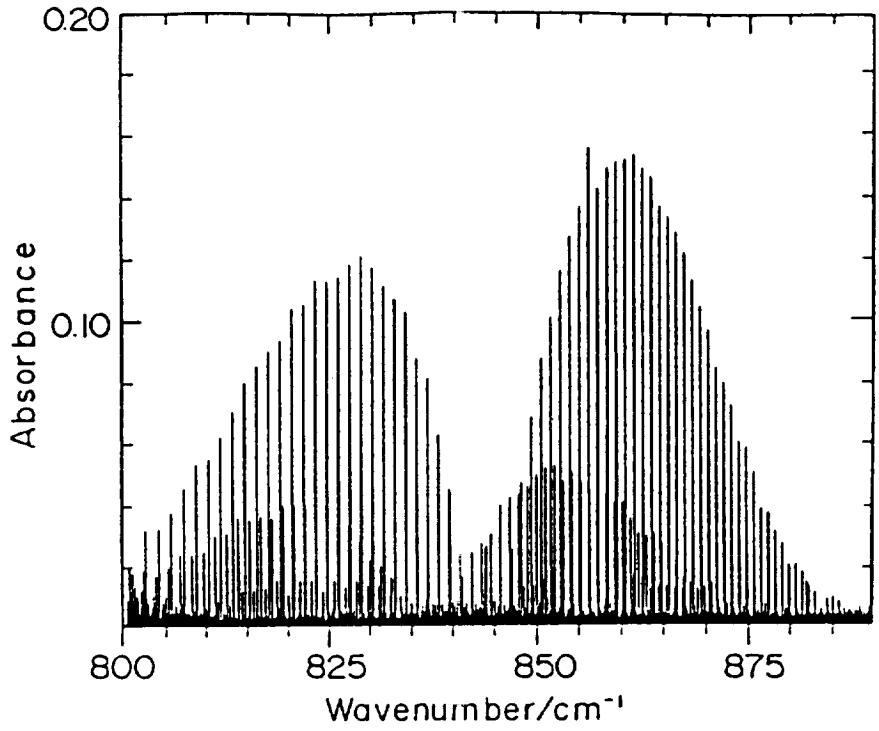

Figure 1 ClO radical infrared absorption spectrum. The spectrum was recorded at 0.004 cm^{-1} resolution in 50 coadded scans. [ClO] = 1.35 $x10^{13}$ molecule cm^{-3}.

A preliminary value of the measured integrated band intensity is S = 9.15 ± 1.5 cm^{-2} atm^{-1} at 296 K. A N_2 collisional broadening coefficient of γ^0 = 0.093 ± 0.018 cm^{-1} atm^{-1} was also determined from spectra recorded at higher pressure, 10 torr N_2. The discrepancy between our FTS band intensity measurements and those of Kostiuk et al. [1986] will be discussed. A source of systematic error in the use of the Cl + O_3 reaction as a quantitative source of ClO radicals will also be discussed.

ClO + ClO Reaction Product

Molina and Molina [1987] have discussed the ClO dimer cycle:

$$ClO + ClO + M \rightarrow Cl_2O_2 + M \quad (1)$$

$$Cl_2O_2 + h\nu \rightarrow Cl + ClOO \quad (2)$$

$$ClOO + M \rightarrow Cl + O_2 + M \quad (3)$$

$$2(Cl + O_3 \rightarrow ClO + O_2) \quad (4)$$

$$\text{NET } 2O_3 \rightarrow 3O_2 \quad (5)$$

and suggested that it may play an important role in the Antarctic ozone depletion. At the temperature, pressure and [ClO] observed in the lower Antarctic stratosphere, the self reaction of ClO to form the dimer, Cl_2O_2, is significant. At these temperatures, 190 - 210 K, the ClO dimer ,assuming a bond energy ~16.5 kcal $mole^{-1}$, would have a long thermal decomposition lifetime, τ ~ 20 hours. The UV absorption spectrum, photolysis rate and reactivity of Cl_2O_2 therefore need to be understood to determine the significance of the ClO dimer cycle. Infrared and UV absorption measurements of the ClO + ClO + M reaction products will be presented. Our observations will be compared with the recent measurements of Molina and Molina [1987].

REFERENCES

Burkholder, J.B., P.D. Hammer, C.J. Howard, A.G. Maki, G. Thompson, and C. Chackerian, Jr., Infrared Measurements of the ClO Radical, J. Mol. Spectrosc. 124, 139, 1987.

Kostiuk, T., J.L. Faris, M.J. Mumma, D. Deming, and J.J. Hillman, Infrared Line Intensities of Chlorine Monoxide, J.Geophys. Res. 91 D2, 2735, 1986.

Margolis, J.S., R.T. Menzies, and E.D. Hinkley, Bandstrength determination of the Fundamental Vibration-Rotation Spectrum of ClO, Appl. Opt. 17, 1680, 1978.

Menzies, R.T., Remote Measurement of ClO in the Stratosphere, Geophys. Res. Lett., 6, 151, 1979.

Menzies, R.T., A Re-Evaluation of Laser Heterodyne Radiometer ClO Measurements, Geophys. Res. Lett., 10, 729, 1983.

Molina, L.T., and M.J. Molina, Production of Cl_2O_2 from the Self-Reaction of the ClO Radical, J. Phys. Chem. 91, 433, 1987.

Mumma, M.J., J.D. Rogers, T. Kostiuk, D. Deming, J.J. Hillman, and D. Zipoy, Is There Any Chlorine Monoxide in the Stratosphere?, Science, 221, 268, 1983.

Rogowski, R.S., C.H. Bair, W.R. Wade, J.M. Hoell, and G.E. Copeland, Infrared Vibration-rotation Spectra of the ClO Radical Using Tunable Diode Laser Spectroscopy, Appl. Opt. 17, 1301, 1978.

ABSTRACT

POLAR OZONE WORKSHOP

May 9-13, 1988, Aspen, Colorado

CHEMISTRY OF THE CLO DIMER AT LOW TEMPERATURES

W. B. DeMore
Chemical Kinetics and Photochemistry Group
Jet Propulsion Laboratory
Pasadena, California 91109

and

E. T. Roux
Department of Chemistry
University of Calgary
Calgary, Alberta, Canada T2N 1N4

The unique conditions of low temperature and high observed ClO concentrations in the Antarctic stratosphere have focussed attention on the possible role of ClO dimers in the photochemistry of that region, particularly as related to ozone depletion. Compared to other aspects of stratospheric chlorine chemistry, very little is known about the formation, structure, thermal decomposition, photochemistry, and chemical reactivity of the dimer. Other possible complexes of ClO, such as

$$ClO + ClO_2 \leftrightarrow Cl_2O_3$$

and

$$ClO + O_2 \leftrightarrow ClO\text{-}O_2$$

are also very uncertain with regard to their importance under laboratory and atmospheric conditions.

We have conducted a series of experiments on the chlorine-catalyzed photodecomposition of O_3 both in the gas phase and in inert solvents such as CF_4 and CO_2 in the temperature range of about 190 - 225 K. The liquid medium was chosen in order to minimize possible surface loss of long-lived ClO dimer, and to aid in the stabilization of transient excited intermediates. The mechanism of dimer formation was as follows:

(1) $$Cl_2 + h\nu \rightarrow Cl + Cl$$

(2) $$Cl + O_3 \rightarrow ClO + O_2$$

(3) $$ClO + ClO \rightarrow Cl_2O_2$$

The experiments were done in cooled low temperature cells, with irradiation from an Osram high pressure mercury arc, filtered to remove radiation below 325nm. Spectral analysis was by means of a Cary Model 2200 UV spectrometer.

The principal objectives were (1) to determine the lifetime of the dimer as a function of temperature, (2) to observe spectral changes in the mixture which could be attributed to dimer or related products, and (3) to observe chemical or photochemical reactions of the dimer.

RESULTS

Gas Phase: A transient absorption spectrum attributed to symmetric ClO dimer was obtained in experiments at 200-220K. (Figure 1). Two methods were used to obtain the spectra: (1) Following partial photodecomposition of the O_3, spectra were recorded and residual absorptions due to O_3, Cl_2, and the empty cell were successively subtracted. (2) After photolysis, a difference spectrum was taken before and after standing for a period of 10-30 minutes. The spectral change on standing corresponded to the same absorption as that obtained by method 1, indicating that the dimer was unstable on a time period of a few minutes. The proposed mechanism for dimer loss is discussed below.

Liquid Phase: These experiments provided further evidence of dimer instability at quite low temperatures. In liquid CO_2 near 225K, photolysis produced a rapid O_3 loss as expected from reactions 1 and 2, but no measurable Cl_2 loss corresponding to dimer formation by reaction 3. Computer simulations, assuming a long dimer lifetime with respect to thermal decomposition, indicated that measurable Cl_2 loss should have been observed. There is evidence that the dimer loss can be explained by the bimolecular self-reaction,

(4) $$Cl_2O_2 + Cl_2O_2 \rightarrow 2Cl_2 + 2O_2$$

Experiments at and below 200K in liquid CF_4 contrasted sharply with the above experiments in liquid CO_2, showing clear evidence of substantial product formation. The observed products included OClO and a material tentatively identified as Cl_2O_3. Spectral changes occurring in the mixtures on standing indicate that dark reactions are also important in the overall process. We consider that the onset of OClO formation follows from the appearance of the asymmetric dimer, ClOClO, as a stable product in the liquid medium. Since these products were not observed in gas phase experiments at the same temperature, it is probable that efficient quenching of the ClOClO reaction intermediate is necessary to prevent isomerization to the more stable ClOOCl structure.

(5) $$ClO + ClO \rightarrow [ClOClO]^*$$

(6) $$[ClOClO]^* \rightarrow ClOOCl$$

(7) $$[ClOClO]^* + M \rightarrow ClOClO$$

Production of OClO can be accounted for by the reaction:

(8) $$Cl + ClOClO \rightarrow Cl_2 + OClO$$

MAJOR CONCLUSIONS

A spectral feature peaking near 245 nm, similar to that previously reported by R. A. Cox and co-workers, is attributed to the symmetric dimer ClOOCl.

The dimer ClOOCl undergoes a bimolecular self-reaction which can become the dominant loss mechanism at low temperatures.

The asymmetric dimer ClOClO, Although present as an excited intermediate in the ClO + ClO reaction, is difficult to stabilize and would not be expected to be produced under the low pressure conditions prevailing in the atmosphere.

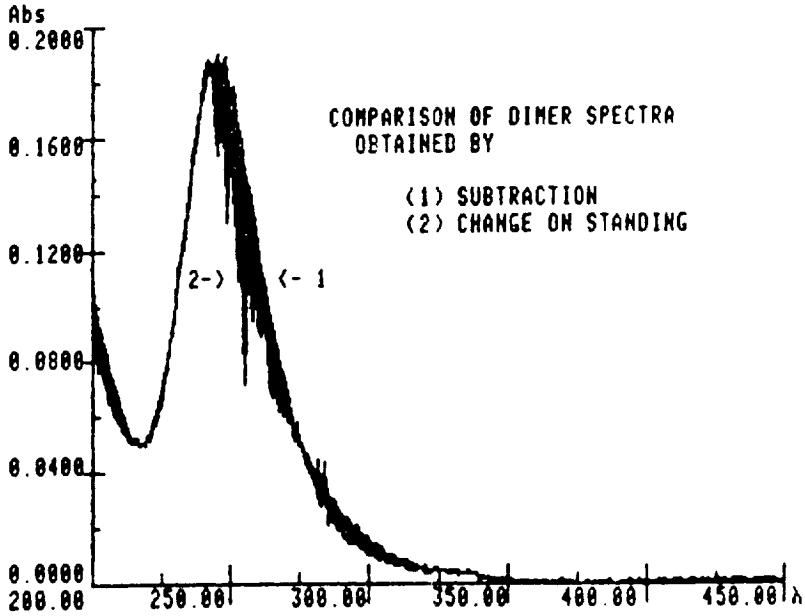

Figure 1.

N89-14603

MODELLING THE ANTARCTIC LOWER STRATOSPHERE

M.P. Chipperfield and J.A. Pyle

Department of Physical Chemistry
University of Cambridge
U.K.

We will present results from modelling studies of the Antarctic lower stratosphere which have attempted to simulate the large springtime ozone losses and corresponding changes in other trace constituents. These studies were carried out in a photochemical box model, a one-dimensional model without transport and in a two-dimensional photochemical-dynamical-radiation model.

The photochemical studies have investigated inter alia the sensitivity of ozone to inclusion in the model of heterogeneous chemistry, and to the inclusion of the ClO dimer. When both of these are incorporated in the model, ozone depletions resembling those found in Halley Bay in 1987 (J.C. Farman, Nature, 329, 1987) can be reproduced. We will discuss the temporal variations (both diurnal and during the August to October period) of a number of important tracers including HCl, $ClONO_2$, OClO and BrO.

The two-dimensional study has concentrated on the difficulty of establishing in the model the dynamical preconditioning of the lower polar stratosphere - low temperatures, low N_2O, etc, high ClO_x. We will present calculations to show: (i) the depletion of ozone during the springtime season, (ii) the effect of large ozone losses on lower latitudes and (iii) the longer term (multi-year) variations of ozone in Antarctica, assuming realistic increases in the atmospheric halogen burden.

The Chemistry of Antarctic Ozone 1960 – 1987

by
R. J. Salawitch, S. C. Wofsy and M. B. McElroy

The ozone abundance over Antarctica has declined rapidly during spring in recent years (Farman et al., 1985), with nearly complete removal between about 11 and 20 km by early October in 1986 and 1987 (Hofmann et al., 1987; Farman et al., in press 1988). Marked declines in ozone were first observed during the 1970's, and rates of depletion appear to have accelerated after 1980 (Farman et al., 1985; Krueger et al., 1987). The present paper examines the factors that influence Antarctic ozone with a view to understanding the observed historical trend. We show that reduced ambient temperatures can dramatically enhance the efficiency of chemical removal processes. Attention is focused on positive feedback between levels of ozone, temperature, and rates for heterogeneous chemical reactions.

Chemical models using recent kinetic data predict rapid loss of Antarctic ozone after sunrise (McElroy et al., 1988, Salawitch et al., 1988, Wofsy et al., 1988), consistent with observations from 1986 and 1987. Key chemical steps require very low temperatures, needed to condense ice containing HCl and HNO_3 to form the polar stratospheric clouds (PSCs). Heterogeneous reactions on PSC particles convert inorganic chlorine to reactive forms in the gas phase, mainly ClO and $(ClO)_2$ and odd nitrogen species are efficiently scavenged from the gas phase (Molina et al., 1987; Tolbert et al., 1987, 1988; Leu, 1988). Trace gas concentrations predicted by these models are consistent with the observations of Farmer et al. (1987) and Solomon et al. (1987), from the 1986 NOZE campaign, and the models yield concentrations of ClO consistent with the ER-2 data of Anderson, Brune and coworkers. About 75% of the computed O_3 removal is associated with reactions of ClO and its dimer (Molina and Molina, 1987), and about 25% with reactions of ClO and BrO (McElroy et al., 1986b).

Model results exploring effects of nighttime heterogeneous chemistry are shown in Figure 1. Conditions at the beginning of polar night were estimated on the basis of detailed photochemical simulations of stratospheric chemistry at various latitudes in fall (June), scaling to Antarctic latitudes along preferred mixing surfaces (McElroy et al., 1986b). Condensation was assumed to begin on July 1, corresponding to the first appearance of PSCs (McCormick and Trepte, 1986). The composition of the ice was fixed at 2 mole % HCl (Wofsy et al., 1988) during the early stages of condensation and HNO_3 was assumed to be completely scavenged from the gas phase (Toon et al., 1986; Crutzen and Arnold, 1986; McElroy et al., 1986a).

Four key heterogeneous reactions were assumed to operate at rates given by Leu (1988) (reactions 1 and 2) and by Tolbert et al. (1988) (reactions 3 and 4):

$$ClNO_3 + HCl(s) \rightarrow HNO_3(s) + Cl_2 \quad (1)$$

$$ClNO_3 + H_2O(s) \rightarrow HNO_3(s) + HOCl \quad (2)$$

$$N_2O_5 + HCl(s) \rightarrow ClNO_2 + HNO_3(s) \quad (3)$$

$$N_2O_5 + H_2O(s) \rightarrow 2HNO_3(s), \quad (4)$$

where (s) denotes solid phase species. Production of nitryl chloride is seen to represent an important component of the net loss of HCl, while odd nitrogen is converted mainly to solid-phase HNO_3. At stratospheric sunrise chlorine species are rapidly converted to

ClO and its dimer, and high levels of these gases are maintained until the clouds evaporate, on 15 September for the simulation shown here.

Concentrations of chlorine radicals decline after the clouds dissipate. The model assumed that 50% of the HNO_3(s) returned to the gas phase when the clouds evaporated, while 50% was removed by precipitation, consistent with the observations of Farmer et al. (1987) in 1986 (McElroy et al., 1988). Photolytic destruction of HNO_3 yields NO_2, which binds chlorine as relatively unreactive $ClNO_3$. Significant conversion of radicals to HCl also occurred, by reaction of Cl with CH_4.

Analysis of these results shows that ozone losses are sensitive to several of our assumptions, most of which relate to the formation and persistence of the PSCs:

(1) If the clouds last longer into the spring, high concentrations of radicals will persist and ozone losses will continue longer, producing larger reductions of ozone by mid-October.

(2) If less nitric acid is returned to the gas phase, formation of $ClNO_3$ would be retarded, high concentrations of ClO would persist, and loses of ozone would be larger.

(3) If the rate of reaction of Cl with CH_4 were slowed, formation of HCl would be retarded. A slower rate could reflect an abundance of CH_4 less than assumed here, or a lower temperature resulting in a slower rate for reaction of Cl and CH_4.

(4) If the height range of the region influenced by clouds were extended, losses of column ozone would be correspondingly increased.

The persistence of the polar vortex itself may give rise to an observational bias, particularly in comparison of model results with monthly averaged data for ozone column in October as reported, for example, by Farman et al. (1985). If the breakdown of the vortex is delayed the October mean concentration of O_3 will be more strongly influenced by the springtime depletion.

The factors cited above all respond in the same way to reductions in stratospheric temperatures. Colder temperatures would extend the time duration and the height range for PSCs. Colder temperatures also would provide efficient precipitation of solid-phase HNO_3. There are intriguing hints that temperatures might indeed have declined in the Antarctic stratosphere, reflecting perhaps reduced solar heating associated with ozone reductions. Persistence of the vortex and downwelling in the vortex (which would bring in air depleted in CH_4) might also be strengthened by diminished heating at low O_3.

Figure 2 illustrates the influence of the above factors on column ozone, for levels of inorganic chlorine appropriate for the time period between 1960 to 1987. The upper curve shows the relatively modest declines in ozone predicted with the model in Figure 1. The lower curve shows the very low ozone columns if PSCs persist to the end of September, if CH_4 is 50% less than assumed in Figure 1, and if 90%, rather than 50%, of stratospheric HNO_3 is assumed to precipitate. The effects of particular changes in model parameters are also shown in Figure 2 (see caption).

The magnitude of the O_3 loss is shown to be sensitive to the efficiency with which HNO_3 is removed from the stratosphere by precipitation and to the persistence and altitude extent of PSCs. Loss of O_3 may be expected to diminish the role of solar heating in October, extending the lifetime of the polar vortex and promoting colder temperatures. These factors could account for the accelerated removal of O_3 observed over the past

several years.

REFERENCES

Crutzen, P. J. and Arnold, F. (1986) Nitric acid cloud formation in the cold Antarctic stratosphere: A major cause for the springtime "ozone hole". *Nature* **324**, 651.

Farman, J. C., Gardiner, B. G., and Shanklin, J. D. (1985) Large losses of total ozone in Antarctica reveal seasonal ClO_x/NO_x interaction. *Nature* **315**, 207.

Farmer, C. B., Toon, G. C., Schaper, P. W., Blavier, J.-F., and Lowes, L. L. (1987) Stratospheric trace gases in the spring 1986 Antarctic atmosphere. *Nature* **329**, 126.

Hofmann, D. J., Harder, J. W., Rolf, S. R., and Rosen, J. M. (1987) Balloon-borne observations of the development and vertical structure of the Antarctic ozone hole in 1986. *Nature* **326**, 59.

Krueger, A. J., Schoeberl, M. R., and Stolarski, R. S. (1987) TOMS observations of total ozone in the 1986 Antarctic spring. *Geophys. Res. Lett.* **14**, 527.

Leu, M.-T. (1988) Laboratory studies of sticking coefficients and heterogeneous reactions important in the Antarctic stratosphere. *Geophys. Res. Lett.*, submitted for publication.

McCormick, M. P. and C. R. Trepte (1986) SAM II measurements of Antarctic PSCs and aerosols. *Geophys. Res. Lett.* **13**, 1276.

McElroy, M. B., Salawitch, R. J., and Wofsy, S. C. (1986a) Antarctic O_3: Chemical mechanisms for the spring decrease. *Geophys. Res. Lett.* **13**, 1296.

McElroy, M. B., Salawitch, R. J., and Wofsy, S. C. (1988) Chemistry of the Antarctic stratosphere. *Planet. Space Sci.*, Jan. 1988.

McElroy, M. B., Salawitch, R. J., Wofsy, S. C., and Logan, J. A. (1986b) Reductions of Antarctic ozone due to synergistic interactions of chlorine and bromine. *Nature* **321**, 759.

Molina, L. T. and Molina, M. J. (1987) Production of Cl_2O_2 from the self-reaction of the ClO radical. *J. Phys. Chem.* **91**, 433.

Molina, M. J., Tso, T.-L., Molina, L. T., and Wang, F. C.-Y. (1987) Antarctic stratospheric chemistry of chlorine nitrate, hydrogen chloride and ice: Release of active chlorine. *Science* **238**, 1253.

Salawitch, R. J., S. C. Wofsy, and M. B. McElroy (1988) Chemistry of OClO in the Antarctic stratosphere: implications for bromine, *Planet. Space Sci.*, Feb. 1988.

Solomon, S., Mount, G. H., Sanders, R. W., and Schmeltekopf, A. L. (1987) Visible spectroscopy at McMurdo Station, Antarctica. 2. Observations of OClO. *J. Geophys. Res.* **92**, 8329.

Tolbert, M. A., M. J. Rossi, R. Malhotra, and D. M. Golden (1987) Reaction of chlorine nitrate with hydrogen chloride and water at Antarctic stratospheric temperatures. *Science* **238**, 1258.

Tolbert, M. A., M. J. Rossi, and D. M. Golden (1988) Heterogeneous chemistry related to Antarctic ozone depletion: Reactions of N_2O_5 with H_2O and HCl on ice surfaces. *Science*, submitted for publication.

Toon, O. B., Hamill, P., Turco, R. P., and Pinto, J. (1986) Condensation of HNO_3 and HCl in the winter polar stratospheres. *Geophys. Res. Lett.* **13**, 1284.

Wofsy, S. C., Molina, M. J., Salawitch, R. J., Fox, L. E., and McElroy, M. B. (1988) Interactions between HCl, NO_x, and H_2O ice in the Antarctic stratosphere: Implications for ozone. *J. Geophys. Res.*, in press.

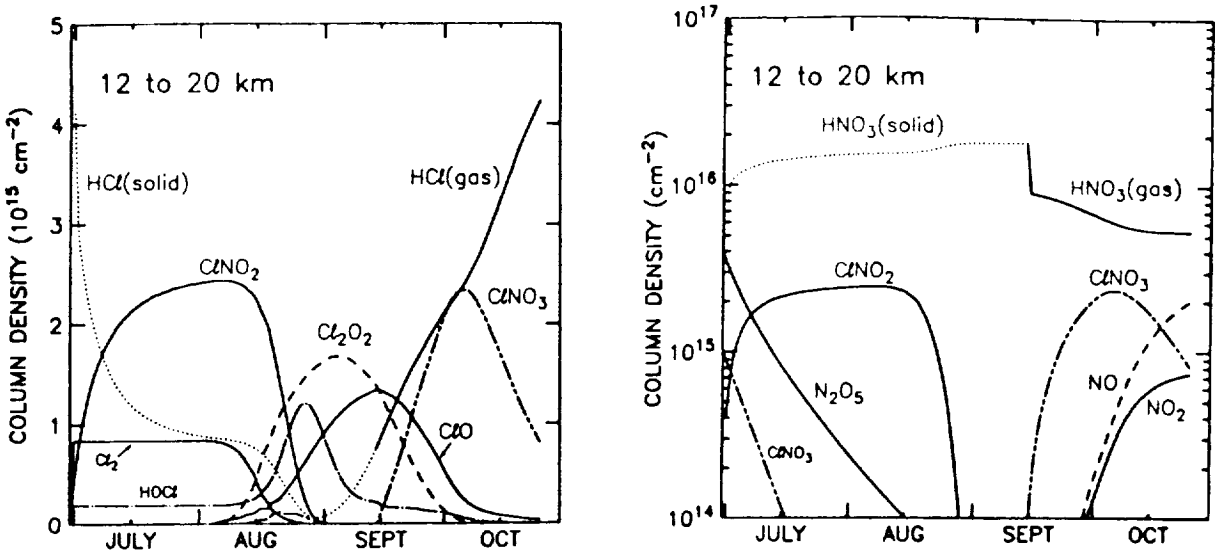

FIGURE 1 COLUMN DENSITY vs TIME

The evolution of the column density between 12 and 20 km for species of the chlorine family (left panel) and nitrogen family (right panel). The calculation used a latitude of 78°S and assumed 3.3 ppb of Cl_x at high altitude, appropriate for 1985. Results are shown for local noon. Polar stratospheric clouds were assumed to exist prior to September 15, with heterogeneous reactions (1) – (4) occurring and HCl and HNO_3 existing in the solid phase. Further details are provided in the text.

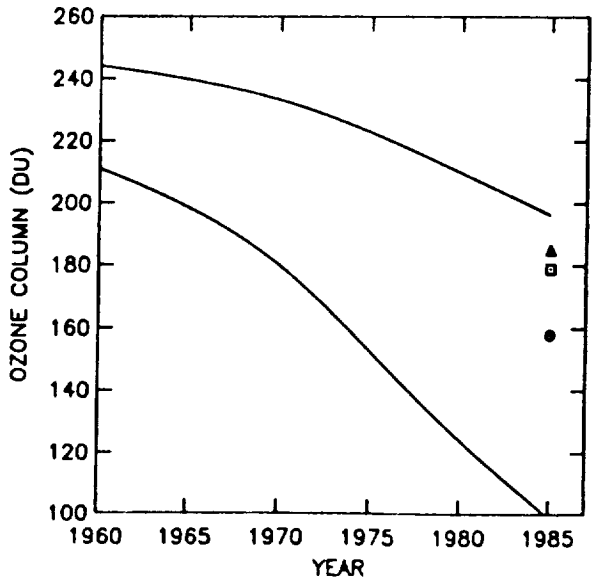

FIGURE 2 OZONE COLUMN vs YEAR, 1960–1987

The ozone column calculated for October 15 at 78°S, using levels of Cl_x appropriate for each year (1.0 ppb for 1960, 1.55 ppb for 1970, 2.4 ppb for 1978, and 3.3 ppb for 1985). The upper curve shows results using the same assumptions used for Figure 1. The points show the effects of changing various model assumptions: the triangle represents reducing the level of CH_4 in the model by 50%; the box represents extending the height range of the ozone loss to 11 to 25 km (vs. 12 to 20 km); the circle represents precipitation of 90% of HNO_3(s) (vs. 50%). The lower curve combines all three of these changes. The effects are not additive due to the non-linearity of the ClO–ClO loss process.

P.J. Crutzen and C. Bruhl:

Modelling the "Antarctic Ozone Hole".

Abstract:

We have performed model calculations of the ozone depletions taking place in the Antarctic lower stratosphere. Making the assumption that odd nitrogen is frozen out on polar stratospheric haze particles, an analysis is given of how much homogeneous reactions can contribute to ozone loss during September - October. Comparisons with observations indicates the potential importance of reactions with HCl in the polar stratospheric cloud particles.

STRATOSPHERIC FEEDBACK FROM CONTINUED INCREASES IN TROPOSPHERIC METHANE

F. Sherwood Rowland and Donald R. Blake
Department of Chemistry, University of California Irvine, 92717

Tropospheric concentrations of methane have increased steadily over the past ten years at an average rate of 16.5 ppbv per year, to a value in January 1988 of 1.69 ppmv. Measurements of CH_4 concentrations in air bubbles trapped in ice cores have shown concentrations of about 0.7 ppmv 200 years ago, with little further change for thousands of years before that. Interpolation earlier into this century suggests a concentration of about 1.1-1.2 ppmv in the 1940s.

The only important pathway believed to be important for transfer of air from the troposphere to the stratosphere is through the tropical tropopause which is cold enough to reduce the mixing ratio of H_2O in that air to about 3 ppmv. The only other major pathway for the delivery of H to the stratosphere is through the simultaneous injection of gaseous CH_4 in the same rising air. Satellite observations of the concentrations of both H_2O and CH_4 have shown that the summed H concentration is approximately constant at 12 ppmv H, the equivalent of 6 ppmv H_2O, corresponding roughly to 3 ppmv H_2O and 1.5 ppmv CH_4. As the trace concentrations of CH_4 in the troposphere have increased from 0.7 to 1.0 to 1.7 ppmv, the total H in the stratosphere has probably risen from about 4.4 to 5.0 to 6.0 to 6.4 ppmv H_2O equivalent. In well-oxidized air with most of its CH_4 converted to H_2O, these H_2O changes can account for as much as 45% more than was present 200 years ago, and 28% more than was there about 40-50 years ago. (These estimates assume that no change has occurred in the average temperature of the tropical tropopause which controls the H_2O concentration in the air entering the stratosphere.)

The formation of clouds in the stratosphere is dependent upon very low temperatures, and generally upon the amount of water vapor available. The possibility of a positive feedback exists, especially in "well-oxidized methane" air that clouds are easier to form than earlier. This could mean enhancement of PSCs in both Antarctic and Arctic locations. Additional H_2O in the stratosphere can also add to some of the greenhouse calculations.

HIGH RESOLUTION FTIR SPECTROSCOPY of the CLO RADICAL

Valerie Lang, Stanley Sander and Randy Friedl
Jet Propulsion Laboratory, California Institute of Technology
4800 Oak Grove Drive, Pasadena CA 91109

The chlorine monoxide radical, ClO, plays a significant role in the catalytic destruction of ozone in the Earth's stratosphere. Because of its atmospheric importance, ClO has been the subject of numerous observational attempts. In order to deduce ClO concentrations from stratospheric infrared measurements, the infrared spectroscopy of ClO must be well characterized.

FTIR spectra of the complete $X^2\Pi_{3/2}$ - $X^2\Pi_{3/2}$ and $X^2\Pi_{1/2}$- $X^2\Pi_{1/2}$ (1-0) fundamental vibrational-rotational bands of $^{35}Cl^{16}O$ and $^{37}Cl^{16}O$ have been obtained at 0.005 cm^{-1} apodized resolution. The short-lived radicals are produced in a discharge-flow chemical reactor which contains a White-type absorption cell. The typical infrared path length is 42 meters. During acquisition of the FTIR spectra, an optical multi-channel analyzer is used to monitor the ClO concentration by observing the $A^2\Pi_i$-$X^2\Pi_i$ electronic band in the uv region. Uv cross sections for ClO were obtained by titrating a known amount of OClO with excess Cl atoms and by titrating ClO with NO.

Approximately 830 individual lines were measured from ClO infrared spectra with the ClO concentration between 1 X 10^{13} and 6 X 10^{13} molecules/ cm^3. The lines were then averaged and fit to a function of m (where m = 0,-J or J+1 for the Q,P and R branches respectively) to obtain the band strength, S_v and the first Herman-Wallis coefficient, α. The total S_v for the two main isotopomers was 13.11 ± 1 cm^{-2} atm^{-1} while α was 0.00412 ± .00062.

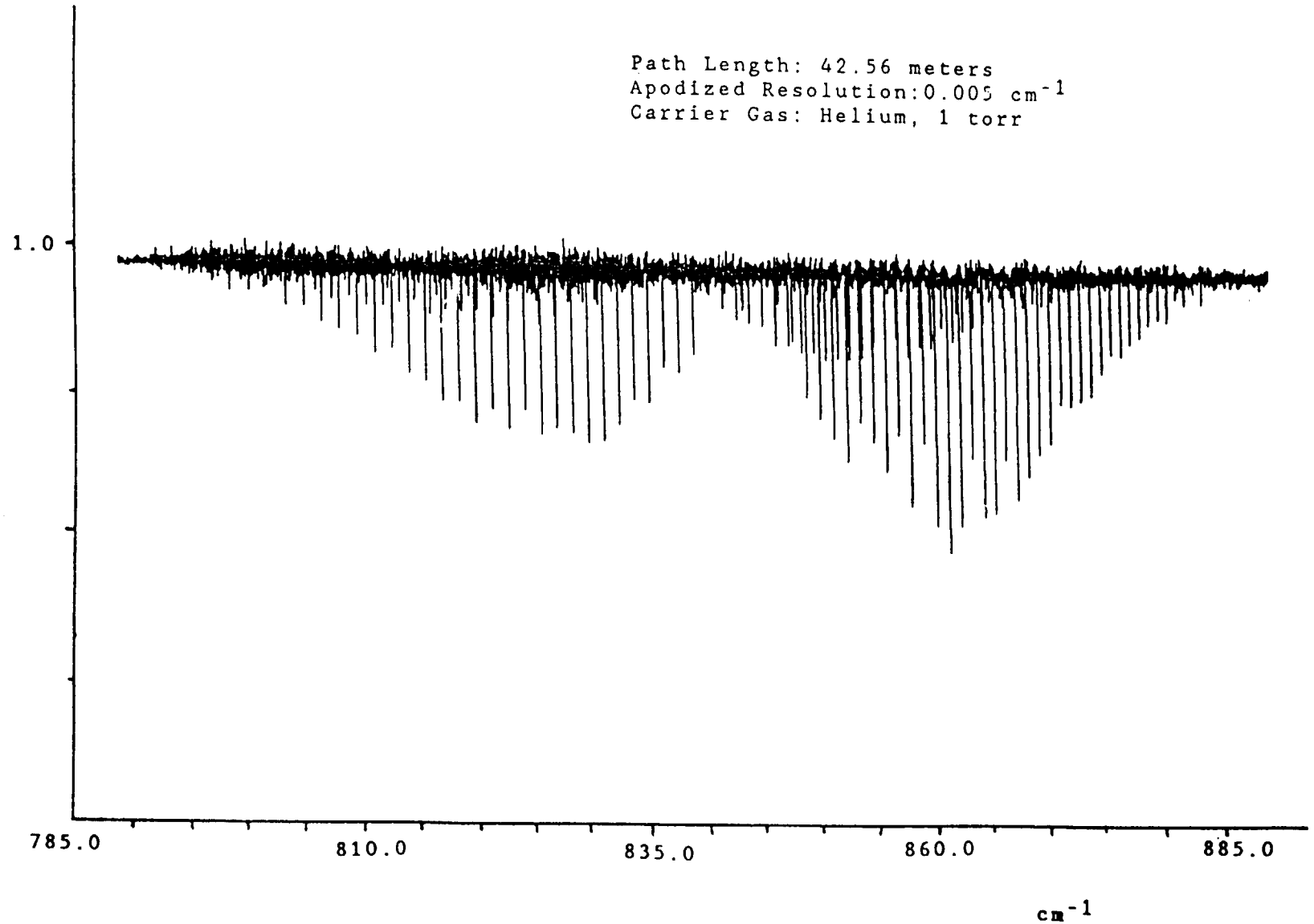
FTIR SPECTRUM of the CLO RADICAL
Path Length: 42.56 meters
Apodized Resolution:0.005 cm-1
Carrier Gas: Helium, 1 torr
1.0
TRANSMITTANCE
785.0
810.0
835.0
860.0
885.0
cm-1

AUTHOR INDEX

AUTHOR	SESSION Oral-Poster
Aikin,A.	I(O)
Akryoshi,H.	VIII(P)
Albritton,D	I(O)
Allen,M.	VIII(P)
Anderson,J.	V(O),V(P),VI(O)
Arnold,F.	VII(O)
Austin,J.	V(O),VIII(O)
Barrett,J.	IV(O),III(P)
Barrie,L.	VII(P)
Bauer,R.	VII(O),VII(P)
Bhartia,P.	I(P)
Blake,D.	IX(O)
Blavier,J.	IV(O),IV(P)
Bloomfield,P	VII(O)
Bojkou,R.	VII(O)
Bouille,B.	VIII(O)
Bowen,S.	V(P)
Bressitte,W.	I(P)
Briegleb,B.	VIII(O)
Brothers,G.	V(P)
Browell,E.	II(O),III(O),VI(O)
Bruhl,C	IX(O)
Brune,W	VII(O),VII(P), V(O),V(P)
Bui,T.	V(P)
Burkholder,J.	IX(O)
Butler,C.	II(O)
Carpenter,J.	II(O),I(P)
Carroll,M.	IV(O)
Chan,K.	V(P),III(O),V(O), VI(O),I(P),VI(P)
Chen,K.	I(P)
Chipperfield,M.	IX(O)
Chubahi,S.	I(O)
Coffey,M.	IV(O),IV(P),VI(O)
Condon,E.	V(P)
Cox,R.	IX(O)
Craven,J.	I(P)
Crisp,D.	VIII(P)
Crutzen,P.	IX(O)
Danielsen,E.	VII(O),VII(P)
Davidouits,P.	III(O),III(P)
Day,R.	V(P)
DeMore,W.	IX(O)
deZafra,R.	IV(O),III(P)
Dritschel,D.	VIII(P)
Emmons,L.	IV(O),III(P)
Eubank,C.	III(O),V(O)
Evans,W.	VII(O)
Fahey,D.	III(O),V(O),VI(O)
Farman,J.	I(O)
Farmer,C.	IV(P),IV(O),II(P)
Fanning,M.	I(P)
Fast,H.	VII(O)
Ferry,G.	II(O),III(O),V(O), VI(O)
Franchois,P.	I(P)
Friedl,R.	IX(O),IX(P)
Fong,W.	II(O)
Gandrud,B.	II(O)
Garcia,M.	VIII(O)
Gardner,J.	III(P)
Gary,B.	V(O),IX(P),VI(O)
Geller,M.	VIII(O)
Gelman,M.	I(P)
Golden,D.	III(O),II(P)
Goldman,A.	IV(O),IX(O)
Goodman,J.	II(O),II(P),IX(P)
Goutail,F.	VII(P)
Grass,R.	I(P)
Gray,L.	VIII(P)
Hammer,P.	IX(O)
Hanson,D.	III(O)
Harder,J.	II(O),I(P)
Harris,N.	VII(O)
Hartmann,D.	VI(O)
Hayman,G.	IX(O)
Haynes,P.	VIII(P)
Heath,D.	I(P)
Heidt,L.	V(P),V(O),VI(O)
Henry,B.	V(O)
Hereford,J.	I(P)
Hoffman,D.	II(O)
Hofmann,D.	I(P)
Howard,C.	IX(O)
Ismail,S.	II(O)
Iwasaka,Y.	VI(P)
Jakoubek,R.	IV(O),VI(O),VII(O), IV(P)
Jaramillo,M.	IV(O),III(P)
Jayne,J.	III(O),III(P)
Johnston,P.	IV(O)
Jones,R.	II(O),V(O),III(O), VI(O),VIII(O)
Kahl,J.	VII(P)
Keating,G.	I(P)
Kelly,K.	VI(O),III(O),I(P)
Kerr,J.	VII(P),VII(O)
Keys,J.	IV(O)
Kiehl,J.	VIII(O)
Kinne,S	II(P)
Klein,E.	VII(O),VII(P)
Knop,G.	VII(O)
Ko,M.	VIII(O),VI(O)
Kolb,C.	III(O),III(P)
Komhyr,W.	I(P)

AUTHOR	SESSION Oral-Poster	AUTHOR	SESSION Oral-Poster
Kooi,S.	II(O)	Pitts,M.	I(P)
Krueger,A.	I(O),II(O),VII(O), I(P),VII(P)	Podolske,J.	V(O),VI(O),I(P), V(P),VI(P)
Kuester,S.	I(P)	Pollock,W.	V(O),V(P)
Kulessa,G.	VII(O),VII(P)	Pommereau,J.	VII(O),VII(P)
Kunzi,K.	VI(P)	Poole,L.	II(O),III(O),II(P)
Lait,L.	VIII(O),VI(O),I(P)	Powell,J.	VI(O)
Lang,V.	IX(P)	Prather,M	VIII(O),VIII(P),VI(O)
Larsen,J.	I(O),IX(P)	Proffitt,M.	VI(O),V(O),I(P),V(P)
Larsen,S.	VII(P)	Pueschel,R.	II(O),III(O),II(P), IX(P)
Leu,M.	III(O)		
Leub,R.	V(P)	Pyle,J.	IX(O),VIII(P)
Livingston,J.	II(O)	Ramaswamy,V.	III(O)
Lowenstein,M.	V(O),VI(O),I(P), III(P),V(P)	Randel,W.	I(O)
		Ravishankara,A.	IV(O),IV(P)
Low,M.	VI(P)	Reitelback,P.	I(P)
Lowes,L.	IV(O)	Rodriquez,J.	VI(O),III(O),V(O), VIII(O)
Lueb,R.	V(O)		
Mankin,W.	IV(O),VI(O),IV(P)	Rosen,J.	II(O),I(P)
Margitan,J.	V(P)	Rosen,R.	VIII(P)
Martin,R.	VI(O)	Rossi,M.	III(O),II(P)
Mathews,W.	IV(O)	Roux,E.	IX(O)
Maversberger,K.	III(O)	Rowland,F.	IX(O),VII(O)
McCormick,P.	I(O),II(O),II(P), IX(P),III(O),VI(O)	Salawitch,R.	IX(O)
		Salstein,S.	VIII(P)
McElroy,M.	IX(O)	Sander,S.	IX(O),IX(P)
McIntye,M.	VIII(O)	Sanders,R.	IV(O),IV(P),VII(O)
McKenna,D.	VIII(O),V(O),VI(O)	Sanford,L.	II(O)
McPeters,R.	I(O)	Schaper,P.	IV(O),IV(P)
Miller,A.	VIII(P)	Schmeltekopf,A.	IV(O),VII(O)
Mohler,G.	IV(P)	Schmidt,U.	VII(O),VII(P)
Mohler,O.	VII(O)	Schnell,R.	VII(P)
Molina,M.	IX(O)	Schoeberl,M.	I(O),VI(O),VIII(O), I(P)
Morley,B.	III(P)		
Mount,G.	VII(O),IV(O),IV(P)	Schubert,B.	VII(O),VII(P)
Murcray,D.	IV(O)	Scott,S.	V(P),III(P)
Murcray,F.	IV(O)	Sheridan,P.	VII(P)
Murphy,D.	VI(O),VI(P),III(O), V(O)	Shia,R.	VIII(P)
		Smith,S.	III(P)
Nash,E.	VIII(O)	Snetsinger,K.	II(O),II(P),IX(P)
Nenny,B.	V(P)	Solomon,P.	IV(O),III(P)
Newman,P.	I(O),I(P),VI(O), VIII(O)	Solomon,S.	IV(O),VII(O),IV(P)
		Sperry,P.	II(O)
Norton,R.	IV(O)	Stan.W.	VII(P)
Oberbeck,V.	II(O)	Starr,W.	IV(P),V(O),VI(O), VII(O),I(P),V(P)
Olaquar,E.	VIII(O)		
Oltmans,S.	II(O),VII(P)	Stearns,C.	I(P)
Orlando,J.	IX(O)	Strahan,S.	I(P),V(O),VI(O),VI(P)
Parrish,A.	IV(O),III(P)	Stolarski,R.	VII(O),VII(P),VIII(O)
Peterson,D.	IV(P),VII(P)	Sze,N.	VI(O),VIII(O)
Pfeilsticker,K.	VII(O)	Szedlmayer,M.	II(O)
Piasecki,J.	III(P)	Taylor,S.	I(P)
Pitari,G.	II(P)	Tolbert,M.	III(O),II(P)

AUTHOR	SESSION Oral-Poster	AUTHOR	SESSION Oral-Poster
Toohey,D.	VII(O),VII(P)		
Toon,G.	IV(O),II(P),IV(P)		
Toon,O.	III(O),II(P),IX(P)		
Torres,A.	I(P)		
Trepte,C.	II(O),I(O)		
Trepte,V.	II(P)		
Tso,T.	IX(O)		
Tuck,A.	II(O),VI(O),V(P),VI(P)		
Tung,K.	VIII(O)		
Turco,R.	III(O)		
VanDoren,J.	III(P),III(O)		
Vedder,J.	V(O),VI(O),IV(P),V(P)		
Verma,S.	II(O),II(P),IX(P)		
Visconti,G.	II(P)		
Wahner,A.	IV(O),IV(P),VI(O)		
Wang,F.	IX(O)		
Watson,L.	III(O),III(P)		
Watson,R.	V(P)		
Weisenstein,D.	VIII(O)		
Wellemeyer,C.	I(O)		
Wen,J.	VIII(P)		
Wilson,J.	III(P)		
Winchester,J.	VII(P)		
Wofsy,S.	IX(O)		
Worsnop,D.	III(O),III(P)		
Wu,M.	VIII(O)		
Yang,H.	VIII(O)		
Yung,Y.	VIII(P)		
Zahniser,M.	III(O),III(P)		
Ziereis,H.	VII(O)		
Zurek,R.	VIII(P)		

POLAR OZONE WORKSHOP

Snowmass, Colorado

May 9 - 13, 1988

LIST OF PARTICIPANTS

Dr. Arthur Aikin
NASA/GSFC
Code 616
Greenbelt, MD 20771

Dr. Patrick Aimedieu
Service d'Aeronomie du CNRS
BP 3
Verrieres le Buisson, FRANCE 91370

Dr. Hideharu Akiyoshi
Kyushu University
Hakozaki, Higashiku
Fukuoka, JAPAN 812

Dr. Daniel F. Albritton
NOAA Aeronomy Laboratory
R/E/AL6
325 Broadway
Boulder, CO 80303

Dr. Donald E. Anderson
Naval Research Laboratory
Code 4141
Washington, DC 20375

Dr. Gail P. Anderson
AFGL/OPI
Hanscom AFB, MA 01731

Dr. James G. Anderson
Harvard University
ESL
40 Oxford Street
Cambridge, MA 02138

Dr. F. Arnold
Max-Planck-Institut for Kerphysik
Postfach 103980
Heidelberg, FRG D6900

Dr. Roger Atkinson
Bureau of Meteorology
P.O. Box 1289K
Melbourne, AUSTRALIA 3001

Dr. John Austin
University of Washington
Department of Atmospheric Sciences
AK-40
Seattle, WA 98195

Dr. Mark Baldwin
Northwest Research Assoc., Inc.
PO Box 3027
Bellevue, WA 98009

Dr. Art Belmont
3216 36th Avenue, NE
Minneapolis, MN 55418

Dr. Pawan K. Bhartia
Science Applications Research
4400 Forbes Blvd
Lanhan, MD 20706

Dr. Rosina Bierbaum
Office of Technology Assessment
U.S. Congress
600 Pennsylvania Ave., SE
Washington, DC 2003

Dr. Christian Blanchette
York Univ
Dept of Earth & Atmos Sci
4700 Keele Street
North York, Ontario, Canada M3J 1P3

Dr. B. W. Boville
York University
Dept. of Earth & Atmos. Sci.
4700 Keele Street
North York, Ontario, CANADA M3J 1P3

Dr. Byron A Boville
National Center for Atmos. Rch.
P.O. Box 3000
1850 Table Mesa Dr.
Boulder, CO 80307

Dr. Guy Brasseur
Belgian Institute for Space Aeronomy
3, Avenue Circulaire
Brussels, BELGIUM 1180

Dr. Edward Browell
NASA Langley Research Ctr
Mail Stop 401-A
Hampton, VA 23665-5225

Dr. Christoph Bruhl
Max Planck Institut fur Chemie
POB 3060
Mainz, FRG D-6500

Dr. William Brune
Harvard University
ESL
40 Oxford Street
Cambridge, MA 02138

Dr. Paul Bui
NASA/Ames Research Center
184 Farley Street
Mountain View, CA 94043

Dr. James B. Burkholder
NOAA/CIRES
R/E/AL2
325 Broadway
Boulder, CO 80303

Dr. C.R. Burnett
Florida Atlantic University
(CRB,KRM), NOAA-EBB
P.O. Box 59
Rollinsville, CO 80474

Dr. E. B. Burnett
Florida Atlantic University
(CRB,KRM), NOAA-EBB
P.O. Box 59
Rollinsville, CO 80474

Dr. K. Roland Chan
NASA/Ames Research Center
MS 245-5
Moffett Field, CA 94035

Dr. Martyn Chipperfield
Cambridge University
Dept of Physical Chemistry
Lensfield Rd
Cambridge, ENGLAND CB2 1EP

Dr. S. Chubachi
Meteorological Research Institute
1-1 Nagamine
Tsukuba, Ibaraki, JAPAN 305

Dr. Michael T. Coffey
National Center for Atmos Rch
Code 1302
1850 Table Mesa Drive
Boulder, CO 80307

Dr. Estelle Condon
NASA Ames Res. Ctr
Code 245-5
1950 Alford Ave
Los Altos, CA 94022

Ms. Liz Cook
Friends of the Earth
530 7th Street, S.E.
Washington, DC 20003

Dr. R. A. Cox
UKAEA
Engineering Sciences Division
Harwell Laboratory
Didcot, Oxfordshire, ENGLAND OX11 ORA

Mr. Charles Crawford
Cable News Network
Science Unit
100 International Blvd.
Atlanta, GA 30348

Dr. Paul Crutzen
Max-Planck-Institute for Chemistry
P.O. Box 3060
Mainz, FRG D6500

Dr. Robert L. De Zafra
State University of New York
Physics Department
Stony Brook, NY 11794

Dr. William B. DeMore
Jet Propulsion Laboratory
Mail Stop 183-301
4800 Oak Grove Dr
Pasadena, CA 91109

Dr. Terry Deshler
University of Wyoming
1010 Kearney
Laramie, WY 82070

Dr. Paul Dickinson
Rutherford Appleton Laboratory
Chilton
Didcot. Oxon, ENGLAND OX11 OQX

Ms. Dianne Dumanoski
Boston Globe
135 Morrissey Blvd.
Boston, MA 02107

Dr. Timothy Dunkerton
Northwest Research Associates, Inc.
P.O. Box 3027
Bellevue, WA 98009

Dr. James E. Dye
National Center for Atmos. Research
Mesoscale & Microscale Met. Div.
P.O. Box 3000
Boulder, CO 80307

Dr. Robert Etkins
NOAA
National Climate Programs Office
11400 Rockville Pike
Rockville, MD 20852

Dr. W. F. J. Evans
Atmospheric Environment Service
4905 Dufferin Street
Downsview, Ontario, CANADA M3H 5T4

Dr. David Fahey
NOAA Aeronomy Lab
R/E/AL6
325 Braodway
Boulder, CO 80303

Dr. Hugh Farber
Farber Associates
2807 Highbrook
Midland, MI 48640

Dr. Joe C. Farman
British Antarctic Survey
Natural Environment Research Council
High Cross Madingley Road
Cambridge, ENGLAND CB3 0ET

Dr. Crofton B. Farmer
Jet Propulsion Laboratory
Mail Stop 183-401
4800 Oak Grove Drive
Pasadena, CA 91109

Dr. Guy V. Ferry
NASA-Ames Research Center
Mail Stop 245-5
Moffett Field, CA 94035

Dr. Giorgio Fiocco
University La Sapieuza
Physics Department
Rome, Italy 00185

Dr. Diane Fisher
Environmental Defense Fund
257 Park Avenue, S. 16th Floor
New York, NY 10010

Dr. Paul R. Franchois
CIRES, Univ. of CO
NOAA/GMCC, R/E/AR4
325 Broadway
Boulder, CO 80303

Mr. Phil Frank
Cable News Network
Science Unit
100 International Blvd.
Atlanta, GA 30348

Dr. Randall R. Friedl
Jet Propulsion Laboratory
Mail Stop 183-301
4800 Oak Grove Dr
Pasadena, CA 91109

Dr. Bruce Gandrud
National Center for Atmos. Rch.
P.O. Box 3000
1850 Table Mesa Dr.
Boulder, CO 80307

Prof. Monika Ganseforth (SPD)
German Parliament
Bundeshaus NH 1518
Bonn 1, FRG 5300

Dr. Wolf Garber
Federal Environmental Agency
Bismarckplatz 1
Berlin, West Germany

Dr. Bruce Gary
Jet Propulsion Lab
MS T-1182-3
4800 Oak Grove Drive
Pasadena, CA 91109

Dr. Marvin A. Geller
NASA Goddard Space Flight Center
Chief, Laboratory for Atmospheres
Code 610
Greenbelt, MD 20771

Dr. Melvyn E. Gelman
NOAA/NMC
Climate Analysis Center
5200 Auth Road
Washington, DC 20233

Dr. Anver Ghazi
Comm. of the European Comm.
200 Rue de la Loi
Brussels, BELGIUM 1049

Dr. G. P. Gobbi
IFA/CNR
Casella Postale 27
Frascati, ITALY 00044

Dr. Sophie Godin
Jet Propulsion Laboratory
Table Mountain Observatory
P.O. Box 367
Wrightwood, CA 92397

Dr. D.M. Golden
SRI International
PS 031
333 Ravenswood Ave
Menlo Park, CA 94025-3493

Mrs. Elizabeth Festa Gormley
Chemical Manufacturers Assoc.
2501 M Street, NW
Washington, DC 20037

Dr. Florence Goutail
CNRA/France
Verriers le Buisson, France

Dr. Claire Granier
Service d'Aeronomie du CNRS
BP 3
Verrieres le Buisson, FRANCE 91371

Dr. Linsley Gray
Akzo Chemie America
8401 West 47th Street
McCook, IL 60525

Dr. Lesley J. Gray
Rutherford Appleton Laboratory
Chilton,
Didcot, Oxon., ENGLAND OX 11 OQX

Dr. Robert F. Hampson
National Bureau of Standards
Bldg 222 RM A147
Gaithersburg, MD 20899

Dr. David Hanson
University of Minnesota
School of Physics and Astronomy
116 Church St., SE
Minneapolis, MN 55455

Dr. Jerald Harder
CIRES/ University of Wyoming
NOAA/ERL R/E/AL5
325 Broadway
Boulder, CO 80303

Dr. Neil Harris
Univ. of CA, Irvine
Department of Chemistry
Irvine, CA 92717

Dr. Dennis Hartmann
University of Washington
Department of Atmospheric Sciences
AK-40
Seattle, WA 98195

Dr. Donald F. Heath
NASA
NOAA/R/E/AL6
325 Broadway
Boulder, CO 80303

Dr. Leroy E. Heidt
National Center for Atmos. Rch.
P.O. Box 3000
1850 Table Mesa Dr.
Boulder, CO 80307

Dr. Henri Heron
Ministry of the Environment
National Agency of Environ Protection
29, Strandgade
Copenhagen K., DENMARK DK-1401

Dr. John S. Hoffman
Environmental Protection Agency
401 M Street, SW
Washington, DC 20460

Dr. D. J. Hofmann
University of Wyoming
Dept. of Physics & Astronomy
Laramie, WY 82071

Dr. J.R. Holton
University of Washington
Atmospheric Sci. AK-40
Seattle, WA 98195

Ms. Janice Hostetter
ORI, Inc./NASA
NASA Hqts.
EPM-20
Washington, DC 20546

Dr. Susan Hovde
NOAA Aeronomy Laboratory
R/E/AL6
325 South Broadway
Boulder, CO 80303

Dr. Carleton J. Howard
NOAA Aeronomy Lab
R/E/AL6
325 Broadway
Boulder, CO 80303

Dr. Ivar Isaksen
University of Oslo
Dept. of Physics
P.O. Box 0316 Blindern
OSLO 3, NORWAY 0316

Dr. Yasunobu Iwasaka
Water Research Institute
Nagoya University
Chikusa'ku
Nagoya, JAPAN 464

Dr. Roger Jacoubek
CIRES
3065 24th St.
Boulder, CO 80302

Dr. Geoff Jenkins
UK Dept of the Environment
B354 Romney House
43 Marsham Street
London, ENGLAND SW1P 3PY

Dr. R. L. Jones
U. K. Meteorological Office
London Road
Bracknell, Berkshire, ENGLAND

Dr. Joe Jordan
Sterling Software Co.
1504 Bay Street, #6
Santa Cruz, CA 95060

Dr. Torben S. Jorgensen
Danish Meteorological Institute
Lyngbyvey 100
Copenhagen, DENMARK 2100

Dr. Jacek Kaminski
York University
Center for Rch in Exp. Spa. Sci
4700 Keele Street
North York, CANADA M3J 1P3

Dr. Gerald M. Keating
NASA Langley Research Center
Mail Stop 401-B
Hampton, VA 23665

Dr. Ken Kelly
NOAA
Sunshine Canyon Drive
Boulder, CO 80303

Mr. Dick Kerr
Science
1333 H Street, NW
Washington, DC 20005

Dr. James B. Kerr
Atmospheric Environment Service
4905 Dufferin Street
Downsview, Ontario, CANADA M3H 5T4

Dr. J. Gordon Keys
Physics and Engineering Lab.,
DSIR, Lauder
Private Bag
Omakau, Central, NEW ZEALAND

Dr. L. Keyser
Jet Propulsion Laboratory
4800 Oak Grove Drive
Pasadena, CA 91109

Dr. Jeffrey T. Kiehl
National Center for Atmos Rch
P.O. Box 3000
Boulder, CO 80307

Dr. Stefan Kinne
NASA/Ames Research Center
MS 245-3
Mountain View, CA 94040

Dr. Malcolm K. W. Ko
Atmospheric & Environmental Rch, Inc.
840 Memorial Drive
Cambridge, MA 02139

Dr. Charles E. Kolb
Aerodyne Research Inc.
45 Manning Road
Billerica, MA 01821-3976

Dr. W. D. Komhyr
NOAA/ ARL/ GMCC
R/E/AR4
325 Broadway
Boulder, CO 80303

Dr. Arlin Krueger
NASA Goddard Space Flight Center
Code 616
Greenbelt, MD 20771

Dr. Klaus F. Kunzi
University of Bern
5, Sidlerstrasse
Bern, SWITZERLAND CH-3012

Dr. Michael J. Kurylo
NASA & NBS
NASA Hqts.
Code EEU
Washington, DC 20546

Dr. Leslie Robert Lait
NASA Goddard Space Flight Center
Code 616
Greenbelt, MD 20771

Mr. Jean Lalonde
CBC Montreal
1400 Dorchester Blvd.
Montreal, CANADA H2L 2M2

Dr. Valerie Lang
Jet Propulsion Laboratory
4800 Oak Grove Drive
Pasadena, CA 90019

Dr. Jack C. Larsen
ST Systems Corporation (STX)
28 Research Drive
Hampton, VA 23666

Dr. Soren H. H. Larsen
University of Oslo
Dept of Physics
P.O. Box 0316 Blindern
Oslo 3, NORWAY 0316

Dr. Ming-Taun Leu
Jet Propulsion Lab
Mail Stop 183-301
4800 Oak Grove Dr
Pasadena, CA 91109

Ms. Barbara Levi
Physics Today
335 East 45th Street
New York, NY 10017

Ms. Yan Liu
Florida Atlantic University
Department of Physics
Boca Raton, FL 33431

Dr. Shaw Liu
NOAA/Aeronomy Lab
325 Broadway
Boulder, CO 80303

Dr. Julius London
University of Colorado
Boulder, CO 80309

Dr. John Lynch
National Science Foundation
DPP/Rm 620
1800 G Street NW
Washington, DC 20550

Dr. William G. Mankin
National Center for Atmos. Rch
Code 1302
1850 Table Mesa Drive
Boulder, CO 80307

Dr. James J. Margitan
Jet Propulsion Lab
Code 183-301
4800 Oak Grove Dr
Pasadena, CA 91109

Dr. David McAllister
Great Lakes Chemical Corp.
P.O. Box 2200
West Layfayette, IN 47906

Dr. M. Patrick McCormick
NASA Langley Research Center
Mail Code 475
Hampton, VA 23665

Dr. Michael B. McElroy
Harvard University
Pierce Hall
29 Oxford Street
Cambridge, MA 02138

Dr. Mack McFarland
E.I. DuPont de Nemours and Co., Inc.
B-13230
Wilmington, DE 19898

Dr. Michael E. McIntyre
University of Cambridge
DAMTP
Silver Street
Cambridge, ENGLAND CB3 9EW

Dr. Daniel McKenna
U. K. Meteorological Office
London Road
Bracknell, Berkshire, ENGLAND

Dr. Gerard Megie
Service d'Aeronomie du CNRS
BP 3
Verrieres le Buisson, FRANCE 91371

Dr. Bernard Mendonca
NOAA
325 Broadway
Boulder, CO 80303

Dr. Kent L. Miller
Utah State University
Center for Atmospheric & Space Sci.
Logan, UT 84322-4405

Dr. K.R. Minschwaner
Florida Atlantic University
(CRB,KRM), NOAA-EBB
P.O. Box 59
Rollinsville, CO 80474

Dr. Mario J. Molina
Jet Propulsion Lab
Mail Code 183-301
4800 Oak Grove Dr
Pasadena, CA 91109

Dr. Bruce Morley
SRI International
PN 375
333 Ravenswood Avenue
Menlo Park, CA 94025

Dr. George Mount
NOAA/Aeronomy Lab
325 Broadway
Boulder, CO 80303

Dr. Christian Muller
Belgium Institute for Space Aeronomy
3 Avenue Circulaire
Brussels, BELGIUM B1118

Dr. David G. Murcray
University of Denver
Department of Physics
Denver, CO 80208-0202

Dr. Frank J. Murcray
University of Denver
Department of Physics
Denver, CO 80208-0202

Dr. Daniel Murphy
NOAA
1556 Sunset Blvd.
Boulder, CO 80303

Mr. John J. Nance
4512 87th Ave West
Tacoma, WA 98466

Dr. Paul A. Newman
Applied Research Corp
NASA/GSFC
Code 616
Greenbelt, MD 20771

Dr. Mike Nicovich
Georgia Tech Research Institute
Georgia Institute of Technology
Atlanta, GA 30322

Dr. Samuel J. Oltmans
NOAA/GMCC
R/E/AR4
325 Broadway
Boulder, CO 80303

Dr. S. Robert Orfeo
Allied-Signal Inc.
20 Peabody Street
Buffalo, NY 14210

Dr. John Orlando
NOAA/CIRES Aeronomy Lab
R/E/AL6
325 Broadway
Boulder, CO 80303

Ms. Flo Ormond
ORI, Inc./NASA
NASA Hqts.
Code EEU
Washington, DC 20546

Dr. Leonard Pfister
NASA/Ames Research Center
MS 245-3
Moffett Field, CA 94035

Dr. Alan Plumb
MIT
Department of Meteorology
and Physical Oceanography
Cambridge, MA 02146

Dr. Rafe Pomerance
World Resources Institute
1735 New York Ave, NW
Suite 400
Washington, DC 10006

Dr. Lamont R. Poole
NASA Langley Research Ctr.
Mail Stop 475
Hampton, VA 23665

Dr. Lars P. Prahm
Danish Meteorological Institute
Lyngbyvey 100
Copenhagen, DENMARK 2100

Dr. Michael H. Proffitt
NOAA/Aeronomy Lab
325 Broadway
Boulder, CO 80303

Dr. James Peterson
NOAA/GMCC
325 Broadway
Boulder, CO 80303

Dr. Stephen Piotrowicz
NOAA/AOML/OCD
4301 Rickenbacher Causeway
Miami, FL 33149

Dr. James Podolske
NASA Ames Research Center
Mail Stop 245-5
Moffett Field, CA 94035

Dr. J.P. Pommereau
CNRS
Verrieres le buisson, France 91371

Dr. Jill Powell
NOAA Aeronomy Laboratory
R/E/AL6
325 South Broadway
Boulder, CO 80303

Dr. Michael Prather
Goddard Institute for Space Studies
NASA
2880 Broadway
NY, NY 10025

Dr. Rudolf Pueschel
NASA/Ames Research Center
MS 245-5
Moffett Field, CA 04035

Dr. John A. Pyle
University of Cambridge
Dept of Physical Chemistry
Lensfield Rd
Cambridge, ENGLAND CB2 1EP

Dr. V. Ramaswamy
Princeton University (GFDL)
AOS Program
(Forrestal Campus) PO Box 308
Princeton, NJ 08542

Dr. A.R. Ravishankara
NOAA Aeronomy Lab
R/E/AL2
325 Braodway
Boulder, CO 80303

Dr. Nathaniel D. Reynolds
University of Alabama
Department of Math and Stats
Huntsville, AL 35899

Ms. Shari Roan
Orange County Register
Accent Dept.
625 North Grand Avenue
Santa Ana, CA 92701

Dr. Jose M. Rodriguez
Atmospheric & Environmental Rch, Inc.
840 Memorial Drive
Cambridge, MA 02139

Dr. James M. Rosen
University of Wyoming
Dept. of Physics and Astronomy
Laramie, WY 82071

Mr. Horst Rademacher
Frankfurter Zeitung
57 Overhill Rd.
Orinda, CA 94563

Dr. William Randel
National Center for Atmos. Research
Code 0904
P.O. Box 3000
Boulder, CO 80307-3000

Dr. Carl A. Reber
NASA/Goddard Space Flight Center
Code 616
Greenbelt, MD 20771

Dr. Behrooz Rezai
Utah State University
Center for Atmospheric & Space Sci.
Logan, UT 84322-4405

Dr. Aidan Roche
Lockheed, Palo Alto Labs.
Code 9790/201
3251 Hanover Street
Palo Alto, CA 94304

Dr. H. K. Roscoe
Clarendon Lab
Dept of Atmospheric Physics
Parks Rd.
Oxford, ENGLAND OX13PU

Dr. F. Sherwood Rowland
University of California
Department of Chemistry
Irvine, CA 92717

Dr. Philip Russell
NASA/Ames Research Center
Mail Stop 245-5
Moffett Field, CA 94035

Dr. Ross J. Salawitch
Harvard University
Pierce Hall
29 Oxford Street
Cambridge, MA 02138

Dr. David A. Salstein
Atmospheric & Environmental Rch, Inc.
840 Memorial Drive
Cambridge, MA 02139

Dr. Stanley Sander
Jet Propulsion Lab
Mail Stop 183-301
4800 Oak Grove Dr
Pasadena, CA 91109

Dr. Ryan Sanders
NOAA Aeronomy Lab
R/E/AL8
325 S. Broadway
Boulder, CO 80303

Dr. Yasushiro Sasano
National Institute for Environmental
16-2 Onogawa, Yatacho
Tsukuba-gun,, JAPAN 305

Dr. Ulrich Schmidt
Institut fur Atmos. Chemie,
KFA Julich
Postfach 1913
Julich, FRG D-5170

Dr. Mark Schoeberl
NASA Goddard Space Flight Center
Code 616
Greenbelt, MD 20771

Dr. Stan G. Scott
NASA/Ames Research Center
12 Maywood Lane
Menlo Park, CA 94025

Dr. W. R. Sheldon
University of Houston
Physics Department
4800 Calhoun
Houston, TX 77004

Dr. Yasushiro Shimizu
Environmental Agency
1-2-2 Kasumigaseki
Chiyoda Ku
Tokyo, JAPAN 100

Dr. Paul C. Simon
Institut d'Aeronomie Spatiale
3 Ave Circulaire
Brussels, BELGIUM B-1180

Dr. Igor Sobolev
C&P Technology, Inc.
5 Rita Way
Orinda, CA 94563

Dr. Philip Solomon
State University of New York
Dept of Earth & Space Sci
Astronomy Program
Stony Brook, NY 11794

Dr. Susan Solomon
NOAA Aeronomy Laboratory
325 S. Broadway
Boulder, CO 80303

Dr. J. Richard Soulen
Technical & Management Services, Inc.
2833 Montclair Drive
P. O. Box 1325
Ellicott City, MD 21043

Dr. Charles R. Stearns
University of Wisconsin
Dept. of Meteorology
1225 W. Dayton St.
Madison, WI 53706

Ms. Sherry Stephens
Univ. of Colorado/NCAR
Campus Box 449
Boulder, CO 80309

Dr. Richard Stolarski
NASA Goddard Space Flight Center
Code 616
Greenbelt, MD 20771

Dr. Susan E. Strahan
NASA Ames Research Center
SSG:245-5
Moffett Field, CA 94035

Dr. N. Sundararaman
World Meteorological Organization
Case Postale 5
Geneva 20, SWITZERLAND CH1211

Dr. Marijke J. Swierstra
South African Council for Sci & Ind Rch
Office of Science and Technology
4801 Massachusetts Ave., NW
Washington, DC 20016

Dr. Brian A. Tinsley
National Science Foundation
1800 G Street, NW
Washington, DC 20550

Dr. Margaret A. Tolbert
SRI International
Chemical Physics Lab
333 Ravenswood Ave
Menlo Park, CA 94025

Dr. Darin Toohey
Harvard University
40 Oxford St.
Cambridge, MA 02139

Dr. Brian Toon
NASA Ames Research Center
MS 245-3
Moffett Field, CA 94035

Dr. Geoffrey C. Toon
Jet Propulsion Laboratory
Mail Stop 183-401
4800 Oak Grove Drive
Pasadena, CA 91109

Dr. Arnold Torres
NASA/GSFC
Wallops Flight Facility
Code 672
Wallops Island, VA 23337

Dr. Chip Trepte
ST Systems Corp. (STX)
28 Research Drive
Hampton, VA 23666

Dr. Tai-Ly Tso
Jet Propulsion Laboratory
Mail Stop 183-301
4800 Oak Grove Dr
Pasadena, CA 91109

Dr. Adrian Tuck
NOAA Aeronomy Lab
R/E/AL6
325 Braodway
Boulder, CO 80303

Dr. Ka Kit Tung
Clarkson Univ
Dept of Math & Comp Sci
Potsdam, NY 13676

Dr. Richard Turco
R&D Associates
P.O. Box 9695
Marina del Rey, CA 90295

Dr. Peter Usher
United Nations Environment Programme
UNEP P.O. Box 30552
Nairobi, KENYA

Dr. Jane Van Doren
Boston College/Aerodyne Research
45 Manning Road
Billerica, MA 01821

Dr. Prasad Varanasi
State Univ of New York
Lab for Planetary Atmos Rch
Stony Brook, NY 11794-2300

Dr. James F. Vedder
NASA Ames Research Center
Mail Stop 245-5
Moffett Field, CA 94035

Dr. M. Verhille
ATOCHEM
Le Defanse 10
Cedex 42
Paris la Defense, France

Dr. Guido Visconti
Universita' degli Studi-lAquila
Dipartimento di Fisica
Piazza Annunziata 1
l'Aquila, ITALY 67100

Dr. A. Wahner
CIRES/NOAA R-E-AL2
325 Broadway
Boulder, CO 80303

Mrs. Jeanne Waters
NOAA Aeronomy Lab
325 Broadway
Boulder, CO 80303

Dr. Ian Watterson
CIRES/Univ. of Colorado
405 Christmas Tree Drive
Boulder, CO 80302

Dr. Peter E. Wilkniss
National Science Foundation
Washington, DC 20550

Dr. J.C. Wilson
Univ of Denver
2390 S. York
Denver, CO 80208

Dr. Steven C. Wofsy
Harvard University
Pierce Hall
29 Oxford Street
Cambridge, MA 02138

Dr. Yuk L. Yung
California Institute of Technology
Div. Geol. & Planetary Sci.
Code 170-25
Pasadena, CA 91125

Dr. Mark Zahniser
Aerodyne Research Inc.
45 Manning Road
Billerica, MA 01821-3976

Prof. R. Zellner
University of Gottingen
Institute fur Physikalische Chemie
Tammannshasse
Gottingen, FRG D-3400

Ms. Pamela S. Zurer
Chemical & Engineering News
1155 16th Street, NW
Washington, DC 20036

NASA
National Aeronautics and Space Administration

Report Documentation Page

1. Report No.	2. Government Accession No.	3. Recipient's Catalog No.
NASA CP-10014		

4. Title and Subtitle	5. Report Date
Polar Ozone Workshop - Abstracts - May 1988	May 1988
	6. Performing Organization Code: 616

7. Author(s)	8. Performing Organization Report No.
A. C. Aikin	88B0234
	10. Work Unit No.

9. Performing Organization Name and Address	11. Contract or Grant No.
Goddard Space Flight Center Greenbelt, Maryland 20771	
	13. Type of Report and Period Covered: Conference Publication

12. Sponsoring Agency Name and Address	14. Sponsoring Agency Code
National Aeronautics and Space Administration Washington, D. C. 20546	

15. Supplementary Notes

16. Abstract

The Polar Ozone Workshop was convened to discuss recent findings on the temporal and spatial behavior of ozone in the polar regions. The underlying photochemical and dynamical causes were examined in detail. The discovery of large decreases in ozone over Antarctica in the spring were described. These results have been verified by ground-based, balloon and satellite instruments. The amount of ozone loss has been increasing since 1979 when the effect was first detected. This ozone hole is associated with the southern hemisphere polar vortex, which confines air in winter so that heterogenous chemical reactions involving chlorine and nitrogen compounds on polar stratospheric clouds can proceed uninterrupted by motions. The return of sunlight in the spring releases chlorine from the clouds leading to the destruction of ozone. Highlights of the Workshop included the presentation of the 1987 aircraft expedition in the Antarctic and the 1988 Arctic aircraft expedition as well as ground-based measurements in Antarctic and Arctic.

17. Key Words (Suggested by Author(s))	18. Distribution Statement
Antarctic Ozone Polar ozone Polar atmospheric circulation Aerosols	Unclassified - Unlimited Subject Category 45

19. Security Classif. (of this report)	20. Security Classif. (of this page)	21. No. of pages	22. Price
Unclassified	Unclassified	329	

National Aeronautics and
Space Administration

Washington, D.C.
20546

Official Business
Penalty for Private Use, $300

Postage and Fees Paid
National Aeronautics and
Space Administration
NASA-451

U.S.MAIL

NASA

POSTMASTER: If Undeliverable (Section 158
Postal Manual) Do Not Return